Photodynamic Activities and Metal Sensing Behavior of Boron Dipyrromethenes and a Silicon(IV) Phthalocyanine

HE, Hui

A Thesis Submitted in Partial Fulfillment
of the Requirements for the Degree of
Doctor of Philosophy
in
Chemistry

The Chinese University of Hong Kong

September 2010

UMI Number: 3483860

All rights reserved

INFORMATION TO ALL USERS
The quality of this reproduction is dependent upon the quality of the copy submitted.

In the unlikely event that the author did not send a complete manuscript
and there are missing pages, these will be noted. Also, if material had to be removed,
a note will indicate the deletion.

UMI®
Dissertation Publishing

UMI 3483860
Copyright 2011 by ProQuest LLC.
All rights reserved. This edition of the work is protected against
unauthorized copying under Title 17, United States Code.

ProQuest®

ProQuest LLC
789 East Eisenhower Parkway
P.O. Box 1346
Ann Arbor, MI 48106-1346

Thesis/Assessment Committee

Professor Kevin Wing Por Leung (Chair)

Professor Dennis Kee Pui Ng (Thesis Supervisor)

Professor Qian Miao (Committee Member)

Professor Wai Kin Chan (External Examiner)

Professor Andrew Cammidge (External Examiner)

Abstract

This thesis describes the synthesis and characterization of several series of functional boron dipyrromethenes (BODIPYs) and a silicon(IV) phthalocyanine. Their applications as efficient photosensitizers in photodynamic therapy and selective fluorescent sensors for metal ions are also reported herein.

Chapter 1 presents an overview of BODIPYs, including their general synthesis, properties, reactivities, and applications. The use of these compounds as photosensitizers for photodynamic therapy and fluorescent sensors for metal ions is highlighted.

Chapter 2 reports the synthesis, spectroscopic characterization, photophysical propreties, and in vitro photodynamic activities of a series of symmetrical distyryl BODIPYs substituted with one to five hydrophilic oligoethylene glycol monomethyl ether chain(s). In general, these compounds are essentially non-aggregated in DMF, resulting in a strong fluorescence emission and relatively high efficiency in generating singlet oxygen. Being formulated with 0.05% Tween 80, these compounds act as efficient photosensitizers. The compound which contains five triethylene glycol monomethyl ether chains exhibits the highest photocytotoxicity with an IC_{50} value as low as 7 nM toward HT29 human colorectal carcinoma cells. The high photodynamic activity of this compound can be attributed to its high

efficiency in generating singlet oxygen, low aggregation tendency, and high cellular uptake. In addition, this compound also has a strong and selective affinity to the endoplasmic reticulum of the cells, causing cell death mainly through apoptosis.

Chapter 3 reports a related study on a series of unsymmetrical distyryl BODIPYs. These compounds possess three triethylene glycol monomethyl ether chains and another substituent at the other styryl group. The effects of this substituent on the photophysical properties, aggregation behavior, cellular uptake, and subcellular localization have been explored. Furthermore, their in vitro photodynamic activities have also been evaluated and compared with those of symmetrical analogues reported in Chapter 2.

Chapter 4 describes a novel ratiometric near-infrared fluorescent dye based on distyryl BODIPY with a 4-dimethylaminophenylethynyl group at the 2- and 6-positions. This compound exhibits a remarkable blue-shift in its absorption and fluorescence emission positions upon protonation with trifluoroacetic acid in organic solvents or HCl in water in the presence of 0.05% Tween 80. These changes can be made reversible upon addition of a base.

Chapter 5 describes two monostyryl BODIPYs which contain two or four water-soluble amide chains as the metal chelators. The photophysical properties of these compounds and their spectral response to various metal ions have been

investigated. The results show that the compound with two amide chains can detect Zn^{2+} ion in MeCN. They bind in a 1:1 stoichiometry with a binding constant of 2.2×10^4 M^{-1}. The fluorescence emission increases remarkably in intensity and shifts substantially to the blue from 620 to 572 nm due to the inhibition of the intramolecular charge transfer. The compound which contains four amide chains can detect Cd^{2+} ion with a high selectivity in phosphate buffered saline.

Chapter 6 reports the synthesis and spectral properties of a silicon(IV) phthalocyanine with two axial bis(2-picolyl)amine moieties which act as the binding sites for metal ions. The effects of various metal ions on its absorption and fluorescence spectra have been examined. The results indicate that this compound shows a relatively high sensitivity to Zn^{2+} ion. Moreover, the proposed binding mode and the sensing mechanism are also discussed.

At the end of this thesis, the ^1H and $^{13}C\{^1H\}$ NMR spectra of all the new compounds are listed in the Appendix.

摘 要

本論文報導了幾個系列的功能氟硼二吡咯染料和一個硅（IV）酞菁染料的合成與表徵。這些化合物作為有效光敏劑在光動力治療和螢光傳感金屬離子的應用也被探索。

第一章概述了氟硼二吡咯染料的合成，性質，反應活性和應用。重點介紹了該類化合物作為有效光敏劑在光動力治療和螢光傳感金屬離子兩方面的應用。

第二章報導了一系列對稱的二（苯乙烯基）－氟硼二吡咯類化合物的合成、光譜表徵、光物理性質和光動力學活性。這些化合物含有一條到五條不等的生物相容的寡（乙二醇）鏈。總體上來說，這些化合物在 N，N－二甲基甲醯胺中基本上是非聚集的，能夠產生強螢光並具有較高的單線態氧量子產率。在含有 0.05%吐溫 80 的細胞介質中，這些化合物能作為有效的光敏劑。含有五條三（乙二醇）鏈的化合物表現出最高的光毒性，對人類肝癌細胞 HT29 其 IC_{50} 值低至 7 nM。這個化合物高的光動力學活性主要是由於高的單線態氧產生能力，低的聚集趨勢和高的細胞攝入量而導致的。此外，該化合物表現出高選擇性地停留在細胞內質網上，且主要通過細胞程式性死亡的方式殺死癌細胞。

第三章報導了一系列不對稱的二（苯乙烯基）－氟硼二吡咯類化合物的相關研究。這些化合物含有相同的三條三（乙二醇）鏈，但在苯乙烯基上含一個不同的取代基。這些取代基對化合物的光物理性質、聚集行為、細胞吸收和亞

細胞定位的影響也被研究。此外，也將他們的光動力學活性與第二章的對稱類似物進行了比較。

第四章報導了一個新型的基於二（苯乙烯基）－氟硼二吡咯的近紅外螢光染料分子，該分子在 2 和 6 號位置上連接了酸性敏感的 4－二甲氨基苯乙炔基，在有機溶劑中加入三氟乙酸或含 0.05%吐溫 80 的水溶液中加入鹽酸，該分子的吸收和螢光光譜發生顯著的藍移。這些變化是高度酸堿可逆的。

第五章報導了兩個基於苯乙烯基－氟硼二吡咯染料的螢光分子，它們分別含有兩條或四條水溶性的能夠作為金屬離子配體的醚胺鏈。這兩個化合物的光譜性質以及它們對金屬離子的響應情況被研究。研究結果表明含有兩條醚胺鏈的化合物在乙腈中能識別鋅離子，兩者結合比為 1:1，結合常數達 $2.2 \times 10^4\ M^{-1}$。由於鋅離子的加入抑制了分子內的電荷轉移過程，其螢光強度顯著增強且伴隨著光譜從 620 藍移到 572 nm。而含有四條醚胺鏈的化合物在磷酸鹽緩衝體系中能高選擇性地識別鎘離子。

第六章報導了軸向上含兩個能作為金屬離子配體的二（2－吡啶甲基）氨基的硅（IV）酞菁的合成與光譜性質。不同金屬離子對它的電子吸收光譜和螢光光譜的影響被考察。研究結果表明該化合物對鋅離子表現出相對高的靈敏度。此外，可能的結合模式和識別機理也被討論。

論文的最後附上所有新化合物的氫譜和碳譜。

Acknowledgment

How time flies! It has passed three years in a twinkling. The past three-year time is on of the most impressive and meaningful periods in my life. I will not forget it forever.

Firstly, I would like to express my sincere and deep gratitude to my supervisor, Prof. Dennis K. P. Ng, for his continuous inspiration, guidance, support, encouragement, and patience during my Ph.D. studies. His wide knowledge, scrupulous attitude, and dedication on research are always an excellent example and a motive force for my future career. Over the past three years, he has taught me a lot in various aspects. He has taught me how to select a research field, design a feasible project, organize and present data in a scientific way. He has also provided a great assistance during the preparation of my graduate seminars and this thesis. He has also given me the opportunity to attend the 15th and 17th Symposium on Chemistry Postgraduate Research in Hong Kong, which have widened my horizon. I have benefited a lot from his vigorous training. Here, I do like to thank him once again.

I would also like to thank Prof. Gigi P. C. Lo for her useful suggestions in my research, help for in vitro study, and some comments on this thesis. Thanks are also given to Prof. Wing-Ping Fong and Sin-Lui Yeung of the Department of Biochemistry for their help for in vitro study in Chapter 2 and 3.

Thanks are also given to my lab-mates, past and present, including Dr. Xuebing Leng, Dr. Jianyong Liu, Dr. Hu Xu, Dr Xiongjie Jiang, Janet T. F. Lau, Yingsi

Huang, Qunling Fang, Meirong Ke, and Wenjing Shi for their help, discussion, and friendship.

Last but not least, I would like to thank my parents, my husband, and my friends for their continuous care, support, understanding, and encouragement during these years.

Table of Contents

List of Figures

List of Schemes

List of Tables

Abbreviations

General:

ε	Molar extinction coefficient
λ_{max}	Absorption maximum
λ_{em}	Emission Maximum
Φ_F	Fluorescence quantum yield
Φ_Δ	Singlet oxygen quantum yield
Φ_T	Triplet state quantum yield
τ_T	Triplet state lifetime
BODIPY	Boron dipyrromethene
ca.	Coarse approximation
Calcd.	Calculated
DDQ	2,3-Dichloro-5,6-dicyano-1,4-benzoquinone
DIPEA	Diisopropylethylamine
DMEM	Dulbecco's Modified Eagle Medium
DMF	N,N-Dimethylformamide
DPBF	1,3-Diphenylisobenzofuran
equiv.	Equivalent
eT	Electron transfer
FEF	Fluorescence enhancement factor
FRET	Fluorescence resonance energy transfer
h	Hours

HOMO	Highest occupied molecular orbital
ICT	Intramolecular charge transfer
ISC	Intersystem crossing
LUMO	Lowest unoccupied molecular orbital
NIR	Near-infrared
PDT	Photodynamic therapy
PET	Photoinduced electron transfer
ROS	Reactive oxygen species
r.t.	Room temperature
TFA	Trifluoroacetic acid
THF	Tetrahydrofuran
UV	Ultraviolet
Vis	Visible
v/v	Volume to volume ratio
ZnPc	Unsubstituted zinc(II) phthalocyanine

Nuclear Magnetic Resonance (NMR) Data:

$\{^1H\}$	Proton decouple
δ	Chemical shift
J	Coupling constant in Hz
ppm	Part per million
s	Singlet
d	Doublet

t	Triplet
dd	Doublet of doublet
m	Multiplet
br s	Broad signal

Mass Spectrometric (MS) Data:

M^+	Molecular ion
ESI	Electrospray ionization
HRMS	High resolution mass spectroscopy

Chapter 1

Introduction: An Overview of Boron Dipyrromethenes

1.1 General

Boron dipyrromethene (hereafter abbreviated as BODIPY) has received much attention as one of the versatile functional dyes over the past two decades. Figure 1.1 shows the skeleton of BODIPYs. It is composed of two units of pyrrole which are connected by a methene bridge in the 8-position and a boron atom, which is coordinated by two fluorine atoms. The first member of the BODIPY family (compound **1.1**) was reported by Treibs and Kreuzer in 1968.[1] Investigations of these dyes were rare until the end of 1980s.[2] The application of this class of dyes for biological labeling has been well recognized.[3] In fact, several BODIPY-based dyes[4] have been designed and commercialized as labeling reagents for biomolecules. As a consequence, BODIPYs have been known as photostable substitutes for fluorescein. Apart from this application, fundamental studies on the chemical reactivity and photophysical properties of these dyes have also been carried out. BODIPYs have many attractive spectral characteristics, such as large absorption coefficient, high fluorescence quantum yield, and long-wavelength emission. Other advantages of BODIPYs include their slow rate of intersystem crossing, good solubility, high chemical robustness, excellent thermal and photochemical stability, and insensitivity

to changes in environment, such as polarity, pH, and oxygen content of the media, etc.[5]

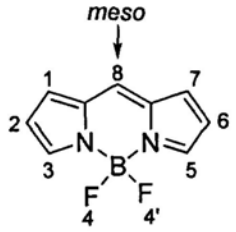

Figure 1.1. The skeleton of BODIPYs.

A small modification of the BODIPY core enables tuning of their stability, photophysical properties, and other characteristics.[5] Non-substituted BODIPY **1.2** had not been reported until Schmitt et al. succeeded in obtaining this compound in 2009.[6] This may be due to the synthetic difficulties as a result of the fact that none of the pyrrole-based carbons are blocked from electrophilic attack. This compound exhibits a high photochemical but low thermal stability. However, the symmetrical 3,5-dimethyl-substituted compound **1.3**[7] was prepared in 1977 and could be considered as a reference to which other simple alkylated BODIPYs can be compared. It exhibits a high photochemical and thermal stability. The absorption and emission maxima appear at 507 and 520 nm, respectively, and the fluorescence quantum yield is up to 0.81 in ethanol. When the symmetric tetra-, hexa-, and hepta-alkylated systems **1.4**,[8] **1.5**, and **1.6**[9] are included in the comparison, a clear trend toward red–shifted electronic absorption and fluorescence emission maxima with increased substitution becomes apparent.

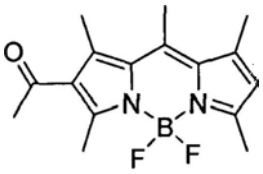

1.1

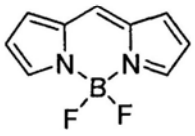

1.2

CH_2Cl_2
$\lambda_{m,abs}$ = 503 nm
$\lambda_{m,em}$ = 512 nm

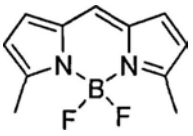

1.3

Φ_F = 0.81, EtOH
$\lambda_{m,abs}$ = 507 nm
$\lambda_{m,em}$ = 520 nm

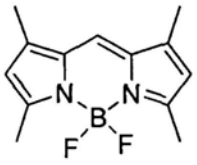

1.4

Φ_F = 0.80, EtOH
$\lambda_{m,abs}$ = 505 nm
$\lambda_{m,em}$ = 516 nm

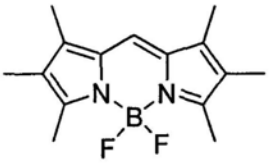

1.5

Φ_F = 0.56, EtOH
$\lambda_{m,abs}$ = 528 nm
$\lambda_{m,em}$ = 536 nm

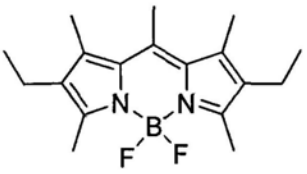

1.6

Φ_F = 0.70, EtOH
$\lambda_{m,abs}$ = 517 nm
$\lambda_{m,em}$ = 546 nm

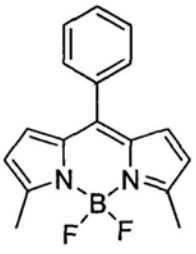

1.7

Φ_F = 0.19, MeOH
$\lambda_{m,abs}$ = 508 nm
$\lambda_{m,em}$ = 521 nm

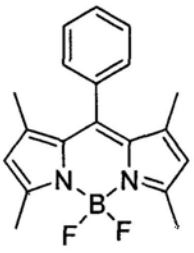

1.8

Φ_F = 0.65, MeOH
$\lambda_{m,abs}$ = 498 nm
$\lambda_{m,em}$ = 508 nm

Alkylation or arylation at the 8-position, namely the *meso* site, has almost no special effect on the electronic absorption and fluorescence emission wavelength even though this substitution position is structurally unique (comparing **1.3** with **1.7**[10] and **1.4** with **1.8**[11]). In addition, the fluorescence quantum yield of compound **1.7** is appreciably lower than that of the more substituted analogue **1.8**. This has been widely attributed to the 1,7-substituents which hinder the rotation of the phenyl group, reducing the possibility of non-radiative decay.

1.2 Synthesis of BODIPYs

The basic synthetic method for BODIPYs is based on the well-known pyrrole condensation reaction, which was developed originally for the synthesis of certain types of porphyrins. A highly electrophilic carbonyl compound such as acyl chloride, acid anhydride, or aldehyde is used to form the methene bridge between the two pyrrole units.

1.2.1 Synthesis from Pyrroles and Acyl Chlorides or Acid Anhydrides

BODIPY dyes can be easily prepared via condensation of acyl chlorides with pyrroles (Scheme 1.1). The transformations involve dipyrromethene hydrochloride salts as intermediates. These intermediates can be handled and purified readily, particularly as the ring-substitution increases, but even so, they are not generally isolated in the synthesis of BODIPY dyes. BODIPYs **1.9**, **1.10**,[12] **1.11**, and **1.12**[13] are selected examples which have been prepared using this method.

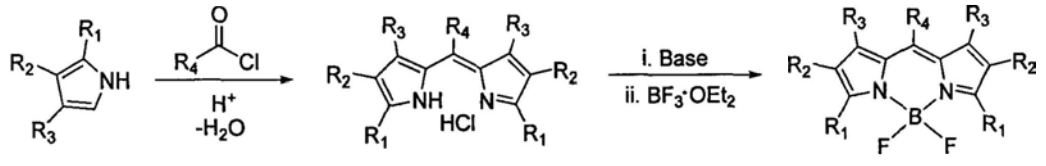

Scheme 1.1. Synthesis of BODIPY dyes from pyrroles and acyl chlorides.

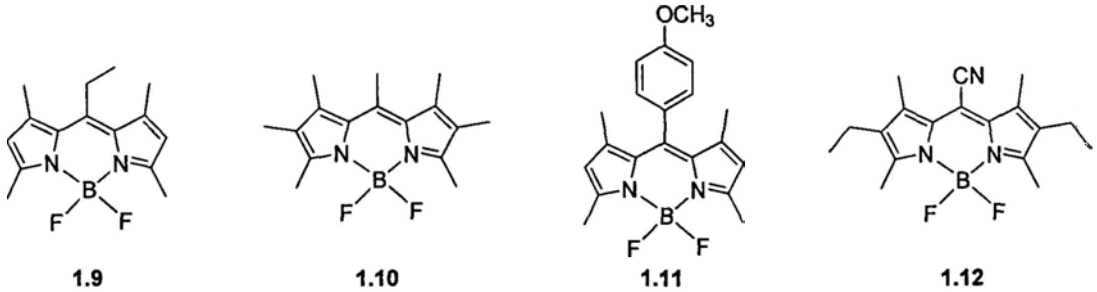

1.9 **1.10** **1.11** **1.12**

Other activated carboxylic acid derivatives can also be used in place of acyl chlorides. Scheme 1.2 shows how the BODIPY derivative **1.13** is prepared from glutaric anhydride.[14] An attractive feature of this reaction is that a free carboxylic acid is attached to BODIPY, which may later be used to conjugate with a probe for targeting.

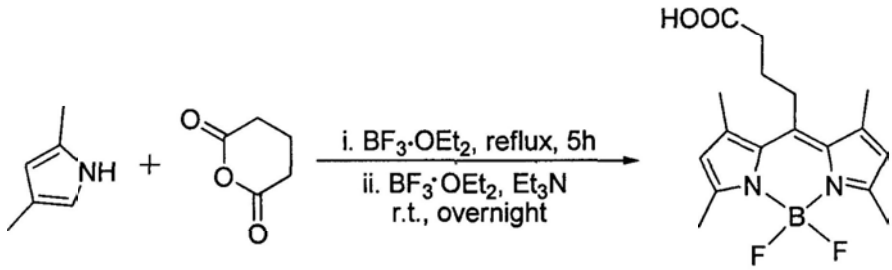

1.13

Scheme 1.2. Synthesis of BODIPY **1.13** from pyrrole and glutaric anhydride.

1.2.2 Synthesis from Pyrroles and Aldehydes

Resembling those depicted in Schemes 1.1 and 1.2, a synthetic procedure of BODIPY dyes from pyrroles and aldehydes is outlined in Scheme 1.3, in which 2,3-dichloro-5,6-dicyano-1,4-benzoquinone (DDQ) or p-chloranil is frequently used as an oxidizing reagent. BODIPYs **1.14**,[15] **1.15**,[16] **1.16**,[17] and **1.17**[18] are selected examples which have been synthesized using this method.

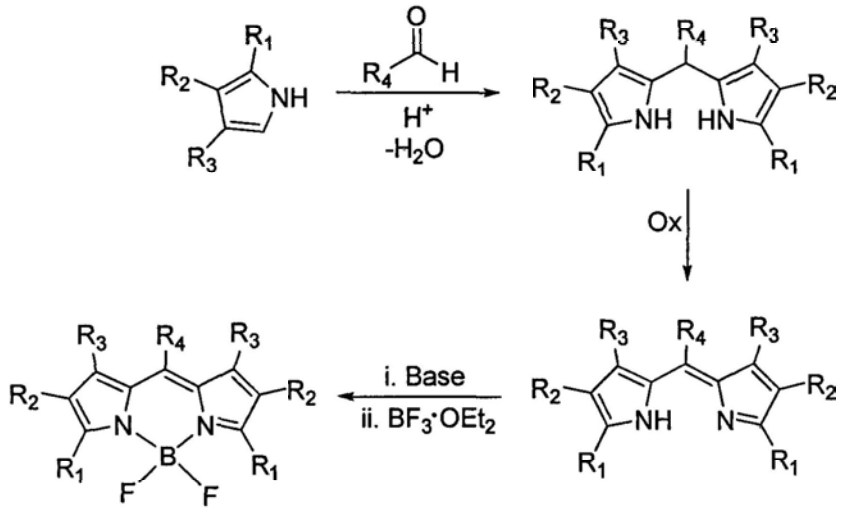

Scheme 1.3. Synthesis of BODIPY dyes from pyrroles and aldehydes.

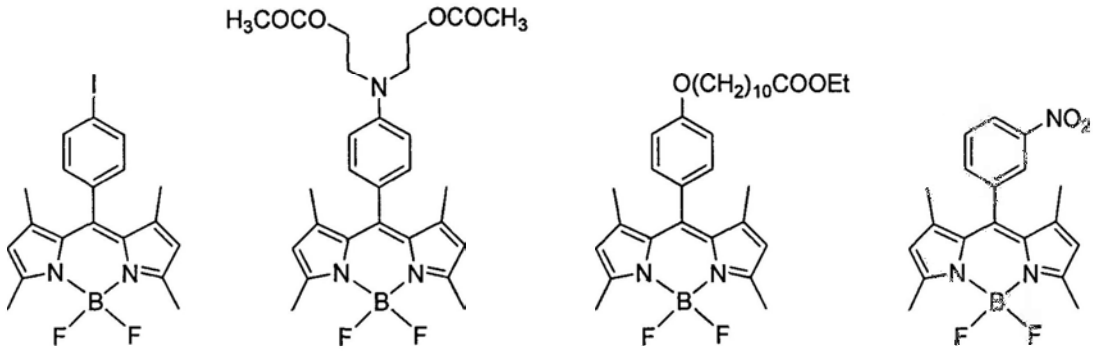

1.14 **1.15** **1.16** **1.17**

α,β-Unsubstituted BODIPYs, such as **1.18**,[19] **1.19**, and **1.20**[20] can also be prepared from the corresponding aldehydes using neat conditions. The aldehyde is dissolved in excess pyrrole at room temperature, and the dipyrromethane intermediate is formed and isolated. The corresponding BODIPY dye can be obtained after oxidation and treatment with boron trifluoride. This mild aldehyde-based approach is preferred, which can prevent some undesirable side reactions of acyl chlorides and unsubstituted pyrrole.

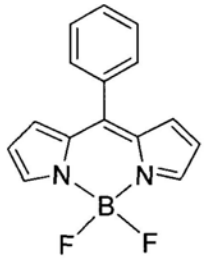

1.18

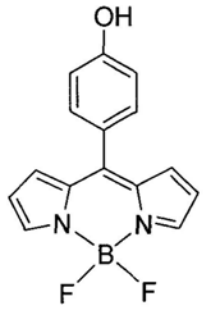

1.19

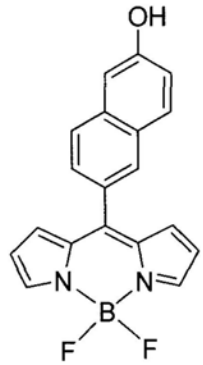

1.20

In general, aliphatic aldehydes are barely applied in the preparation of BODIPY derivatives. The synthesis of vinylic thioether substituted BODIPY **1.21** is an exception. For the preparation of this compound, a catalytic amount of ytterbium(III) trifluoromethane sulfonamide was used to mediate the condensation process. After oxidation with DDQ, the intermediate dipyrromethane was treated with boron trifluoride to obtain the product, though in a very poor yield.[21]

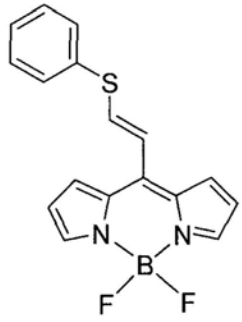

1.21

By using these synthetic methods, numerous BODIPY derivatives have been prepared from the readily available pyrroles. These are direct and convenient methods to access symmetrically substituted BODIPY dyes.

1.2.3 Synthesis from Pyrroles and Ketopyrroles

Generally, unsymmetrically substituted BODIPY dyes are prepared via

condensation of ketopyrrole intermediates with another pyrrole compound without a blocking group at the *o*-position (Scheme 1.4). BODIPY **1.22** is one of the examples prepared by using this method.[22] In fact, this method has been successfully applied in the synthesis of a series of BODIPY-based biological labels.[23]

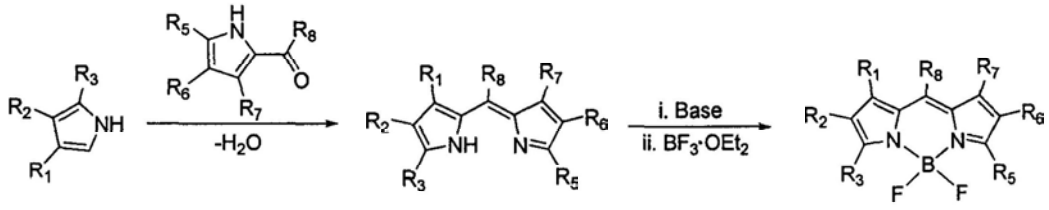

Scheme 1.4. General synthetic route for unsymmetrical BODIPY dyes.

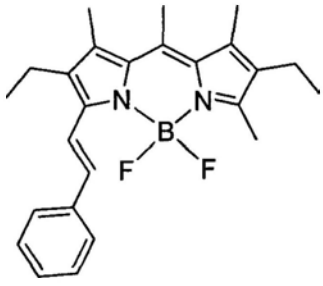

1.22

1.3 Reactivity of BODIPYs

1.3.1 Electrophilic Substitution

An examination of the various mesomeric structures of BODIPY reveals that the 2,6-positions bear the least positive charge, so they should be most susceptible to electrophilic attack (Figure 1.2). Sulfonation, halogenation, and nitration are some common reactions. A general route leading to electrophilic substitution at the 2,6-positions is shown in Scheme 1.5.

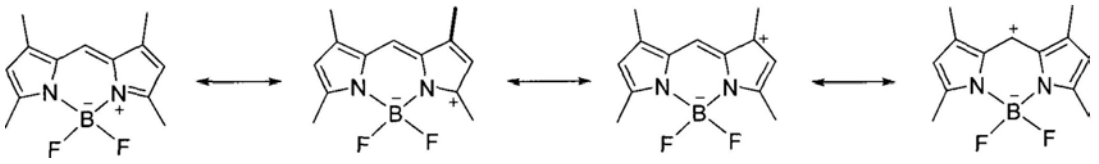

Figure 1.2. Mesomeric structures of tetramethyl-BODIPY.

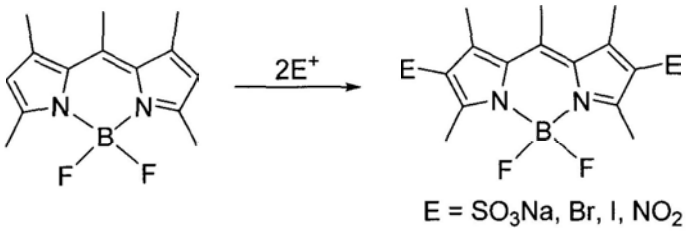

Scheme 1.5. A general route of electrophilic substitution at the 2,6-positions of tetramethyl-BODIPY.

Treibs and Kreuzer[1] first realized that BODIPY dyes readily undergo electrophilic substitution reactions at the 2,6-positions in the presence of chlorosulfonic acid. This reaction was exploited later by Boyer et al. as a means to synthesize some water-soluble analogues.[13] To date, a handful of sulfonated BODIPY dyes have been prepared by treating tetra- or penta-substituted BODIPYs with chlorosulfonic acid at –50°C, followed by neutralization with a base. Monosulfonated analogues can be obtained when only one equiv. of chlorosulfonic acid is used. In general, introduction of sulfonate groups does not significantly change the absorption and fluorescence emission maxima relative to the unsulfonated analogues. The sulfonated BODIPY dyes **1.23** and **1.24** have been found to have a higher stability than the parent dyes in aqueous media.[12,24]

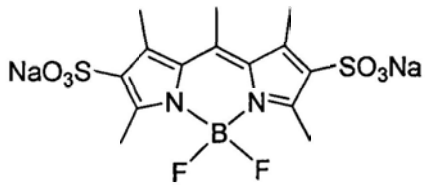

1.23

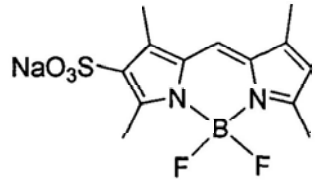

1.24

2,6-Dibromo-pentamethyl BODIPY **1.25** was prepared by slow addition of Br_2 into 1,3,5,7,8-pentamethyl-substituted BODIPY.[12] Similarly, 2,6-diiodo-tetramethyl BODIPY **1.26**[25] was obtained by treating 1,3,5,7-tetramethyl-substituted BODIPY with iodine and iodic acid. Predictably, introduction of bromo or iodo substituents onto the BODIPY core causes a significant red-shift of both the absorption and fluorescence emission maxima, but quenches the fluorescence due to the internal heavy-atom effect. Compound **1.26** is much more resistant to photo-bleaching than Rose Bengal because the BODIPY core has a more positive oxidation potential than the xanthone unit of Rose Bengal. Compound **1.26** is also an efficient photosensitizer. The 2,6-difluoro and 2,6-dichloro substituted BODIPY derivatives **1.27**[26] and **1.28**[27] have also been used as electroluminescent devices and sensitizers.

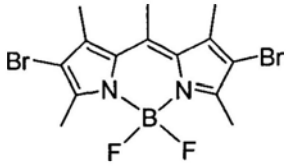

1.25

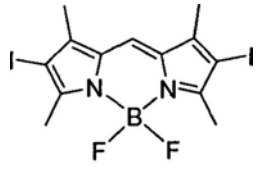

1.26

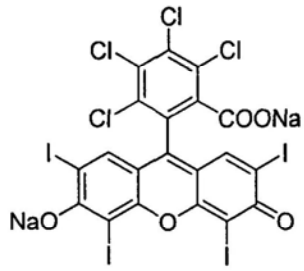

Rose Bengal

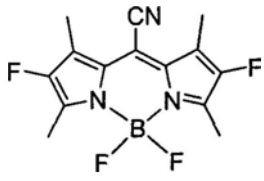

1.27

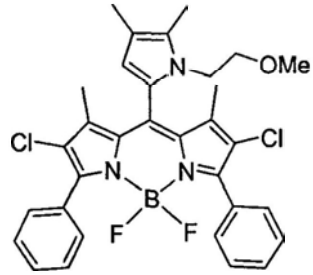

1.28

The 2,6-dinitro BODIPY dye **1.29** can be obtained via nitration of the pentamethyl-BODIPY with nitric acid at 0°C. Its fluorescence quantum yield is dramatically decreased after incorporation of the nitro groups due to strong electron transfer.[12,28]

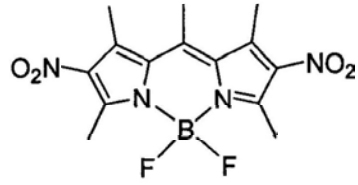

1.29

1.3.2 Nucleophilic Substitution

A flexible approach to generate 3- and/or 5-substituted BODIPYs is to utilize appropriately substituted pyrroles as precursors. Recently, a powerful method which involves nucleophilic substitution of 3,5-dichloro-BODIPY **1.30**[29] has received

considerable attention. Different nucleophilic species, such as alkoxides, amines, and thioalkoxides, as well as the diethyl malonate anion can be used. More importantly, the substitution process can be controlled, giving selectively mono- or di-substituted product (Scheme 1.6).

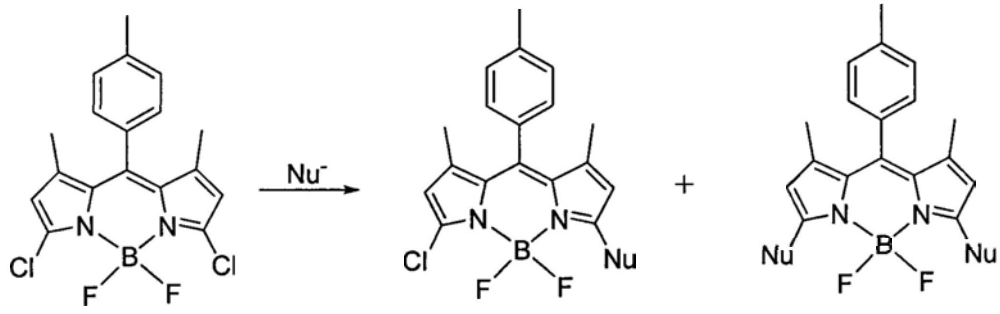

1.30 **1.31** **1.32**

Scheme 1.6. Nucleophilic substitution of BODIPY **1.30**.

The 3- and 5-substituents have some significant effects on the photophysical characteristics of the dyes. For example, introduction of two amino groups in BODIPY **1.33**[29a] or a thioester moiety in BODIPY **1.34**[29c] results in remarkable red-shifts in their absorption and emission postions. Their fluorescence quantum yields are also reduced compared with the unsubstituted analogues.

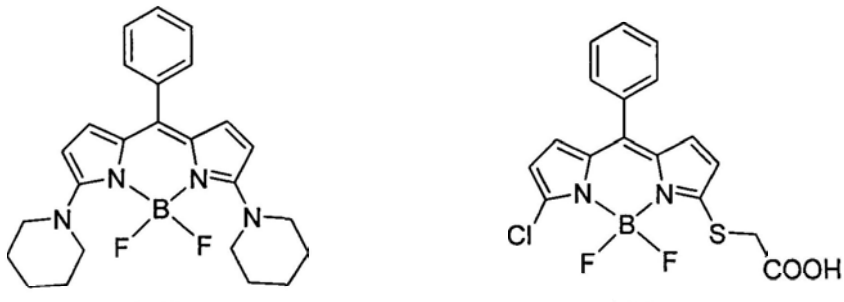

1.33 **1.34**

8-(ω-Haloalkyl)-BODIPY dye **1.35** is an useful building block, which can be readily functionalized by nucleophilic substitution reactions (Scheme 1.7).[30] A series of novel BODIPY analogues **1.36** have been prepared by this method which can be used for chemoselective labeling of cysteine residues and chemosensors for metal ions.[30a]

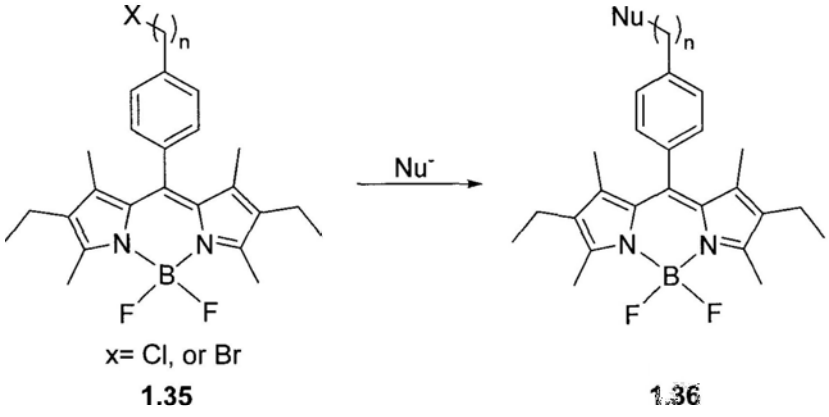

Scheme 1.7. Preparation of BODIPY **1.36** via nucleophilic substitution reactions at the 8-position.

1.3.3 Reactions of the Active Methyl Groups

BODIPYs bearing methyl groups at the 3,5-positions can be functionalized at the methyl carbon atoms owing to their acidic nature and the strong nucleophilic character of the resulting carbanions. These methyl groups can be deprotonated under mild conditions. The resulting carbanions react readily with aromatic aldehydes to generate a mixture of monostyryl substituted BODIPY (MS-BODIPY) **1.37** and distyryl substituted BODIPY (DS-BODIPY) **1.38** (Scheme 1.8).[3b,31]

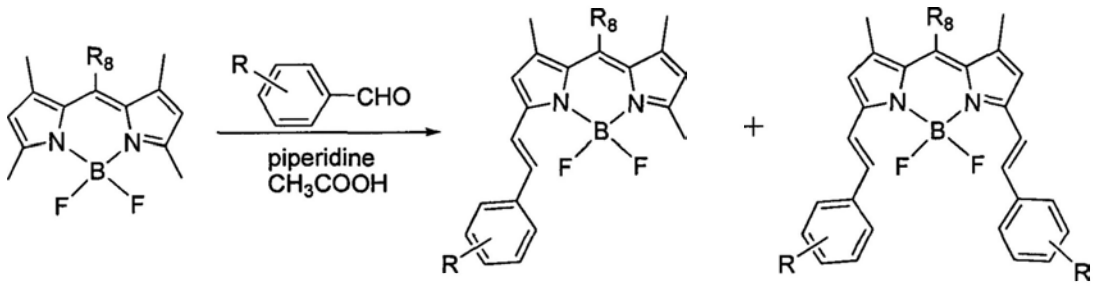

1.37 **1.38**

Scheme 1.8. Condensation of methylated BODIPYs with aromatic aldehydes.

This synthetic procedure has been used to extend the degree of π-electron conjugation, which consequently induces a pronounced bathochromic shift to both the absorption and fluorescence emission maxima. Generally, MS-BODIPYs and DS-BODIPYs without special groups exhibit the emission maxima at ca. 570 and 640 nm, respectively, while their parent BODIPYs without styryl substituents show an emission maximum at ca. 500 nm. When a strong electron-donating group, such as dimethylamino group is directly attached to the styryl group, a considerable red shift will be observed due to intramolecular charge transfer (ICT). For example, MS-BODIPY **1.39** and DS-BODIPY **1.40** exhibit the emission maximum at 738 and 791 nm, respectively.[32] However, when the dimethylamino group is located at the *meso*-position, the red shift is less substantial because this *meso*-substituent is nonplanar to the π system and exerts less influence on the photophysical properties of the BODIPYs.[33]

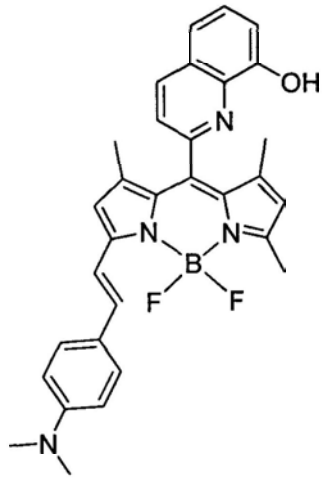

1.39

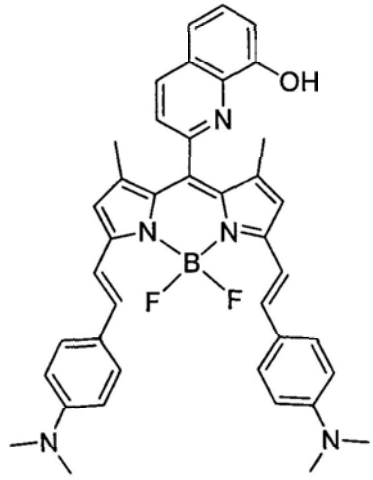

1.40

1.3.4 Metal-Catalyzed Cross-Coupling Reactions

Further extension of the conjugation and building of more sophisticated structures can be achieved by using palladium-catalyzed coupling reactions. The reactive halo groups can either be directly linked to the BODIPY core or the aryl substituents.[34] The halogen atoms can be introduced to the BODIPY core by using halogen-containing pyrrole precursors or by electrophilic halo substitution.[12,25] Various types of coupling reactions, such as Sonogashira, Heck, Stille, and Suzuki reactions, have been applied to connect alkynyl, ethenyl, and aryl groups to the BODIPY frameworks (Scheme 1.9). Interestingly, the B-F bonds remain intact during these cross-coupling reactions.

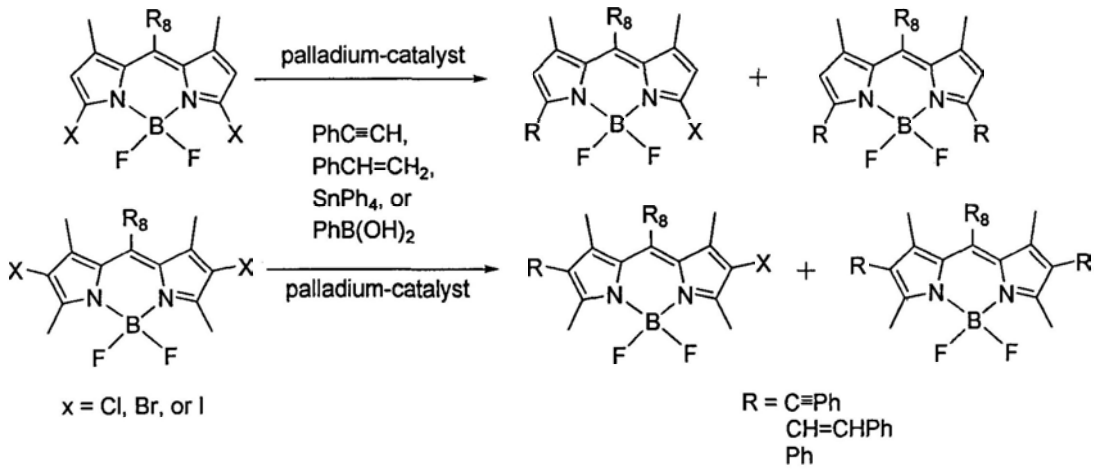

Scheme 1.9. Palladium-catalyzed cross-coupling reactions of BODIPYs.

The extended conjugation of the resulting coupled products leads to red-shift of their absorption and emission maxima. The absorption maxima for the mono-substituted compound **1.41** and the di-substituted analogue **1.42**, for example, are red-shifted by 48 and 97 nm, respectively, compared with the non-alkynylated analogue. The mono-substituted BODIPY **1.41** can be further modified by nucleophilic substitution (see Section **1.3.2**) or cross coupling reactions to give unsymmetrical derivatives.[36]

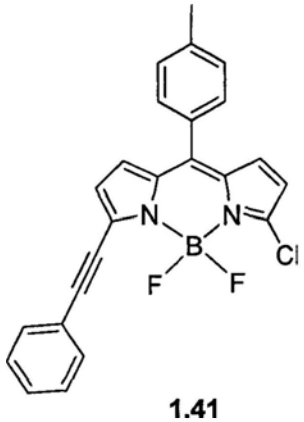

1.41

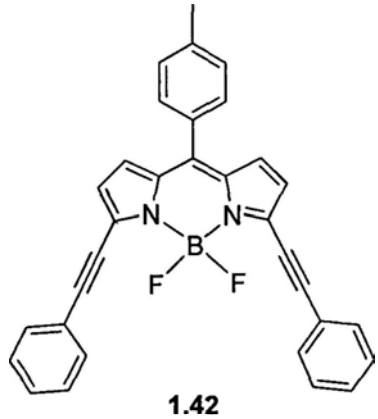

1.42

1.3.5 Substitution of Fluoride in the BF_2-Group

Substitution of the fluoride groups of BODIPYs had been rarely reported before Murase et al. filed a patent in 2002.[37] In this case, phenylmagnesium chloride was used to carry out the replacement. The organometallic approach has been further developed by Ulrich et al.,[38] who introduce aryl,[39] ethynylaryl,[40] and ethynyl[41] subunits in place of the fluoride. Depending on the nature of the substrate, organolithium or Grignard reagents are commonly used to substitute the fluoride groups (Scheme 1.10). This strategy has led to a dramatic increase in the versatility of BODIPY dyes, such as **1.43**,[42] **1.44**,[39] **1.45**,[38] and **1.46**.[41] In particular, it allows the construction of sophisticated arrays in which different functional groups are linked up together at the boron sites.

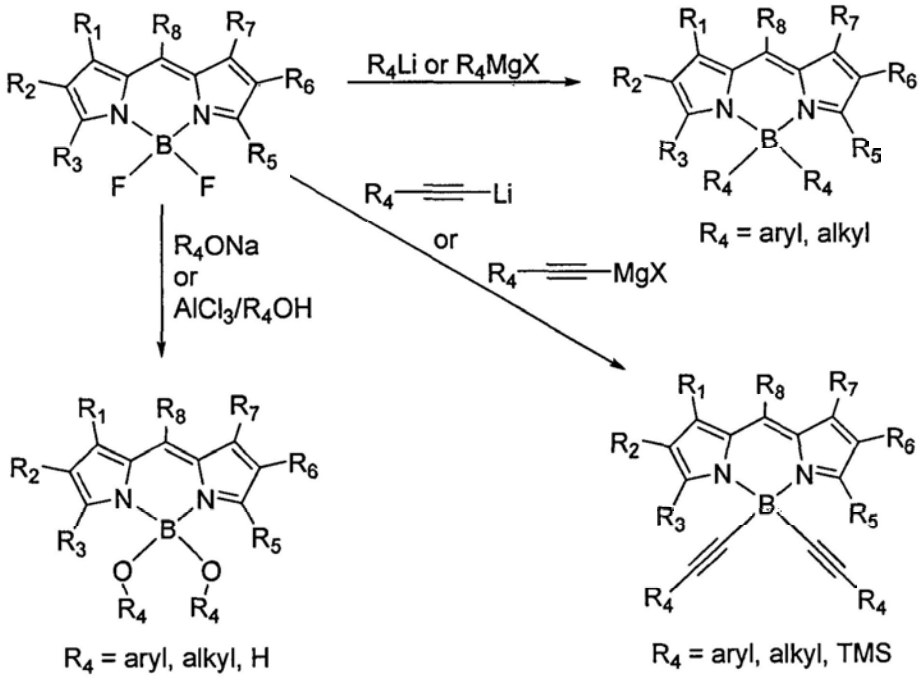

Scheme 1.10. Substitution of the fluoride groups in the BF_2 moiety of BODIPYs.

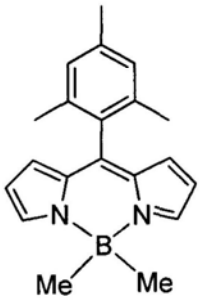

1.43

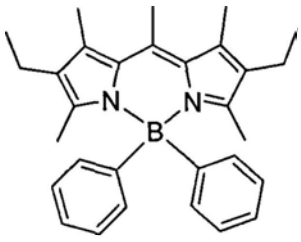

1.44

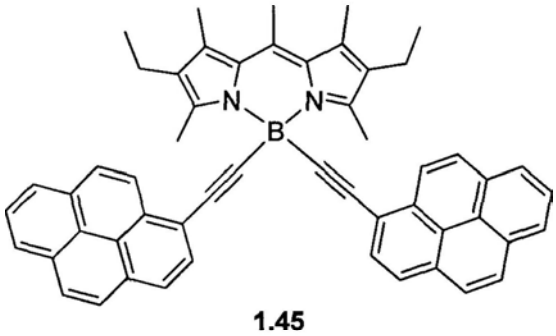

1.45

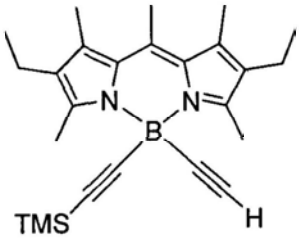

1.46

Compound **1.47** was prepared by intramolecular displacement of the fluoride groups with the *o*-phenoxyl groups located at the 3,5-positions in the presence of BBr_3.[43] The fluoride can also be readily replaced with hydroxyl groups in the presence of a strong Lewis acid. Compound **1.48**, for example, was prepared by treatment of the corresponding BODIPY with $AlCl_3$ in dry CH_2Cl_2 followed with water.[44]

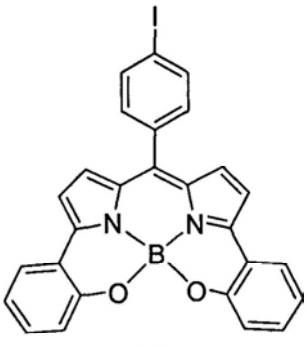

1.47

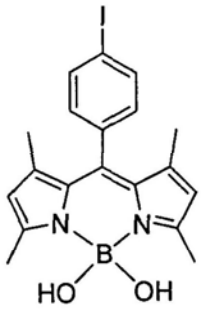

1.48

1.4 BODIPYs as Efficient Photosensitizers for Photodynamic Therapy

1.4.1 Photodynamic Therapy

1.4.1.1 *The Development of Photodynamic Therapy*

The use of light for therapy was found three thousand years ago, but it was only in the last century that photodynamic therapy (PDT) was developed.[45] A German medical student Rabb reported the killing of the microorganism *paramecia* with the combination of acridine and light at the end of 19th century.[46] A few years later, von Tappeiner and Jesionek treated skin tumors with topically applied eosin and white light.[47] They went on to demonstrate the requirement of oxygen in the photosensitization reaction, and in 1904 introduced the term "phododynamic action" to describe this phenomenon,[48] which was regarded as the milestone of PDT.

PDT is an innovative approach for the treatment of a range of cancers and wet age-related macular degeneration.[49] The treatment involves a combination process of a photosensitizer, light, and oxygen. Each component is non-toxic by itself, but their combination can lead to cellular and tissue damage. The photosensitizer is a photosensitive compound which can be preferentially retained in malignant cells or tissues. When a cancer is identified, a photosensitizer can be administered into body by various means, such as intravenous injection or topical application to the skin. Upon irradiating with visible light in an appropriate region, the photosensitizer is activated, and then transfers its electron or energy to molecular oxygen to generate reactive oxygen species (ROS). Because of the high reactivity and short lifetime of

ROS, their biochemical reactions take place only in the immediate locale of the photosensitizer. Therefore, the biological responses are induced only in the particular areas of tissue which are exposed to light. Hence, the targeting of PDT is accomplished mainly by the precise application of light through modern fiber optics and endoscopy. Photosensitizers encapsulated in various carriers, such as polymeric micelles and liposomes, can also increase their selectivity toward tumor cells.[49e,49i]

PDT has several potential advantages over traditional cancer treatment methods.[49f] First of all, it is comparatively non-invasive and can be targeted accurately, mainly through the precise application of light. In addition, repeated doses can be given to patients without the total-dose limitations associated with radiotherapy. It also does not have multi-drug resistant problem which is the main drawback of chemotherapy.[50] The healing process usually results in little or no scarring. Furthermore, PDT can usually be done in an outpatient or day-care setting, which is convenient to patients. Finally, this method does not seem to have significant and long-term side effects.

1.4.1.2 *The Mechanisms of Photodynamic Therapy*

1.4.1.2.1 Photophysical Mechanism

The photophysical mechanism involved in PDT is shown in Figure 1.3. Upon illumination, the photosensitizer at its ground state (S_0) absorbs the energy to the first excited singlet state (S_1). This excited state can return to S_0 by emitting fluorescence or lose its energy via intersystem crossing (ISC) to populate the much longer-lived

triplet state (T_1). The excited triplet state then interacts with tissue oxygen ($^3O_2$) in either a Type I or Type II mechanism. In Type I mechanism, an electron transfer reaction occurs leading to the generation of super oxide ($O_2^{\cdot-}$). Alternatively, the triplet state can undergo an energy transfer with oxygen to form singlet oxygen ($^1O_2$) and this process is classified as the Type II mechanism. Singlet oxygen is a highly reactive oxygen species that can react rapidly with numerous biologically important substrates, resulting in oxidative damage and ultimately cell death. It is generally believed that the Type II mechanism predominates during PDT and singlet oxygen is the most important cytotoxic species produced.[51]

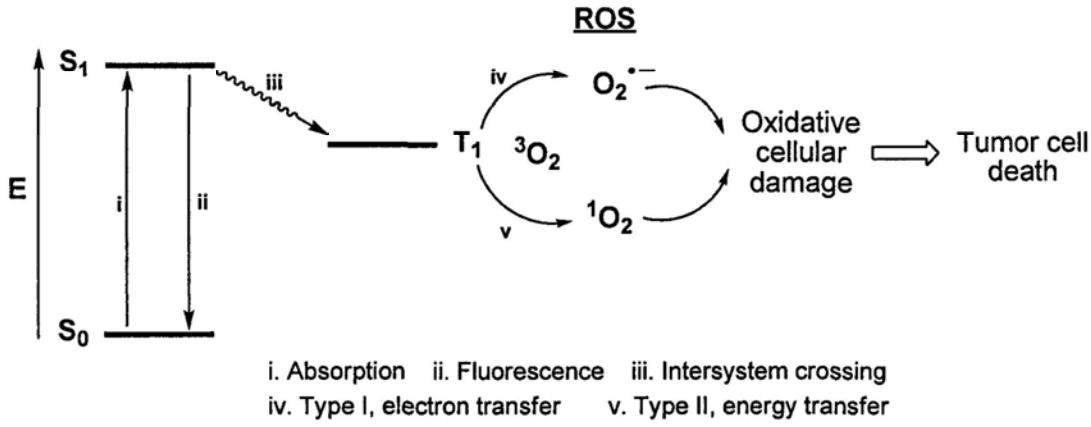

Figure 1.3. The photophysical mechanism involved in PDT.

1.4.1.2.2 Cellular Mechanism

Significant effort has been directed toward understanding the cellular mechanism of PDT in recent years. Cell death in a necrotic fashion can be induced by organelle damage, such as membrane lipid peroxidation, disruption of lysosomal membrane, membrane enzyme inhibition or damage to nuclear components.[52] Apoptosis is a type of programmed cell death.[53] It is a process of deliberate suicide

by unwanted cells. In contrast to necrosis, apoptosis results in acute tissue injury, which is carried out in an ordered process. The cell genotype and the PDT dose have been found to determine whether the cell death occurs by apoptosis or necrosis.[54] For instance, under low light doses, apoptosis was the predominant process of cell death when murine leukemia P388 cells were treated with chloroaluminum phthalocyanine, whereas necrosis was observed for high light doses.[54a]

1.4.1.2.3 In vivo Mechanism

There are three main ways to induce tumor destruction in vivo by PDT. Firstly, PDT can damage the tumor-associated vasculature, leading to tumor infarction. The viability of tumor cells depends on the amount of nutrients supplied by the blood vessels. It was reported that a greater percentage of tumor cells in vivo die after PDT treatment because the vascular shutdown starves them of oxygen and nutrients.[55] Secondly, PDT can generate ROS which can kill tumor cells directly when the photosensitizer concentration is high within the tumor at the time of illumination. In vivo studies showed that PDT can reduce the number of tumor cells through direct photodamage.[56] Finally, several studies showed that PDT induces immune modulation, either immune stimulating mediated by natural killer cells and macrophages or immune suppressing. It was suggested that the modulation of immune effects may play a role in PDT-induced destruction of tumors.[57]

1.4.2 Photosentizers for Photodynamic Therapy

Photosensitizers are compounds that are capable of absorbing light of a specific wavelength and transforming it into useful energy. In the case of PDT, this would involve the production of lethal cytotoxic agents. In fact, there are hundreds of natural and synthetic dyes that can function as photosensitizers for PDT. Several comprehensive reviews have appeared, summarizing various types of photosensitizers used in PDT.[49g-i,51]

The first-generation photosensitizers are hematoporphyrin derivatives (HpD). In the 1960s, Liposn et al. found that hematoporphyrin derivatives (HpD) were useful photosensitizing agents.[58] HpD consist of a mixture of several monomeric and oligomeric compounds. Photofrin (**1.49**), which is the most active component in HpD, was isolated by high performance liquid chromatography or size exclusion gel chromatography.[59] The oligomeric units are mainly linked with ester and ether bonds.[60] Photofrin, which was first approved in 1993 in Canada for the treatment of bladder cancer, is also the most commonly used phtosensitizer in clinic to date. However, this drug has a number of drawbacks.[59c] Firstly, it consists of about 60 ingredients and therefore it is difficult to reproduce its composition.[61] Secondly, the longest-wavelength absorption band appears at 630 nm with a low molar extinction coefficient of 1170 M^{-1} cm^{-1}. The biological effects after irradiation at this wavelength occur only to a tissue depth of about 5 mm. Thirdly, it is basically non-selective toward tumors.[62] Most importantly, the sensitizer is retained in

cutaneous tissues for 2-3 months. Patients are therefore required to avoid bright light for a long period of time.[63]

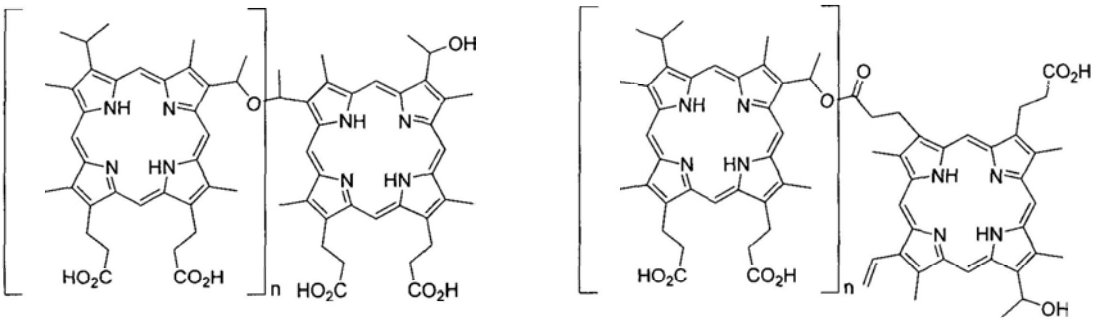

The ether and ester-linked components in Photofrin (**1.49**)

In general, an ideal photosensitizer should meet the following criteria:[64] low dark toxicity but strong photocytotoxicity; high selectivity toward tumor in order to reduce side effects in peritumoral tissues; long-wavelength (e. g. 600-800 nm) absorption in order to enhance light penetration; high extinction coefficient; rapid removal from the body thus inducing a low systemic toxicity; desirable photophysical properties including high triplet state quantum yield ($\Phi_T > 0.4$), long triplet state lifetime ($\tau_T > 20$ μs), and ability to effectively produce singlet oxygen and other ROS.

The second-generation photosensitizers have been developed with the goal of overcoming some of the shortcomings of Photofrin. The first group of second-generation photosensitizers is porphyrin derivatives. Tetrasulfonated porphyrin **1.50**[65] and tetra(hydroxyphenyl)porphyrin **1.51**[66] are representative examples of this series. The second group consists of chlorins and bacteriochlorins, like chlorin e6 **1.52**,[67] benzoporphyrin derivative **1.53**,[68] tin etiopurpurin **1.54**,[69] and *meso*-tetra(hydroxyphenyl) chlorin **1.55**.[70] The third group of potential candidates is

expanded porphyrins such as lutetium texaporphyrin **1.56**.[71] The fourth group is phthalocyanine-based photosensitizers such as the disulfonated aluminium phthalocyanine **1.57**[72] and silicon phthalocyanine Pc4 (**1.58**).[73] The compounds **1.52-1.58** have been approved for clinical use or trial.[71]

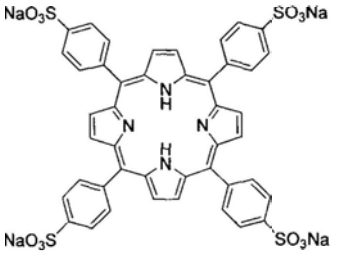

1.50

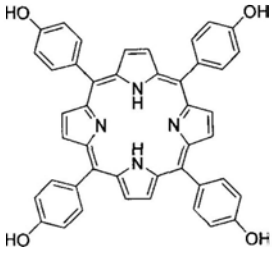

1.51

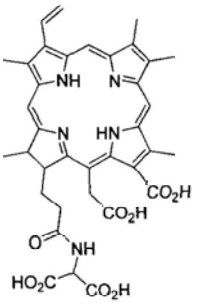

1.52

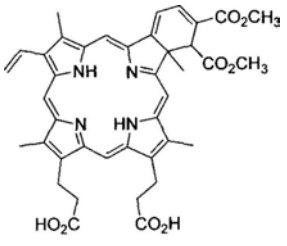

1.53

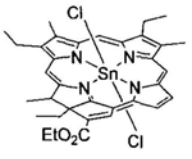

1.54

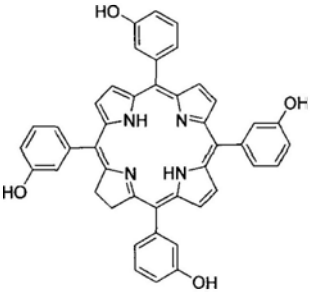

1.55

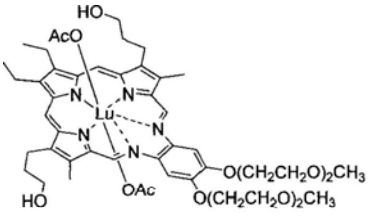

1.56

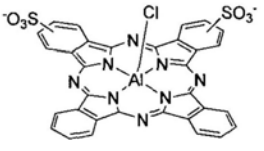

1.57

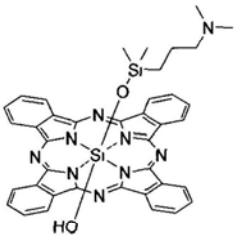

1.58

1.4.3 BODIPYs as Efficient Photosensitizers

Recently, BODIPYs containing heavy atoms, such as bromine and iodine, directly on the core have been found to act as efficient photosensitizers. In 2005, Nagano et al. reported diiodo-BODIPY **1.26**, which was an efficient singlet oxygen

generator.[25] Its singlet oxygen generating efficiency was 1.3 fold higher than that of Rose Bengal, while the non-iodo substituted analogue was not able to generate singlet oxygen. The high efficiency in generating singlet oxygen was achieved due to internal heavy-atom effect. The introduction of iodine atoms into the molecule promoted the intersystem crossing ($S_1 \rightarrow T_1$), thereby enhancing the formation of singlet oxygen.[74]

More recently, Akkaya et al. have demonstrated that the dibromo distyryl BODIPY **1.59**, which has nine hydrophilic triethylene glycol chains, is a very efficient singlet oxygen generator.[75] The compound has a strong absorption at 660 nm, which is considered to be well within the therapeutic window of mammalian tissue. It exhibits good photo-induced cytotoxicity against K562 cells with an IC_{50} value of less than 200 nM. The dark toxicity is negligible at the concentration range studied. The results suggest that it can act as a satisfactory photodynamic agent.

In addition, Lee et al. have reported a BODIPY **1.60**, which shows good photocytotoxicity against HL-60, HSC-2, and HK1 cell lines.[76] It has a selective and high affinity to the mitochondria of the HSC-2 cells. It induces cell death through mitochondria-dependent apoptosis rather than through damage to nucleic materials. In addition, this compound is able to induce complete vascular occlusion, which is considered favorable in PDT treatment of cancer. In spite of shorter wavelength absorption, it still has potential to be explored as a clinically useful photosensitizing agent, especially for the treatment of superficial tissues.

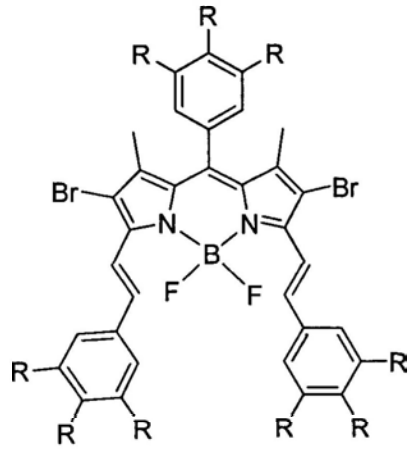

$R = O(CH_2CH_2O)_3CH_3$

1.59

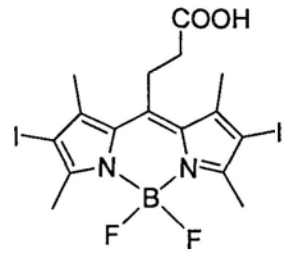

1.60

In light of the very few examples of BODIPY-based photosensitizers, there is much room for further development in this area.

1.5 BODIPYs as Fluorescent Sensors for Metal Ions

1.5.1 Fluorescent Sensing for Metal Ions

Besides the application of PDT, BODIPY dyes can also be used as fluorescent sensors for metal ions which are essential in biological metabolism and many other processes. s-Block metal ions, including Na^+, K^+, Mg^{2+}, and Ca^{2+} ions are involved in biological processes such as transmission of nerve impulses, muscle contraction, and regulation of cell activities, etc. In medicine, it is important to control the Li^+ level in serum of patients under treatment for manic depression and K^+ level in the case of high blood pressure. Referring to Al^{3+} ion, its toxicity is well recognized and there is a controversy about its possible implication in Alzheimer's disease. In chemical oceanography, it has been demonstrated that some nutrients are required for the

survival of microorganisms in sea water which contain Zn^{2+}, Fe^{2+}, and Mn^{2+} ions as enzyme cofactors. Finally, highly toxic Hg^{2+}, Pb^{2+}, and Cd^{2+} ions are well known to cause several diseases and environmental problems. Therefore early detection of these ions in the environment is desirable.[77]

For the purpose of quantitative determination of these metal ions, great efforts have been devoted to the design and development of appropriate chemosensors.[78] The main issue in the design of effective chemosensors involves association of a selective molecular recognition event with a physical signal which is highly sensitive to its occurrence. Colorimetric and/or ratiometric responses can be observed and recorded as output signals if appropriate chromophores or fluorophores are available. For the optical and fluorimetric-based sensors, the latter type shows a higher sensitivity.[79] It also has an additional advantage of being able to differentiate analytes by time-resolved measurements.[80]

In general, for fluorimetric determination of metal ions, chemosensors are composed of two components, namely an ionophore and a fluorophore, which can be bridged via a spacer or not (Figure 1.4). The ionophore is responsible for selective and efficient binding of metal ions which depends on the ligand topology and the characteristics of the metal ions, such as their ionic radius, charge, coordination number, and hardness, etc. The fluorophore provides the means of signaling this binding by changing its photophysical properties, such as emission position, intensity, and lifetime, etc.[77] The most commonly used ionophores are dipicolylamine **1.61**,[81] amino substituted diacetic aid **1.62**,[82] and crown ethers such as **1.63**.[83] Fluorescein

1.64,[84] rhodamine **1.65**,[85] and BODIPY[5] are well known fluorophores for this application.

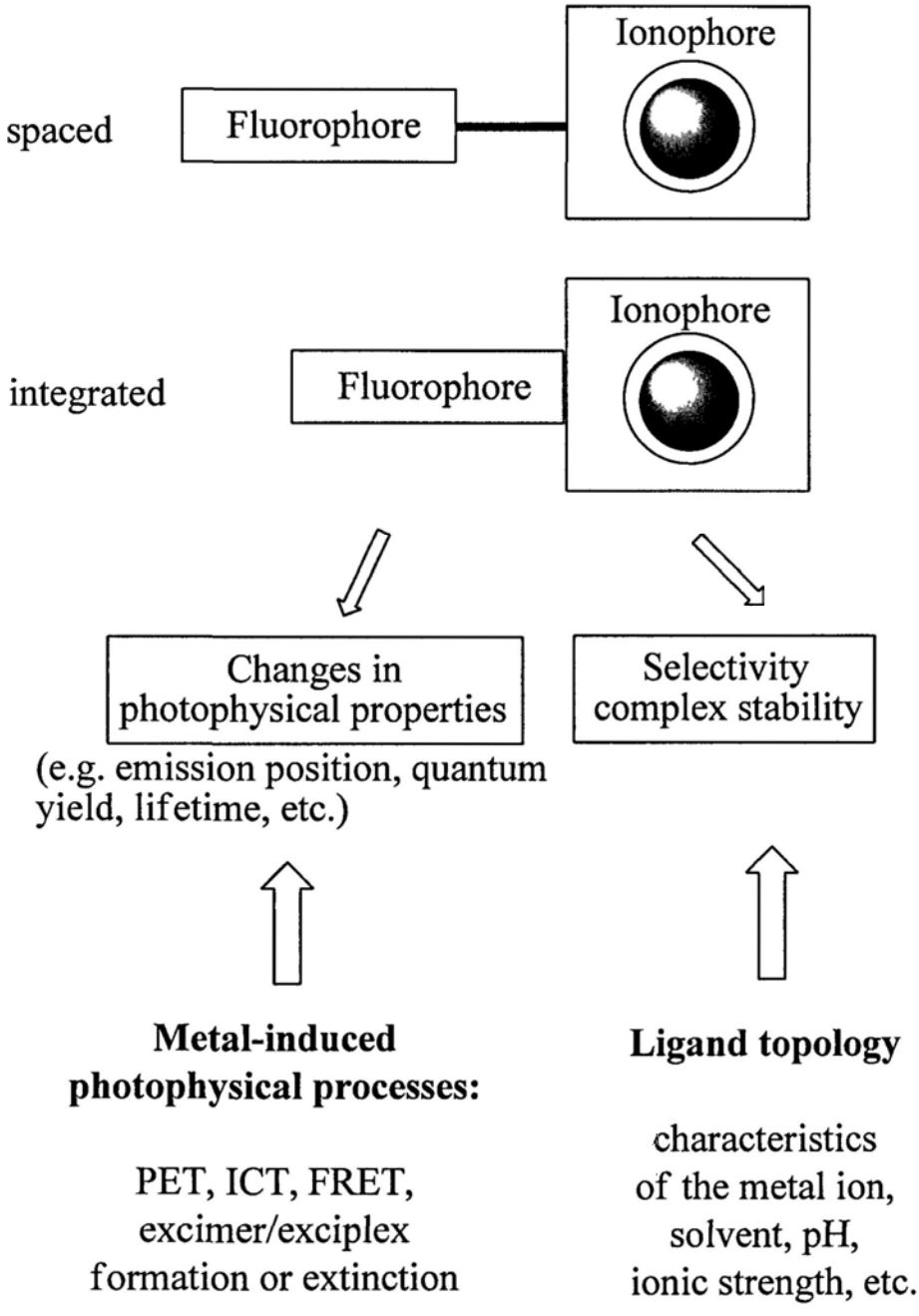

Figure 1.4. Main aspects of fluorescent sensors for metal ions.

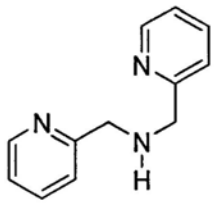

1.61

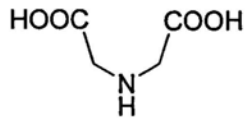

1.62

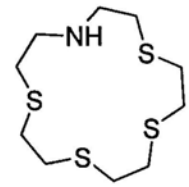

1.63

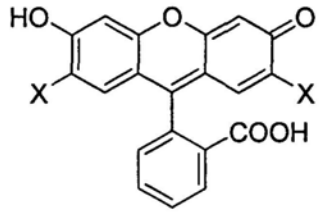

X = H, F, Cl

1.64

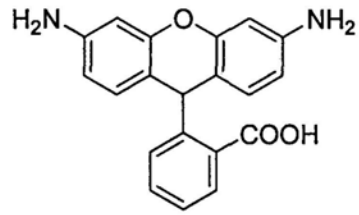

1.65

There are several mechanisms that control the response of a fluorophore upon metal binding. These include photoinduced electron transfer (PET), intramolecular charge transfer (ICT), fluorescence resonance energy transfer (FRET), and excimer/exciplex formation or extinction.[78] PET and ICT are the most common sensing mechanisms, which are briefly introduced in the following sections.

1.5.2 BODIPY-Based Fluorescent PET Sensors

Figure 1.5 illustrates how a metal ion can control the PET process in a fluorescent sensor. The ionophore (also called the metal ion receptor) is usually an electron donor (e. g. amino group) and the fluorophore serves as an electron acceptor. Upon excitation of the fluorophore, an electron locating at the highest occupied molecular orbital (HOMO) is promoted to the lowest unoccupied molecular orbital (LUMO), which enables PET from the HOMO of the donor (belonging to the free

ionophore) to that of the fluorophore, causing fluorescence quenching of the latter. Upon metal binding, the redox potential of the donor is raised so that the relevant HOMO becomes lower in energy than that of the fluorophore. Consequently, PET is not possible and fluorescence quenching is suppressed. Hence, the fluorescence intensity is enhanced upon metal binding.[77]

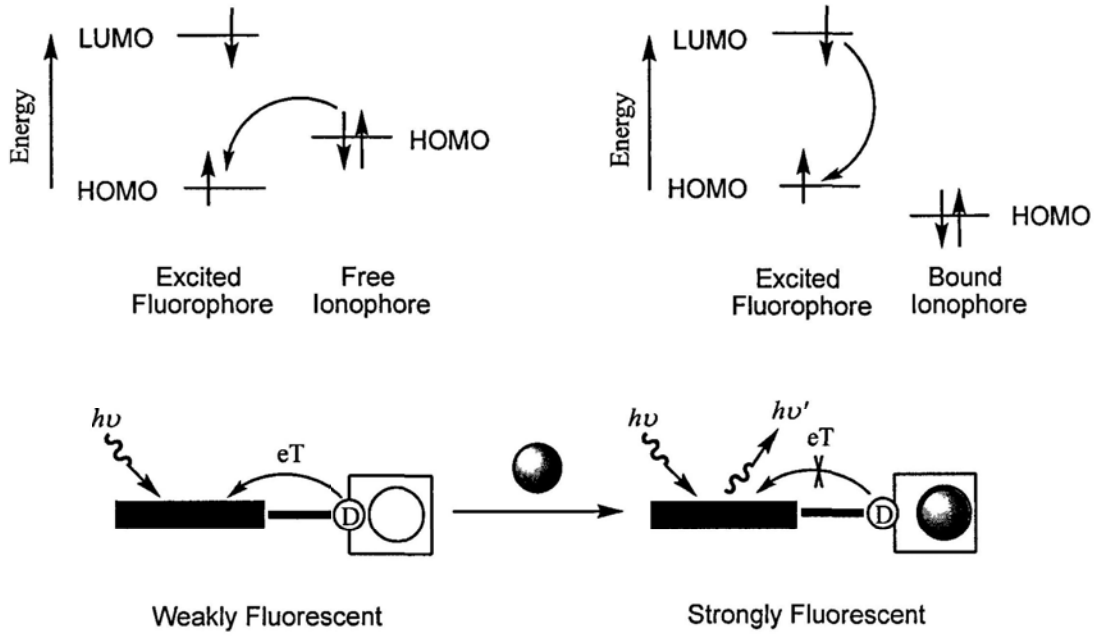

Figure 1.5. A schematic diagram showing the working principle of fluorescent PET sensors.

For constructing PET systems, a common strategy is to incorporate either an amino donor or a nitro acceptor close to the fluorescent dye so that electron transfer can compete with the fluorescence process. This approach can also be used to design fluorescent probes as pH indicators. The thermodynamics of the system have to be poised such that efficient electron transfer occurs in the "off" state, thereby ensuring minimal fluorescence. Coordination of the proton or metal ion to the quencher

changes the redox potential to such a level that fluorescence is restored. Thus, the "on" state displays the fluorescence properties inherent to the dye.

Peng et al. have utilized this principle to prepare a BODIPY-based turn-on PET sensor **1.66**.[86] In this compound, di-(2-picolyl)amine is the ionophore and 1,3,5,7-tetramethyl-BODIPY is the fluorophore. Fluorescence emission of this compound is pH-independent under a large physiological pH range. When it is bound with Zn^{2+} ion, its fluorescence quantum yield increases from 0.08 to 0.86 due to the inhibition of the PET process. This compound can detect Zn^{2+} ion with a high selectivity and sensitivity down to nanomolar in aqueous solution. The low toxicity and good cell-permeability has made it a new Zn^{2+} sensor suitable for biological application. Similarly, compound **1.67**,[87] reported by Boens et al., can recognize Ca^{2+} ion in the neutral 3-(N-morpholino)propanesulfonic acid (MOPS) buffer solution.

Chang et al. have prepared compound **1.68**,[88] which is the first Cu^{+}-selective fluorescent probe with visible excitation and emission profiles. It gives a 10-fold turn-on response for detecting this ion, and features excellent selectivity for Cu^{+} ion over other biologically relevant metal ions, including Cu^{2+} ion. Moreover, confocal microscopy experiments have established that this probe can be used for detecting Cu^{+} levels within living HEK 293 cells. The same group has reported a unique Ni^{2+}-responsive fluorescent sensor **1.69**,[89] which can detect changes in Ni^{2+} levels inside living A549 cells.

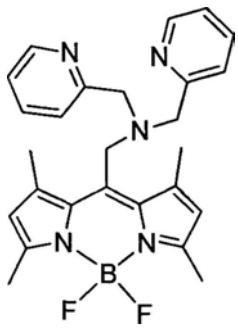

1.66

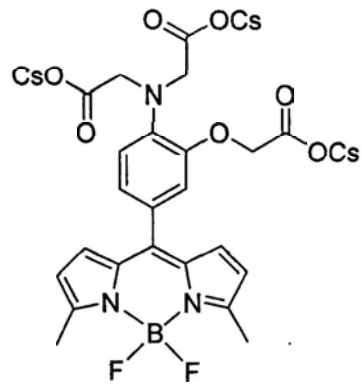

1.67

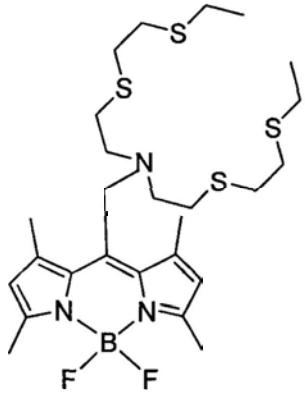

1.68

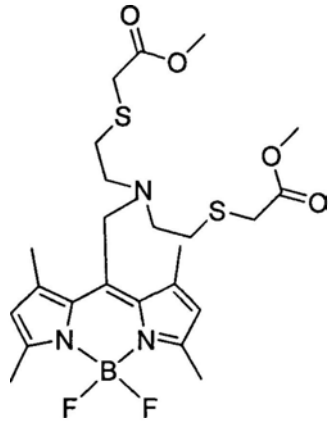

1.69

Compared with BODIPY-based metal sensors, pH-responsive BODIPY dyes remain little studied. Akkaya et al. have reported calix[4]arene substituted BODIPY **1.70**,[90] which exhibits a high fluorescence quantum yield at low pH values. However, as the pH value increases, phenol is deprotonated to generate a phenolic anion, promoting PET from the oxygen to BODIPY core. Therefore, this compound exhibits a lower quantum yield at higher pH value. Boens et al. have synthesized a series of phenol-substituted BODIPYs **1.71a-d**,[91] which show a large fluorescent enhancement upon increasing the acidity of the solution. They can be used as fluorescent pH probes in aqueous solution for the pH range from 7.5 to 9.3, depending on the substituents.

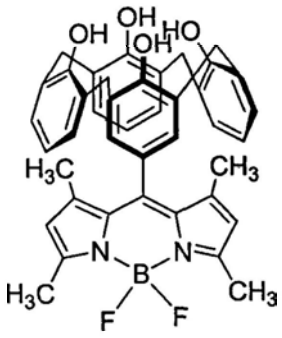

1.70

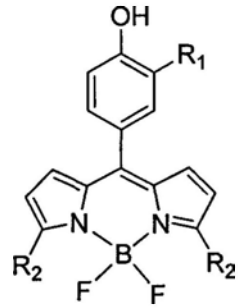

a: $R_1 = H$, $R_2 = H$
b: $R_1 = H$, $R_2 = CH_3$
c: $R_1 = H$, $R_2 = Cl$
d: $R_1 = Cl$, $R_2 = CH_3$

1.71

The PET process described above is usually called reductive PET. It occurs from an ionophore to the excited fluorophore. The other kind of PET from an excited fluorophore to the ionophore, which is called oxidative or reverse PET.[92] Upon metal binding, the ionophore becomes more electron-deficient. Therefore, PET from an excited fluorophore to the ionophore is promoted and the fluorescence of the fluorophore is quenched.

Oxidative PET is well known[93] but rarely utilized in sensing application. Akkaya et al. have described **1.72**.[92] Its fluorescence is quenched by an oxidative PET from the excited BODIPY unit to the bipyridyl unit complexed to metal ions. The closed shell diamagnetic Zn^{2+} ion is one of the most effective quenchers of fluorescence in this system, demonstrating that the quenching is not simply related to the facilitated intersystem crossing. Later, Ziessel et al. have reported another Zn^{2+}-responsive oxidative PET sensor based on terpyridine-functionalized BODIPY.[94] Kim et al. have reported calix[4]arene-functionalized BODIPY **1.73**.[95] Its fluorescence is quenched upon addition of Ca^{2+} ion. The quenching phenomenon

is attributed to the reverse PET from the excited BODIPY unit to calix[4]arene unit complexed to Ca^{2+} ion.

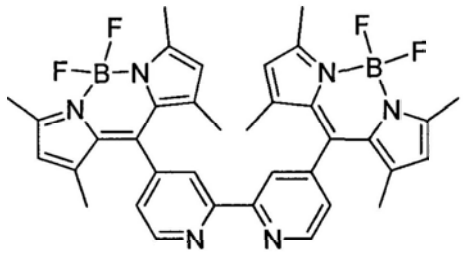

1.72

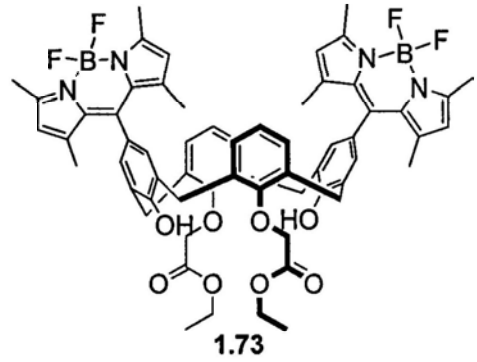

1.73

1.5.3 BODIPY-Based Fluorescent ICT Sensors

When a fluorophore with an electron-donating group (often an amino group) is conjugated to an electron-withdrawing group, intramolecular charge transfer can occur from the donor to the acceptor upon excitation by light. The consequent change in dipole moment results in a Stokes shift that depends on the microenvironment of the fluorophore and polarity probes have been designed on this basis.[96] It can thus be anticipated that metal ions in close interaction with the donor or the acceptor moiety will change the photophysical properties of the fluorophore because the complexed cation affects the efficiency of intramolecular charge transfer.[97]

When a group (like an amino group) playing the role of an electron donor within the fluorophore interacts with a metal ion, the latter reduces the electron-donating character of this group. Owing to the resulting reduction of conjugation, a blue shift of the absorption peak is expected together with a decrease of the molar extinction coefficient. Conversely, a metal ion interacting with the

acceptor group of the fluorophore enhances the electron-withdrawing character of this group. Thus the absorption peak is red-shifted and the molar extinction coefficient is increased (Figure 1.6). The fluorescence spectra are in principle shifted in the same direction as the absorption spectra do. In addition to these shifts, changes in fluorescence quantum yields and lifetimes are often observed. All these photophysical changes are obviously dependent on the charge and the size of the cation, and selectivity of these effects is expected.[77,78]

The photophysical changes upon metal binding can also be described in terms of charge dipole interaction.[98] Let us consider only the case where the dipole moment in the excited state is larger than that in the ground state. Then, when the cation interacts with the donor group, the excited state is more strongly destabilized by the cation than the ground state, and a blue shift of the absorption and emission band is expected. Conversely, when the cation interacts with the acceptor group, the excited state is more stabilized by the cation than the ground state, and this leads to a red shift of the absorption and emission band.[77]

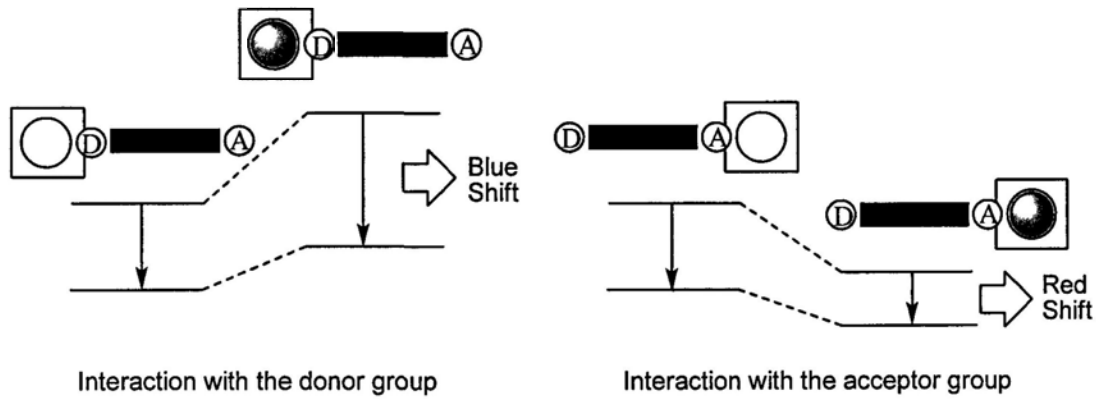

Figure 1.6. Principle of metal ion recognition by fluorescent ICT sensors.

Rurack et al. have devised a highly sensitive fluorescent ICT sensor **1.74**.[99] In acetonitrile, free **1.74** exhibits a dual fluorescence emission at 509 (locally excited, LE emission) and 749 nm (charge transfer, CT emission). After binding with metal ions, the intensity of the CT emission at the longer wavelength decreases and eventually vanishes, while the intensity of LE emission at the shorter wavelength increases with emission enhancement factors of 5900 for Hg^{2+} ion, 2500 for Cu^{2+} ion, and 2200 for Ag^{+} ion. The LE emission enhancement and CT emission quenching are owing to the inhibition of ICT process because the electron-donating ability of the donor is reduced after binding with metal ions. Later, this group has also reported another crown ether substituted BODIPY **1.75**, which exhibits a selective ratiometric signaling for Fe^{3+} ion in buffer solution.[100]

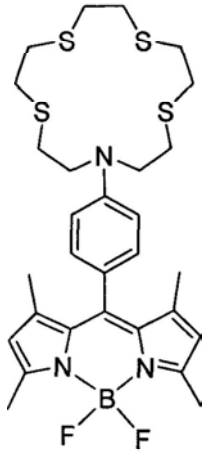

1.74

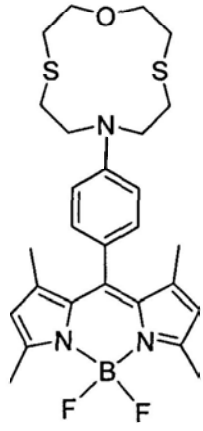

1.75

Boens et al. have synthesized the azacrown ether-functionalized BODIPY **1.76**.[101] This compound exhibits a high selectivity for K^{+} ion over other alkali metal ions. Both the absorption and fluorescence emission maxima shift hypsochromically by 24 and 45 nm, respectively. Later, another similar compound has been reported

which can detect Ca^{2+} ion.[102] Very recently, Chang et al. have presented a new type of ratiometric Cu^{+}-specific fluorescent sensor **1.77**, which can function in living systems. It shows a high selectivity for Cu^{+} ion over other metal ions and a ca. 20-fold fluorescence ratio change with visible excitation and emission profiles.[103]

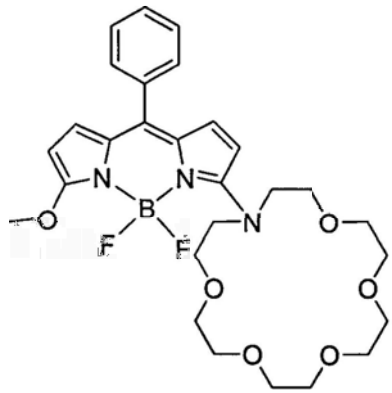

1.76

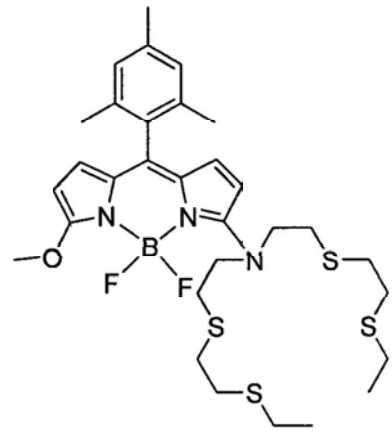

1.77

Rurack et al. have reported an unsymmetrical MS-BODIPY dye **1.78**.[104] Its fluorescence emission appears at a very long wavelength in the near infrared region (731 nm) due to the strong electron-donating ability of the dimethylamino group. After protonation, the electron-donating property of the dimethylamino group is altered and the ICT process is switched off. Then the fluorescence emission wavelength returns to normal range at 563 nm and the fluorescence quantum yield is greatly increased. Another MS-BODIPY dye **1.79** has been reported by Peng et al., which can be used for selective imaging of Cd^{2+} ion in living cells. It can distinguish Cd^{2+} from Zn^{2+} ion by using both normal and ratiometric fluorescence microscopy.[105] Some other examples of MS-BODIPY-based ICT sensors have also been reported in the literature.[106]

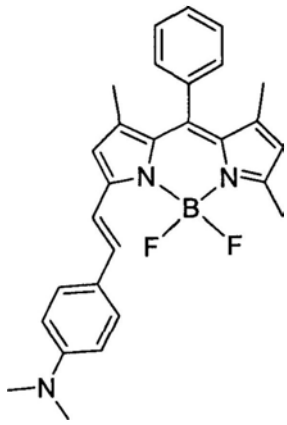

1.78

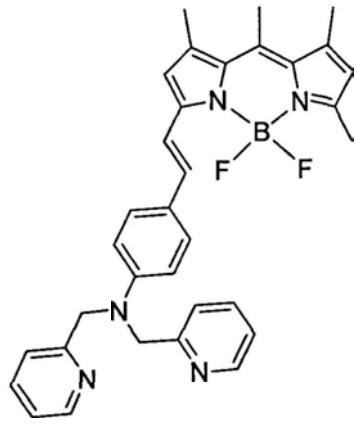

1.79

Akkaya et al. have reported two novel symmetrical DS-BODIPY dyes.[107] Both **1.80** and **1.81** display opposite spectral shifts upon protonation with TFA in organic solvents. This bidirectional switching of the dyes has been shown to be directly related to the donor and acceptor characteristics of the substituents attached to the BODIPY core. The spectral response of these two dyes could be very useful in the design of novel near-infrared (NIR) fluorescent ratiometric pH probes. Later, this group has described a novel unsymmetrical DS-BODIPY dye **1.82**.[108] Its emission band shifts hypsochromically from 730 to 680 nm upon binding with Zn^{2+} ion. This compound represents one of the very few water-soluble fluorescent chemosensors emitting in the NIR region. Very recently a NIR DS-BODIPY-based ratiometric fluorescent chemosensor for Hg^{2+} has also been reported.[109]

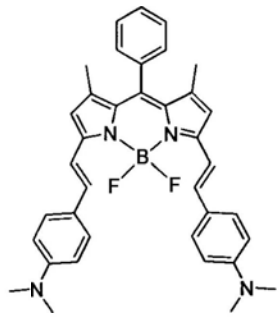

1.80

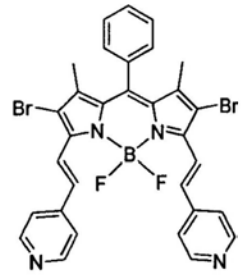

1.81

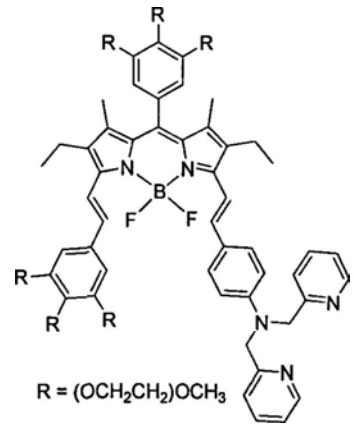

1.82

In summary, PET only induces changes in fluorescence intensity, while ICT can induce changes in both the fluorescence intensity and the emission position. Therefore, ICT-based sensors are generally more attractive.

1.6 Objectives of this Study

Because BODIPYs have many desirable properties which can be modified readily, we aimed to explore their functions and applications, particularly as efficient photosensitizers for photodynamic therapy and selective fluorescent sensors for metal ions. The results are reported in the following Chapters.

1.7 References

1 Treibs, A.; Kreuzer, F. H. *Justus Liebigs Ann. Chem.* **1968**, *718*, 208.

2 (a) Falk, H.; Hofer, O.; Lehner, H. *Monatsh. Chem.* **1974**, *105*, 169. (b) Vosdewael, E.; Pardoen, J. A.; Vankoeveringe, J. A.; Lugtenburg, J. *Recl. Trav. Chim. Pays-bas* **1977**, *96*, 306. (c) Wories, H. J.; Koek, J. H.; Lodder, G.;

Lugtenburg, J.; Fokkens, R.; Driessen, O.; Mohn, G. R. *Recl. Trav. Chim. Pays-bas* **1985**, *104*, 288.

3 (a) Haughland, R. P.; Kang, H. C. *US Patent US4774339* **1988**. (b) Monsma, F. J.; Barton, A. C.; Kang, H. C.; Brassard, D. L.; Haughland, R. P.; Sibley, D. R. *J. Neurochem.* **1989**, *52*, 1641.

4 Registered trademark of Molecular Probes; http://probes.Invitrogen.com.

5 (a) Loudet, A.; Burgess, K. *Chem. Rev.* **2007**, *107*, 4891. (b) Ulrich, G.; Ziessel, R.; Harriman, A. *Angew. Chem. Int. Ed.* **2008**, *47*, 1184.

6 Schmitt, A.; Hinkeldey, B.; Wild, M.; Jung, G. *J. Fluoresc.* **2009**, *19*, 755.

7 Vos, de Wael, E.; Pardoen, J. A.; Van, Koeveringe, J. A.; Lugtenburg, J. *Recl. Trav. Chim. Pays-Bas* **1977**, *96*, 306.

8 Bandichhor, R.; Thivierge, C.; Bhuvanesh, N. S. P.; Burgess, K. *Acta Crystallogr. Sect. E: Struct. Rep. online* **2006**, *E62*, o4310.

9 Goeb, S.; Ziessel, R. *Tetrahedron Lett.* **2008**, *49*, 2569.

10 Qin,W.; Baruah, M.; der Auweraer, M. V.; De Schryver, F. C.; Boens, N. *J. Phys. Chem. A* **2005**, *109*, 7371.

11 Gabe, Y.; Urano, Y.; Kikuchi, K.; Kojima, H.; Nagano, T. *J. Am. Chem. Soc.* **2004**, *126*, 3357.

12 Shah, M.; Thangaraj, K.; Soong, M.-L.; Wolford, L. T.; Boyer, J. H.; Politzer, I. R.; Pavlopoulos, T. G. *Heteroat. Chem.* **1990**, *1*, 389.

13 Boyer, J. H.; Haag, A. M.; Sathyamoorthi, G.; Soong, M. L.; Thangaraj, K.; Pavlopoulos, T. G. *Heteroat. Chem.* **1993**, *4*, 39.

14 Li, Z.; Mintzer, E.; Bittman, R. *J. Org. Chem.* **2006**, *71*, 1718.

15 Wagner, R. W.; Lindsey, J. S. *Pure Appl. Chem.* **1996**, *68*, 1373.

16 Qi, X.; Jun, E. J.; Kim, S.-J.; Hong, J. S. J.; Yoon, Y. J.; Yoon, J. *J. Org. Chem.* **2006**, *71*, 2881.

17 Yamada, K.; Toyota, T.; Takakura, K.; Ishimaru, M.; Sugawara, T. *New J. Chem.* **2001**, *25*, 667.

18 Ueno, T.; Urano, Y.; Kojima, H.; Nagano, T. *J. Am. Chem. Soc.* **2006**, *128*, 10640.

19 Wagner, R. W.; Lindsey, J. S. *Pure Appl. Chem.* **1996**, *68*, 1373.

20 Baruah, M.; Qin, W.; Basaric, N.; De Borggraeve, W. M.; Boens, N. *J. Org. Chem.* **2005**, *70*, 4152.

21 Goud, T. V.; Tutar, A.; Biellmann, J.-F. *Tetrahedron* **2006**, *62*, 5084.

22 Costela, A.; García -Moreno, I.; Pintado-Sierra, M.; Amat-Guerrib, F.; Lirasc, M.; Sastred, R.; Arbeloa, F. L.; Prieto, J. B.; Arbeloa, I. L. *J. Photochem. Photobiol. A: Chem.* **2008**, *1998*, 192.

23 Monsma, F. J.; Barton, A. C.; Kang, H. C.; Brassard, D. L.; Haughland, R. P.; Sibley, D. R. *J. Neurochem.* **1989**, *52*, 1641.

24 (a)Wories, H. J.; Koek, J. H.; Lodder, G.; Lugtenburg, J.; Fokkens, R.; Driessen, O.; Mohn, G. R. *Recl. Trav. Chim. Pays-Bas* **1985**, *104*, 288. (b) Morgan, L. R.; Boyer, J. H. *US Patent 5189029* **1995**.

25 Yogo, T.; Urano, Y.; Ishitsuka, Y.; Maniwa, F.; Nagano, T. *J. Am. Chem. Soc.* **2005**, *127*, 12162.

26 Suzuki, T.; Tanaka, T.; Higashiguchi, I.; Oda, A. *JP Patent 11176572* **1999**.

27 (a) Takuma, K.; Misawa, T.; Sugimoto, K.; Nishimoto, T.; Tsukahara, H.; Tsuda, T.; Imai, G.; Kogure, H. *JP Patent 10273504* **1998**. (b) Imai, G.; Kogure, H.; Ogiso, A.; Misawa, T.; Nishimoto, T.; Tsukahara, H.; Takuma, K. *JP Patent 2000039716* **2000**.

28 (a) Pavlopoulos, T. G.; Boyer, J. H.; Shah, M.; Thangaraj, K.; Soong, M. L. *Appl. Opt.* **1990**, *29*, 3885. (b) Boyer, J. H.; Thangarai, K.; Soong, M. L.; Sathyamoorthi, G.; Ross, T. M.; Haag, A. M. *Proc. Int. Conf. Lasers* **1991**, 739.

29 (a) Rohand, T.; Baruah, M.; Qin, W.; Boens, N.; Dehaen, W. *Chem. Commun.* **2006**, 266. (b) Baruah, M.; Qin, W.; Vallee, R. A. L.; Beljonne, D.; Rohand, T.; Dehaen, W.; Boens, N. *Org. Lett.* **2005**, *7*, 4377. (c) Dilek, O.; Bane, S. L. *Bioorg. Med. Chem. Lett.* **2009**, *19*, 6911.

30 (a) Kalai, T.; Hideg, E.; Jeko, J.; Hideg, K. *Tetrahedron Lett.* **2003**, *44*, 8497. (b) Amat-Guerri, F.; Liras, M.; Carrascoso, M. L.; Sastre, R. *Photochem. Photobiol.* **2003**, *77*, 577. (c) Guo, B.; Peng, X.; Cui, A.; Wu, Y.; Tian, M.; Zhang, L.; Chen, X.; Gao, Y.; *Dyes Pigm.* **2007**, *73*, 206.

31 (a) Saki, N.; Dinc, T.; Akkaya, E. U. *Tetrahedron* **2006**, *62*, 2721. (b) Sathyamoorthi, G.; Wolford, L. T.; Haag, A. M.; Boyer, J. H. *Heteroat. Chem.* **1994**, *5*, 245.

32 Yu, Y.-H.; Descalzo, A. B.; Shen, Z.; Rohr, H.; Liu, Q.; Wang, Y.-W.; Spieles, M.; Li, Y.-Z.; Rurack, K.; You, X.-Z. *Chem. Asian J.* **2006**, *1*, 176.

33 Rurack, K.; Kollmannsberger, M.; Daub, J. *New J. Chem.* **2001**, *25*, 289.

34 *Handbook of Organopalladium Chemistry for Organic Synthesis*; Negishi, E., Eds.; Wiley: New York, **2002**.

35 Wan, C.-W.; Burghart, A.; Chen, J.; BergstrLm, F.; Johansson, L. B.-A.; Wolford, M. F.; Kim, T. G.; Topp, M. R.; Hochstrasser, R. M.; Burgess, K. *Chem. Eur. J.* **2003**, *9*, 4430.

36 Rohand, T.; Qin, W.; Boens, N.; Dehaen, W. *Eur. J. Org. Chem.* **2006**, 4658.

37 Murase, S.; Tominaga, T.; Kohama, A. *Eur Patant 1253151a* **2002**.

38 Ulrich, G.; Goze, C.; Guardigli, M.; Roda, A.; Ziessel, R. *Angew. Chem. Int. Ed.* **2005**, *44*, 3694.

39 Goze, C.; Ulrich, G.; Mallon, L. J.; Allen, B. D.; Harriman, A.; Ziessel, R. *J. Am. Chem. Soc.* **2006**, *128*, 10231.

40 Goze, C.; Ulrich, G.; Ziessel, R. *J. Org. Chem.* **2007**, *72*, 313.

41 Goze, C.; Ulrich, G.; Ziessel, R. *Org. Lett.* **2006**, *8*, 4445.

42 Kee, H. L.; Kirmaier, C.; Yu, L.; Thamyongkit, P.; Youngblood, W. J.; Calder, M. E.; Ramos, L.; Noll, B. C.; Bocian, D. F.; Scheidt, W. R.; Birge, R. R.; Lindsey, J. S.; Holten, D. *J. Phys. Chem. B* **2005**, *109*, 20433.

43 Kim, H.; Burghart, A.; Welch, M. B.; Reibenspies, J.; Burgess, K. *Chem. Commun.* **1999**, 1889.

44 Tahtaoui, C.; Thomas, C.; Rohmer, F.; Klotz, P.; Duportail, G.; Mly, Y.; Bonnet, D.; Hibert, M. *J. Org. Chem.* **2007**, *72*, 269.

45 (a) Daniell, M. D.; Hill, J. S. *Aust. NZ J. Surg.* **1991**, *61*, 340. (b) Ackroyd, R.; Kelty, C.; Brown, N.; Reed, M. *Photochem. Photobiol.* **2001**, *74*, 656.

46 Raab, O. *Zeitung Biol.* **1900**, *39*, 524.

47 von Tappeiner, H.; Jesionek, A. *Muench Med. Wochenschr.* **1903**, *47*, 2042.

48 von Tappeiner, H.; Jesionek, A. *Dtsch. Arch. Klin. Med.* **1904**, *80*, 427.

49 For some recent reviews on PDT, see (a) MacDonald, I. J.; Dougherty, T. J. *J. Porphyrins Phthalocyanines* **2001**, *5*, 105. (b) Oleinick, N. L.; Morris, R. L.; Belichenko, I. *Photochem. Photobiol. Sci.* **2002**, *1*, 1. (c) Vrouenraets, M. B.; Visser, G. W. M.; Snow, G. B.; van Dongen, G. A. M. S. *Anticancer Res.* **2003**, *23*, 505. (d) Dolmans, D. E. J. G. J.; Fukumura, D.; Jain, R. K. *Nature Rev. Cancer* **2003**, *3*, 380. (e) Brown, S. B.; Brown, E. A.; Walker, I. *Lancet Oncol.* **2004**, *5*, 497. (f) Detty, M. R.; Gibson, S. L.; Wagner, S. J. *J. Med. Chem.* **2004**, *47*, 3897. (g) Nyman, E. S.; Hynninen, P. H. *Photochem. Photobiol. B: Biol.* **2004**, *73*, 1. (h) Wilson, B. C.; Patterson, M. S. *Phys. Med. Biol.* **2008**, *53*, R61. (i) Celli, J. P.; Spring, B. Q.; Rizvi, I.; Evans, C.; Samkoe, K. S.; Verma, S.; Pogue, B. W.; Hasan, T. *Chem. Rev.* **2010**, *110*, 2795.

50 Capella, M. A. M.; Capella, L. S. *J. Biomed. Sci.* **2003**, *10*, 361.

51 *Chemical Aspects of Photodynamic Therapy*; Bonnett, R., Eds.; Gordon and Breach: Amsterdam, **2000**.

52 Castano, A. P.; Demidova, T. N.; Hamblin, M. R. *Photodiag. Photodyn. Ther.* **2004**, *1*, 279.

53 (a) Oleinick, N. L.; Morris, R. L.; Belichenko, I. *Photochem. Photobiol. Sci.* **2002**, *1*, 1. (b) Almeida, R. D.; Manadas, B. J.; Carvalho, A. P.; Duarte, C. B. *Biochimi. Biophys. Acta* **2004**, *1704*, 59. (c) Macdonald, I. J.; Dougherty, T. J. *J. Porphyrins phthalocyanines* **2001**, *5*, 105.

54 (a) Luo, Y.; Kessel, D. *Photochem. Photobiol.* **1997**, *66*, 479. (b) Ben-Hur, E.; Oetjen, J.; Horowitz, B. *Photochem. Photobiol.* **1997**, *65*, 456. (c) He, X. Y.; Sikes, R. A.; Thomsen, S.; Chung, L. W. K.; Jacques, S. L. *Photochem. Photobiol.* **1994**, *59*, 468. (d) Noodt, B. B.; Berg, K.; Stokke, T.; Peng, Q.; Nesland, J. M. *Br. J. Cancer* **1996**, *74*, 22. (e) Castano, A. P.; Demidova, T. N.; Hamblin, M. R. *Photodiag. Photodyn. Ther.* **2005**, *2*, 1.

55 Dougherty, T. J.; Gomer, C. J.; Henderson, B. W.; Jori, G.; Kessel, D.; Korbelik, M.; Moan, J.; Peng, Q. *J. Natl. Cancer Inst.* **1998**, *90*, 889.

56 (a) Christensen, T.; Feren, K.; Moan, J.; Pettersen, E. *Br. J. Cancer* **1981**, *44*, 717. (b) Fingar, V. H.; Wieman, T. J.; Wiehle, S. A; Cerrito, P. B. *Cancer Res.* **1992**, *52*, 4914.

57 Korbelik, M.; *J. Clin. Laser Med. Surg.* **1996**, *14*, 329. (b) Musser, D. A; Fiel, R. J. *Photochem. Photobiol.* **1991**, *53*, 119. (c) Korbelik, M.; Dougherty, G. J. *Cancer Res.* **1999**, *59*, 1941.

58 Lipson, R. L.; Blades, E. J.; Olsen, A. M. *J. Natl. Cancer Inst.* **1961**, *26*, 1.

59 (a)Dougherty, T. J.; Potter, W. R.; Weishaupt, K. R. *Prog. Clin. Biol. Res.* **1984**, *170*, 301. (b) Bonnett, R. *Chem. Soc. Rev.* **1995**, *24*, 19. (c) Wöhrle, D.; Hirth, A.; Bogdahn-Rai, T.; Schnurpfeil, G.; Shopova, M. *Russ. Chem. Bull.*

1998, *47*, 807. (d) Dougherty, T. J.; Marcus, S. L. *Eur. J. Cancer* **1992**, *28A*, 1734.

60 Brown, S. B.; Truscott, T. G. *Chem. Br.* **1993**, *29*, 955.

61 Moore, C. M.; Pendse, D.; Emberton, M. *Nat. Clin. Pract. Urol.* **2009**, *6*, 18.

62 Orenstein, A.; Kostenich, G.; Roitman, L.; Shechtman, Y.; Kopolovic, Y.; Ehrenberg, B.; Malik, Z. *Br. J. Cancer* **1996**, *73*, 937.

63 (a) Philips, D. *Prog. Reaction Kinetics* **1997**, *22*, 175. (b) Sibata, C. H.; Colussi, V. C.; Oleinick, N. L.; Kinsella, T. J. *Expert Opin. Pharmacother.* **2001**, *2*, 917.

64 (a) Lunardi, C. N. Tedesco, A. C. *Curr. Org. Chem.* **2005**, *9*, 813. (b) Tedesco, A. C.; Rotta, J. C.; Lunardi, C. N. *Curr. Org. Chem.* **2003**, *7*, 187. (c) Lang, K.; Mosinger, J.; Wagnerová, D. M. *Coord. Chem. Rev.* **2004**, *248*, 321.

65 (a) Kessel, D.; Thompson, P.; Saatio, K.; Nantwi, K. D. *Photochem. Photobiol.* **1987**, *45*, 787. (b) Wilkinson, F.; Helman, W. P.; Ross, A. B.; *J. Phys. Chem. Ref. Data* **1993**, *22*, 113.

66 Stilts, C. E.; Nelen, M. I.; Hilmey, D. G.; Davies, S. R.; Gollnick, S. O.; Oseroff, A. R.; Gibson, S. L.; Hilf, R.; Detty, M. R. *J. Med. Chem.* **2000**, *43*, 2403.

67 Nelson, J. S.; Roberts, W. G.; Berns, M. W. *Cancer Res.* **1987**, *47*, 4681. (b) Roberts, W. G.; Shiau, F. Y.; Nelson, J. S.; Smith, K. M.; Berns, M. W. *J. Natl. Cancer. Inst.* **1988**, *80*, 330. (c) Leach, M. W.; Higgins, R. J.; Autry, S. A.; Boggan, J. E.; Lee, S. J.; Smith, K. M. *Photochem. Photobiol.* **1993**, *58*, 653.

68 Pandey, R. K.; Potter, W. R.; Meunier, I.; Sumlin, A. B.; Smith, K. M. *Photochem. Photobiol.* **1995**, *62*, 764.

69 Morgan, A. R.; Rampersaud, A.; Keck, R. W.; Selman, S. H. *Photochem. Photobiol.* **1987**, *46*, 441.

70 Ma, L.; Moan, J.; Berg, K. *Int. J. Cancer* **1994**, *57*, 883.

71 Serra, A.; Pineiro, M.; Pereira, N.; Gonsalves, A. R.; Laranjo, M.; Abrantes, M.; Botelho, F. *Oncol. Rev.* **2008**, *2*, 235.

72 Nyman, E. S.; Hynninen, P. H. *J. Photochem. Photobiol. B: Biol.* **2004**, *73*, 1.

73 Farooq, F. T.; Berlin, J.; Baron, E.; Faulx, A. L.; Marks, J. M.; Chak, A. *Castrointest. Endosc.* **2007**, *65*, AB155.

74 *Modern Molecular Photochemistry*; Turro, N. J., Eds.; University science Books: Sausalito, CA, **1991**.

75 Atilgan, S.; Ekmekci, Z.; Dogan, A. L.; Guc, D.; Akkaya, E. U. *Chem. Commun.* **2006**, 4398.

76 Lim, S. H.; Thivierge, C.; Nowak-Sliwinska, P.; Han, J.; van den Bergh, H.; Wagnières, G.; Burgess, K.; Lee, H. B. *J. Med. Chem.* **2010**, *53*, 2865.

77 Valeur, B.; Leray, I. *Coord. Chem. Rev.* **2000**, *205*, 3.

78 Kim, J. S.; Quang, D. T. *Chem. Rev.* **2007**, *107*, 3780.

79 (a) Fabbrizzi, L.; Poggi, A. *Chem. Soc. Rev.* **1995**, *24*, 197. (b) Dixon, A. J.; Benham, G. S. *Int. Lab.* **1988**, *4*, 38. (c) Tan, W.; Shi, Z. Y.; Kopelman, R. *Anal. Chem.* **1992**, *64*, 2985. (d) Sharp, S. L.; Warmack, R. J.; Goudonnet, J. P.; Lee, I.; Ferrell, T. L. *Acc. Chem. Res.* **1993**, *26*, 377.

80 *Molecular fluorescence*; Valeur, B., Eds.; Wiley-VCH: Weinheim, Germany, **2001**.

81 (a) Walkup. G. K.; Burdette, S. C.; Lippard, S. J.; Tsien, R. Y. *J. Am. Chem. Soc.* **2000**, *122*, 5644. (b) Komatsu, K.; Kikuchi, K.; Kojima, H.; Urano, Y; Nagano, T. *J. Am. Chem. Soc.* **2005**, *127*, 10197. (c) Tomat, E.; Nolan, E. M.; Jaworski, J.; Lippard, S. J. *J. Am. Chem. Soc.* **2008**, *130*, 15776.

82 (a) Gunnlaugsson, T.; Lee, T. C.; Parkesh, R. *Org. Lett.* **2003**, *5*, 4065. (b) Gunnlaugsson, T.; Leeb, T. C.; Parkesha, R. *Tetrahedron* **2004**, *60*, 11239. (c) Que, E. L.; Chang, C. J. *J. Am. Chem. Soc.* **2006**, *128*, 15942.

83 (a) Yang, L.; McRae, R.; Henary, M. M.; Patel, R.; Lai, B.; Vogt, S.; Fahrni, C. J. *PNAS* **2005**, *102*, 11179. (b) Yooh, S.; Miller, E. W.; He, Q.; Do, P. H.; Chang, C. J. *Angew. Chem. Int. Ed.* **2007**, *46*, 6658.

84 (a) Hirano, T.; Kikuchi, K.; Urano, Y; Higuchi, T.; Nagano, T. *J. Am. Chem. Soc.* **2002**, *122*, 12399. (b) Hirano, T.; Kikuchi, K.; Urano, Y; Nagano, T. *J. Am. Chem. Soc.* **2002**, *124*, 6555. (c) Carol, P.; Sreejith, S.; Ajayaghosh, A. *Chem. Asia J.* **2007**, *2*, 338. (d) Zhang, X.; Hays, D.; Smith, S. J.; Friedle, S.; Lippard, S. J. *J. Am. Chem. Soc.* **2008**, *130*, 15788.

85 (a) Xiang, Y.; Tong, A.-J. *Org. Lett.* **2006**, *8*, 1549. (b) Ko, S.-K.; Yang, Y.-K.; Tae, J.; Shin, I. *J. Am. Chem. Soc.* **2006**, *128*, 14150. (c) Yang, Y.-K.; Ko, S.-K.; Shin, I.; Tae, J. *Nat. Protoc.* **2007**, *2*, 1740. (d) Zhang X.; Shiraishi, Y.; Hirai, T. *Org. Lett.* **2007**, *9*, 5039. (e)Jian, J. D.; Jiang, L. F.; Ping, P. S.; Jing, Y. W.; Hong, L. L.; Shi, G. S. *Org. Lett.* **2010**, *12*, 476.

86 Wu, K.; Peng, X.; Guo, B.; Fan, J.; Zhang, Z.; Wang, J.; Cui, A.; Gao, Y. *Org. Biomol. Chem.* **2005**, *3*, 1387.

87 Basarić, N.; Baruah, M.; Qin, W.; Metten, B.; Smet, M.; Dehaen, W.; Boens, N. *Org. Biomol. Chem.* **2005**, *3*, 2755.

88 (a) Zeng, L.; Miller, E. W.; Pralle, A.; Isacoff, E. Y.; Chang, C. J. *J. Am. Chem. Soc.* **2006**, *128*, 10. (b) Miller, E. W.; Zeng, L.; Domaille, D. W.; Chang, C. J. *Nat. Protocols* **2006**, *1*, 824.

89 Dodani, S. C.; He, Q.; Chang, C. J. *J. Am. Chem. Soc.* **2009**, *131*, 18020.

90 Baki, C. N.; Akkaya, E. U. *J. Org. Chem.* **2001**, *66*, 1512.

91 Baruah, M.; Qin, W.; Basarić, N.; De Borggraeve, W. M.; Boens, N. *J. Org. Chem.* **2005**, *70*, 4152.

92 Turfan, B.; Akkaya, E. U. *Org. Lett.* **2002**, *4*, 2857.

93 *Molecular Fluorescence*; Valeur, B., Eds.; Wiley-VCH: Weinheim, Germany, **2002**.

94 Goze, C.; Ulrich, G.; Charbonnière, L.; Cesario, M.; Prangé, T.; Ziessel, R. *Chem. Eur. J.* **2003**, *9*, 3748.

95 Kim, H. J.; Kim, J. S. *Tetrahedron Lett.* **2006**, *47*, 7051.

96 *Molecular Luminescence Spectroscopy*; Valeur, B., Schulman, S. G., Eds.; Wiley: New York, **1993**.

97 *Fluorescent Chemosensors for Ion and Molecule Recognition*; Valeur, B., Bourson, J., Pouget, J., Czarnik, A. W., Eds.; ACS Symposium Series 538, American Chemical Society, Washington, DC, **1993**.

98 Löhr, H. G.; Vögtle, F. *Acc. Chem. Res.* **1985**, *18*, 65.

99 Rurack, K.; Kollmannsberger, M.; Resch-Genger, U.; Daub, J. *J. Am. Chem. Soc.* **2000**, *122*, 968.

100 Bricks, J.; Kovalchuk, A.; Trieflinger, C.; Nofz, M.; Büschel, M.; Tolmachev, A. I.; Daub, J.; Rurack, K. *J. Am. Chem. Soc.* **2005**, *127*, 13522.

101 Baruah, M.; Qin, W.; Vallée, R. A. L.; Beljonne, D.; Rohand, T.; Dehaen, W.; Boens, N. *Org. Lett.* **2005**, *7*, 4377.

102 Móczár, I.; Huszthy, P.; Maidics, Z.; Kádár, M.; Tóth, K. *Tetrahedron* **2009**, *65*, 8250.

103 Domaille, D. W.; Zeng, L.; Chang, C. J. *J. Am. Chem. Soc.* **2010**, *132*, 1194.

104 Rurack, K.; Kollmannsberger, M.; Daub, J. *Angew. Chem. Int. Ed.* **2001**, *40*, 385.

105 Peng, X.; Du, J.; Fan, J.; Wang, J.; Wu, Y.; Zhao, J.; Sun, S.; Xu, T. J. *J. Am. Chem. Soc.* **2007**, *129*, 1500.

106 (a) Yuan, M.; Li, Y.; Li, J.; Li, C.; Liu, X.; Lv, J.; Xu, J.; Liu, H.; Wang, S.; Zhu, D. *Org. Lett.* **2007**, *9*, 2313. (b) Cheng, T.; Xu, Y.; Zhang, S.; Zhu, W.; Qian, X.; Duan L. *J. Am. Chem. Soc.* **2008**, *130*, 16160.

107 Deniz, E.; Isbasar, G. C.; Bozdemir, Ö. A.; Yildirim, L. T.; Siemiarczuk, A.; Akkaya, E. U. *Org. Lett.* **2008**, *10*, 3401.

108 Atilgan, S.; Ozdemir, T.; Akkaya, E. U. *Org. Lett.* **2008**, *10*, 4065.

109 Atilgan, S.; Kutuk, I.; Ozdemir, T. *Tetrahedron Lett.* **2010**, *51*, 892.

Chapter 2

Synthesis, Characterization, and Photodynamic Activities of Novel Distyryl BODIPYs

2.1 Introduction

Photodynamic therapy (PDT) is a noninvasive technique for the treatment of malignant tumors and age-related macular degeneration. It involves the combined use of harmless visible light and a nontoxic photosensitizing drug.[1] The photosensitizer of minimal dark toxicity is first introduced into the body, which accumulates preferentially in the tumor. The tumor is then selectively irradiated with low-energy light of wavelength that can pass through the body's therapeutic window (650-900 nm), resulting in excitation of the photosensitizer to generate reactive oxygen species (ROS) and thus irreversibly damage the tumor cells. Therefore, development of efficient photosensitizers for PDT is of much current interest.[2]

Haematoporphyrin derivatives (HpD) are the first generation photosensitizers.[3] Subsequently, other porphyrin derivatives, chlorins, bacteriochlorins, and phathlocyanines have been studied as the second generation PDT agents.[4] Recently, distyryl BODIPYs substituted by heavy atoms in the pyrrole rings have been reported to be another promising class of photosensitizers owing to their strong absorption in the 650-680 nm region and high efficiency to generate singlet oxygen.[5] BODIPY-based photosensitizers, however, remain very little studied. To our

knowledge, only a few examples have been reported so far.[5,6] Therefore, we have explored a novel series of distyryl BODIPYs for the use of PDT. Their synthesis, spectroscopic and photophysical properties, as well as their in vitro photodynamic activities are reported in this Chapter.

2.2 Results and Discussion

2.2.1 Molecular Design and Chemical Synthesis

BODIPY derivatives are promising fluorescent dyes for various applications. They show appealing properties including high extinction coefficients, high fluorescence quantum yields, relatively resistant to photo-bleaching, and ease of chemical modifications. The BODIPY unit originally has an absorption peak near 500 nm. However, by Knoevenagel condensation reaction of the methyl groups, their absorptions can be turned to the red visible region.[7] As part of our continuing efforts in the development of photosensitizers for PDT, we have synthesized a series of iodinated distyryl BODIPYs containing different number of triethylene glycol or polyethylene glycol chains. Polyethylene glycols are well-known pharmaceutical vehicles, which can prolong circulating half-life, minimize nonspecific uptake, and enable specific tumor-targeting through the enhanced permeability and retention (EPR) effect.[8] It is hoped that these biocompatible ethylene glycol units can enhance the water solubility and cellular uptakes of the distyryl BODIPYs. In addition, two iodo groups were introduced at the 2- and 6-positions of the BODIPY core to

promote the intersystem crossing and hence the singlet oxygen formation through the heavy atom effect.

Scheme 2.1 shows the synthetic route used to prepare the target compounds **2.11a-2.11d**. Treatment of 4-hydroxybenzaldehyde (**2.1**) with tosylated triethylene glycol monomethyl ether **2.2** and K_2CO_3 in N,N-dimethylformamide (DMF) gave triethylene glycol monomethyl substituted benzaldehyde **2.3**. It reacted with excess 2,4-dimethylpyrrole, followed by sequential oxidation by 2,3-dichloro-5,6-dicyano-1,4-benzoquinone (DDQ) and complexation with boron trifluoride to afford triethylene glycol monomethyl substituted BODIPY **2.5**. The 2 and 6 positions of the BODIPY skeleton were iodinated using a mixture of iodic acid and iodine to give the diiodo BODIPY **2.6**. Nucleophilic substitution reaction of tosylate **2.2** or **2.7** with 3,4-dihydroxybenzaldehyde (**2.8**) to afford the disubstituted benzaldehyde **2.9c** or **2.9d**. The tosylate **2.7** was prepared from the commercially available polyethylene glycol methyl ether having an average molecular weight of 550. Afterwards, treatment of diiodo BODIPY **2.6** with benzaldehydes **2.3**, **2.9c**, **2.9d**, and **2.10** in the presence of piperidine led to double Knoevenagel condensation giving the corresponding distyryl BODIPYs **2.11a-2.11d**. All of these compounds were soluble in common organic solvents and possessed a high stability, which facilitated the purification by silica gel column chromatography and size exclusion chromatography.

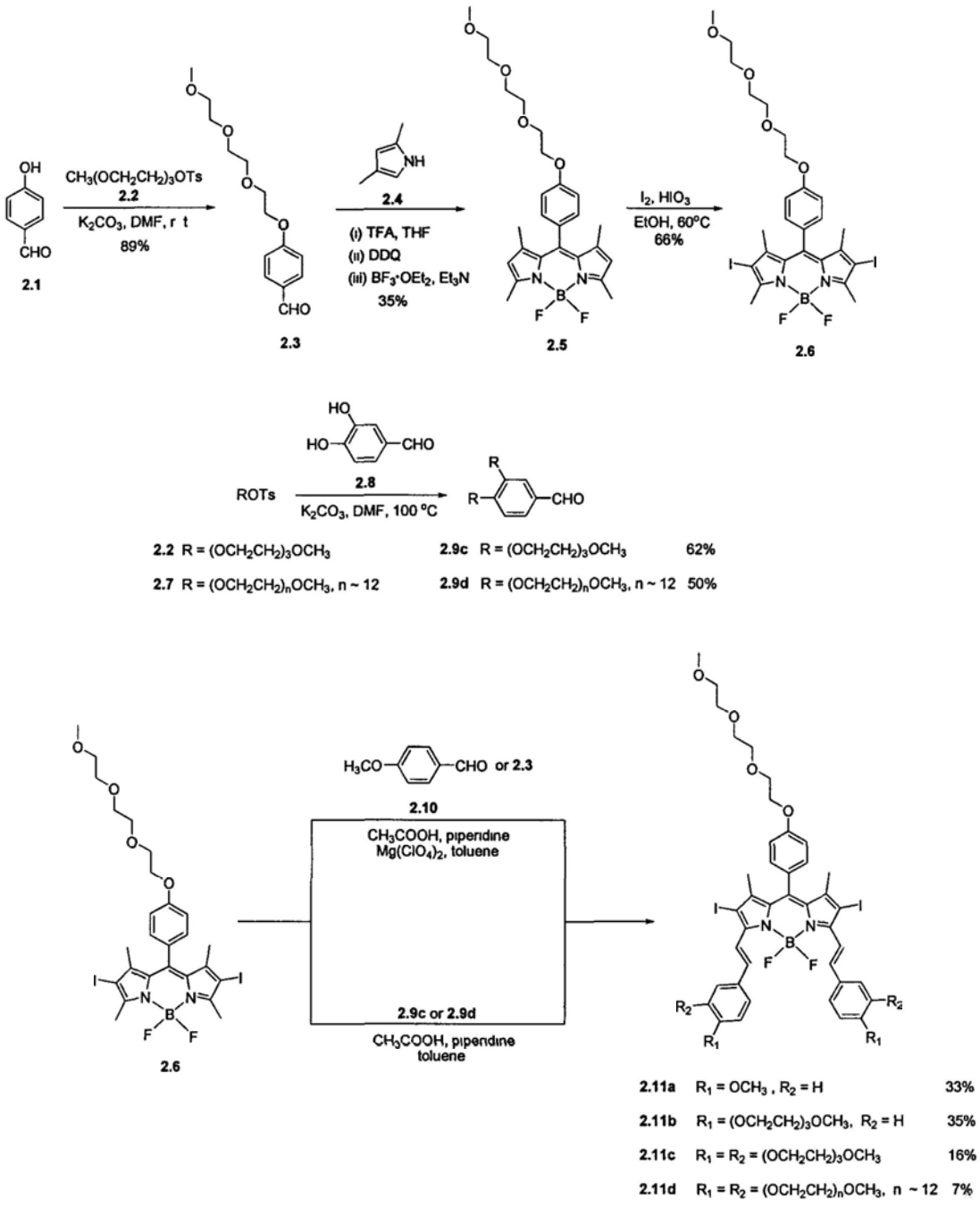

Scheme 2.1. Synthesis of distyryl BODIPYs **2.11a-2.11d**.

2.2.2 Spectroscopic Characterization and Photophysical Properties

All of the new compounds were fully characterized with various spectroscopic methods and elemental analysis. The data are given in the Experimental Section. Figure 2.1 shows the ^{1}H NMR spectrum of compound **2.11a** in $CDCl_3$. The

downfield signals from 6.9 to 8.2 ppm are due to the aryl and vinyl protons. The upfield signals from 3.3 to 4.3 ppm are attributed to the triethylene glycol chain and methoxy protons. The singlet around 1.5 ppm is due to the methyl protons at the pyrrole rings. For the other three compounds **2.11b-2.11d**, the assignment of the ^{1}H NMR signals is similar to that of **2.11a**. As expected, the number and length of the ethylene glycol chains did not exert a significant influence on the chemical shifts of these signals.

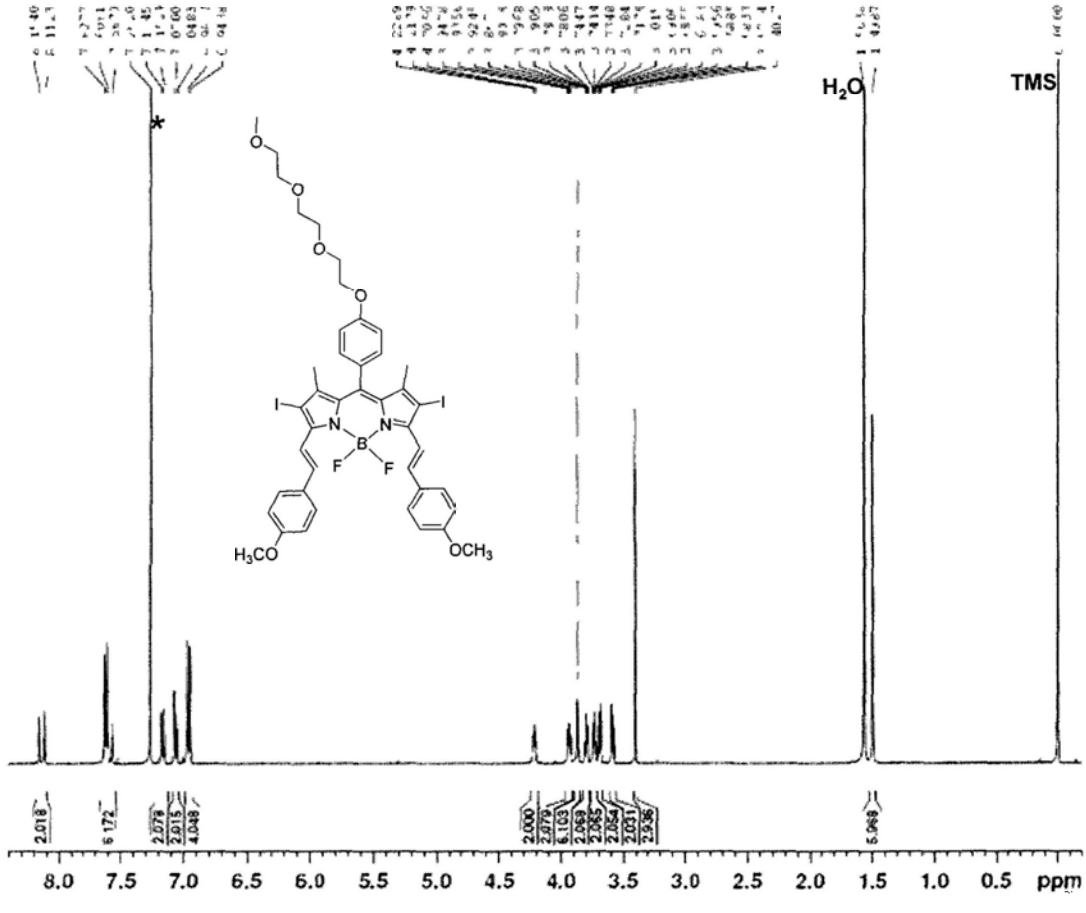

Figure 2.1. ^{1}H NMR spectrum of **2.11a** in $CDCl_3$; * indicates residual solvent signal.

The $^{13}C\{^{1}H\}$ NMR data of these distyryl BODIPYs were also in accord with the structures though some of the aryl carbon signals and the chain CH_2 signals were overlapped.

The ESI mass spectra of all the distyryl BODIPYs were also recorded. The molecular ion $[M + Na]^+$ isotopic cluster could be detected for all the cases. The isotopic distribution was in good agreement with the corresponding simulated pattern. The identity of these species was also confirmed by accurate mass measurements. In the ESI mass spectrum of **2.11d**, two major envelopes for the $[M]^{2+}$ and sodiated $[M + Na]^+$ species were observed (Figure 2.2). Within these envelopes, the clusters are separated by 22 or 44 mass units, respectively, corresponding to the molecular mass of the repeating unit of polyethylene glycol.

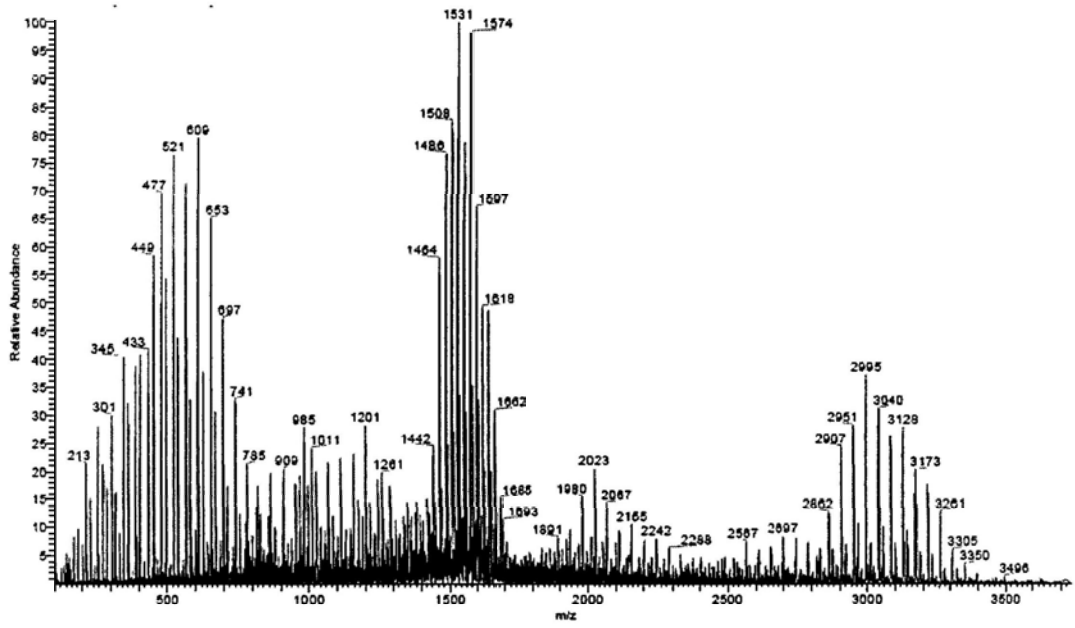

Figure 2.2. ESI mass spectrum of **2.11d**.

The electronic absorption and fluorescence spectra of distyryl BODIPYs **2.11a-2.11d** were recorded in DMF and the data are summarized in Table 2.1. It was

observed that the Q-band absorption became slightly weakened and red-shifted upon introduction of the polyethylene glycol chains (Figure 2.3(a)). The absorption positions of the Soret bands were also significantly changed for compounds **2.11c** and **2.11d**. In order to investigate the aggregation behavior of these compounds, their absorption spectra were recorded at different concentrations. Taking the spectrum of **2.11c** as an example, it showed two broad Soret bands peaking at 331 and 387 nm, a vibronic band at 460 nm, and an intense Q band, which strictly follows the Lambert Beer's law (Figure 2.4). Similar results were obtained for the other three compounds. The results suggested that all these compounds are not significantly aggregated in DMF.

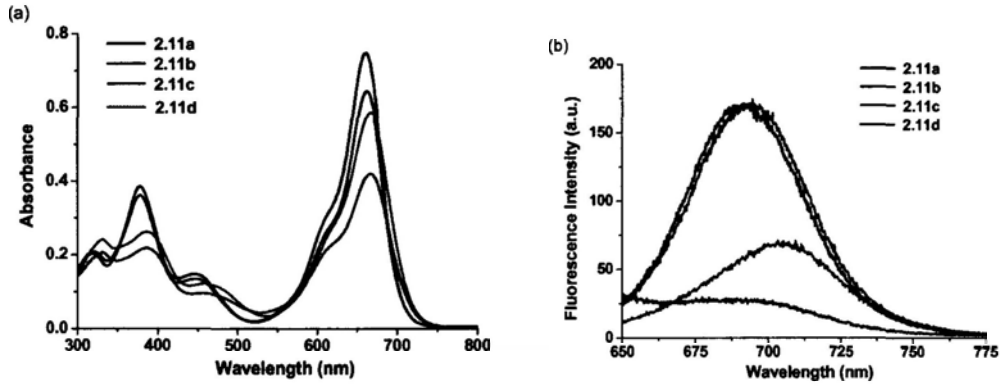

Figure 2.3. Electronic absorption (a) and fluorescence emission spectra (excited at 610 nm) (b) of **2.11a-2.11d** (8 μM) in DMF.

Table 2.1. Electronic absorption and photophysical data for compounds **2.11a-2.11d** in DMF.

Compound	λ_{max} (nm) (log ε)	λ_{em} (nm)[a]	Φ_F[b]	Φ_Δ[c]
2.11a	319 (4.40), 378 (4.66), 447 (4.24), 661 (4.96)	689	0.19	0.42
2.11b	320 (4.40), 379 (4.64), 447 (4.21), 662 (4.90)	690	0.18	0.45
2.11c	331 (4.48), 387 (4.51), 460 (4.18), 667 (4.85)	703	0.09	0.43
2.11d	331 (4.38), 386 (4.41), 457 (4.05), 667 (4.70)	701	0.04	0.37

[a] Excited at 610 nm. [b] Relative to ZnPc (Φ_F = 0.28 in DMF). [c] Relative to ZnPc (Φ_Δ = 0.56 in DMF).

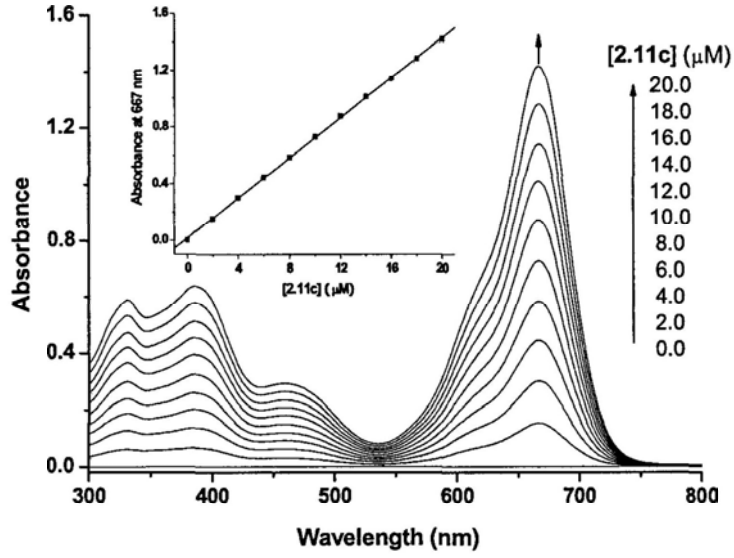

Figure 2.4. Electronic absorption spectra of **2.11c** at various concentrations in DMF. The inset plots the Q-band absorbance versus the concentration of **2.11c**.

The fluorescence emission spectra of these compounds were also recorded in DMF. Upon excitation at 610 nm, compounds **2.11a-2.11d** showed a fluorescence emission at 689-703 nm with a fluorescence quantum yield (Φ_F) of 0.04-0.19 relative to unsubstituted zinc(II) phthalocyanine (ZnPc) (Φ_F = 0.28)[9] (Figure 2.3(b) and

Table 2.1). The relatively weak fluorescence emission may be attributed to the two iodo moieties, which promote the intersystem crossing and triplet state population. It was also observed that pegelation led to weakening and red shift of the fluorescence emission. It is in accord with the general observation that the lower the energy of the Q band, the smaller the Φ_F value.[10] It has been suggested that the excited state becomes unstable as the HOMO-LUMO gap decreases, probably due to the ease of electron transfer.

The singlet oxygen quantum yields (Φ_Δ) of these compounds were also determined using 1,3-diphenylisobenzofuran (DPBF) as the scavenger. The concentration of the quencher was monitored spectroscopically at 415 nm along with time, from which the values of Φ_Δ could be determined by the method described previously.[11] These data are also summarized in Table 2.1. Figure 2.5 compares the rates of decay of DPBF using these compounds and ZnPc as the photosensitizers. It can be seen that all these compounds can induce photo-bleaching of DPBF and their efficiencies are comparable except **2.11d**. The lowest singlet oxygen generation efficiency of **2.11d** is probably due to the stronger dipole-dipole interaction of the longer polyethylene glycol chains, which enhances the aggregation of the dye.

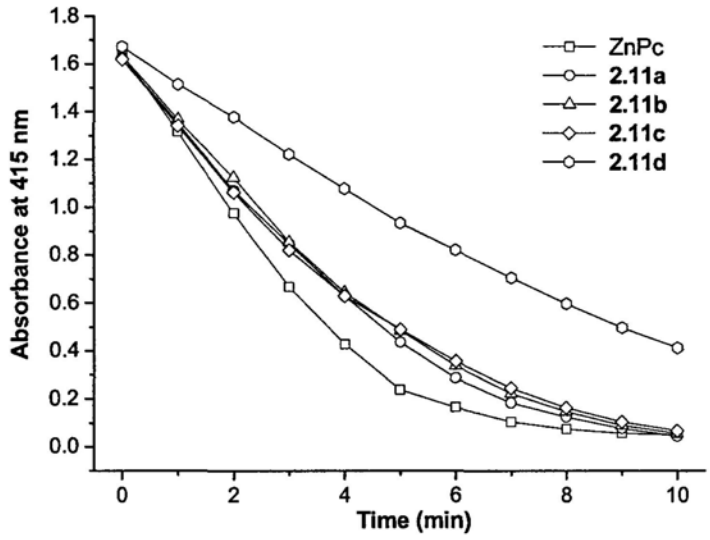

Figure 2.5. Comparison of the rates of decay of DPBF (initial concentration = 75 μM) in DMF, as monitored spectroscopically at 415 nm, using **2.11a-2.11d** as the photosensitisers (4 μM) and ZnPc (4 μM) as the reference.

2.2.3 In Vitro Photodynamic Activities

The in vitro photodynamic activities of **2.11a-2.11d** in Tween 80 emulsions were investigated against HT29 human colorectal carcinoma cells. Figure 2.6 shows the dose dependent survival curves for **2.11a-2.11d.** It can be seen that all of the compounds are essentially noncytotoxic in the absence of light. However, they become cytotoxic upon illumination with red light ($\lambda > 610$ nm), except compound **2.11d**, which is essentially noncytotoxic. Compound **2.11c**, which contains five triethylene glycol chains, is significantly more potent with an IC_{50} value of 7 nM. The IC_{50} and IC_{90} values, defined as the dye concentrations required to kill 50% and 90% of the cells, respectively, are summarized in Table 2.2. The photoactivity follows the order **2.11c** > **2.11b** > **2.11a** > **2.11d**. It was found that the potency

increases as the number of triethylene glycol chains increases. However, compound **2.11d**, bearing four polyethylene glycol moieties, only shows little photocytotoxicity on the cells up to 8 μM.

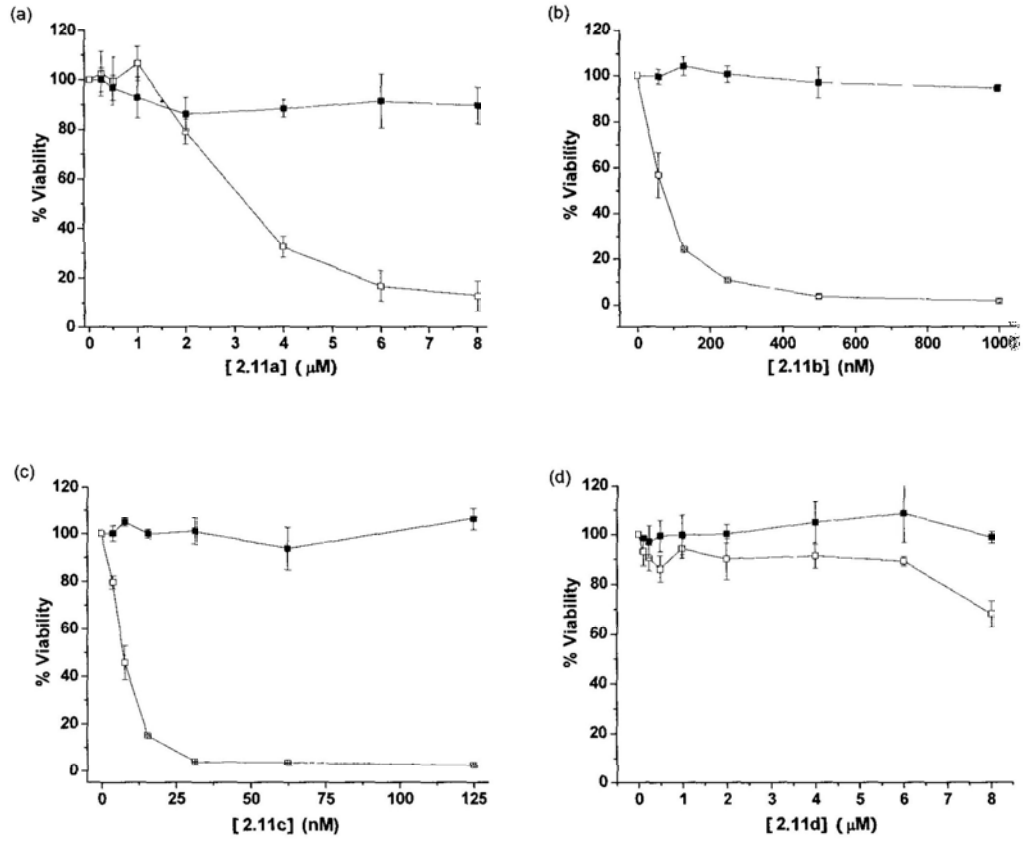

Figure 2.6. Effects of **2.11a-2.11d** on HT29 cells in the absence (closed symbol) and presence (open symbol) of light ($\lambda > 610$ nm, 40 mW cm^{-2}, 48 J cm^{-2}). Data are expressed as mean values ± S.E.M. of three independent experiments, each performed in quadruplicate.

Table 2.2. IC_{50} and IC_{90} values of compounds **2.11a-2.11d** against HT29 cells.[a]

Compound	IC_{50}	IC_{90}
2.11a	3.3 μM	> 8 μM
2.11b	78 nM	270 nM
2.11c	7 nM	22 nM
2.11d	> 8 μM	> 8 μM

[a] Defined as the dye concentrations required to kill 50% and 90% of the cells, respectively, in the presence of light (λ > 610 nm, 40 mW cm^{-2}, 48 J cm^{-2}).

To account for their different photodynamic activities, their aggregation behavior in DMEM culture medium was examined by absorption and fluorescence spectroscopic methods. Figure 2.7(a) shows the UV-Vis spectra of compounds **2.11a-2.11d** in DMEM medium. It can be seen that the Q bands of compounds **2.11a-2.11c** remain very sharp and intense, while that of **2.11d** is significantly broadened and split into two weaker peaks. These observations indicate that compounds **2.11a-2.11c** are essentially non-aggregated in the culture medium. However, compound **2.11d**, having four polymeric ethylene glycol moieties, is significantly more aggregated in the medium. These conclusions were also supported by their different fluorescence spectra. As shown in Figure 2.7(b), an intense fluorescence emission can be observed for compounds **2.11a** and **2.11b**, while compound **2.11c** only shows moderate fluorescence emission and compound **2.11d** gives the least fluorescence emission. As molecular aggregation provides an efficient nonradiative relaxation pathway for the singlet excited state of the dyes, the

fluorescence intensity as well as efficiency at generating singlet oxygen will be reduced as the aggregation tendency increases.[12] Thus, these results explain why analogue **2.11d** shows the lowest photocytotoxicity among this series of compounds.

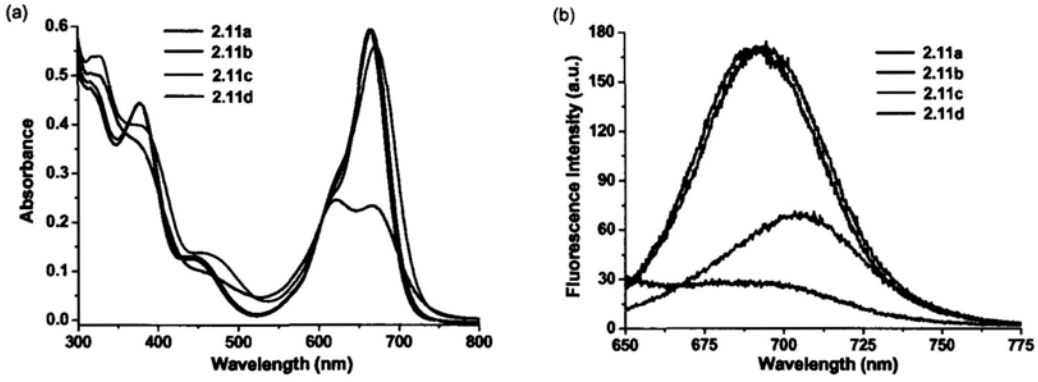

Figure 2.7. Electronic absorption (a) and fluorescence emission spectra (excited at 610 nm) (b) of **2.11a-2.11d** (8 μM), formulated with 0.05% Tween 80 in the DMEM culture medium.

To further explain the photocytotoxicity results, fluorescence microscopic studies were also carried out to investigate the cellular uptake of these compounds. HT29 cells were incubated respectively with all these compounds (1 μM) for 2 h. Upon excitation at 633 nm, the bright field and fluorescence images of the cells were then captured (Figure 2.8(a)), and the intracellular fluorescence intensities were also determined (Figure 2.8(b)). It was found that compound **2.11c** showed a much stronger intracellular fluorescence throughout the cytoplasm. The apparent intensity, which reflects the extent of cellular uptake and aggregation of the dyes, follows the order: **2.11c** > **2.11b** > **2.11a** and **2.11d**, which is in good agreement with the trend in photocytotoxicity.

(a)

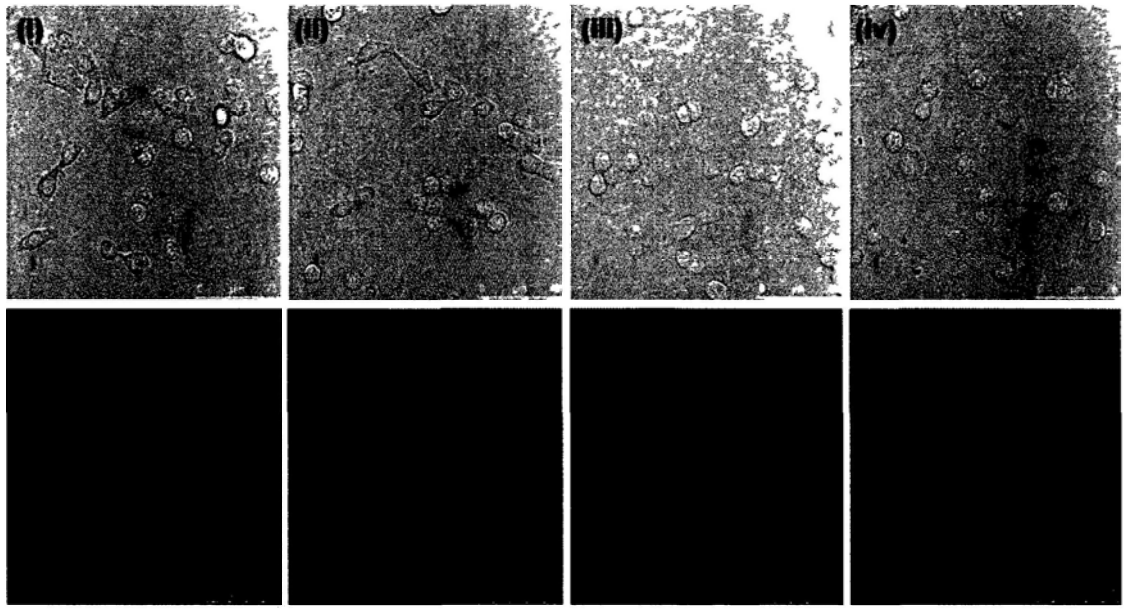

(b)

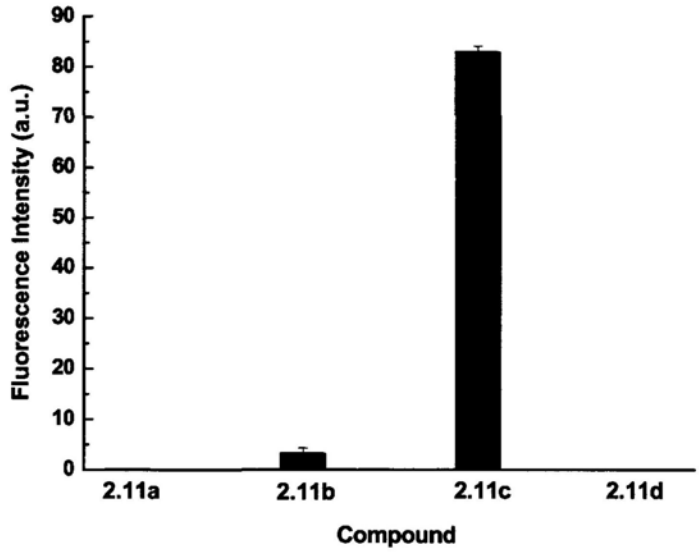

Figure 2.8. (a) Visualization of bright field (upper row) and intracellular fluorescence (lower row) images of HT29 cells after incubation with (i) **2.11a**, (ii) **2.11b**, (iii) **2.11c**, and (iv) **2.11d** (1 μM) for 2 h. (b) Comparison of the intracellular fluorescence intensity of compounds **2.11a-2.11d**. Data are expressed as the mean ± standard deviation (number of cells = 50).

Owing to the highest potency of **2.11c**, its subcellular localization was also investigated. The cells were stained respectively with LysoTracker DND 26, MitoTracker Green FM, and ER-Tracker Green, which are specific fluorescence dyes for lysosomes, mitochondria, and endoplasmic reticulum, respectively. As shown in Figure 2.9, the fluorescence caused by the ER-Tracker Green (excited at 488 nm, monitored at 510-560 nm) is well superimposed with the fluorescence caused by **2.11c** (excited at 633 nm, monitored at 650-720 nm), indicating that **2.11c** has a strong and selective affinity to the endoplasmic reticulum. The endoplasmic reticulum is known to play an important role in the biosynthesis, transport of proteins and lipids, and the release of intracellular calcium.[13] It has been reported that accumulation of photosensitizers in the endoplasmic reticulum results in more efficient triggering of cell death and higher cytotoxicity upon illumination. By contrast, the fluorescence images of **2.11c** and the LysoTracker (or MitoTracker) cannot be overlapped (Figure 2.10), which indicates that **2.11c** is not localized in the lysosomes and the mitochondria.

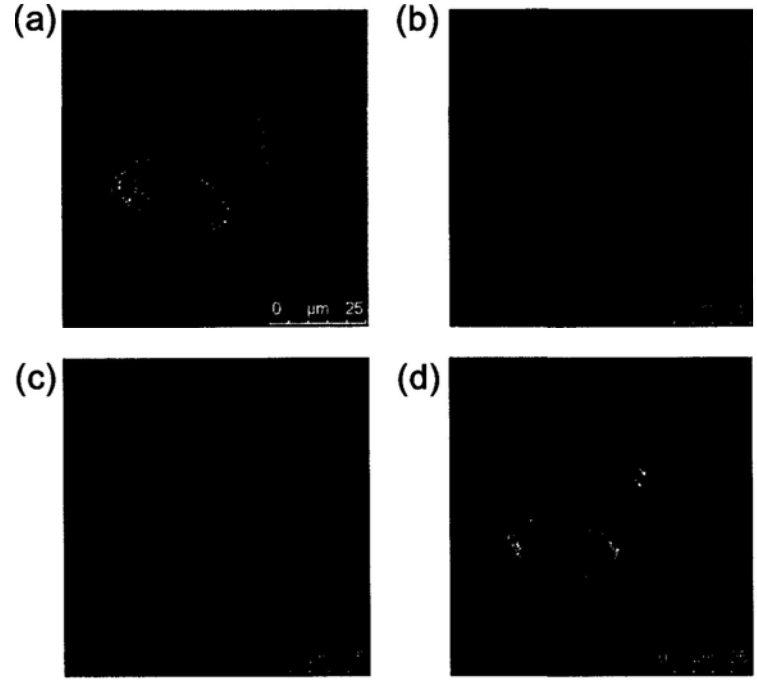

Figure 2.9. Visualization of intracellular fluorescence of HT29 cells using filter sets specific for (b) ER-Tracker (in green) and (c) compound **2.11c** (in red). The corresponding superimposed image is given in (d), while the bright field image is shown in (a).

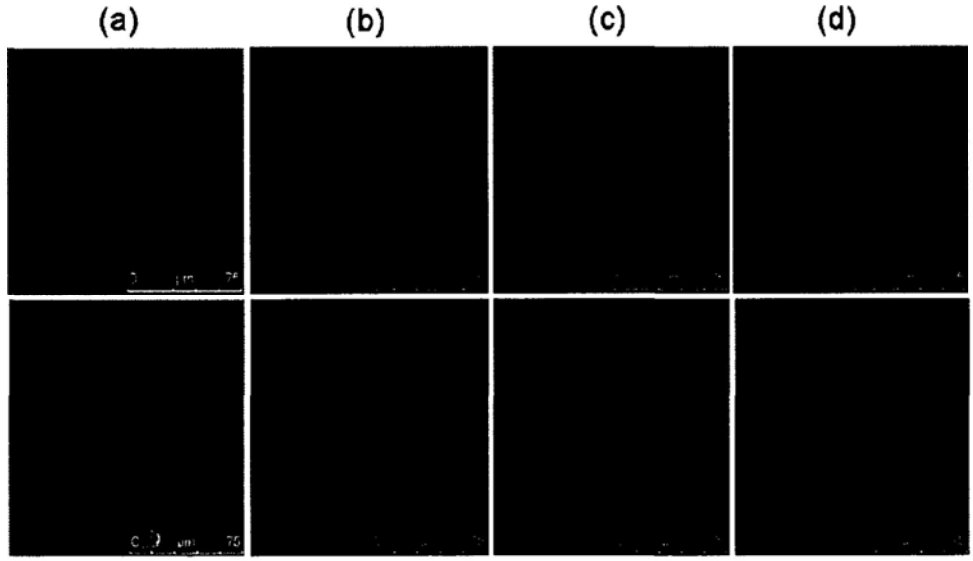

Figure 2.10. Visualization of intracellular fluorescence of HT29 cells using filter sets specific for (b) LysoTracker (upper low), MitoTracker (lower low) (in green), and (c) **2.11c** (in red). The corresponding superimposed image is given in (d), while the bright field image is shown in (a).

To study the mode of cell death induced by compound **2.11c**, a flow cytometric assay of Annexin V (Annexin-V) / Propodium Iodide (PI) co-staining was employed. The population of cells at different phases of cell death, namely viable (Annexin-V^-/PI^-), early apoptotic (Annexin-V^+/PI^-), and necrotic or late-stage apoptotic (Annexin-V^+/PI^+), was examined at different drug doses. As shown in Figure 2.11, the percentage of cells in the early apoptotic stage (i.e. externalization of phospholipid phosphatidylserine but not membrane leakage) increased from less than 10% for both the light (without compound **2.11c**) and dark (with 32 nM of compound **2.11c**) controls to more than 60% after the treatment with **2.11c** (32 nM) upon irradiation. The percentage of apoptotic cells increased with the concentration of **2.11c**. A significant amount of necrotic cells (less than 30%) was also observed.

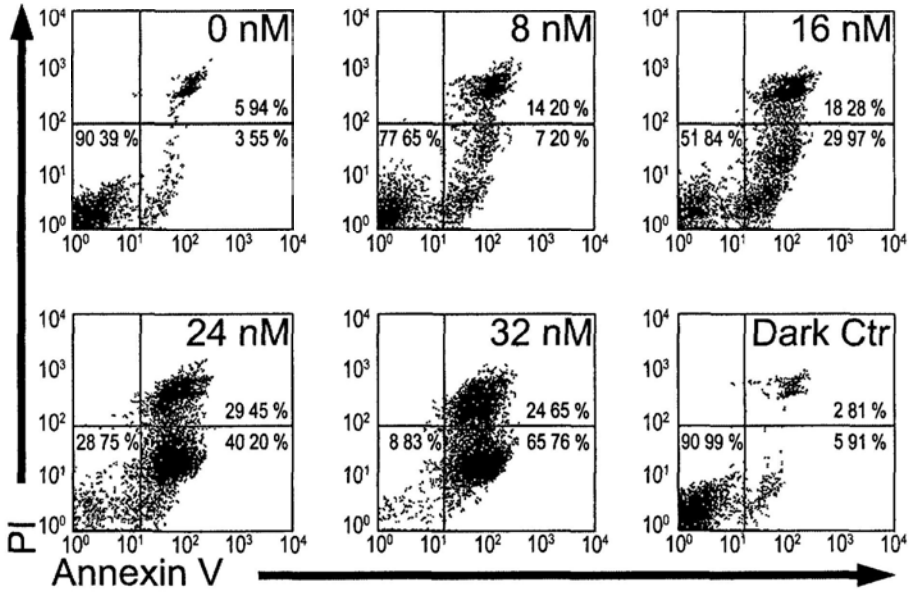

Figure 2.11. Flow cytometric analysis of cell death mechanism induced by compound **2.11c** upon PDT treatment in HT29 cells. Data are expressed as mean values ± S.E.M. of three independent experiments, each performed in quadruplicate.

2.3 Conclusion

In conclusion, we have prepared and characterized a series of distyryl BODIPYs substituted with different ethylene glycol moieties. Their in vitro photodynamic activities, cellular uptake, and aggregation behavior in the culture medium have also been investigated. Compound **2.11c** is a highly promising photosensitizer, which shows an extremely high photocytotoxicity, high cellular uptake, and selective affinity to the endoplasmic reticulum of the cells. Flow cytometric study has also revealed that compound **2.11c** can induce apoptosis upon PDT treatment.

2.4 Experimental Section

2.4.1 General

All the reactions were performed under an atmosphere of nitrogen. DMF, tetrahydrofuran (THF), toluene, and pyridine were distilled from barium oxide, sodium benzophenone ketyl, sodium, and potassium hydroxide, respectively. Chromatographic purifications were performed on silica gel (Macherey-Nagel, 70-230 mesh) columns with the indicated eluents. Size exclusion chromatography was carried out on Bio-Rad Bio-Beads S-X1 beads (200-400 mesh). All other solvents and reagents were of reagent grade and used as received. Compound **2.2**[14] and **2.7**[15] were prepared as described.

^{1}H and $^{13}C\{^{1}H\}$ NMR spectra were recorded on a Bruker DPX 300 (^{1}H, 300; ^{13}C, 75.4 MHz) or AVANCE II 400 (^{1}H, 400; ^{13}C, 100.6 MHz) spectrometer in $CDCl_3$, CD_2Cl_2, or D_2O. Spectra were referenced internally using the residual solvent

[^{1}H: δ 7.26 (for $CDCl_3$), 5.32 (for CD_2Cl_2), or 4.79 (for D_2O)] or solvent (^{13}C: δ 77.2 for $CDCl_3$) resonances relative to $SiMe_4$. Electrospray ionization (ESI) mass spectra were measured on a Thermo Finnigan MAT 95 XL mass spectrometer. Elemental analyses were performed by the Shanghai Institute of Organic Chemistry, Chinese Academy of Sciences.

2.4.2 Electronic Absorption and Photophysical Studies

Electronic absorption and fluorescence emission spectra were recorded on a Cary 5G UV-Vis-NIR spectrophotometer and a Hitachi F-7000 spectrofluorometer, respectively. The excitation and emission slit widths were 5 nm and 10 nm, respectively. The fluorescence quantum yields were determined by the equation: $\Phi_{F(sample)} = (F_{sample}/F_{ref})(A_{ref}/A_{sample})(n_{sample}^2/n_{ref}^2)\Phi_{F(ref)}$,[16] where F, A, and n are the measured fluorescence (area under the emission peak), the absorbance at the excitation position, and the refractive index of the solvent, respectively. The unsubstituted zinc (II) phthalocyanine (ZnPc) in DMF was used as the reference [$\Phi_{F(ref)} = 0.28$].[9] To minimize re-absorption of radiation by the ground-state species, the emission spectra were obtained in very dilute solutions where the absorbance at 610 nm was less than 0.03.

Singlet oxygen quantum yields (Φ_Δ) were measured by the method described by Wöhrle et al.[11] with some modifications. A mixture of DPBF (75 μM) and the photosensitizer (4 μM) in DMF was illuminated with red light coming from a 100 W halogen lamp after passing through a water tank for cooling and a color glass filter

(Newport, cut-on 610 nm). The decrease of the DPBF absorption at 415 nm was monitored along with time. The quantum yield of the photoreaction Φ_{DPBF} was defined as: $\Phi_{DPBF} = -(V_R/I_{abs})\cdot(c_t-c_0)/t$, where V_R is the reaction volume and I_{abs} is related to the light intensity, which was not directly determined, c_0 and c_t are the DPBF concentrations prior to and after irradiation, respectively, and t is the irradiation time in second. The value of $(I_{abs}/V_R)\cdot\Phi_{DPBF}$ was determined for each irradiation cycle using the extinction coefficient for DPBF ($\varepsilon = 23{,}000$ $dm^3mol^{-1}cm^{-1}$ at 415 nm). The singlet oxygen quantum yield Φ_Δ is related to Φ_{DPBF} according to the equation: $1/\Phi_{DPBF} = 1/\Phi_\Delta + (1/\Phi_\Delta)(k_d/k_a)(1/[DPBF])$, where k_d is the decay rate constant of singlet oxygen and k_a is the rate constant of the reaction of DPBF with singlet oxygen. By comparing the slope or y-intercept of the plot $(V_R/I_{abs})\cdot(1/\Phi_{DPBF})$ versus 1/[DPBF] with those derived from the experiment using the reference ZnPc as the sensitizer ($\Phi_\Delta = 0.56$ in DMF) under the same conditions, the Φ_Δ value of the sensitizer could be determined. The ratio of the slope or y-intercept should be inversely proportional to their ratio of Φ_Δ.

2.4.3 Synthesis

4-Triethylene glycol monomethyl ether substituted benzaldehyde 2.3.[17] A mixture of 2-hydroxybenzaldehyde (**2.1**) (0.98 g, 8.0 mmol), tosylated triethylene glycol monomethyl ether **2.2** (2.14 g, 6.7 mmol), and K_2CO_3 (4.67 g, 33.8 mmol) in DMF (40 mL) was stirred overnight at ambient temperature. The reaction mixture was mixed with water (50 mL), then extracted with CH_2Cl_2 (50 mL × 3). The

combined organic portion was washed with brine, dried over anhydrous $MgSO_4$, and then evaporated in vacuo. The crude product was purified by silica gel column chromatography using hexane/ethyl acetate (1:1, v/v) as the eluent to give a light yellow oil (1.61 g, 89 %). ^{1}H NMR (300 MHz, $CDCl_3$): δ 9.87 (s, 1 H, CHO), 7.83 (d, J = 8.7 Hz, 2 H, ArH), 7.02 (d, J = 8.7 Hz, 2 H, ArH), 4.22 (t, J = 4.5 Hz, 2 H, OCH_2), 3.89 (t, J = 5.1 Hz, 2 H, OCH_2), 3.75-3.55 (m, 8 H, OCH_2), 3.38 (s, 3 H, OCH_3).

Triethylene glycol monomethyl substituted BODIPY 2.5. To a solution of compound **2.3** (0.81 g, 3.0 mmol) and 2,4-dimethylpyrrole (**2.4**) (0.63 g, 6.6 mmol) in THF (90 mL) was added several drops of trifluoroacetic acid. The mixture was stirred at ambient temperature overnight, then a solution of 2,3-dichloro-5,6-dicyano-p-benzoquinone (0.68 g, 3.0 mmol) in THF (120 mL) was added. The mixture was stirred continuously for another 4 h. After the addition of triethylamine (18 mL, 0.13 mol), $BF_3{\cdot}OEt_2$ (18 mL, 0.15 mol) was added dropwise to the mixture, which was cooled in an ice-water bath. The mixture was kept stirring at ambient temperature overnight, then filtered through a pad of celite. The residue was rinsed with CH_2Cl_2 (50 mL), then the combined filtrate was rotary evaporated to dryness. The residue was redissolved in CH_2Cl_2 (100 mL) and washed with water (100 mL × 2). The organic portion was dried over anhydrous $MgSO_4$, and then evaporated in vacuo. The crude product was purified by silica gel column chromatography using CH_2Cl_2/ethyl acetate (10:1, v/v) as the eluent to give an orange-yellow solid (0.51 g, 35%). ^{1}H NMR (400 MHz, $CDCl_3$): δ 7.16 (d, J = 8.4

Hz, 2 H, ArH), 7.02 (d, J = 8.4 Hz, 2 H, ArH), 5.97 (s, 2 H, pyrrole-H), 4.18 (t, J = 4.8 Hz, 2 H, O-CH_2), 3.91 (t, J = 4.8 Hz, 2 H, OCH_2), 3.79-3.76 (m, 2 H, OCH_2), 3.72-3.66 (m, 4 H, OCH_2), 3.58-3.56 (m, 2 H, OCH_2), 3.39 (s, 3 H, OCH_3), 2.55 (s, 6 H, CH_3), 1.42 (s, 6 H, CH_3); $^{13}C\{^1H\}$ NMR (100.6 MHz, $CDCl_3$): δ 159.4, 155.2, 143.2, 141.9, 131.9, 129.2, 127.2, 121.2, 115.2, 72.0, 70.9, 70.7, 70.6, 69.8, 67.5, 59.1, 14.6; MS (ESI): isotopic clusters peaking at *m/z* 467 {20%, $[M - F]^+$}, 509 {100%, $[M + Na]^+$}, and 525 {20%, $[M + K]^+$}; HRMS (ESI): *m/z* calcd for $C_{26}H_{33}BF_2N_2NaO_4$ $[M + Na]^+$: 509.2394, found: 509.2398. Anal. calcd for $C_{26}H_{33}BF_2N_2O_4$: C, 64.21; H, 6.84; N, 5.76. Found: C, 64.17; H, 6.97; N, 5.77.

Diiodo BODIPY 2.6. Iodic acid (0.35 g, 2 mmol) dissolved in a minimum amount of water was added dropwise to a mixture of BODIPY **2.5** (0.51 g, 1 mmol) and iodine (0.63 g, 2.5 mmol) in EtOH. The mixture was heated at 60 °C for 2h. After cooling, the mixture was evaporated in vacuo. The crude product was purified by silica gel chromatography using CH_2Cl_2/ethyl acetate (25:1, v/v) as the eluent followed by recrystallization from CH_2Cl_2 and hexane to afford a bright red solid (0.49 g, 66 %). ^1H NMR (400 MHz, $CDCl_3$) : δ 7.12 (d, J = 8.8 Hz, 2 H, ArH), 7.05 (d, J = 8.8 Hz, 2 H, ArH), 4.20 (t, J = 4.8 Hz, 2 H, OCH_2), 3.92 (t, J = 4.8 Hz, 2 H, OCH_2), 3.80-3.77 (m, 2 H, OCH_2), 3.73-3.72 (m, 2 H, OCH_2), 3.69-3.67 (m, 2 H, OCH_2), 3.59-3.56 (m, 2 H, OCH_2), 3.40 (s, 3 H, OCH_3), 2.64 (s, 6 H, CH_3), 1.44 (s, 6 H, CH_3); $^{13}C\{^1H\}$ NMR (100.6 MHz, $CDCl_3$): δ 159.9, 156.7, 145.5, 141.7, 131.8, 129.1, 126.9, 115.6, 85.7, 72.0, 71.0, 70.8, 70.7, 69.8, 67.7, 59.2, 17.3, 16.1; MS (ESI): an isotopic cluster peaking at *m/z* 761{100%, $[M + Na]^+$}; HRMS (ESI): *m/z*

calcd for $C_{26}H_{31}BF_2I_2N_2NaO_4$ $[M + Na]^+$: 761.0324, found: 761.0327. Anal. calcd for $C_{26}H_{31}BF_2I_2N_2O_4$: C, 42.31; H, 4.23; N, 3.80. Found: C, 42.40; H, 4.50; N, 3.57.

3,4-Bis(triethylene glycol monomethyl ether) substituted benzaldehyde 2.9c.[17] A mixture of 3,4-dihydroxybenzaldehyde (**2.8**) (1.38 g, 10 mmol), tosylated triethylene glycol monomethyl ether **2.2** (6.05 g, 22 mmol), and K_2CO_3 (6.91 g, 50 mmol) in DMF (40 mL) was stirred at 100°C for 4 days. The mixture was then poured into water and the mixture was extracted with CH_2Cl_2 (100 mL × 3). The combined organic portion was washed with saturated brine (100 mL), dried over anhydrous $MgSO_4$, and then evaporated in vacuo. The crude product was purified by silica gel column chromatography using CH_2Cl_2/acetone (10:1, v/v) as the eluent to give a colorless oil (2.67 g, 62%). ^{1}H NMR (400 MHz, $CDCl_3$): δ 9.84 (s, 1 H, CHO), 7.44 (d, J = 7.6 Hz, 1 H, ArH), 7.43 (s, 1 H, ArH), 7.00 (d, J = 8.0 Hz, 1 H, ArH), 4.27-4.21 (m, 4 H, OCH_2), 3.93-3.89 (m, 4 H, OCH_2), 3.77-3.75 (m, 4 H, OCH_2), 3.69-3.64 (m, 8 H, OCH_2), 3.56-3.54 (m, 4 H, OCH_2), 3.38 (s, 3 H, OCH_3).

3,4-Bis(polyethylene glycol monomethyl ether) substituted benzaldehyde 2.9d. A mixture of 3,4-dihydroxybenzaldehyde (**2.8**) (0.43 g, 3.1 mmol), tosylated polyethylene glycol monomethyl ether **2.7** (5.05 g, 7.2 mmol), and K_2CO_3 (2.47 g, 17.9 mmol) in DMF (40 mL) was stirred at 100°C for 4 days. The mixture was filtered through a pad of celite and the residue was rinsed with CH_2Cl_2 (100 mL). The filtrate was rotary evaporated to dryness. The crude product was purified by silica gel column chromatography using CH_2Cl_2/acetone (10:1, v/v) as the eluent to give a colorless oil (1.88 g, 50%). ^{1}H NMR (400 MHz, $CDCl_3$): δ 9.84 (s, 1 H, CHO),

7.44 (d, J = 8.4 Hz, 1 H, ArH), 7.43 (s, 1 H, ArH), 7.01 (d, J = 8.0 Hz, 1 H, ArH), 4.21-4.27 (m, 4 H, OCH_2), 3.88-3.92 (m, 4 H, OCH_2), 3.73-3.75 (m, 4 H, OCH_2), 3.64-3.66 (m, ca. 80 H, OCH_2), 3.54-3.56 (m, 4 H, OCH_2), 3.38 (s, 6 H, OCH_3). MS (ESI): an isotopic clusters peaking at *m/z* 1246 {65%, $[M + Na]^+$ for n = 12}.

Distyryl BODIPY 2.11a. A mixture of diiodo BODIPY **2.6** (0.20 g, 0.27 mmol), 4-methoxybenzaldehyde (**2.10**) (0.11 g, 0.81 mmol), glacial acetic acid (0.41 mL, 7.2 mmol), piperidine (0.46 mL, 4.7 mmol), and a small amount of $Mg(ClO_4)_2$ in toluene (60 mL) was refluxed for 2 h. The water formed during the reaction was removed azeotropically with a Dean-Stark apparatus. The mixture was concentrated under reduced pressure. The residue was purified by silica gel column chromatography using ethyl acetate/hexane (1:1, v/v) as the eluent. The green colored fraction was collected and rotary evaporated. It was then further purified by size exclusion chromatography with Bio-beads S-X1 beads using THF as the eluent followed by recrystallization from CH_2Cl_2 and hexane to afford a green solid (86 mg, 33%). ^1H NMR (400 MHz, $CDCl_3$): δ 8.13 (d, J = 16.8 Hz, 2 H, CH=CH), 7.62 (d, J = 8.4 Hz, 4 H, ArH), 7.59 (d, J = 15.6 Hz, 2 H, CH=CH), 7.16 (d, J = 8.8 Hz, 2 H, ArH), 7.06 (d, J = 8.8 Hz, 2 H, ArH), 6.95 (d, J = 8.8 Hz, 4 H, ArH), 4.22 (t, J = 4.8 Hz, 2 H, OCH_2), 3.94 (t, J = 4.8 Hz, 2 H, OCH_2), 3.87 (s, 6 H, OCH_2), 3.81-3.78 (m, 2 H, OCH_2), 3.74-3.72 (m, 2 H, OCH_2), 3.70-3.68 (m, 2 H, OCH_2), 3.40 (s, 3 H, OCH_3), 1.50 (s, 6 H, CH_3); $^{13}C\{^1H\}$ NMR (100.6 MHz, $CDCl_3$): δ 160.8, 159.9, 150.5, 145.9, 139.2, 138.7, 133.4, 129.7, 129.4, 127.6, 116.9, 115.6, 114.4, 82.8, 72.1, 71.1, 70.8, 70.8, 69.9, 67.7, 59.2, 55.6, 17.9; MS (ESI): an isotopic cluster peaking at *m/z* 997

{100%, $[M + Na]^+$}; HRMS (ESI): *m/z* calcd for $C_{42}H_{43}BF_2I_2N_2NaO_6$ $[M + Na]^+$: 997.1164, found:997.1164. Anal. calcd for $C_{42}H_{43}BF_2I_2N_2O_6$: C, 51.77; H, 4.45; N, 2.87. Found: C, 51.93; H, 4.84; N, 2.77.

Distyryl BODIPY 2.11b. According to the procedure described for **2.11a**, a mixture of diiodo BODIPY **2.6** (51 mg, 69 μmol), 4-triethylene glycol monomethyl ether substituted benzaldehyde **2.3** (56 mg, 0.2 mmol), glacial acetic acid (0.1 mL, 1.7 mmol), piperidine (0.12 mL, 1.2 mmol), and a small amount of $Mg(ClO_4)_2$ in toluene (20 mL) was refluxed for 2 h. The crude product was purified by silica gel column chromatography using $CHCl_3$ as the eluent, followed by size exclusion chromatography using THF as the eluent to afford a green solid (30 mg, 35%). ^1H NMR (400 MHz, $CDCl_3$): δ 8.13 (d, J = 16.4 Hz, 2 H, CH=CH), 7.60 (d, J = 8.8 Hz, 4 H, ArH), 7.58 (d, J = 18.0 Hz, 2 H, CH=CH), 7.16 (d, J = 8.4 Hz, 2 H, ArH), 7.06 (d, J = 8.4 Hz, 2 H, ArH), 6.96 (d, J = 8.8 Hz, 4 H, ArH), 4.18-4.23 (m, 6 H, OCH_2), 3.94 (t, J = 4.8 Hz, 2 H, OCH_2), 3.90 (t, J = 4.8 Hz, 4 H, OCH_2), 3.66-3.81 (m, 18 H, OCH_2), 3.55-3.60 (m, 6 H, OCH_2), 3.40 (s, 3 H, OCH_3), 3.39 (s, 6 H, OCH_3), 1.50 (s, 6 H, CH_3); $^{13}C\{^1H\}$ NMR (100.6 MHz, $CDCl_3$): δ 160.1, 159.9, 150.5, 145.9, 139.1, 138.7, 133.4, 129.8, 129.7, 129.4, 127.6, 116.9, 115.6, 115.1, 82.8, 72.1, 71.0, 70.8, 70.7, 69.8, 67.7, 59.2, 17.9; MS (ESI): an isotopic cluster peaking at *m/z* 1262 {100%, $[M + Na]^+$}. HRMS (ESI): *m/z* calcd for $C_{54}H_{67}BF_2I_2N_2NaO_{12}$ $[M + Na]^+$: 1261.2737, found: 1261.2723. Anal. calcd for $C_{54}H_{67}BF_2I_2N_2O_{12}$: C, 52.36; H, 5.45; N, 2.26. Found: C, 52.44; H, 5.63; N, 2.13.

Distyryl BODIPY 2.11c. A mixture of diiodo BODIPY **2.6** (0.29 g, 0.4 mmol), 3,4-bis(triethylene glycol monomethyl ether) substituted benzaldehyde **2.9c** (0.52 g, 1.2 mmol), glacial acetic acid (0.8 mL, 14.0 mmol), and piperidine (1.0 mL, 10.1 mmol) in toluene (80 mL) was refluxed for 2 h. The water formed during the reaction was removed azeotropically with a Dean-Stark apparatus. The mixture was concentrated under reduced pressure, then the residue was purified by silica gel column chromatography using $CHCl_3$/MeOH (100:3) as the eluent, followed by size exclusion chromatography using THF as the eluent. The product was obtained as a green solid (96 mg, 16%). ^{1}H NMR (400 MHz, CD_2Cl_2): δ 8.08 (d, J = 16.4 Hz, 2 H, CH=CH), 7.52 (d, J = 16.4 Hz, 2 H, CH=CH), 7.29 (dd, J = 1.6 Hz, 8.4 Hz, 2 H, ArH), 7.21 (d, J = 8.4 Hz, 2 H, ArH), 7.17 (d, J = 1.6 Hz, 2 H, ArH), 7.10 (d, J = 8.4 Hz, 2 H, ArH), 6.97 (d, J = 8.4 Hz, 2 H, ArH), 4.20-4.24 (m, 10 H, OCH_2), 3.85-3.89 (m, 10 H, OCH_2), 3.69-3.72 (m, 10 H, OCH_2), 3.56-3.66 (m, 20 H, OCH_2), 3.47-3.54 (m, 10 H, OCH_2), 3.35 (s, 3 H, OCH_3), 3.33 (s, 6 H, OCH_3), 3.31 (s, 6 H, OCH_3), 1.53 (s, 6 H, CH_3); ^{13}C{^{1}H} NMR (100.6 MHz, $CDCl_3$): δ 159.8, 150.4, 148.9, 145.8, 139.2, 138.8, 133.4, 130.4, 129.6, 127.4, 121.6, 117.2, 115.5, 114.3, 114.2, 83.1, 71.9, 70.9, 70.7, 70.6, 70.5, 69.8, 69.7 (two overlapping signals), 69.1, 68.7, 67.6, 59.1, 59.0, 17.8; MS (ESI): an isotopic cluster peaking at *m/z* 1585 {100%, $[M + Na]^+$}. HRMS (ESI): *m/z* calcd for $C_{68}H_{95}BF_2I_2N_2NaO_{20}$ $[M + Na]^+$: 1585.4521, found:1585.4557. Anal. calcd for $C_{68}H_{95}BF_2I_2N_2O_{20}$: C, 52.25; H, 6.13; N, 1.79. Found: C, 51.97; H, 6.27; N, 1.64.

Distyryl BODIPY 2.11d. According to the procedure described for **2.11c**, a mixture of diiodo BODIPY **2.6** (0.29 g, 0.4 mmol), 3,4-bis(polyethylene glycol monomethyl ether) substituted benzaldehyde **2.9d** (1.42 g, 1.2 mmol), glacial acetic acid (0.8 mL, 14.0 mmol), and piperidine (1.0 mL, 10.1 mmol) in toluene (80 mL) was refluxed for 2 h. The crude product **2.11d** was purified by silica gel column chromatography using $CHCl_3$/MeOH (10:1) as the eluent, followed by size exclusion chromatography using THF as the eluent to afford an oily green product (92 mg, 7%). ^{1}H NMR (400 MHz, CD_2Cl_2): δ 8.08 (d, J = 16.4 Hz, 2 H, CH=CH), 7.52 (d, J = 16.4 Hz, 2 H, CH=CH), 7.30 (d, J = 8.4 Hz, 2 H, ArH), 7.22 (d, J = 8.4 Hz, 2 H, ArH), 7.16 (s, 2 H, ArH), 7.10 (d, J = 8.4 Hz, 2 H, ArH), 6.98 (d, J = 8.4 Hz, 2 H, ArH), 4.20-4.25 (m, 10 H, OCH_2), 3.87-3.89 (m, 10 H, OCH_2), 3.70-3.72 (m, 10 H, OCH_2), 3.54-3.67 (m, *ca.* 164 H, OCH_2), 3.49-3.51 (m, 10 H, OCH_2), 3.35 (s, 3 H, OCH_3), 3.33 (s, 12 H, OCH_3), 1.53 (s, 6 H, CH_3). MS (ESI): isotopic clusters peaking at *m/z* 1574 {98%, $[M]^{2+}$ for n = 12} and 3173 {20%, $[M + Na]^+$ for n = 12}.

2.4.4 In vitro Studies (in collaboration with Prof. Fong's Lab)

2.4.4.1 Cell Line and Culture Conditions

The HT29 human colorectal carcinoma cells (from ATCC, no. HTB-38) were maintained in Dulbecco's modified Eagle's medium (DMEM; Invitrogen, cat no.10313-021) supplemented with fetal calf serum (10%), penicillin-streptomycin (100 units mL^{-1} and 100 mg mL^{-1}, respectively), L-glutamine (2 mM), and transferrin (10 mg mL^{-1}). Approximately 3×10^4 cells per well in the media were

inoculated in 96-multiwell plates and incubated overnight at 37 °C in a humidified 5% CO_2 atmosphere.

2.4.4.2 Photocytotoxicity Assay

Distyryl BODIPYs **2.11a-2.11d** were first dissolved in DMF to give 1.6 mM solutions, which were diluted to 80 μM with an aqueous solution of Tween 80 (Arcos, 0.5% by volume). The solutions were filtered with a 0.22 μm filter, then diluted with the culture medium to appropriate concentrations. The cells, after being rinsed with PBS, were incubated with 100 μL of these distyryl BODIPY solutions for 2 h at 37 °C under 5% CO_2. The cells were then rinsed again with PBS and refed with 100 μL of the culture medium before being illuminated at ambient temperature. The light source consisted of a 300 W halogen lamp, a water tank for cooling, and a color glass filter (Newport) cut-on 610 nm. The fluence rate ($\lambda > 610$ nm) was 40 mW cm^{-2}. An illumination of 20 min led to a total fluence of 48 J cm^{-2}.

Cell viability was determined by means of the colorimetric MTT assay.[19] After illumination, the cells were incubated at 37 °C under 5% CO_2 overnight. An MTT (Sigma) solution in PBS (3 mg mL^{-1}, 50 μL) was added to each well followed by incubation for 2 h under the same environment. A solution of sodium dodecyl sulfate (SDS, Sigma; 10% by weight, 50 μL) was then added to each well. The plate was incubated in an oven at 60 °C for 30 min, then 80 μL of iso-propanol was added to each well. The plate was agitated on a Bio-Rad microplate reader at ambient temperature for 10 s before the absorbance at 540 nm at each well was taken. The

average absorbance of the blank wells, which did not contain the cells, was subtracted from the readings of the other wells. The cell viability was then determined by the following equation: % viability = $[\Sigma(A_i/A_{control} \times 100)]/n$, where A_i is the absorbance of the ith data (i = 1, 2, ..., n), $A_{control}$ is the average absorbance of the control wells in which the distyryl BODIPY was absent, and n (= 4) is the number of the data points.

2.4.4.3 Intracellular Fluorescence Studies

About 1.2 × 10^5 HT29 cells in the culture medium (2 mL) were seeded on a coverslip and incubated overnight at 37 °C under 5% CO_2. The medium was removed, then the cells were incubated with solutions of distyryl BODIPYs **2.11a-2.11d** in the medium (1 μM, 2 mL) for 2 h under the same conditions. The cells were rinsed with PBS and then viewed with a Leica SP5 confocal microscope equipped with a 633 helium neon laser. Emission signals from 650-720 nm (gain = 750 V) were collected and the images were digitized and analyzed by Leica Application Suite Advanced Fluorescence. The intracellular fluorescence intensities (total 50 cells for each sample) were also determined.

2.4.4.4 Subcellular Localization Studies

About 1.2 × 10^5 HT29 cells in the culture medium (2 mL) were seeded on a coverslip and incubated overnight at 37 °C under 5% CO_2. The medium was then removed. The cells were incubated with a solution of **2.11c** in the medium (1 μM,

2 mL) for 2 h under the same conditions. For the study using ER-Tracker, the cells were incubated with ER-Tracker green (Molecular Probe; 1 μM in PBS) under the same conditions for a further 30 min. For the study using LysoTracker and MitoTracker, the cells were incubated with LysoTracker green DND 26 (Molecular Probe; 0.2 μM in the medium) or MitoTracker Green FM (Molecular Probe; 0.1 μM in the medium) for a further 10 min. For all the cases, the cells were then rinsed with PBS and viewed with a Leica SP5 confocal microscope equipped with a 488 nm Argon laser and a 633 helium neon laser. All the Trackers were excited at 488 nm and monitored at 510-560 nm, whereas compound **2.11c** was excited at 633 nm and monitored at 650-720 nm. Images were digitized and analyzed using Leica Application Suite Advanced Fluorescence. The subcellular localization of **2.11c** was revealed by comparing the intracellular fluorescence images caused by the ER-Tracker, LysoTracker, or MitoTracker and this dye.

2.4.4.5 Flow Cytometric Studies for Cell Death Mechanism

Approximately 6×10^5 HT29 cells were seeded on a 35 mm dish and incubated for 24 h at 37 °C under 5% CO_2. The cells were then treated with **2.11c** at various concentrations and incubated under the same conditions for 2 h. The cells were then rinsed three times with PBS and refed with 100 μL of the culture medium before being illuminated at ambient temperature. After 20 h incubation, the cells were rinsed by PBS and then harvested by 0.25% Trypsin-EDTA (500 μL, Invitrogen) for 5 min, followed by centrifugation at 2400 rpm for 3 min. The pellet was then washed

again by PBS and then subject to centrifugation. The cells were suspended in 1 mL of binding buffer (10 mM HEPES, 140 mM NaCl, 25 mM $CaCl_2$, pH 7.4) containing 5 μL Annexin V-GFP and 2 μg/mL propidium iodide. After incubation in darkness for 15 min at room temperature, the signals of Annexin V-GFP and propidium iodide were measured by the BD FACSCanto flow cytometer (Becton Dickinson) with 10^4 cells counted in each sample. Both Annexin V-GFP and propidium iodide were excited by a 488 nm argon laser while the emitted fluorescence was monitored at 500-560 nm for Annexin V-GFP and at > 670 nm for propidium iodide. The data collected were analyzed by using WinMDI 2.9.

2.5 References

1 (a) Bonnett, R. *Chem. Soc. Rev.* **1995**, *24*, 19. (b) Dolmans, D. E. J. G. J.; Fukumura, D.; Jain, R. K. *Nat. Rev. Cancer* **2003**, *3*, 380. (c) Castano, A. P.; Mroz, P.; Hamblin, M. R. *Nat. Rev. Cancer* **2006**, *6*, 535. (d) Wilson, B. C.; Patterson, M. S. *Phys. Med. Biol.* **2008**, *53*, R61. (e) Celli, J. P.; Spring, B. Q.; Rizvi, I.; Evans, C.; Samkoe, K. S.; Verma, S.; Pogue, B. W.; Hasan, T. *Chem. Rev.* **2010**, *110*, 2795.

2 Oleinick, N. L.; Morris, R. L.; Belichenko, I. *Photochem. Photobiol. Sci.* **2002**, *1*, 1.

3 (a) Dougherty, T. J.; Potter, W. R.; Weishaupt, K. R. *Prog. Clin. Biol. Res.* **1984**, *170*, 301. (b) Kessel, D.; Thompson, P.; Saatio, K.; Nantwi, K. D. *Photochem. Photobiol.* **1987**, *45*, 787. (c) Wilkinson, F.; Helman, W. P.; Ross,

A. B. *J. Phys. Chem. Ref. Data* **1993**, *22*, 113.

4 (a) Nelson, J. S.; Roberts, W. G.; Berns, M. W. *Cancer Res.* **1987**, *47*, 4681. (b) Roberts, W. G.; Shiau, F. Y.; Nelson, J. S.; Smith, K. M.; Berns, M. W. *J. Natl. Cancer. Inst.* **1988**, *80*, 330. (c) Leach, M. W.; Higgins, R. J.; Autry, S. A.; Boggan, J. E.; Lee, S. J.; Smith, K. M. *Photochem. Photobiol.* **1993**, *58*, 653. (d) Nyman, E. S.; Hynninen, P. H. *J. Photochem. Photobiol. B: Biol.* **2004**, *73*, 1.

5 Atilgan, S.; Ekmekci, Z.; Dogan, A. L.; Guc, D.; Akkaya, E. U. *Chem. Commun.* **2006**, 4398.

6 (a) Yogo, T.; Urano, Y.; Ishitsuka, Y.; Maniwa, F.; Nagano, T. *J. Am. Chem. Soc.* **2005**, *127*, 12162. (b) Ozlem, S.; Akkaya, E. U. *J. Am. Chem. Soc.* **2009**, *131*, 48. (c)Erbas, S.; Gorgulu, A.; Kocakusakogullari, M.; Akkaya, E. U. *Chem. Commun.* **2009**, 4956. (d) Lim, S. H.; Thivierge, C.; Nowak-Sliwinska, P.; Han, J.; van den Bergh, H.; Wagnières, G.; Burgess, K.; Lee, H. B. *J. Med. Chem.* **2010**, *53*, 2865.

7 (a) Loudet, A.; Burgess, K. *Chem. Rev.* **2007**, *107*, 4891. (b) Ulrich, G.; Ziessel, R.; Harriman, A. *Angew. Chem. Int. Ed.* **2008**, *47*, 1184.

8 (a) Stolnik, S.; Illum, L.; Davis, S. S. *Adv. Drug Deliv. Rev.* **1995**, *16*, 195. (b) Torchilin, V. P. *Pharm. Res.* **2007**, *24*, 1. (c) van Vlerken, L. E.; Vyas, T. K.; Amiji, M. M. *Pharm. Res.* **2007**, *24*, 1405.

9 Scalise, I.; Durantini, E. N. *Bioorg. Med. Chem.* **2005**, *13*, 3037.

10 (a) Kobayashi, N.; Sasaki, N.; Higashi, Y.; Osa, T. *Inorg. Chem.* **1995**, *34*, 1636. (b) Kobayashi, N.; Ogata, H.; Nonaka, N.; Luk'yanets, E. A. *Chem. Eur.*

J. **2003**, *9*, 5123.

11 Maree, M. D.; Kuznetsova, N.; Nyokong, T. *J. Photochem. Photobiol. A: Chem.* **2001**, *140*, 117.

12 (a) Spikes, D. J. *Photochem. Photobiol.* **1986**, *43*, 691. (b) Dhami, S.; Phillips, D. *J. Photochem. Photobiol. A: Chem.* **1996**, *100*, 77. (c) Howe, L.; Zhang, J. Z. *J. Phys. Chem. A* **1997**, *101*, 3207. (d) Suchetti, C. A.; Durantini, E. N. *Dyes Pigments* **2007**, *74*, 630.

13 Sibrian-Vazquez, M.; Jensen, T. J.; Hammer, R. P.; Vicente, M. G. H. *J. Med. Chem.* **2006**, *49*, 1364.

14 Snow, A. W.; Foos, E. E. *Synthesis* **2003**, *4*, 509.

15 Rivera, E.; Belletête, M.; Natansohn, A.; Durocher, G. *Can. J. Chem.* **2003**, *81*, 1076.

16 Eaton, D. F. *Pure Appl. Chem.* **1988**, *60*, 1107.

17 Lottner, C.; Bart, K. C.; Bernhardt, G.; Brunner, H. *J. Med. Chem.* **2002**, *45*, 2079.

18 Nielsen, C. B.; Johnsen, M.; Arnbjerg, J.; Pittelkow, M.; McIlroy, S. P.; Ogilby, P. R.; Jorgensena, M. *J. Org. Chem.* **2005**, *70*, 7065.

19 Tada, H.; Shiho, O.; Kuroshima, K.; Koyama, M.; Tsukamoto, K. *J. Immunol. Methods* **1986**, *93*, 157.

Chapter 3

Synthesis, Characterization, and Photodynamic Activities of Novel Unsymmetrical Distyryl BODIPYs

3.1 Introduction

Distyryl BODIPYs are promising photosensitizers which have much received current attention.[1] In Chapter 2, we have reported a series of symmetrical distyryl BODIPYs which contain one to five hydrophilic oligoethylene glycol monomethyl ether chain(s). We found that the photocytotoxic potency increases as the number of triethylene glycol chains increases. However, when the length of oligoethylene glycol chains increases, the photocytotoxicity becomes lower. In order to further enhance the photodynamic activity, we modified these compounds by keeping three triethylene glycol chains to ensure their hydrophilicity and introducing another substituent at the other styryl group. In this Chapter, we describe a series of unsymmetrical distyryl BODIPYs, including their preparation, spectroscopic and photophysical properties, as well as in vitro photodynamic activities.

3.2 Results and Discussion

3.2.1 Molecular Design and Chemical Synthesis

Since naphthalene ring can lead to a bathochromic effect through extending the π-conjugation system, we attempted to introduce a naphthalene ring into the distyryl

BODIPY skeleton to shift the absorption and emission maxima to the red. Alternatively, if an auxochromic amine group is added into the distyryl BODIPY skeleton, the absorption and emission maxima should also shift. The amino group can also be protonated or alkylated to give hydrophilic BODIPYs. Accordingly, distyryl BODIPY **3.6a-3.6e** have been designed and synthesized.

Scheme 3.1 shows the synthetic route used to prepare the target compounds **3.6a-3.6e**. Treatment of diiodo BODIPY **2.6** with 3,4-bis(triethylene glycol monomethyl ether) substituted benzaldehyde **2.9c** via Knoevenagel condensation gave monostyryl BODIPY **3.1**. Treatment of 2-N,N-dimethylaminoethanol (**3.2**) with methylsulfonyl chloride (**3.3**) afforded mesylated 2-N,N-dimethylaminoethanol **3.4**, which then reacted with 4-hydroxybenzaldehyde (**2.1**) to give amino-substituted benzaldehyde **3.5d**. Treatment of monostyryl BODIPY **3.1** with benzaldehydes **3.5a-3.5d** via a further Knoevenagel condensation afforded the corresponding unsymmetrical distyryl BODIPYs **3.6a-3.6d**. Treatment of **3.6d** with excess iodomethane in chloroform gave the cationic N-methylated derivative **3.6e**. All of these compounds had good solubility in common organic solvents and possessed a high stability, which facilitated the purification by silica gel column chromatography and size exclusion chromatography.

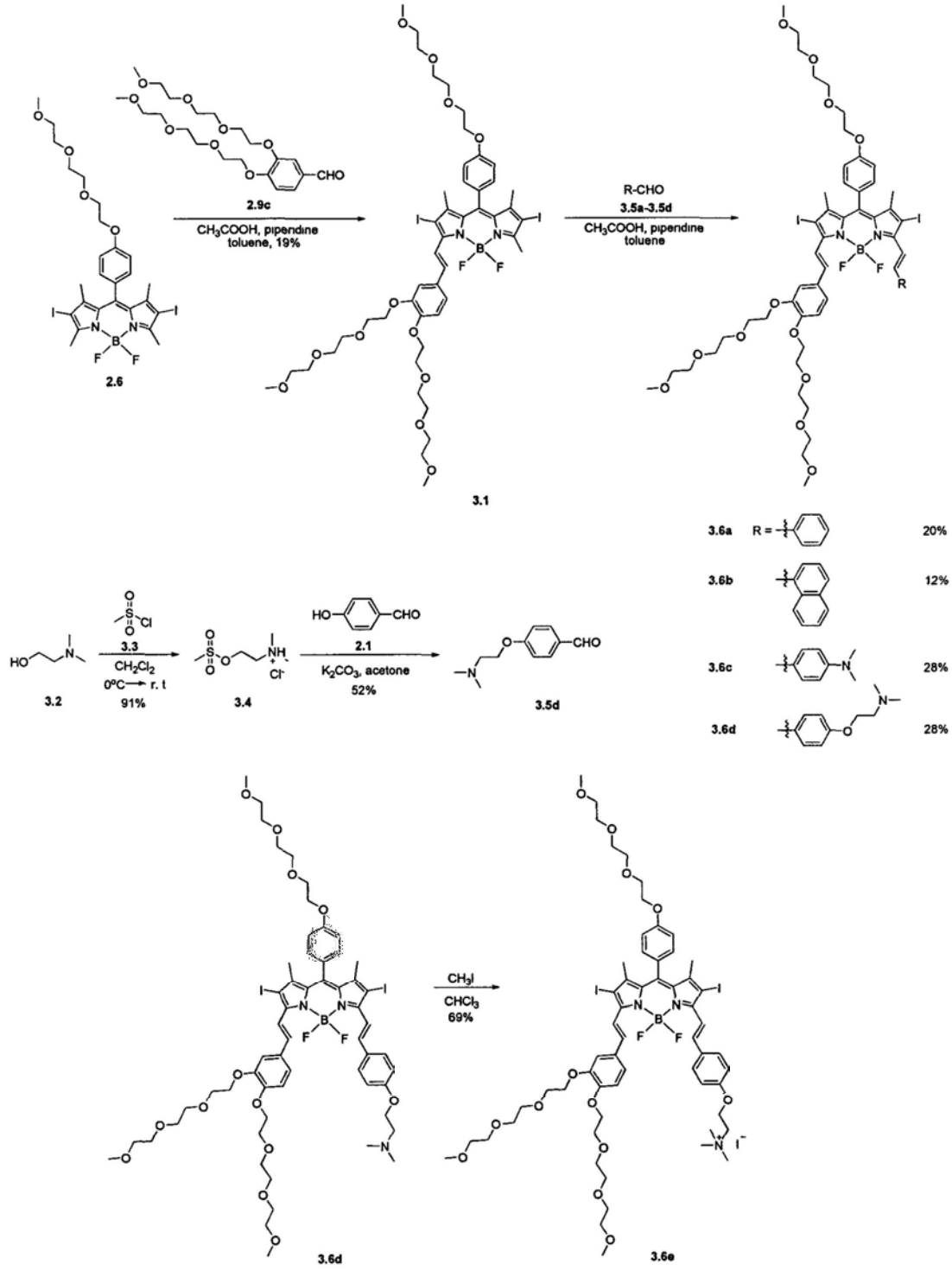

Scheme 3.1. Synthesis of unsymmetrical distyryl BODIPYs **3.6a-3.6e**.

3.2.2 Spectroscopic Characterization and Photophysical Properties

All of the new compounds were fully characterized with various spectroscopic

methods and the data are given in Section 3.4. Figure 3.1 shows the ^{1}H NMR spectrum of compound **3.6d** in CD_2Cl_2. The downfield signals from 6.9 to 8.2 ppm are due to the aryl and vinyl protons. The signals from 3.3 to 4.3 ppm are attributed to the triethylene glycol chain protons. The two triplets at 2.7 and 4.1 ppm are due to the methylene protons near the amino group. The singlet around 2.3 ppm is due to the N-methyl protons. The singlet around 1.5 ppm is due to the methyl protons in the pyrrole rings. For the other four compounds, the assignment of ^{1}H NMR signals is similar to that of **3.6d**. As expected, the substituents at the benzene rings exert a significant influence on the chemical shifts of these signals. Additionally, for the methylated derivative **3.6e**, the signals of the methylene protons near the ammonium group and the N-methyl protons are significantly shifted downfield compared with non-methylated analogue **3.6d**.

The $^{13}C\{^1H\}$ NMR data of these compounds were also in accord with the structures though some of the aryl carbon signals and the chain CH_2 signals were overlapped.

All of these compounds were further characterized with ESI mass spectrometry. The isotopic distribution as well as the exact mass for the $[M + Na]^+$ (for **3.6a-3.6c**), $[M + H]^+$ (for **3.6d**), or $[M - I]^+$ (for **3.6e**) species were in good agreement with the calculated ones.

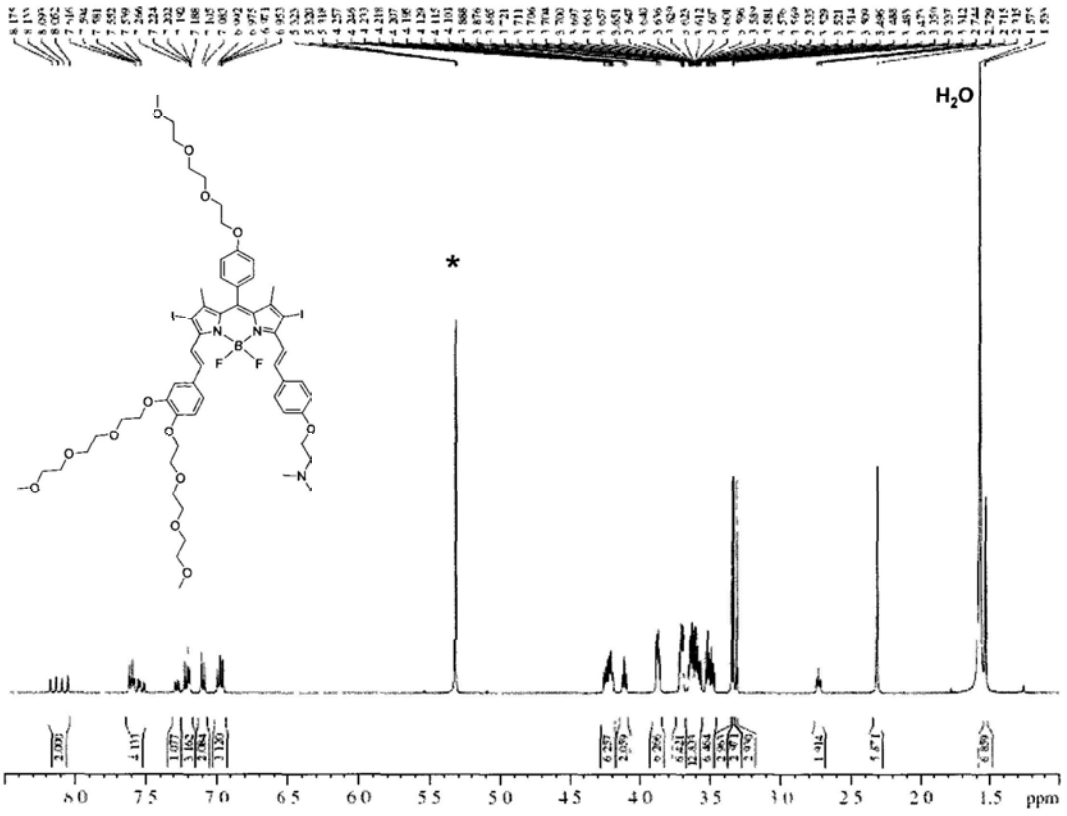

Figure 3.1. ^{1}H NMR spectrum of **3.6d** in CD_2Cl_2; * indicates residual solvent signal.

The electronic absorption and fluorescence spectra of distyryl BODIPYs **3.6a-3.6e** were measured in DMF and the data are summarized in Table 3.1. It was observed that the Q-band absorption of **3.6b-3.6e** was red-shifted compared with that of **3.6a**. Particularly **3.6c**, in which a dimethylamino group is directly attached to the benzene ring, exhibited a remarkable red-shift in the absorption due to the strong intramolecular charge transfer (ICT) (Figure 3.2(a) and Table 3.1). In order to investigate the aggregation behavior of these compounds, their absorption spectra were recorded at different concentrations. The spectrum of **3.6a**, for example, showed a broad Soret band peaking at 340 nm, a vibronic band at 450 nm, and an intense and sharp Q band at 653 nm, which strictly followed the Lambert Beer's law

(Figure 3.3). Similar results were obtained for the other four compounds. It indicated that all these compounds are essentially non-aggregated in DMF.

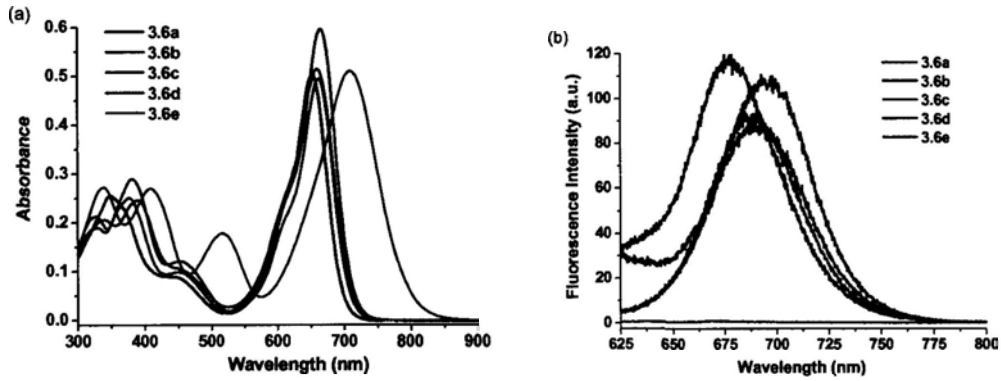

Figure 3.2. Electronic absorption (a) and fluorescence emission spectra (excited at 610 nm) (b) of **3.6a-3.6e** (8 μM) in DMF.

Table 3.1. Electronic absorption and photophysical data for compounds **3.6a-3.6e** in DMF.

Compound	λ_{max} (nm) (log ε)	λ_{em}(nm)[a]	Φ_F[b]	Φ_Δ[c]
3.6a	340 (4.55), 450 (4.12), 653 (4.88)	677	0.19	0.48
3.6b	340 (4.44), 390 (4.54), 465 (4.19), 659 (4.88)	688	0.15	0.38
3.6c	339 (4.53), 410 (4.53), 517 (4.35), 709 (4.81)	-	-	0.05
3.6d	327 (4.43), 382 (4.58), 453 (4.21), 665 (4.91)	695	0.18	0.40
3.6e	327 (4.40), 377 (4.57), 450 (4.19), 661 (4.89)	686	0.15	0.48

[a] Excited at 610 nm. [b] Relative to ZnPc (Φ_F = 0.28 in DMF). [c] Relative to ZnPc (Φ_Δ = 0.56 in DMF).

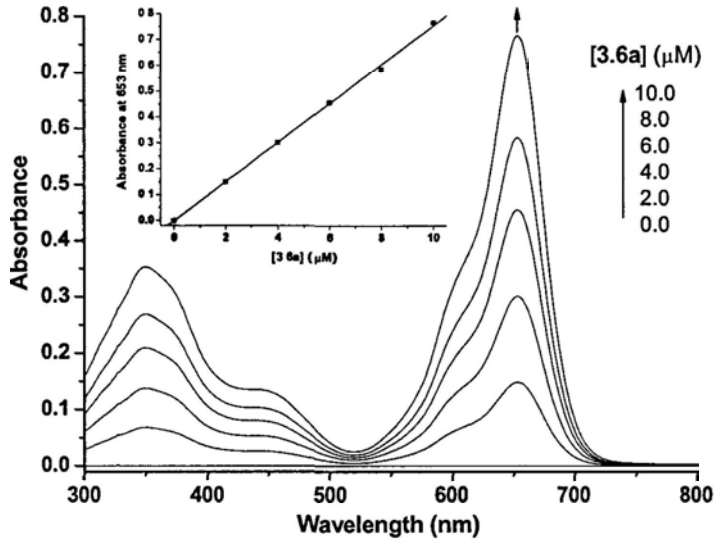

Figure 3.3. Electronic absorption spectra of **3.6a** at various concentrations in DMF. The inset plots the Q-band absorbance versus the concentration of **3.6a**.

The fluorescence emission spectra of these compounds were also recorded in DMF. Upon excitation at 610 nm, compounds **3.6a-3.6e** showed a fluorescence emission at 677-695 nm with a quantum yield (Φ_F) of 0.15-0.19 relative to ZnPc (Φ_F = 0.28).[2] Compounds **3.6b**, **3.6d**, and **3.6e** exhibited a red-shifted fluorescence emission relative to **3.6a**, while **3.6c** was basically non-fluorescent due to the strong ICT process (Figure 3.2(b) and Table 3.1). The red shift of fluorescence emission is consistent with the absorption data.

The efficiency of these compounds in generating singlet oxygen, as reflected by the rate of decay of the singlet oxygen quencher, 1,3-diphenylisobenzofuran (DPBF), was also compared. As shown in Figure 3.4, all of these compounds can induce the photo-bleaching of DPBF and their efficiencies are similar except **3.6c**. The singlet oxygen quantum yields (Φ_Δ) relative to ZnPc (Φ_Δ = 0.56),[3] are listed in Table 3.1.

The poor efficiency of compound **3.6c** in generating singlet oxygen is probably attributed to the strong ICT process.

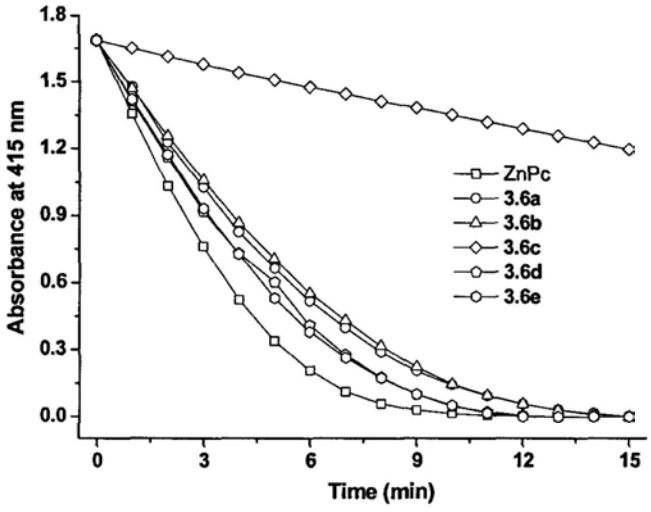

Figure 3.4. Comparison of the rates of decay of DPBF (initial concentration = 75 μM) in DMF, as monitored spectroscopically at 415 nm, using **3.6a-3.6e** as the photosensitisers (4 μM) and ZnPc (4 μM) as the reference.

3.2.3 In Vitro Photodynamic Activities

The in vitro photodynamic activities of **3.6a-3.6e** in Tween 80 emulsions were investigated against HT29 human colorectal carcinoma cells. Figure 3.5 compares the effects of these compounds on the cell line both in the absence and presence of light. It can be seen that all of these compounds are essentially noncytotoxic in the dark, but upon illumination, they exhibit a substantial cytotoxicity. Compound **3.6a** exhibits a good photocytotoxicity with an IC_{50} value of 41 nM. The photocytotoxic potency is comparable with that of its symmetrical analogue **2.11b**. Compound **3.6d** and **3.6e** are significantly more potent with the same IC_{50} value of 17 nM. The

photocytotoxicity of **3.6b** and **3.6c** is significantly lower than that of **3.6a**, **3.6d**, and **3.6e**. The corresponding IC_{50} and IC_{90} values are compiled in Table 3.2. The results show that the photoactivity follows the order **3.6d** ≈ **3.6e** > **3.6a** > **3.6c** > **3.6b**.

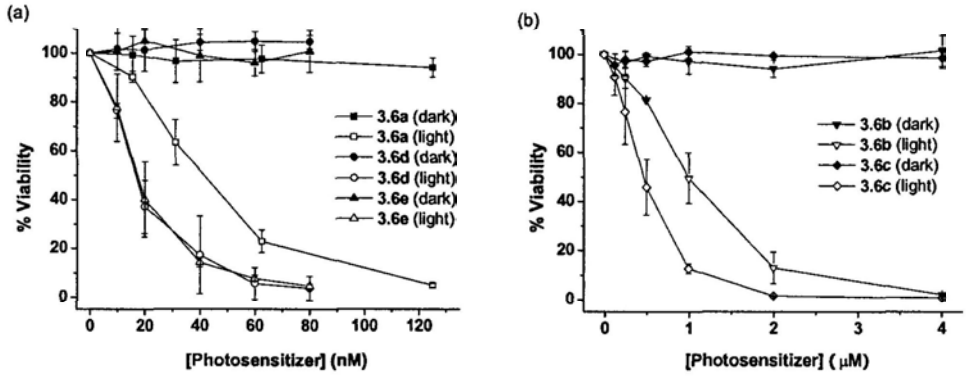

Figure 3.5. Effects of **3.6a-3.6e** on HT29 cells in the absence (closed symbol) and presence (open symbol) of light (λ > 610 nm, 40 mW cm^{-2}, 48 J cm^{-2}). Data are expressed as mean values ± S.E.M. of three independent experiments each performed in quadruplicate.

Table 3.2. IC_{50} and IC_{90} values of compounds **3.6a-3.6e** against HT29 cells.[a]

Compound	IC_{50}	IC_{90}
3.6a	41 nM	107 nM
3.6b	1.0 μM	2.60 μM
3.6c	0.47 μM	1.26 μM
3.6d	17 nM	51 nM
3.6e	17 nM	52 nM

[a] Defined as the dye concentrations required to kill 50% and 90% of the cells, respectively, in the presence of light (λ > 610 nm, 40 mW cm^{-2}, 48 J cm^{-2}).

To account for their different photocytotoxicity, their aggregation behavior in DMEM culture medium was examined by absorption and fluorescence spectroscopic methods. As shown in Figure 3.6(a), the Q bands of compounds **3.6a-3.6e** remain sharp and intense. It indicates that all of these compounds are essentially non-aggregated in the culture medium. This conclusion is also supported by their fluorescence spectra (Figure 3.6(b)). An intense fluorescence emission can be observed for all the compounds except **3.6c**, which is non-fluorescent due to the strong ICT process. Similar results were observed in DMF. Therefore, these results showing their similar aggregation tendency cannot explain why these compounds show different photocytotoxicity.

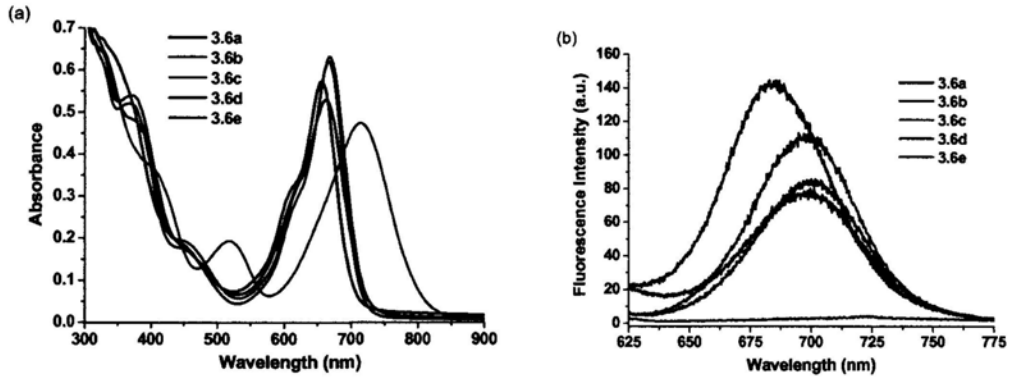

Figure 3.6. Electronic absorption (a) and fluorescence emission spectra (excited at 610 nm) (b) of **3.6a-3.6e** (8 μM), formulated with 0.05% Tween 80 in the DMEM culture medium.

We then performed fluorescence microscopic studies to investigate the cellular uptake of these compounds. HT29 cells were incubated respectively with all these compounds (2 μM) for 2 h. Upon excitation at 633 nm, the bright field and

fluorescence images of the cells were then captured (Figure 3.7(a)), and the intracellular fluorescence intensities were determined (Figure 3.7(b)). It was found that compounds **3.6d** and **3.6e** showed much stronger intracellular fluorescence throughout the cytoplasm. The apparent intensity followed the order: **3.6d** ≈ **3.6e** > **3.6a** > **3.6b** > **3.6c**, which is generally in agreement with the trend in photocytotoxicity except **3.6c**. Since **3.6c** is non-fluorescent in the medium, no fluorescence would be observed even if **3.6c** is present in the cytoplasm. Therefore, it is inappropriate to use this method to evaluate the cellular uptake of **3.6c**. Another method should be employed to measure its cellular uptake. However, in the light of the low photocytotoxicity of **3.6c**, we put our focus on the highly photocytotoxic compounds **3.6a**, **3.6d**, and **3.6e**.

(a)

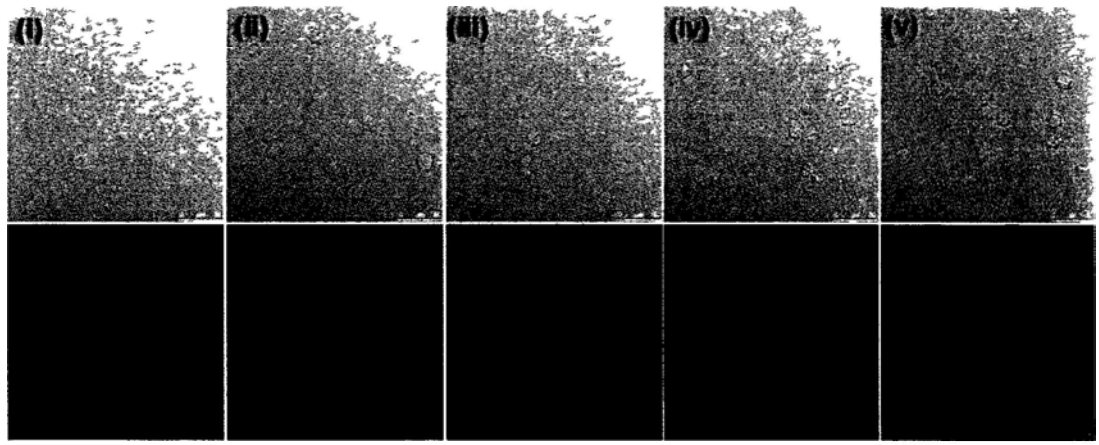

(b)

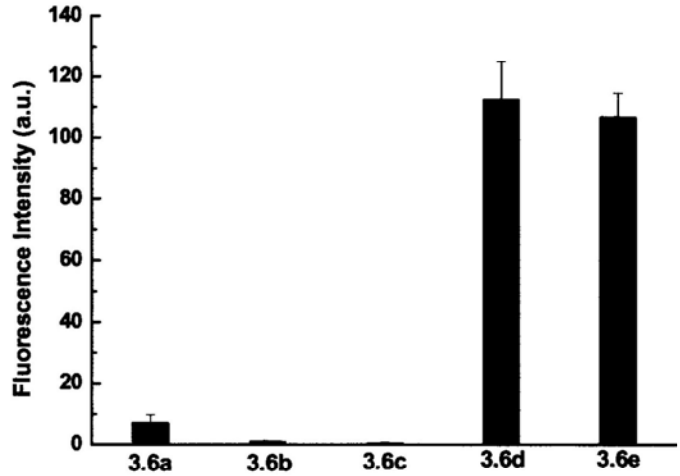

Figure 3.7. (a) Visualization of bright field (upper row) and intracellular fluorescence (lower row) images of HT29 cells after incubation with (i) **3.6a**, (ii) **3.6b**, (iii) **3.6c**, (iv) **3.6d**, and (v) **3.6e** (2 μM) for 2 h. (b) Comparison of the intracellular fluorescence intensity of compounds **3.6a-3.6e**. Data are expressed as the mean ± standard deviation (number of cells = 50).

Owing to the high photocytotoxicity of compounds **3.6a**, **3.6d**, and **3.6e**, their subcellular localization was also investigated. The cells were stained respectively with LysoTracker DND 26, MitoTracker Green FM, and ER-Tracker Green, which

are specific fluorescence dyes for lysosomes, mitochondria, and endoplasmic reticulum, respectively. As shown in Figure 3.8, the fluorescence caused by the ER-Tracker Green (excited at 488 nm, monitored at 510-570 nm) is well superimposed with the fluorescence caused by **3.6a** (excited at 633 nm, monitored at 670-720 nm), indicating that **3.6a** has a strong and selective affinity to the endoplasmic reticulum. By contrast, the fluorescence images of **3.6a** and the LysoTracker (or MitoTracker) cannot be overlapped well, which indicates that **3.6a** is not localized in the lysosomes and the mitochondria. For compound **3.6d**, the fluorescence caused by the LysoTracker Green is well superimposed with the fluorescence caused by **3.6d**, while the fluorescence of the ER-Tracker or MitoTracker cannot be overlapped well with that of **3.6d** (Figure 3.9). It indicates that **3.6d** has a strong and selective affinity to the lysosome. It is well known that the interior of the lysosome is acidic, while compound **3.6d** contains an amine group. Therefore, **3.6d** is preferentially localized in the lysosome of the cells. For compound **3.6e**, the fluorescence is clearly concentrated on the membrane of the cells. The fluorescence of ER-Tracker, LysoTracker, and Mitotracker cannot be overlapped well with that of **3.6e** (Figure 3.10). The results show that compounds **3.6a**, **3.6d**, and **3.6e** localize at various cellular compartments. Compound **3.6a**, **3.6d**, and **3.6e** show a strong and selective affinity to the endoplasmic reticulum, lysosome, and membrane of the cells, respectively.

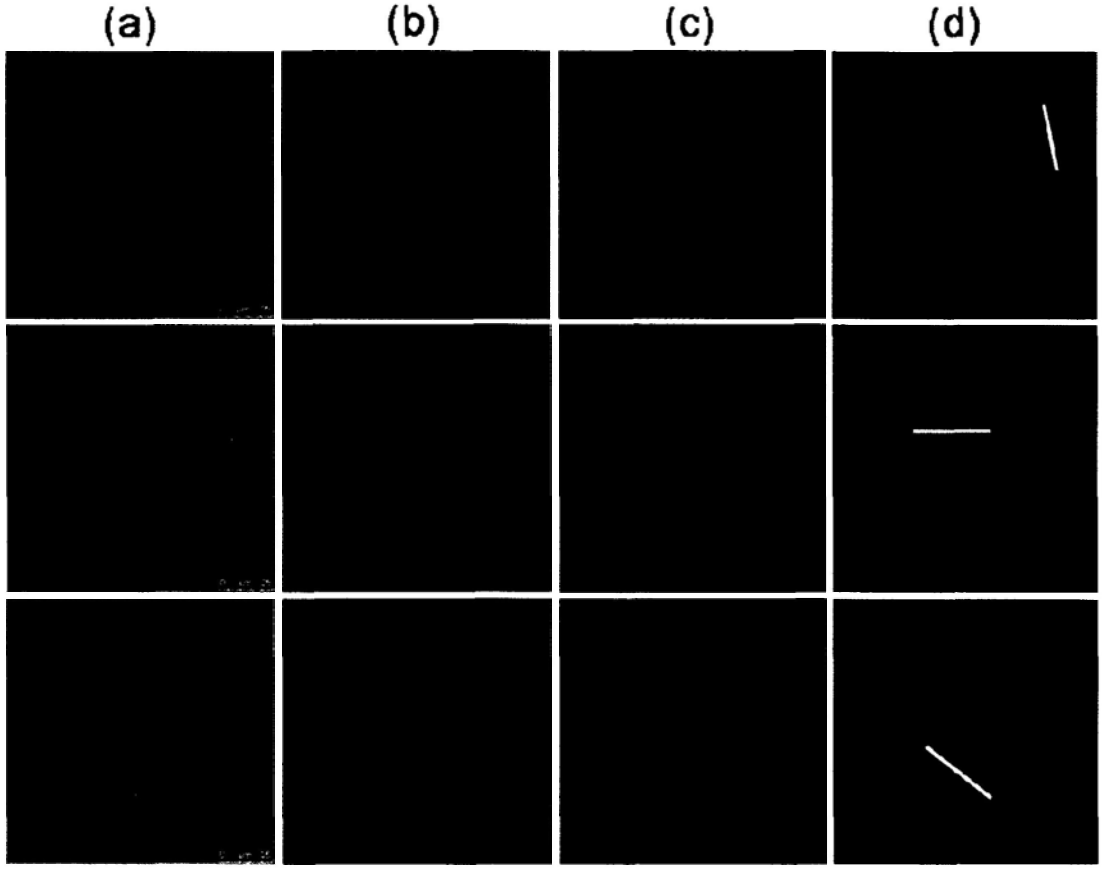

Figure 3.8. Visualization of intracellular fluorescence of HT29 cells using filter sets specific for ER-Tracker (top), LysoTracker (middle), or MitoTracker (bottom) (shown in column (b), in green), and **3.6a** (shown in column (c), in red). The corresponding superimposed images are given in column (d), while the bright field images are shown in column (a).

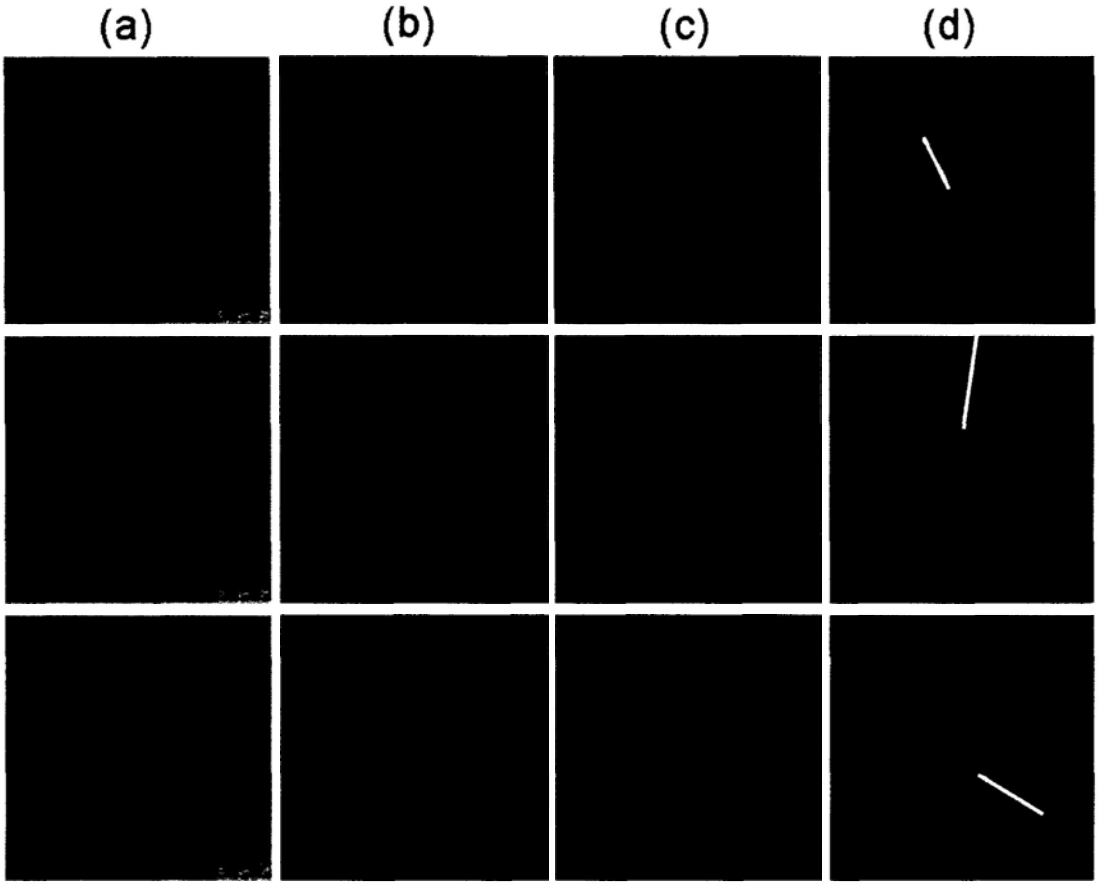

Figure 3.9. Visualization of intracellular fluorescence of HT29 cells using filter sets specific for ER-Tracker (top), LysoTracker (middle), or MitoTracker (bottom) (shown in column (b), in green), and **3.6d** (shown in column (c), in red). The corresponding superimposed images are given in column (d), while the bright field images are shown in column (a).

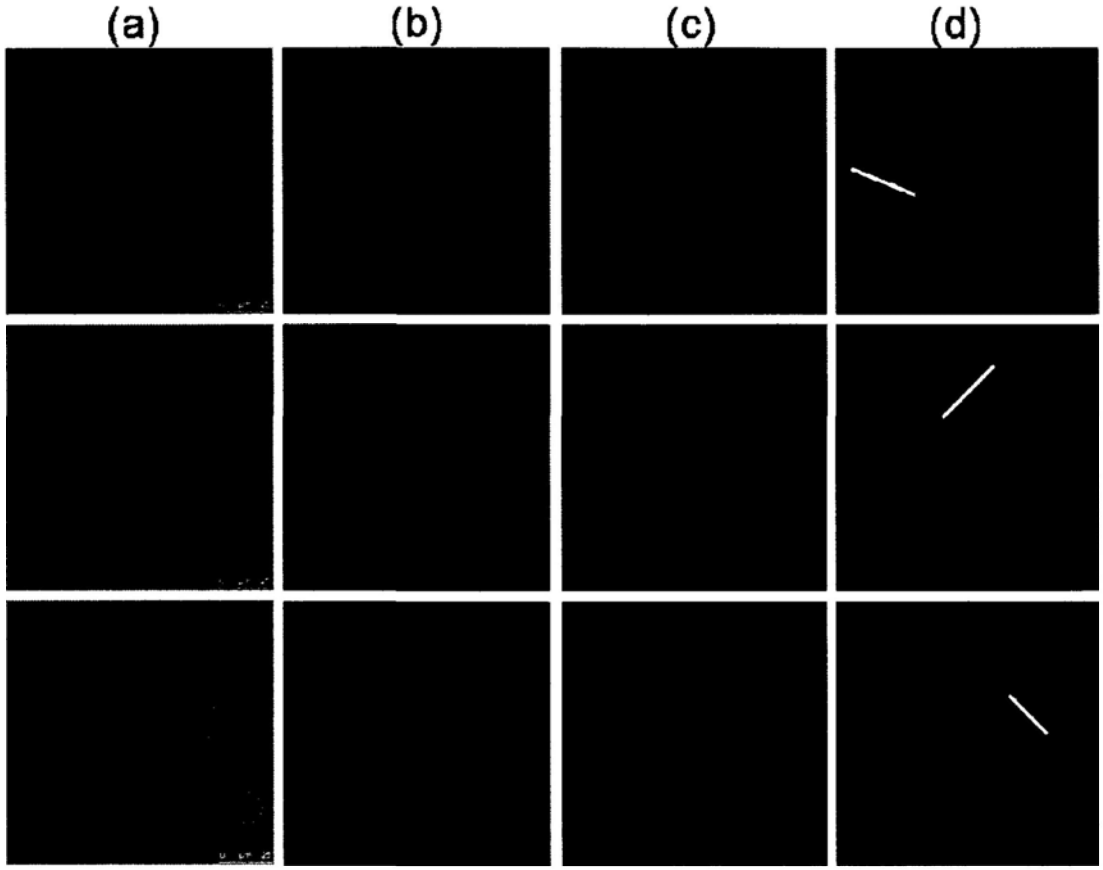

Figure 3.10. Visualization of intracellular fluorescence of HT29 cells using filter sets specific for ER-Tracker (top), LysoTracker (middle), or MitoTracker (bottom) (shown in column (b), in green), and **3.6e** (shown in column (c), in red). The corresponding superimposed images are given in column (d), while the bright field images are shown in column (a).

3.3 Conclusion

In conclusion, we have prepared and characterized a series of unsymmetrical distyryl BODIPYs. Their aggregation behavior in the culture medium, cellular uptake, subcellular localization, and in vitro photodynamic activities have also been evaluated and compared. Compounds **3.6a**, **3.6d**, and **3.6e** are highly potent photosensitizers, which show extremely high photocytotoxicity and high cellular

uptake. It is interesting that they localize at various cellular compartments. Compounds **3.6a**, **3.6d**, and **3.6e** show a strong and selective affinity to the endoplasmic reticulum, lysosome, and membrane of the cells, respectively.

3.4 Experimental Section

3.4.1 General

Experimental details regarding the purification of solvents, instrumentation, and in vitro studies are described in Section 2.4.1. The preparation of diiodo BODIPY **2.6** and benzaldehyde **2.9c** are also reported in Section 2.4.3.

3.4.2 Synthesis

Monostyryl BODIPY 3.1. A mixture of distyryl BODIPY **2.6** (0.29 g, 0.4 mmol), 3,4-bis(triethylene glycol monomethyl ether) substituted benzaldehyde **2.9c** (0.17 g, 0.4 mmol), glacial acetic acid (0.4 mL, 7.0 mmol), and piperidine (0.5 mL, 5.1 mmol) in toluene (40 mL) was refluxed for 2 h. The water formed during the reaction was removed azeotropically with a Dean-Stark apparatus. The mixture was concentrated under reduced pressure. The residue was purified by silica gel column chromatography using $CHCl_3$ as the eluent. The purple fraction was collected and rotary evaporated. It was further purified by size exclusion chromatography with Bio-beads S-X1 beads using THF as the eluent to afford a purple solid (78 mg, 19%). ^{1}H NMR (400 MHz, CD_2Cl_2): δ 8.05 (d, J = 16.8 Hz, 1 H, CH=CH), 7.47 (d, J = 16.8 Hz, 1 H, CH=CH), 7.23 (d, J = 8.4 Hz, 1 H, ArH), 7.19 (d, J = 8.8 Hz, 1 H,

ArH), 7.18 (s, 1 H, ArH), 7.09 (d, J = 8.8 Hz, 2 H, ArH), 6.96 (d, J = 8.4 Hz, 2 H, ArH), 4.19-4.25 (m, 6 H, OCH_2), 3.85-3.89 (m, 6 H, OCH_2), 3.69-3.72 (m, 6 H, OCH_2), 3.59-3.65 (m, 12 H, OCH_2), 3.49-3.53 (m, 6 H, OCH_2), 3.35 (s, 3 H, OCH_3), 3.33 (s, 3 H, OCH_3), 3.32 (s, 3 H, OCH_3), 1.52 (s, 3 H, CH_3), 1.48 (s, 3 H, CH_3); $^{13}C\{^1H\}$ NMR (100.6 MHz, $CDCl_3$): δ 159.9, 156.8, 150.4, 149.1, 146.2, 145.2, 140.4, 139.1, 132.8, 132.4, 130.5, 129.4, 127.2, 122.1, 117.1, 115.6, 114.3, 113.6, 86.2, 82.5, 72.1, 71.0, 70.8, 70.7, 70.6, 69.9, 69.8, 69.7, 69.1, 68.8, 67.7, 59.2, 17.8, 17.4, 16.3; MS (ESI): isotopic clusters peaking at *m/z* 1173 {100%, $[M + Na]^+$} and 1189 {45%, $[M + K]^+$}; HRMS (ESI): *m/z* calcd for $C_{47}H_{62}BF_2I_2N_2NaO_{12}$ $[M + Na]^+$: 1173.2424, found:1173.2430.

Mesylated 2-N,N-dimethylaminoethanol 3.4.[4] Methylsulfonyl chloride (**3.3**) (2.75 g, 24 mmol) was added dropwise into a solution of 2-N,N-dimethylaminoethanol (**3.2**) (1.78g, 20 mmol) in CH_2Cl_2 (50 mL) at 0 °C. The mixture was stirred for 2 h, then the white solid formed was filtrated and rinsed with CH_2Cl_2 (100 mL) (3.71g, 91%). ^1H NMR (400 MHz, D_2O): δ 4.65 (t, J = 5.2 Hz, 2 H, OCH_2), 3.59 (t, J = 5.2 Hz, 2 H, NCH_2), 3.26 (s, 3 H, CH_3), 2.95 (s, 6 H, NCH_3).

Amino-substituted benzaldehyde 3.5d.[5] A mixture of 4-hydroxybenzaldehyde (**2.1**) (1.83 g, 15 mmol), mesylated 2-N,N-dimethylaminoethanol **3.4** (3.67 g, 18 mmol), and K_2CO_3 (10.35 g, 75 mmol) in acetone (200 mL) was refluxed for 2 days. The reaction mixture was concentrated in vacuo. The residue was mixed with water (50 mL), then the mixture was extracted with CH_2Cl_2 (50 mL × 3). The combined organic portion was washed with saturated brine (50 mL), dried over anhydrous

$MgSO_4$, and then evaporated in vacuo. The crude product was purified by silica gel column chromatography using CH_2Cl_2/MeOH (15:1, v/v) as the eluent to give a colorless oil (1.51 g, 52 %). ^{1}H NMR (400 MHz, $CDCl_3$): δ 9.89 (s, 1 H, CHO), 7.84 (d, J = 8.8 Hz, 2 H, ArH), 7.03 (d, J = 8.8 Hz, 2 H, ArH), 4.15 (t, J = 5.6 Hz, 2 H, OCH_2), 2.77 (t, J = 5.6 Hz, 2 H, NCH_2), 2.35 (s, 6 H, NCH_3).

Distyryl BODIPY 3.6a. According to the procedure described for monostyryl BODIPY **3.1**, a mixture of **3.1** (99.5 mg, 0.087 mmol), benzaldehyde (**3.5a**) (92 mg, 0.87 mmol), glacial acetic acid (0.45 mL, 7.9 mmol), and piperidine (0.63 mL, 6.4 mmol) in toluene (30 mL) was refluxed for 2 h. The blue crude product was purified by silica gel column chromatography using $CHCl_3$ as the eluent, followed by size exclusion chromatography with Bio-beads S-X1 beads using THF as the eluent to afford a greenish solid (21 mg, 20%). ^{1}H NMR (400 MHz, CD_2Cl_2): δ 8.15 (d, J = 16.4 Hz, 1 H, CH=CH), 8.11 (d, J = 16.4 Hz, 1 H, CH=CH), 7.69 (d, J = 15.6 Hz, 1 H, CH=CH), 7.66 (d, J = 7.2 Hz, 2 H, ArH), 7.55 (d, J = 16.8 Hz, 1 H, CH=CH), 7.43 (t, J = 7.2 Hz, 2 H, ArH), 7.37 (d, J = 7.2 Hz, 1 H, ArH), 7.28 (d, J = 8.4 Hz, 1 H, ArH), 7.22 (d, J = 8.8 Hz, 2 H, ArH), 7.21 (s, 1 H, ArH), 7.10 (d, J = 8.8 Hz, 2 H, ArH), 6.98 (d, J = 8.4 Hz, 1 H, ArH), 4.20-4.26 (m, 6 H, OCH_2), 3.86-3.89 (m, 6 H, OCH_2), 3.70-3.72 (m, 6 H, OCH_2), 3.57-3.66 (m, 12 H, OCH_2), 3.48-3.54 (m, 6 H, OCH_2), 3.35 (s, 3 H, OCH_3), 3.34 (s, 3 H, OCH_3), 3.32 (s, 3 H, OCH_3), 1.54 (s, 6 H, CH_3); ^{13}C{^{1}H} NMR (100.6 MHz, $CDCl_3$): δ 159.9, 151.1, 150.6, 149.9, 149.1, 146.7, 145.6, 139.7, 139.3, 139.2, 136.9, 133.7, 133.3, 130.5, 129.6, 129.2, 128.9, 127.7, 127.4, 122.1, 119.0, 117.2, 115.6, 114.4, 113.9, 83.3, 82.8, 72.1, 71.0, 70.8,

70.7, 70.6, 69.9, 69.8, 69.7, 69.2, 68.9, 67.7, 59.2, 59.1, 17.9, 17.8; MS (ESI): isotopic clusters peaking at *m/z* 1261 {100%, $[M + Na]^+$} and 1277 {30%, $[M + K]^+$}; HRMS (ESI): *m/z* calcd for $C_{54}H_{67}BF_2I_2N_2NaO_{12}$ $[M + Na]^+$: 1261.2737, found:1261.2757.

Distyryl BODIPY 3.6b. According to the procedure described for monostyryl BODIPY **3.1**, a mixture of **3.1** (0.13 g, 0.11 mmol), naphthaldehyde (**3.5b**) (0.17 g, 1.09 mmol), glacial acetic acid (0.57 mL, 10.0 mmol), and piperidine (0.79 mL, 8.0 mmol) in toluene (40 mL) was refluxed for 2 h. The blue crude product was purified by silica gel column chromatography using $CHCl_3$ as the eluent, followed by size exclusion chromatography with Bio-beads S-X1 beads using THF as the eluent to afford a greenish solid (20 mg, 12%). ^1H NMR (400 MHz, CD_2Cl_2): δ 9.02 (d, *J* = 16.8 Hz, 1 H, CH=CH), 8.36 (d, *J* = 8.0 Hz, 1 H, ArH), 8.14 (d, *J* = 16.8 Hz, 1 H, CH=CH), 8.00 (d, *J* = 7.2 Hz, 1 H, ArH), 7.92 (d, *J* = 7.6 Hz, 1 H, ArH), 7.90 (d, *J* = 8.0 Hz, 1 H, ArH), 7.78 (d, *J* = 16.8 Hz, 1 H, CH=CH), 7.54-7.62 (m, 4 H, CH=CH, ArH), 7.28 (d, *J* = 8.4 Hz, 1 H, ArH), 7.24 (d, *J* = 8.8 Hz, 2 H, ArH), 7.20 (s, 1 H, ArH), 7.11 (d, *J* = 8.4 Hz, 2 H, ArH), 6.97 (d, *J* = 8.4 Hz, 1 H, ArH), 4.20-4.23 (m, 6 H, OCH_2), 3.86-3.90 (m, 4 H, OCH_2), 3.82 (t, *J* = 4.8 Hz, 2 H, OCH_2), 3.47-3.72 (m, 24 H, OCH_2), 3.36 (s, 3 H, OCH_3), 3.34 (s, 3 H, OCH_3), 3.31 (s, 3 H, OCH_3), 1.58 (s, 3 H, CH_3), 1.56 (s, 3 H, CH_3); $^{13}C\{^1H\}$ NMR (100.6 MHz, $CDCl_3$): δ 159.9, 151.2, 150.6, 150.0, 149.1, 146.6, 145.6, 139.8, 139.3, 135.9, 134.4, 133.9, 133.7, 133.4, 131.8, 130.5, 129.6, 128.8, 127.4, 126.8, 126.1, 126.0, 124.5, 124.0, 122.1, 121.1, 117.2, 115.6, 114.3, 113.8, 83.5, 83.2, 72.0, 71.0, 70.9, 70.8, 70.7, 70.6, 69.8, 69.7,

69.1, 68.8, 67.7, 59.2, 59.1, 17.9, 17.8; MS (ESI): isotopic clusters peaking at *m/z* 1311 {100%, $[M + Na]^+$} and 1327 {40%, $[M + K]^+$}; HRMS (ESI): *m/z* calcd for $C_{58}H_{69}BF_2I_2N_2NaO_{12}$ $[M + Na]^+$: 1311.2893, found:1311.2891.

Distyryl BODIPY 3.6c. According to the procedure described for monostyryl BODIPY **3.1**, a mixture of **3.1** (0.11 g, 0.1 mmol), 4-dimethylaminobenzaldehyde (**3.5c**) (0.15 g, 1.0 mmol), glacial acetic acid (0.52 mL, 9.1 mmol), and piperidine (0.73 mL, 7.4 mmol) in toluene (30 mL) was refluxed for 2 h. The blue crude product was purified by silica gel column chromatography using $CHCl_3$ as the eluent, followed by size exclusion chromatography with Bio-beads S-X1 beads using THF as the eluent to afford a greenish solid (36 mg, 28%). ^1H NMR (400 MHz, CD_2Cl_2): δ 8.25 (d, J = 16.4 Hz, 1 H, CH=CH), 8.02 (d, J = 16.4 Hz, 1 H, CH=CH), 7.56 (d, J = 8.8 Hz, 2 H, ArH), 7.54 (d, J = 16.8 Hz, 1 H, CH=CH), 7.51 (d, J = 16.4 Hz, 1 H, CH=CH), 7.27 (d, J = 8.8 Hz, 1 H, ArH), 7.21 (d, J = 8.4 Hz, 2 H, ArH), 7.28 (d, J = 8.4 Hz, 1 H, ArH), 7.19 (s, 1 H, ArH), 7.08 (d, J = 8.4 Hz, 2 H, ArH), 6.98 (d, J = 8.4 Hz, 1 H, ArH), 6.74 (d, J = 8.8 Hz, 2 H, ArH), 4.19-4.27 (m, 6 H, OCH_2), 3.86-3.89 (m, 6 H, OCH_2), 3.70-3.72 (m, 6 H, OCH_2), 3.57-3.65 (m, 12 H, OCH_2), 3.49-3.54 (m, 6 H, OCH_2), 3.35 (s, 3 H, OCH_3), 3.34 (s, 3 H, OCH_3), 3.31 (s, 3 H, OCH_3), 1.53 (s, 3 H, CH_3), 1.51 (s, 3 H, CH_3); $^{13}C\{^1H\}$ NMR (100.6 MHz, $CDCl_3$): δ 159.7, 151.8, 151.5, 150.0, 149.0, 148.8, 146.5, 144.1, 140.8, 138.0, 137.4, 133.7, 132.9, 130.9, 129.8, 129.6, 127.7, 124.9, 121.7, 117.7, 115.5, 114.5, 114.1, 113.9, 112.2, 83.4, 82.2, 72.0, 71.0, 70.9, 70.8, 70.7, 70.6, 69.9, 69.8, 69.7, 69.1, 68.8, 67.6, 59.2, 59.1, 40.4, 18.0, 17.6; MS (ESI): isotopic clusters peaking at *m/z* 1304 {100%, $[M + Na]^+$} and

1321 {40%, $[M + K]^+$}; HRMS (ESI): *m/z* calcd for $C_{56}H_{72}BF_2I_2N_3NaO_{12}$ $[M + Na]^+$: 1304.3159, found:1304.3165.

Distyryl BODIPY 3.6d. According to the procedure described for monostyryl BODIPY **3.1**, a mixture of **3.1** (96.2 mg, 0.083 mmol), amino-substituted benzaldehyde **3.5d** (0.16 g, 0.83 mmol), glacial acetic acid (0.5 mL, 8.8 mmol), and piperidine (0.73 mL, 7.1 mmol) in toluene (30 mL) was refluxed for 2 h. The blue crude product was purified by silica gel column chromatography using $CHCl_3$ as the eluent, followed by size exclusion chromatography with Bio-beads S-X1 beads using THF as the eluent to afford a greenish solid (31 mg, 28%). ^1H NMR (400 MHz, CD_2Cl_2): δ 8.15 (d, *J* = 16.8 Hz, 1 H, CH=CH), 8.07 (d, *J* = 16.4 Hz, 1 H, CH=CH), 7.61 (d, *J* = 8.8 Hz, 2 H, ArH), 7.56 (d, *J* = 16.8 Hz, 1 H, CH=CH), 7.53 (d, *J* = 16.4 Hz, 1 H, CH=CH), 7.28 (d, *J* = 8.4 Hz, 1 H, ArH), 7.21 (d, *J* = 8.8 Hz, 2 H, ArH), 7.19 (s, 1 H, ArH), 7.09 (d, *J* = 8.8 Hz, 2 H, ArH), 6.98 (d, *J* = 8.4 Hz, 1 H, ArH), 6.96 (d, *J* = 8.8 Hz, 2 H, ArH), 4.20-4.26 (m, 6 H, OCH_2), 4.12 (t, *J* = 5.6 Hz, 2 H, OCH_2), 3.88 (t, *J* = 4.4 Hz, 6 H, OCH_2), 3.70-3.72 (m, 6 H, OCH_2), 3.57-3.66 (m, 12 H, OCH_2), 3.47-3.54 (m, 6 H, OCH_2), 3.35 (s, 3 H, OCH_3), 3.34 (s, 3 H, OCH_3), 3.31 (s, 3 H, OCH_3), 2.73 (t, *J* = 5.6 Hz, 2 H, NCH_2), 2.32 (s, 6 H, NCH_3), 1.53 (s, 6 H, CH_3),; $^{13}C\{^1H\}$ NMR (100.6 MHz, $CDCl_3$): δ 160.0, 159.8, 150.6, 150.4, 150.3, 149.0, 146.0, 145.7, 139.2, 139.1, 138.7, 133.4, 133.3, 130.5, 129.7, 129.6, 129.3, 127.5, 121.9, 117.3, 116.8, 115.6, 115.0, 114.3, 114.0, 82.9, 72.0, 71.0, 70.9, 70.8, 70.7, 70.6, 69.9, 69.8, 69.7, 69.1, 68.8, 67.7, 66.1, 59.2, 59.1, 58.3, 46.0, 17.8; MS (ESI): isotopic clusters peaking at *m/z* 1326 {95%, $[M + H]^+$}and 1347 {10%, [M +

Na]$^+$}; HRMS (ESI): *m/z* calcd for $C_{58}H_{77}BF_2I_2N_3O_{13}$ [M + H]$^+$: 1326.3621, found:1326.3592.

Distyryl BODIPY 3.6e. A mixture of **3.6d** (48.1 mg, 0.036 mmol) and a large excess of iodomethane (2 mL) in chloroform (15 mL) was stirred at room temperature for 30 min. Diethyl ether (50 mL) was then added for precipitation. The precipitate formed was collected by filtration, washed with diethyl ether, and then dried in vacuo (33 mg, 62%). ^{1}H NMR (400 MHz, CD_2Cl_2): δ 8.14 (d, J = 17.2 Hz, 1 H, CH=CH), 8.09 (d, J = 17.3 Hz, 1 H, CH=CH), 7.65 (d, J = 8.8 Hz, 2 H, ArH), 7.59 (d, J = 16.8 Hz, 1 H, CH=CH), 7.54 (d, J = 16.4 Hz, 1 H, CH=CH), 7.26 (d, J = 8.4 Hz, 1 H, ArH), 7.21 (d, J = 8.8 Hz, 2 H, ArH), 7.20 (s, 1 H, ArH), 7.10 (d, J = 8.8 Hz, 2 H, ArH), 7.03 (d, J = 8.8 Hz, 1 H, ArH), 6.98 (d, J = 8.4 Hz, 2 H, ArH), 4.56 (br s, 2 H, NCH_2), 4.20-4.26 (m, 6 H, OCH_2), 4.04 (t, J = 4.4 Hz, 2 H, OCH_2), 3.87-3.89 (m, 6 H, OCH_2), 3.70-3.72 (m, 6 H, OCH_2), 3.59-3.64 (m, 12 H, OCH_2), 3.50-3.54 (m, 6 H, OCH_2), 3.37 (s, 9 H, OCH_3), 3.35 (s, 3 H, OCH_3), 3.34 (s, 3 H, OCH_3), 3.31 (s, 3 H, OCH_3), 1.54 (s, 6 H, CH_3),; ^{13}C{^{1}H} NMR (100.6 MHz, $CDCl_3$): δ 159.8, 158.1, 150.5, 150.1, 148.9, 146.1, 145.9, 139.3, 139.0, 138.4, 133.4, 133.3, 130.8, 130.3, 129.6, 129.3, 127.3, 121.7, 117.5, 117.2, 115.6, 115.0, 114.3, 114.2, 83.1, 82.9, 72.0, 71.9, 70.9, 70.7, 70.6, 70.5, 70.4, 69.8, 69.7, 69.6, 69.2, 68.8, 67.6, 65.1, 62.4, 59.1, 59.0, 54.5, 54.4, 17.8, 17.7; MS (ESI): an isotopic cluster peaking at *m/z* 1340 {100%, [M – I]$^+$}; HRMS (ESI): *m/z* calcd for $C_{59}H_{79}BF_2I_2N_3O_{13}$ [M – I]$^+$: 1340.3758, found: 1340.3780.

3.5 References

1 (a) Yogo, T.; Urano, Y.; Ishitsuka, Y.; Maniwa, F.; Nagano, T. *J. Am. Chem. Soc.* **2005**, *127*, 12162. (b) Atilgan, S.; Ekmekci, Z.; Dogan, A. L.; Guc, D.; Akkaya, E. U. *Chem. Commun.* **2006**, 4398. (c) Ozlem, S.; Akkaya, E. U. *J. Am. Chem. Soc.* **2009**, *131*, 48. (d) Erbas, S.; Gorgulu, A.; Kocakusakogullari, M.; Akkaya, E. U. *Chem. Commun.* **2009**, 4956. (e) Lim, S. H.; Thivierge, C.; Nowak-Sliwinska, P.; Han, J.; van den Bergh, H.; Wagnières, G.; Burgess, K.; Lee, H. B. *J. Med. Chem.* **2010**, *53*, 2865..

2 Scalise, I.; Durantini, E. N. *Bioorg. Med. Chem.* **2005**, *13*, 3037.

3 Maree, M. D.; Kuznetsova, N.; Nyokong, T. *J. Photochem. Photobiol. A: Chem.* **2001**, *140*, 117.

4 Kraemer, N. H.; Linde, H. F. G. *Arch. Pharm.* **1991**, *324,* 527.

5 Strohfeldt, K.; Muller-Bunz, H.; Pampillon, C.; Sweeney, N. J.; Tacke, M. *Eur. J. Inorg. Chem.* **2006**, *22*, 4621.

Chapter 4

A Ratiometric Near-Infrared pH-Responsive Fluorescent Dye Based on Distyryl BODIPY

4.1 Introduction

Development of organic chromophores with spectral properties in the near-infrared (NIR) and red visible regions continues to attract considerable research interest. These chromophores with controllable photophysical properties in the 650-900 nm spectral region are potentially useful for a diverse range of material and biological applications, such as optical data storage,[1] photoconductors,[2] electrochromic devices,[3] chemosensors,[4] immunoassay labels and bioconjugated probes,[5] and in vitro and in vivo imaging agents.[6] Specifically, NIR dyes are promising candidates as biomedical diagnostic agents due to the low auto-fluorescence of endogenous chromophores in this spectral region and the deeper light penetration.[7]

Biochemical processes frequently involve protonation and deprotonation of biomolecules with concomitant changes in the pH of the surrounding.[4b] Hence, H^+ is one of the most important targets among the species of interests in biological systems. Currently, several classes of pH-responsive dyes have been described, such as fluoresceins,[8] tricarbocyanines,[4b,9] BODIPYs,[10] and aza-BODIPYs.[11] Distyryl BODIPYs are desirable candidates for this application because their absorption and

fluorescence emission maxima appear in the NIR region. They also have good solubility and high photo- and therm-stability, and can be chemically modified readily.[12] We report herein a novel NIR pH-responsive fluorescent dye based on a distyryl BODIPY, which is connected to two pH-sensitive dimethylamino groups at the 2- and 6-positions via an arylethynyl bridge.

4.2 Results and Discussion

4.2.1 Molecular Design and Chemical Synthesis

It is well known that dimethylamino group has a very strong electron-donating ability and is acid-sensitive. If it is conjugated to a distyryl BODIPY skeleton, a strong intramolecular charge transfer (ICT) will occur resulting in a remarkably red shift in the absorption and fluorescence positions. When this group is protonated, the electron-donating ability is vanished. Hence, the ICT process is inhibited and the absorption and fluorescence emission will shift to the normal range. Based on this consideration, distyryl BODIPY **4.2** has been designed and synthesized.

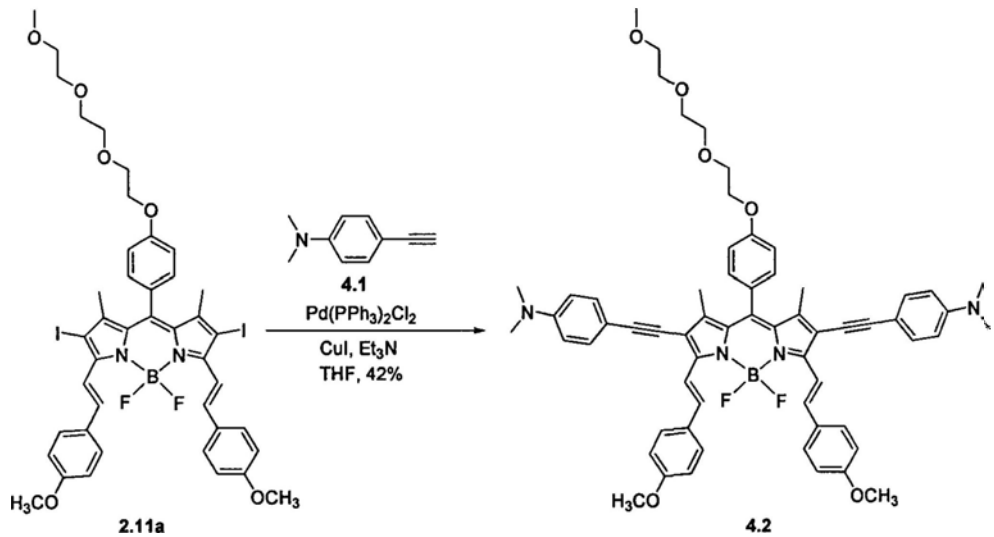

Scheme 4.1. Synthesis of the target compound **4.2**.

As shown in Scheme 4.1, this compound was prepared readily by palladium-catalyzed Sonogashira coupling reaction of distyryl BODIPY **2.11a** with 4-dimethylaminophenylethyne (**4.1**). It was purified by silica gel column chromatography and fully characterized with various spectroscopic methods and elemental analysis.

Figure 4.1 shows the ^{1}H NMR spectrum of compound **4.2** in CD_2Cl_2. The downfield signals from 6.6 to 8.6 ppm are due to the aryl and vinyl protons. The upfield signals from 2.9 to 4.3 ppm are attributed to the triethylene glycol chain, methoxy groups, and N-methyl protons. The singlet around 1.6 ppm is due to the methyl protons at the pyrrole rings.

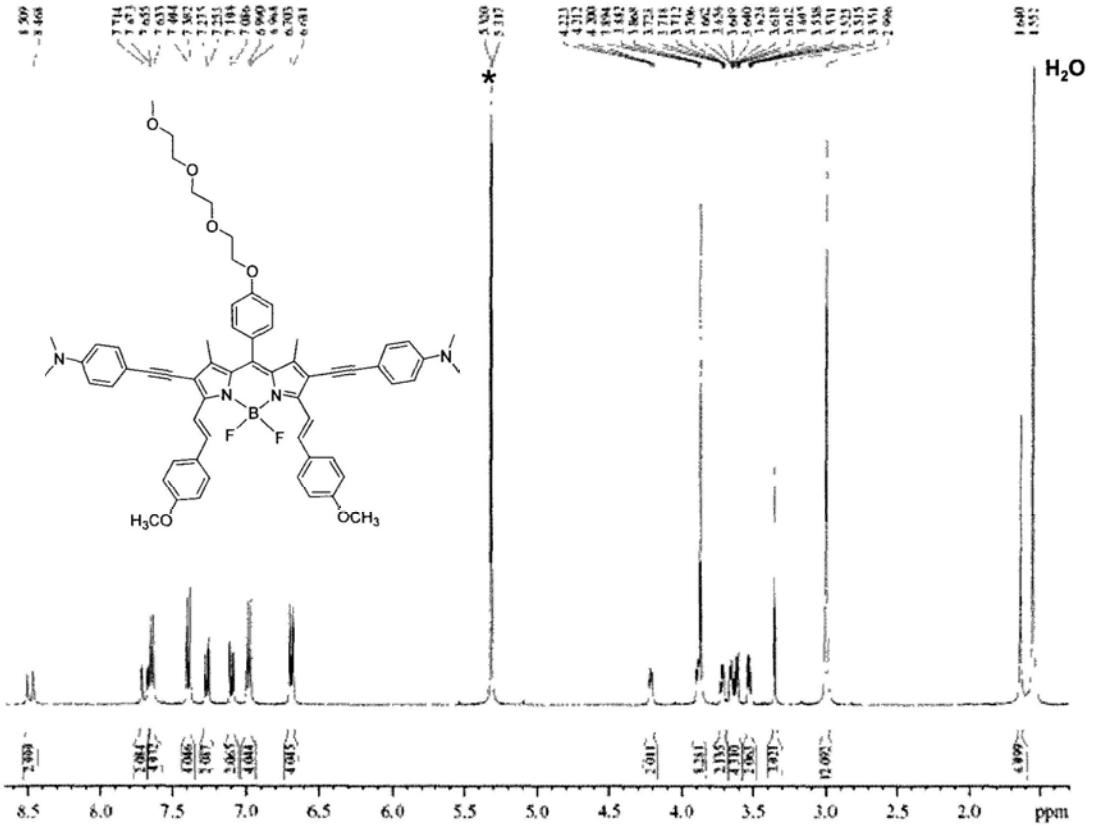

Figure 4.1. ^{1}H NMR spectrum of **4.2** in CD_2Cl_2; * indicates residual solvent signal.

The $^{13}C\{^1H\}$ NMR spectra of this compound showed clearly the expected number of signals. This compound was further characterized with ESI mass spectrometry. The isotopic distribution as well as the exact mass for the $[M + H]^+$ species was in good agreement with the calculated one.

4.2.2 pH-Responsive Photophysical Properties of 4.2 in $CHCl_3$

The electronic absorption spectrum of **4.2** was first recorded in $CHCl_3$. It showed a Soret band at 401 nm with a shoulder at 365 nm, an intense and sharp Q band at 708 nm, together with a vibronic band at 510 nm. The Q band strictly followed the Lambert Beer's law showing that the compound is not significantly aggregated in $CHCl_3$ (Figure 4.2). Upon addition of trifluoroacetic acid (TFA), the Q band at 708 nm gradually decreased in intensity and two new bands at 622 and 678 nm emerged giving three isosbestic points at 409, 475, and 554 nm (Figure 4.3). Furthermore, the color of the solution turned from grass green to blue green upon addition of 140 mM of TFA (Figure 4.4). It can be explained that in the presence of TFA, the 4-dimethylamino groups were protonated. ICT process was inhibited resulting in a blue shift.

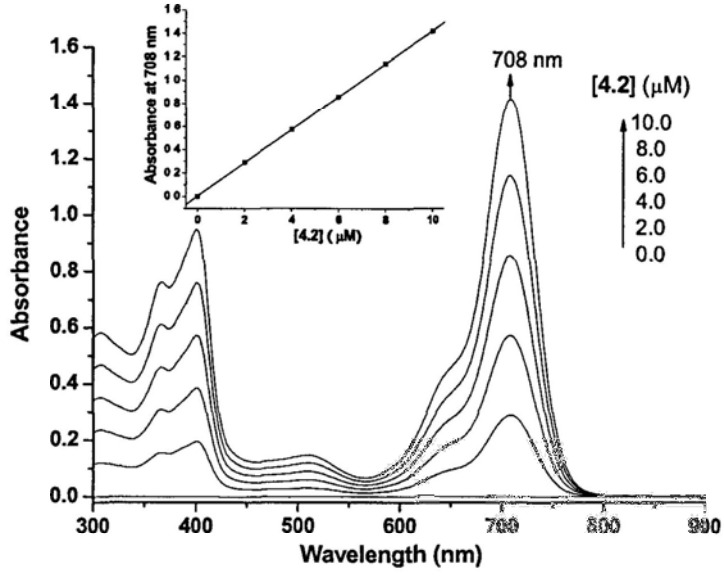

Figure 4.2. Electronic absorption spectra of **4.2** at various concentrations in $CHCl_3$. The inset plots the Q-band absorbance versus the concentration of **4.2**.

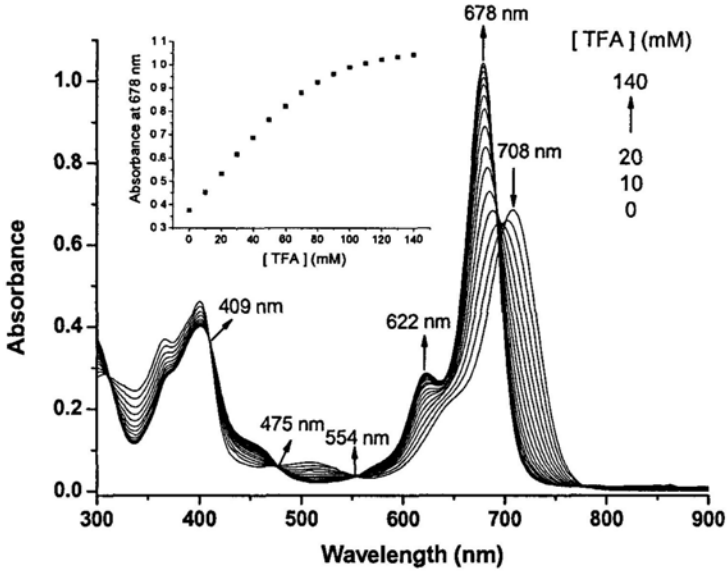

Figure 4.3. Change in absorption spectrum of **4.2** (5 μM) in $CHCl_3$ upon addition of TFA (0-140 mM). The inset plots the Q-band absorbance at 678 nm versus the concentration of TFA.

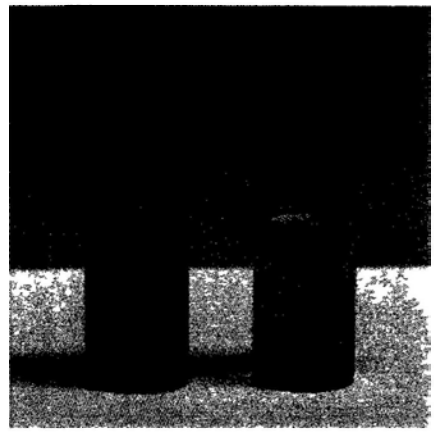

Figure 4.4. The color observed for a solution of **4.2** (10 μM) in $CHCl_3$ in the absence (left) and presence (right) of 140 mM of TFA.

In the absence of TFA, compound **4.2** in $CHCl_3$ gave a weak fluorescence at 736 nm with a fluorescence quantum yield of 0.005, relative to ZnPc in DMF (Φ_F = 0.28).[13] Upon addition of TFA from 0 to 34 mM, the emission shifted to 694 nm and increased in intensity gradually giving a very large blue shift of 42 nm (Figure 4.5). Further addition of TFA (up to 140 mM) further increased the fluorescence intensity at 694 nm. The fluorescence quantum yield reached the value of 0.46 after addition of 140 mM of TFA (Figure 4.6). Moreover, the fluorescence emission turned to bright red (Figure 4.7). The fluorescence enhancement and blue shift of emission maximum further testified that the ICT process was blocked after protonation.

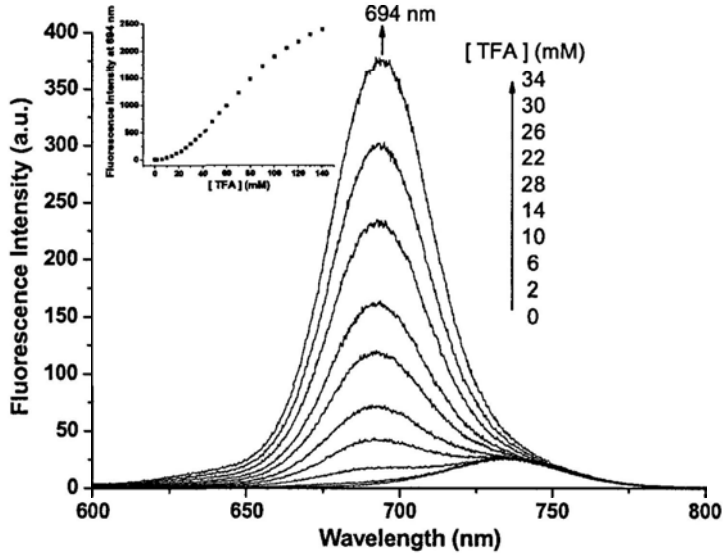

Figure 4.5. Change in fluorescence spectrum (excited at 409 nm) of **4.2** (1 μM) in $CHCl_3$ upon addition of TFA (0-34 mM). The inset plots the fluorescence intensity at 694 nm versus the concentration of TFA.

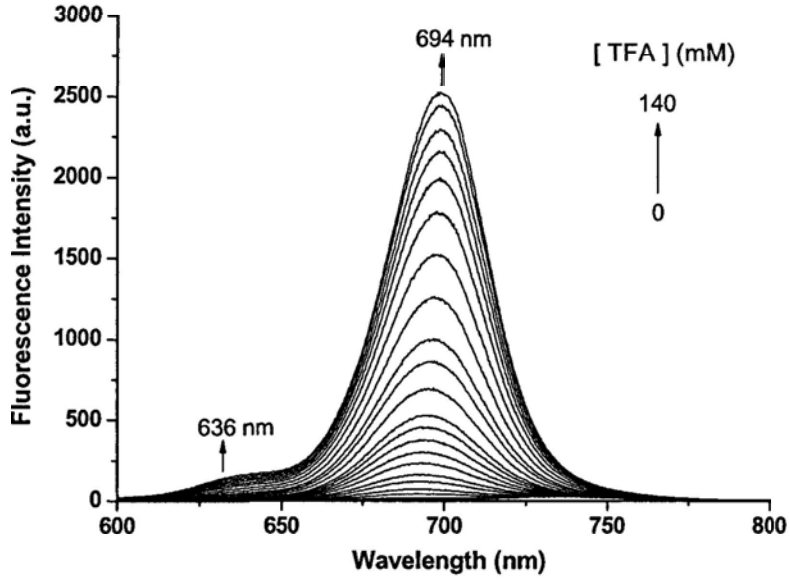

Figure 4.6. Change in fluorescence spectrum (excited at 409 nm) of **4.2** (1 μM) in $CHCl_3$ upon addition of TFA (0-140 mM).

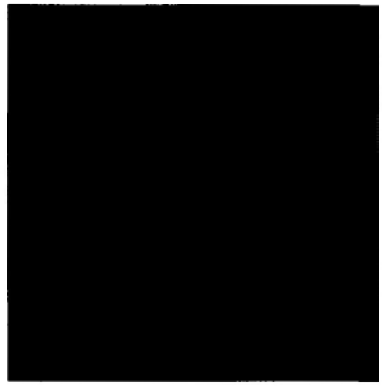

Figure 4.7. The fluorescence observed for a solution of **4.2** (10 μM) in $CHCl_3$ in the absence (left) and presence (right) of 140 mM of TFA.

4.2.3 pH-Responsive Photophysical Properties of 4.2 in H_2O with 0.05% Tween 80

In contrast to the electronic absorption spectrum recorded in $CHCl_3$, the spectrum of **4.2** in H_2O exhibited a very broad Q band indicating that it is highly aggregated in H_2O. Upon addition of 0.05% (v/v) Tween 80, which is a common non-ionic surfactant, the Q band was sharpened showing that the aggregation of **4.2** was significantly reduced (Figure 4.8(a)). In fact, the Q band at 717 nm also strictly followed the Lambert Beer's law (Figure 4.9). It is worth noting that in more polar solvents, such as DMF and H_2O with 0.05% Tween 80, compound **4.2** was nearly non-fluorescent (Figure 4.8(b)). This can be explained by the stronger ICT effect in polar media resulting in a weaker fluorescence.[12b]

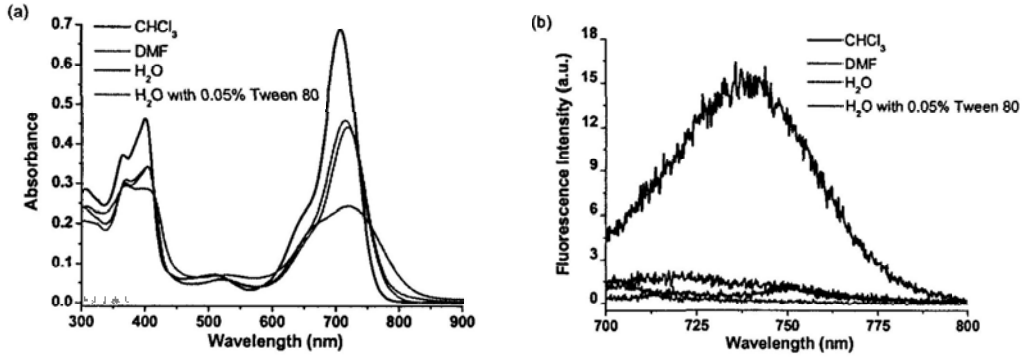

Figure 4.8. Electronic absorption (a) and fluorescence emission spectra (excited at 640 nm) (b) of **4.2** (5 μM) in different solvents.

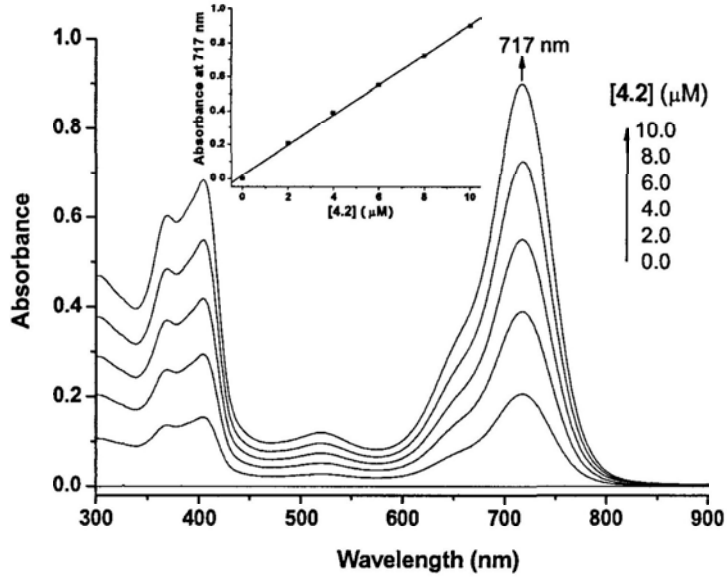

Figure 4.9. Electronic absorption spectra of **4.2** at various concentrations in H_2O with 0.05% Tween 80. The inset plots the Q-band absorbance versus the concentration of **4.2**.

Since compound **4.2** is essentially non-aggregated in H_2O with 0.05% Tween 80, its pH-dependent effects were studied under this condition. Figure 4.10 shows the changes in absorption spectrum of **4.2** at different pH values. With decreasing the pH value from 5.95 to 0.38, the Q band at 717 nm shifted gradually to the blue, giving

two new bands at 628 and 682 nm with three isosbestic points at 423, 481, and 570 nm. The color of the solution also changed from grass green to blue green (Figure 4.11). The results are consistent with those obtained in $CHCl_3$ and can be explained similarly. A sigmoidal plot[14] of the absorbance at 682 nm versus the pH afforded an apparent p*Ka* value of 0.95 ± 0.07 (the inset of Figure 4.10).

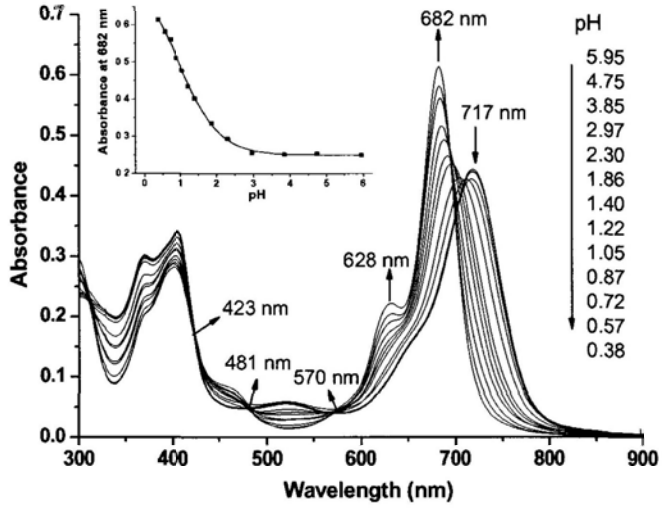

Figure 4.10. Electronic absorption spectra of **4.2** (5 μM) in H_2O with 0.05% Tween 80 at different pH. The inset plots the Q-band absorbance at 682 nm versus the pH value.

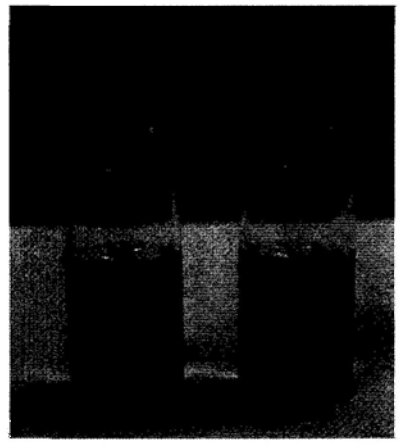

Figure 4.11. The color observed for a solution of **4.2** (10 μM) in H_2O with 0.05% Tween 80 at pH = 5.95 (left) and 0.38 (right).

As shown in Figure 4.12, with decreasing the pH value from 5.95 to 0.38, the fluorescence emissions at 640 and 697 nm gradually enhance and the fluorescence quantum yield finally reaches a value of 0.15 (Table 4.1). The fluorescence of the solution also turns from light blue to bright red (Figure 4.13). As shown in the inset of Figure 4.12, a sigmoidal plot[14] of the fluorescence intensity at 697 nm versus the pH affords an apparent p*Ka* value of 0.83 ± 0.02, which is very close to that obtained from the absorption data. Hence, this compound is pH-responsive not only in organic solvents, but also in aqueous media.

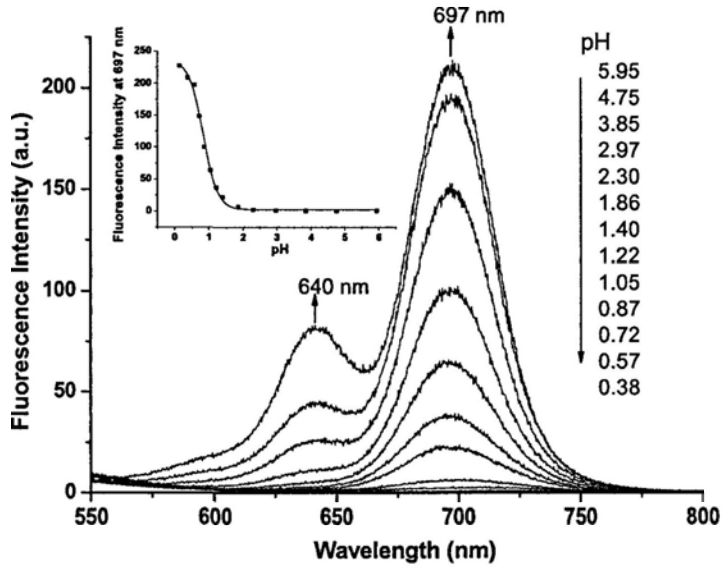

Figure 4.12. Fluorescence emission spectra (excited at 423 nm) of **4.2** (1 μM) in H_2O with 0.05% Tween 80 at different pH. The inset plots the fluorescence emission intensity at 697 nm versus the pH value.

Figure 4.13. The fluorescence observed for a solution of **4.2** (10 μM) in H_2O with 0.05% Tween 80 at pH = 5.95 (left) and 0.38 (right).

Table 4.1. Electronic absorption and fluorescence data for **4.2** in different conditions.

Solvent	Acidic condition	λ_{max} (nm) (log ε)	λ_{em} (nm)	Φ_F[a]
$CHCl_3$	[TFA] = 0	708 (5.15)	736	0.005
	[TFA] = 140 mM	622 (4.76), 678 (5.32)	636, 694	0.46
H_2O with 0.05% Tween 80	pH = 5.95	717 (4.95)	-	-
	pH = 0.38	628 (4.64), 682 (5.09)	640, 697	0.15

[a] Using ZnPc in DMF as the reference (Φ_F = 0.28).

To examine whether these pH-dependent changes are reversible, sodium hydroxide (12 M) and HCl (12 M) aqueous solutions were used to change the pH back and forth between 0.38 and 5.95. The ratios of the absorbance at 682 to 717 nm were measured and the results are shown in Figure 4.14. It is clear that this process has a high reversibility.

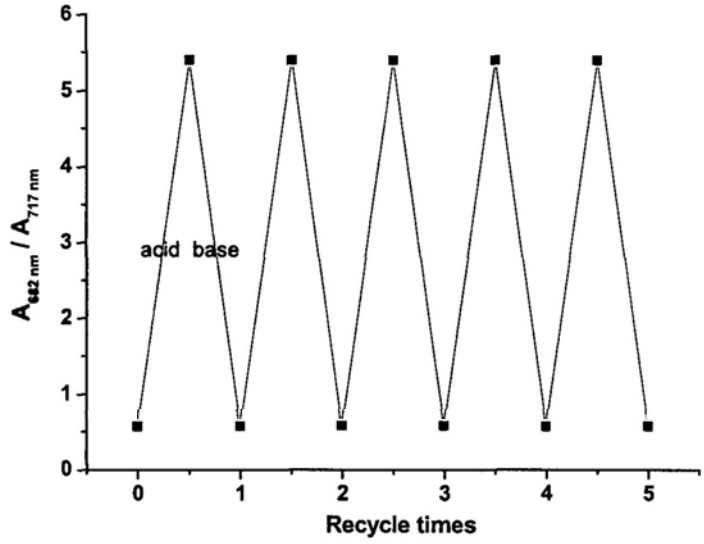

Figure 4.14. Change of the ratio of the absorbance at 682 to 717 nm of **4.2** (5 μM) in H_2O with 0.05% Tween 80. The pH value changes back and forth between 0.38 and 5.95.

4.3 Conclusion

In summary, we have described a novel near-infrared fluorescent dye **4.2** based on distyryl BODIPY. It exhibits pH-responsive changes in absorption and emission properties in $CHCl_3$ and H_2O with 0.05% Tween 80. Moreover, these changes have a high reversibility.

4.4 Experimental Section

4.4.1 General

Experimental details regarding the purification of solvents and instrumentation are described in Section 2.4.1. The preparation of distyryl BODIPY **2.11a** has been reported in Section 2.4.3.

The acidity of the Tween 80 aqueous solution was modulated by adding HCl. All pH measurements were made with a pH meter (Irion Model 420A).

The P*Ka* values were determined by the sigmoidal fit,[9] which is a nonlinear curve fitting model. The function used was the Boltzmann: $y = y_2 + (y_1 - y_2)/\{1 + \exp[(x\text{-}P\mathit{Ka})/dx]\}$, where y is the absorbance or emission intensity of **4.2** at different pH value, y_1 is the initial y value, y_2 is the final y value, and x is the pH value.

4.4.2 Synthesis

Compound 4.2. A mixture of **2.11a** (0.12 g, 0.12 mmol), $Pd(PPh_3)_2Cl_2$ (9 mg, 0.012 mmol), CuI (6 mg, 0.03 mmol), 4-dimethylaminophenylethyne (**4.1**) (52 mg, 0.36 mmol), and triethylamine (5 mL) in THF (30 mL) was stirred at room temperature overnight. The volatiles were removed in vacuo, then the dark green residue was extracted with CH_2Cl_2 (100 mL). The extract was washed with water (30 mL × 2), dried over anhydrous $MgSO_4$, then concentrated under reduced pressure. The mixture was chromatographed using CH_2Cl_2/ethyl acetate (25:1, v/v) as eluent to give a dark green solid (52 mg, 42%). ^{1}H NMR (400 MHz, CD_2Cl_2): δ 8.49 (d, J = 16.4 Hz, 2 H, CH=CH), 7.69 (d, J = 16.4 Hz, 2 H, CH=CH), 7.64 (d, J = 8.8 Hz, 4 H, ArH), 7.39 (d, J = 8.8 Hz, 4 H, ArH), 7.26 (d, J = 8.8 Hz, 2 H, ArH), 7.10 (d, J = 8.8 Hz, 2 H, ArH), 6.98 (d, J = 8.8 Hz, 4 H, ArH), 6.69 (d, J = 8.8 Hz, 4 H, ArH), 4.21 (t, J = 4.4 Hz, 2 H, OCH_2), 3.88 (t, J = 5.2 Hz, 2 H, OCH_2), 3.87 (s, 6 H, OCH_3), 3.73-3.71 (m, 2 H, OCH_2), 3.66-3.61 (m, 4 H, OCH_2), 3.54-3.52 (m, 2 H, OCH_2), 3.35 (s, 3 H, OCH_3), 3.00 (s, 12 H, NCH_3), 1.64 (s, 6 H, CH_3); $^{13}C\{^1H\}$ NMR (100.6

MHz, $CDCl_3$): δ 160.6, 159.6, 151.9, 150.1, 143.7, 138.5, 138.3, 133.2, 132.2, 130.2, 129.9, 129.3, 127.5, 117.2, 115.2, 114.5, 114.4, 112.0, 110.5, 99.5, 82.0, 72.0, 71.0, 70.7, 70.6, 69.8, 67.6, 59.2, 55.5, 40.3, 13.5; MS (ESI): isotopic clusters peaking at *m/z* 1009 {100%, $[M + H]^+$} and 1347 {30%, $[M - F]^+$}; HRMS (ESI): *m/z* calcd for $C_{62}H_{64}BF_2N_4O_6$ $[M + H]^+$: 1009.4881, found:1009.4897. Anal. calcd for $C_{62}H_{65}BF_2N_4O_7$ (**5**·H_2O): C, 72.51; H, 6.38; N, 5.46. Found: C, 72.19; H, 6.00; N, 5.19.

4.5 References

1 Mustroph, H.; Stollenwerk M.; Bressau, V. *Angew. Chem. Int. Ed.* **2006**, *45*, 2016.

2 Law, K. Y. *Chem. Rev.* **1993**, *93*, 449.

3 Rurack, K.; Kollmannsberger M.; Daub, J. *Angew. Chem. Int. Ed.* **2001**, *40*, 385.

4 (a) Zen, J.-M.; Patonay, G. *Anal. Chem.* **1991**, *63*, 2934; (b) Zhang, Z.; Achilefu, S. *Chem. Commun.* **2005**, 5887.

5 Gómez-Hens, A.; Aguilar-Caballos, M. P. *Trends Anal. Chem.* **2004**, *23*, 127.

6 Ntziachristos, V.; Ripoll, J.; Wang, L. V.; Weissleder, R. *Nat. Biotechnol.* **2005**, *23*, 313.

7 Weissleder, R. *Nat. Biotechnol.* **2001**, *19*, 316.

8 (a) Ohkuma, S.; Poole, B. *Proc. Nat Acad. Sci.* **1978**, *5*, 3327. (b) Thomas, J. A.; Buchsbaum, R. N.; Zimniak, A.; Racker, E. *Biochemistry* **1979**, *18*, 2210.

(c) Jones, J. M.; Lorton, S. P.; Bavister, B. D. *Cytometry* **1995**, *19*, 235. (d) Graber, M. L.; DiLillo, D. C.; Friedman, B. L.; Pastoriza-Munoz, E. *Anal. Biochem.* **1986**, *156*, 202. (e) Rink, T. J.; Tsien, R. Y.; Pozzan, T. *J. Cell Biol.* **1982**, *95*, 189. (f) Tsien, R. Y. *Methods Cell Biol.* **1989**, *30*, 127. (g) Bright, G. R.; Fisher, G. W.; Rogowska, J.; Taylor, D. L. *Methods Cell Biol.* **1989**, *30*, 157. (h) Whitaker, J. E.; Haugland, R. P.; Prendergast, F. G. *Anal. Biochem.* **1991**, *194*, 330. (h) Liu, J.; Diwu, Z.; Klaubert, D. H. *Bioorg. Med. Chem. Lett.* **1997**, *7*, 3069.

9 (a) Hilderbrand, S. A.; Kelly, K. A.; Niedre, M. Weissleder, R. *Bioconjugate Chem.* **2008**, *19,* 1635. (b) Tang, B.; Yu, F.; Li, P.; Tong, L.; Duan, X.; Xie, T.; Wang, X. *J. Am. Chem. Soc.* **2009**, *131*, 3016.

10 (a) Kollmannsberger, M.; Gareis, T.; Heinl, S.; Breu, J.; Daub, J. *Angew. Chem. Int. Ed.* **1997**, *36*, 1333. (b) Rurack, K.; Kollmannsberger, M.; Daub, J. *Angew. Chem. Int. Ed.* **2001**, *40*, 385. (c) Baki, C. N.; Akkaya, E. U. *J. Org. Chem.* **2001**, *66,* 1512. (d) Baruah, M.; Qin, W.; Basarić, N.; De Borggraeve, W. M.; Boens, N. *J. Org. Chem.* **2005**, *70*, 4152. (e) Yu, Y.-H.; Descalzo, A. B.; Shen, Z.; Röhr, H.; Liu, Q.; Wang, Y.-W.; Spieles, M.; Li, Y.-Z.; Rurack, K.; You, X.-Z. *Chem. Asia. J.* **2006**, *1*, 176. (f) Bonardi, L.; Ulrich, G.; Ziessel, R. *Org. Lett.* **2008**, *10*, 2183. (g) Deniz, E.; Isbasar, G. C.; Bozdemir, O. A.; Yildirim, L. T.; Siemiarczuk, A.; Akkaya, E. U. *Org. Lett.* **2008**, *10*, 3401. (h) Ziessel, R.; Ulrich, G.; Harriman, A.; Alamiry, M. A. H.; Stewart, B.; Retailleau, P. *Chem. Eur. J.* **2009**, *15*, 1359.

11 (a) McDonnell, S. O.; Hall, M. J.; Allen, L. T.; Byrne, A.; Gallagher, W. M.; O'Shea, D. F. *J. Am. Chem. Soc.* **2005**, *127*, 16360. (b) Hall, M. J.; Allen, L. T.; O'Shea, D. F. *Org. Biomol. Chem.* **2006**, *4*, 776. (c) McDonnell, S. O.; O'Shea, D. F. *Org. Lett.* **2006**, *8*, 3493. (d) Killoran, J.; McDonnell, S. O.; Gallagher, J. F.; O'Shea, D. F. *New J. Chem.* **2008**, *32*, 483. (e) Murtagh, J. M.; Frimannsson, D. O.; O'Shea, D. F. *Org. Lett.* **2009**, *11*, 5386.

12 (a) Loudet, A.; Burgess, K. *Chem. Rev.* **2007**, *107*, 4891. (b) Ulrich, G.; Ziessel, R.; Harriman, A. *Angew. Chem. Int. Ed.* **2008**, *47*, 1184.

13 Scalise, I.; Durantini, E. N. *Bioorg. Med. Chem.* **2005**, *13*, 3037.

14 Killoran, J.; McDonnell, S. O.; Gallagher, J. F.; O'Shea, D. F. *New. J. Chem.* **2008**, *32*, 483.

Chapter 5

Highly Sensitive and Selective Fluorescent Sensors Based on Monostyryl BODIPY for Zinc and Cadmium Ions

5.1 Introduction

Both zinc and cadmium are Group 12 elements which play important roles in our daily life. Zinc is the second most abundant transition metal in the human body, where it plays an important role in many biological processes.[1] It is also believed that disorder of zinc homeostasis is implicated in a number of diseases,[2] such as Alzheimer's disease. Cadmium poses severe harm for human health and the environment. Excessive exposure of the body to cadmium will lead to renal dysfunction, calcium metabolism disorders, and an increased incidence of certain form of cancers.[3] Therefore it is meaningful to develop sensitive and specific methods to detect Zn^{2+} and Cd^{2+} ions. Fluorescence signaling is an excellent choice due to its high detection sensitivity and intrinsic operation simplicity. Hence the design and development of novel fluorescent sensors which can selectively detect and image Zn^{2+} and Cd^{2+} ions has received much current interest.[1c-d, 4] Generally, Zn^{2+} and Cd^{2+} ions have very similar chemical properties, so the discrimination between them is very difficult. To date, only a few examples have been reported.[4e-g] BODIPY dyes are desirable fluorophores because of their large extinction coefficients, high quantum yields, ease of chemical modifications, good solubility

and stability in many solvent systems.[5] Recently, this class of dyes has been widely used as metal sensors.[4e-g,6] We report in this Chapter two fluorescent sensors based on monostyryl BODIPY, containing different number of polyamide chains, which exhibit a high selectivity for Zn^{2+} and Cd^{2+} ions.

5.2 Results and Discussion

5.2.1 Chemical Synthesis and Spectroscopic Characterization

Scheme 5.1 shows the synthetic route used to prepare the target compounds **5.8a** and **5.8b**. Nucleophilic substitution of ethyl bromoacetate (**5.2**) with aniline (**5.1a**) or 1,2-benzenediamine (**5.1b**) under a basic condition gave the intermediate **5.3a** or **5.3b**.[7,6g] Vilsmeier reaction of these compounds with phosphorus oxychloride (**5.4**) in DMF afforded the ester substituted benzaldehydes **5.5a** and **5.5b**.[6g] Condensation of triethylene glycol monomethyl substituted BODIPY **2.5** with aldehyde **5.5a** or **5.5b**, followed by amidation with 2-aminoethanol (**5.7**) afforded the monostyryl BODIPY **5.8a** or **5.8b**.

All of these compounds were purified by silica gel column chromatography and characterized with various spectroscopic methods. Taking the ^1H NMR spectrum of monostyryl BODIPY **5.8a** as an example (Figure 5.1), the three singlets at 1.43, 1.46 and 2.58 ppm are due to the methyl protons in the pyrrole rings. The broad signal at 2.90 ppm is due to the hydroxyl protons. The signals from 3.3 to 4.2 ppm are attributed to the triethylene glycol chain and all the methylene protons. The two singlets at 5.99 and 6.57 ppm are due to the pyrrole ring protons. The singlet at 7.96

ppm is due to the amide protons. The other signals from 6.5 to 7.5 ppm are due to the aryl and vinyl protons. For the other target compound **5.8b**, the assignment of ^1H NMR signals is similar to that of **5.8a**.

The $^{13}C\{^1H\}$ NMR data of these monostyryl BODIPYs were also in accord with the structures though some of aromatic carbon signals and the chain CH_2 signals were overlapped.

All of these compounds were further characterized with ESI mass spectrometry. The isotopic distribution as well as the exact mass for the $[M]^+$ (for **5.6a**, **5.8a**, and **5.8b**) and $[M + Na]^+$ (for **5.6b**) species were in good agreement with the calculated ones.

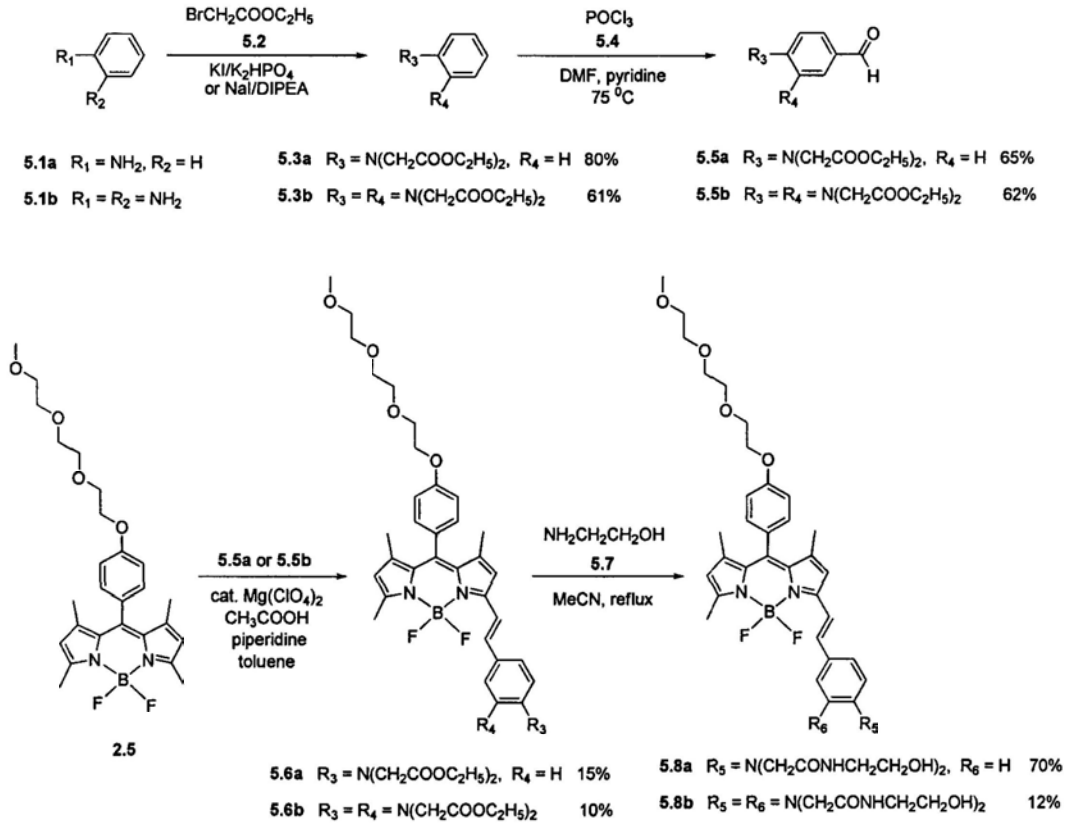

Scheme 5.1. Synthesis of monostyryl BODIPYs **5.8a** and **5.8b**.

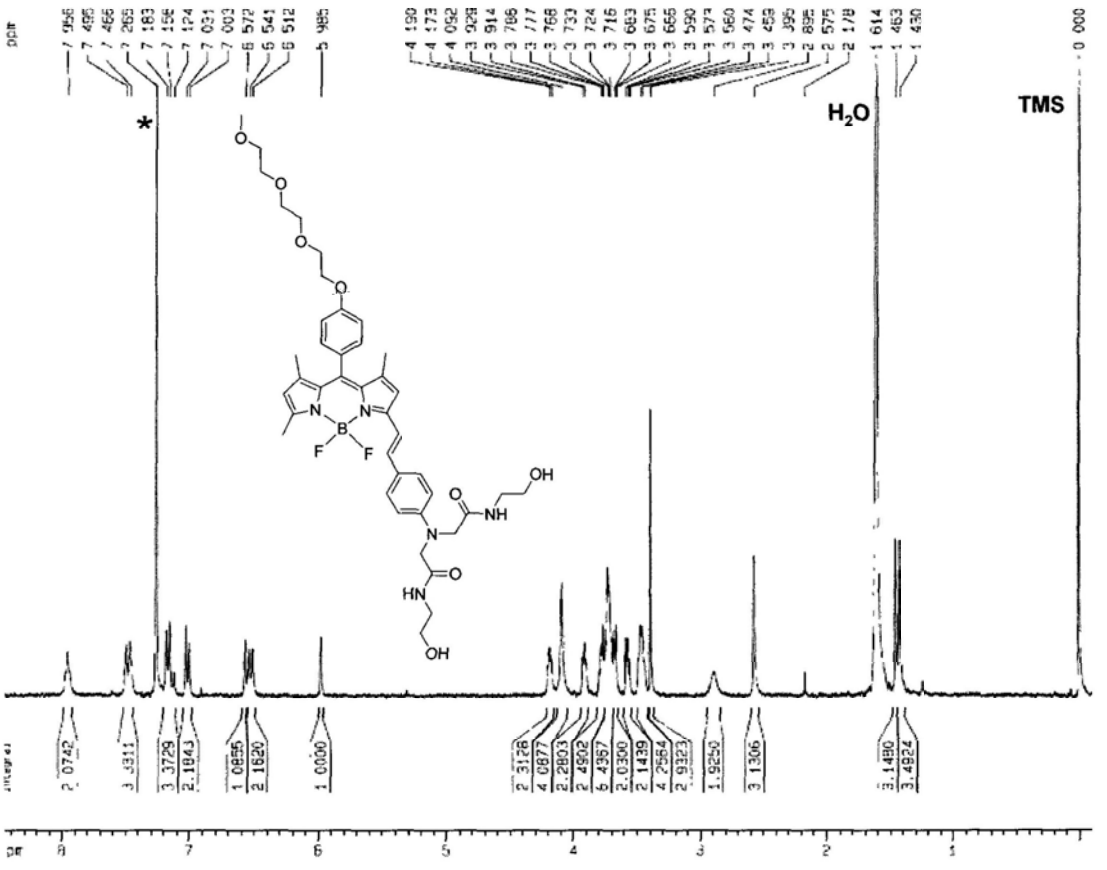

Figure 5.1. ^{1}H NMR spectrum of **5.8a** in $CDCl_3$; * indicates residual solvent signal.

5.2.2 Spectral Response of 5.8a to Various Metal Ions in MeCN

The electronic absorption spectrum of **5.8a** in MeCN exhibited an absorption band at 586 nm (Figure 5.2). Upon addition of Zn^{2+} ion, this band was attenuated while a new peak appeared at shorter wavelength positioned at 563 nm, and the color of the solution turned from light blue to light purple (Figure 5.3). Three isosbestic points at 350, 452, and 571 nm were clearly observed during the spectral titration, indicating the formation of a well-defined **5.8a**-Zn^{2+} complex. The response of the absorption spectrum of **5.8a** toward a variety of metal ions was also examined in MeCN. A similar but weaker effect was observed for Pb^{2+} ion. Addition of Hg^{2+} ion led to a bathochromic shift of 7 nm for the absorption. Addition of Cu^{2+} ion greatly

decreased the maximum band at 586 nm, which eventually disappeared. At the same time, two new peaks at 500 and 700 nm appeared with two isosbestic points at 430 and 521 nm. Other metal ions such as Cd^{2+}, Mg^{2+}, Ca^{2+}, Na^{+}, and K^{+} ions induced a little effect on the absorption spectrum of **5.8a**. All these spectral changes are shown in Figure 5.4.

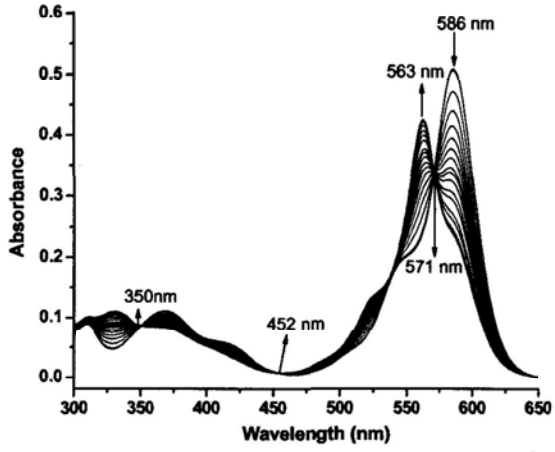

Figure 5.2. Change in electronic absorption spectrum of **5.8a** in MeCN (4 μM) upon addition of Zn^{2+} ion (0-200 μM).

Figure 5.3. The observed color change of **5.8a** in MeCN (4 μM) upon addition of metal ions. From left to right: control, in the presence of Zn^{2+} ion (200 μM), and in the presence of Cd^{2+} ion (200 μM).

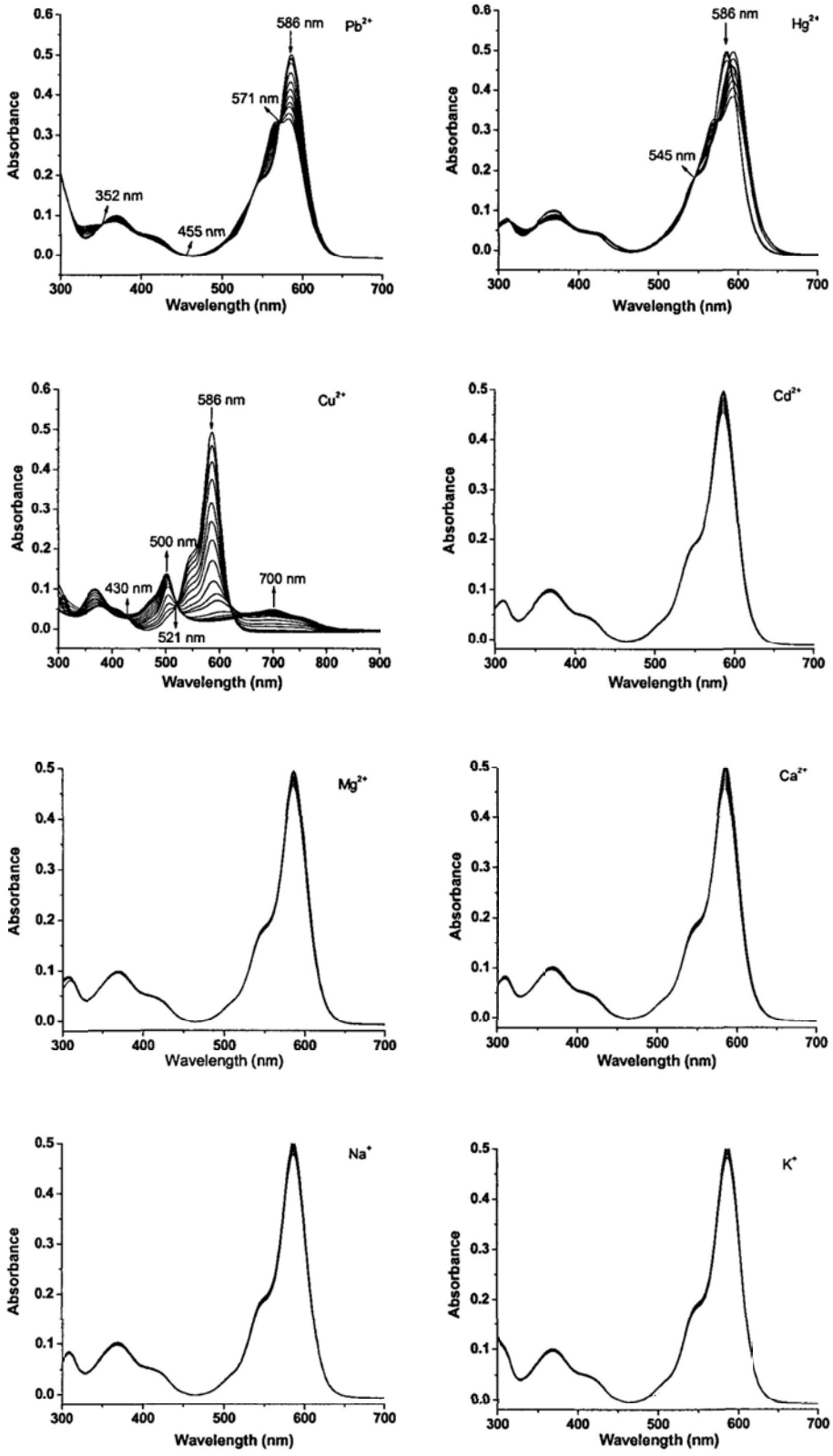

Figure 5.4. Changes in electronic absorption spectrum of **5.8a** in MeCN (4 μM) upon addition of various metal ions (0-200 μM).

As shown in Figure 5.5, free **5.8a** exhibited a weak fluorescence emission at 620 nm with a fluorescence quantum yield (Φ_F) of 0.066.[8] Upon addition of Zn^{2+} ion, the fluorescence emission intensity at 620 nm remained essentially unchanged, while a new emission band at 572 nm emerged, of which the intensity dramatically increased. The fluorescence quantum yield increased to 0.33 when 200 equiv. of Zn^{2+} ion was added. The fluorescence of the solution also turned from red to yellow (Figure 5.6). The remarkable change in emission position and intensity resulted from suppressing the intramolecular charge transfer (ICT) process because the electron-donating ability of the nitrogen atoms in **5.8a** was dramatically reduced upon coordination with Zn^{2+} ion.

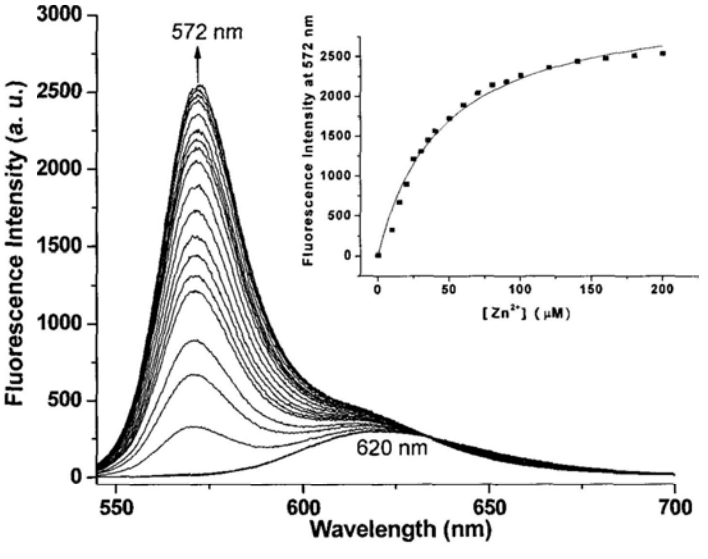

Figure 5.5. Change in fluorescence emission spectrum (excited at 535 nm) of **5.8a** in MeCN (1 μM) upon addition of Zn^{2+} ion (0-200 μM). The insert shows a nonlinear curve fitting of the fluorescence intensity at 572 nm of **5.8a** versus the concentration of Zn^{2+} ion.

The response of the fluorescence of **5.8a** toward a variety of metal ions was also examined in MeCN. The spectral changes are shown in Figure 5.8. Addition of Hg^{2+} ion quenches the emission band at 620 nm and a new band at 575 nm appears. Addition of Cu^{2+} ion also quenches the emission band at 620 nm in a more effective manner, and a very weak band at 560 nm also appears. Addition of Pb^{2+} ion enhances the fluorescence intensity of the bands at 575 and 620 nm. Other metal ions such as Cd^{2+}, Mg^{2+}, Ca^{2+}, Na^{+}, and K^{+} ions have no significant effects on the fluorescence spectrum of **5.8a**. Figure 5.9 compiles the effects of all these metal ions. It is clear that **5.8a** can detect Zn^{2+} ion with a high selectivity and sensitivity.

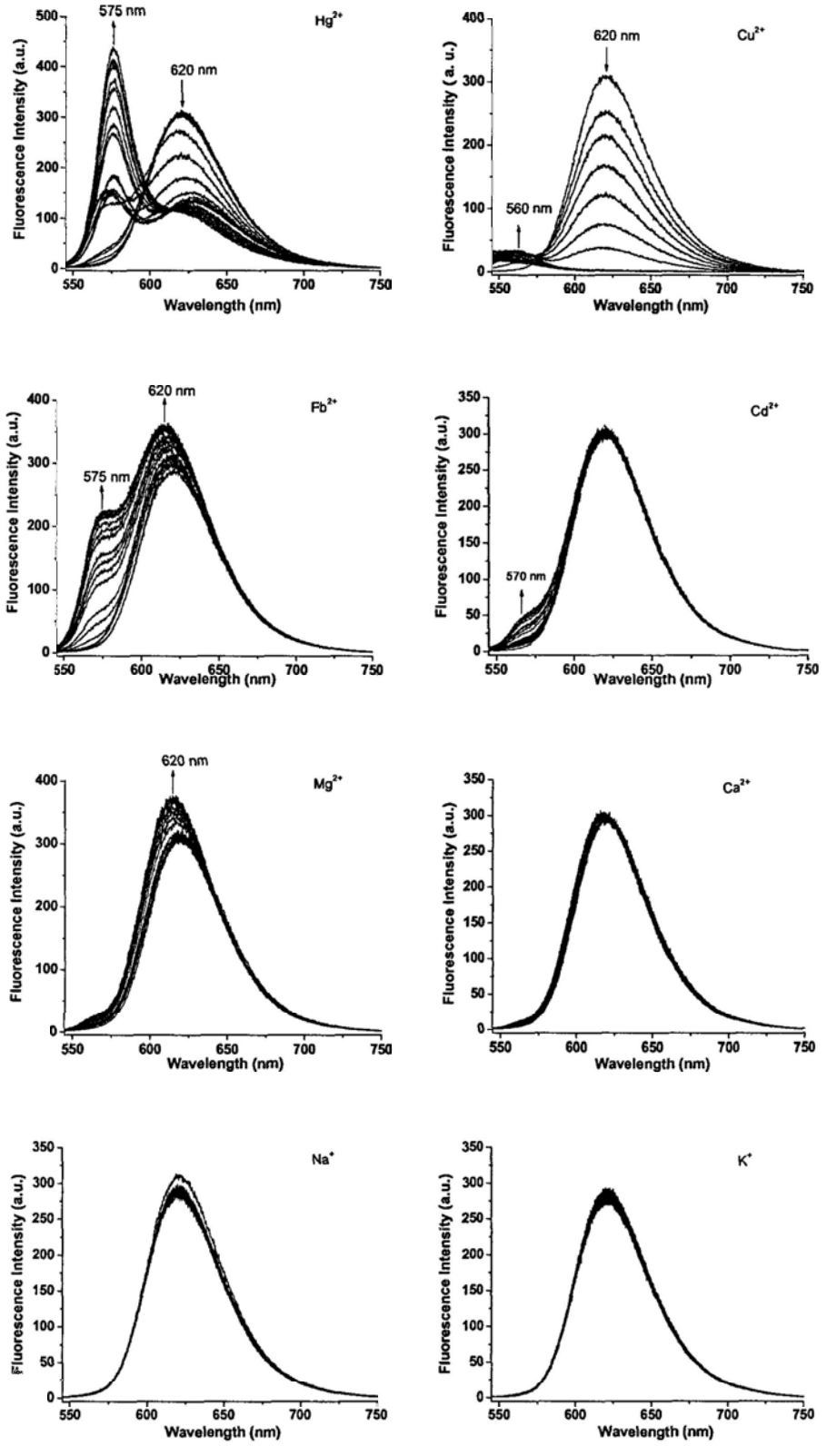

Figure 5.8. Changes in fluorescence emission spectrum (excited at 535 nm) of **5.8a** in MeCN (1 μM) upon addition of various metal ions (0-200 μM).

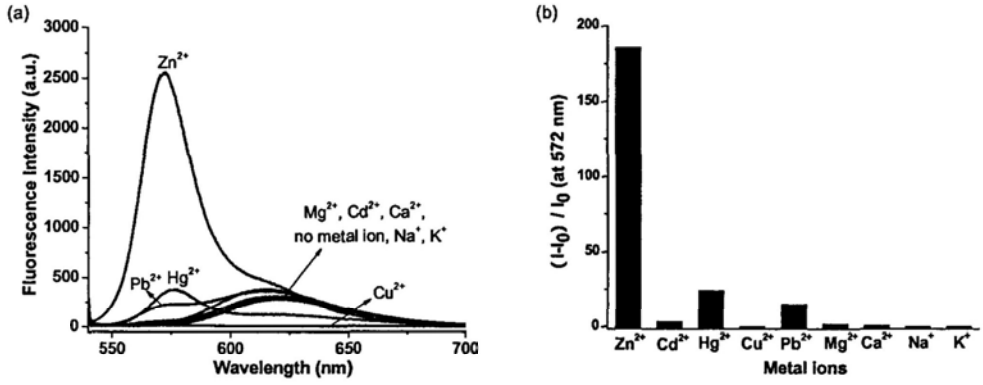

Figure 5.9. Fluorescence emission spectra (a) and change in fluorescence intensity at 572 nm (b) of **5.8a** in MeCN (1 μM) in the presence of 200 equiv. of various metal ions.

5.2.3 Spectral Response of 5.8b to Various Metal Ions in Phosphate Buffered Saline (PBS)

The electronic absorption spectrum of **5.8b** in PBS solution (0.01M, pH = 7.4, containing 0.0027 M KCl and 0.137 M NaCl) exhibited an absorption band at 573 nm (Figure 5.10). Upon addition of Cd^{2+} ion, the band at 573 nm was slightly attenuated, and the color of the solution remained essentially unchanged. The response of the absorption spectrum of **5.8b** toward a series of metal ions was also examined in PBS. As shown in Figure 5.11, all these metal ions, including Zn^{2+}, Hg^{2+}, Cu^{2+}, Pb^{2+}, Mg^{2+}, Ca^{2+}, Na^{+}, and K^{+} have little effect on the absorption spectrum of **5.8b**.

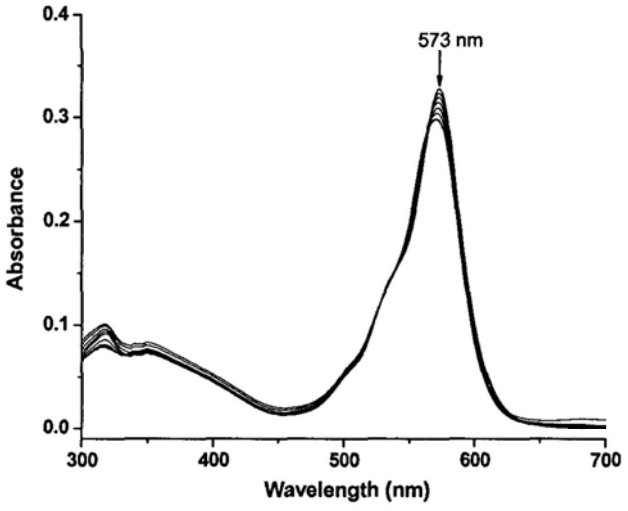

Figure 5.10. Change in electronic absorption spectrum of **5.8b** in PBS (6 μM) upon addition of Cd^{2+} ion (0-80 μM).

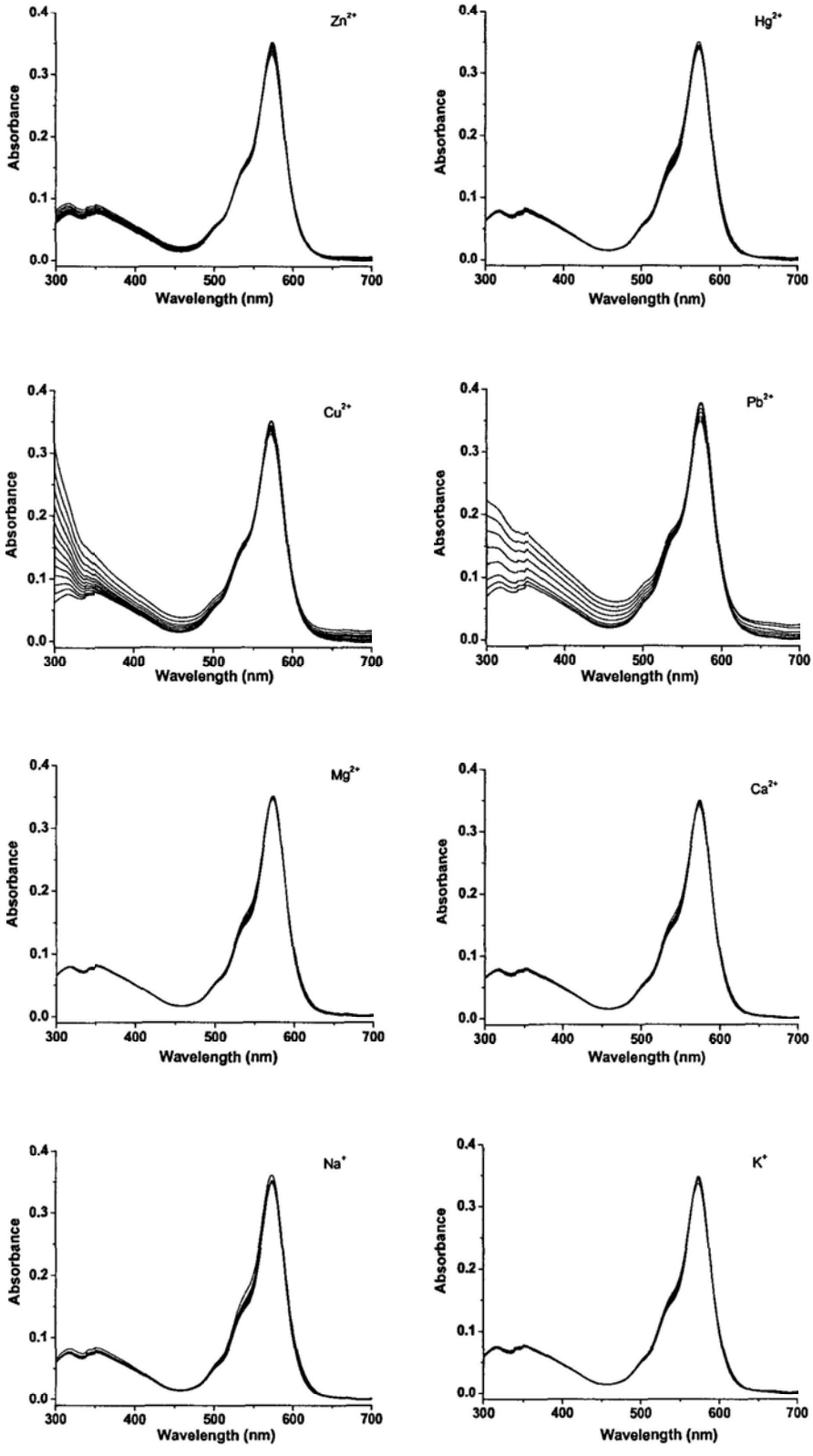

Figure 5.11. Changes in electronic absorption spectrum of **5.8b** in PBS (6 μM) upon addition of various metal ions (0-80 μM).

Free **5.8b** exhibited a weak fluorescence emission at 570 nm in aqueous media with a fluorescence quantum yield of 0.005. The fluorescence intensity was found to be independent of the pH from 4 to 9 (Figure 5.12). Therefore, we performed the metal binding studies in PBS solution (0.01M, pH = 7.4, containing 0.0027 M KCl and 0.137 M NaCl). Upon addition of Cd^{2+} ion, the fluorescence intensity at 570 nm of **5.8b** increased significantly with a hypsochromic shift of 5 nm (Figure 5.13). The fluorescence quantum yield increased by ca.15 fold (Φ_F = 0.076). As shown in Figure 5.14, the fluorescence of the solution turned from light purple to yellow. These changes can be attributed to the binding of the nitrogen atoms in **5.8b** with Cd^{2+} ion which inhibits the ICT process. A Job's plot indicated that **5.8b** chelated Cd^{2+} ion with 1:2 stoichiometry (Figure 5.15). The association constants K_1 and K_2 were determined to be $(4.4 \pm 0.9) \times 10^4$ M^{-1} and $(1.3 \pm 0.1) \times 10^4$ M^{-1}, respectively, by a 1:2 nonlinear least-squares analysis[10] of fluorescence intensity at 565 nm versus the concentration of Cd^{2+} ion (the inset of Figure 5.13).

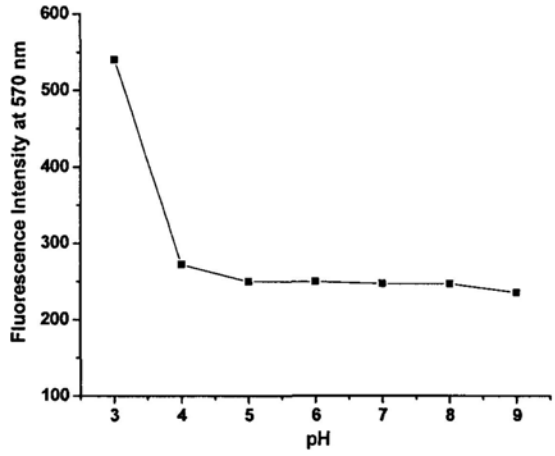

Figure 5.12. Change in the fluorescence intensity at 570 nm of **5.8b** in aqueous media (1 μM) with the pH value.

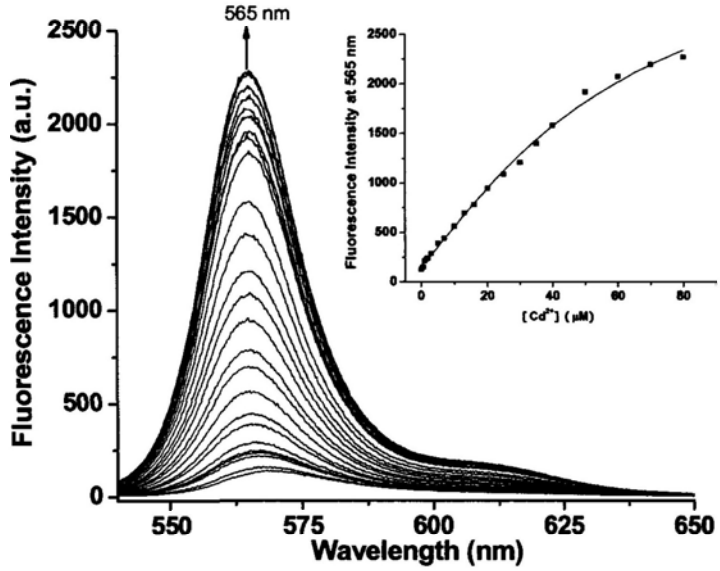

Figure 5.13. Change in fluorescence emission spectrum (excited at 530 nm) of **5.8b** in PBS (1 μM) upon addition of Cd^{2+} ion (0-80 μM). The insert shows a nonlinear curve fitting for the fluorescence intensity at 565 nm of **5.8b** versus the concentration of Cd^{2+} ion.

Figure 5.14. The observed fluorescence change of **5.8b** in PBS (10 μM) upon addition of metal ions. From left to right: control, in the presence of Zn^{2+} ion (200 μM), and in the presence of Cd^{2+} ion (200 μM).

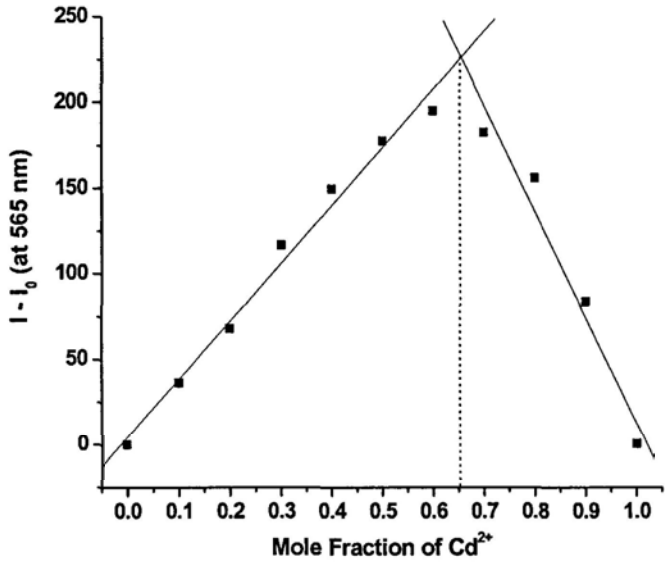

Figure 5.15. Job's plot for the binding of **5.8b** with Cd^{2+} ion. The total concentration of **5.8b** and Cd^{2+} ion was fixed at 4 μM.

The response of the fluorescence of **5.8b** toward a series of metal ions was also examined in PBS. A similar but less intense effect was observed for Hg^{2+} ion. However, the effects of other metal ions, including Zn^{2+}, Cu^{2+}, Pb^{2+}, Mg^{2+}, Ca^{2+}, Na^{+}, and K^{+} exerted only a weak effect on the fluorescence spectrum, as shown in Figure 5.16. It can clearly be seen in Figure 5.17 that compound **5.8b** shows a high selectivity toward Cd^{2+} ion.

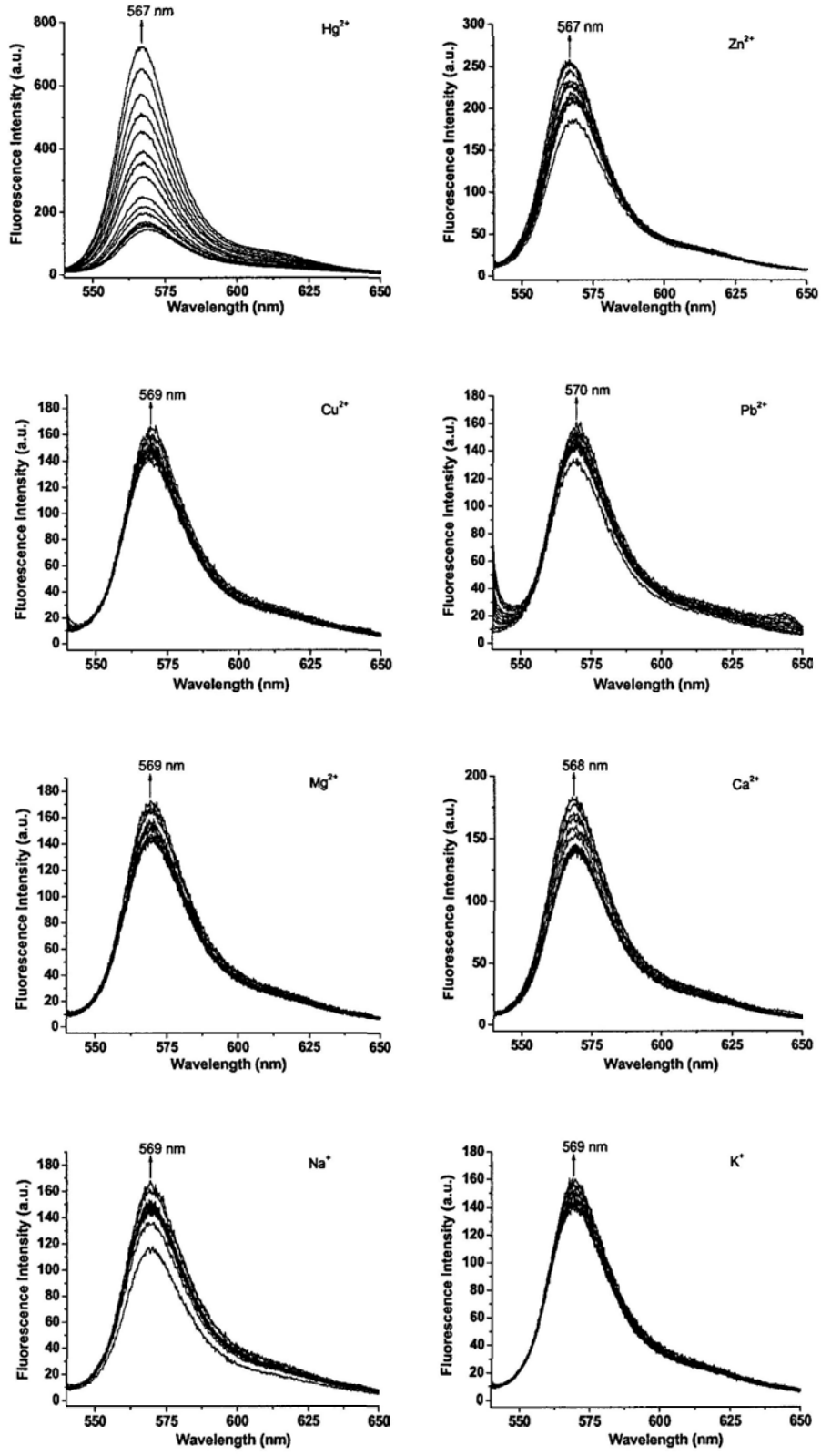

Figure 5.16. Changes in fluorescence emission spectrum (excited at 530 nm) of **5.8b** in PBS (1 μM) upon addition of various metal ions (0-80 μM).

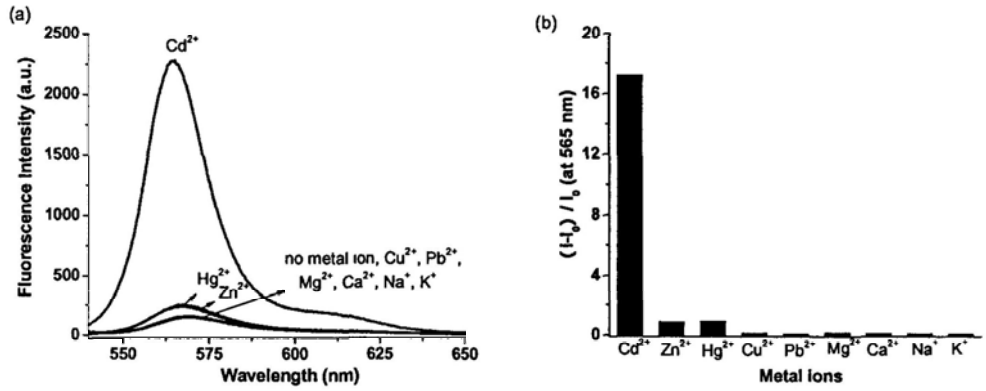

Figure 5.17. Fluorescence emission spectra (a) and change in fluorescence intensity at 565 nm (b) of **5.8b** in PBS (1 μM) in the presence of 80 equiv. of various metal ions.

Competition experiments were also conducted. When 80 equiv. of various metal ions was respectively added into a solution of **5.8b** in PBS containing 80 equiv. of Cd^{2+} ion, the emission spectra displayed a similar pattern and the intensity at 565 nm was not significantly changed as shown in Figure 5.18. The results suggest that compound **5.8b** has a stronger binding to Cd^{2+} ion compared with the other metal ions.

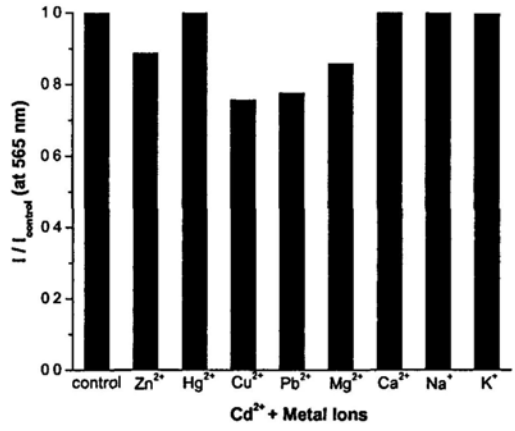

Figure 5.18. Change in fluorescence intensity at 565 nm of **5.8b** in PBS (1 μM) containing 80 equiv. of Cd^{2+} ion upon addition of 80 equiv. of various metal ions.

5.3 Conclusion

We have developed two fluorescent sensors **5.8a** and **5.8b** based on a monostyryl BODIPY fluorophore and a polyamide ionophore. Compound **5.8a** shows a high selectivity toward Zn^{2+} ion in MeCN, while compound **5.8b** exhibits a high selectivity toward Cd^{2+} ion in aqueous media. Both of them can distinguish Zn^{2+} and Cd^{2+} ions.

5.4 Experimental Section

5.4.1 General

Experimental details regarding the purification of solvents and instrumentation have been described in Section 2.4.1. The preparation of triethylene glycol monomethyl substituted BODIPY **2.5** has been reported in Section 2.4.3.

The salts used in this study were $Zn(ClO_4)_2{\cdot}6H_2O$, $Cd(ClO_4)_2{\cdot}H_2O$, $Hg(ClO_4)_2{\cdot}3H_2O$, $Cu(ClO_4)_2{\cdot}6H_2O$, $Pb(ClO_4)_2{\cdot}3H_2O$, $Mg(ClO_4)_2{\cdot}6H_2O$, $Ca(ClO_4)_2{\cdot}4H_2O$, $NaClO_4$, and $KClO_4$.

Fluorescence quantum yields were determined by using Rhodamine B in EtOH as the reference [$\Phi_{F(ref)} = 0.49$].[8]

The association constants were determined by nonlinear least-squares analysis. For the binding of **5.8a** with Zn^{2+} ion, the 1:1 binding equation was used: $y = I_0 + (I_1 - I_0)\{c_0 + x + 1/K - [(c_0 + x + 1/K)^2 - 4c_0x]^{1/2}\}/2c_0$,[9] where y is the emission intensity of **5.8a** in the absence or presence of Zn^{2+} ion, I_0 is the initial emission intensity of Zn^{2+}-free **5.8a**, I_1 is the ultimate emission intensity of **5.8a** in the

presence of Zn^{2+} ion, c_0 is the initial concentration of **5.8a**, x is the concentration of Zn^{2+} ion, K is the association constant of **5.8a** with Zn^{2+} ion. For the binding of **5.8b** with Cd^{2+} ion, the 1:2 binding equation was used: $y = (I_0 + I_1K_1x + I_2K_1K_2x^2)/(1 + K_1x + K_1K_2x^2)$,[10] where y is the emission intensity of **5.8b** in the absence or presence of Cd^{2+} ion, I_0 is the initial emission intensity of Cd^{2+}-free **5.8b**, I_1 is the ultimate emission intensity of a 1:1 **5.8b**-Cd^{2+} complex, K_1 is the first association constant of **5.8b** with Cd^{2+} ion, I_2 is the ultimate emission intensity of a 1:2 **5.8b**-$2Cd^{2+}$ complex, K_2 is the second association constant of **5.8b** with Cd^{2+} ion, x is the concentration of Cd^{2+} ion. In fact, in the case of lower concentrations, where a 1:1 complex was suggested, the equation $y = (I_0 + I_1K_1x)/(1 + K_1x)$ was first used to obtain K_1 and I_1.[10]

5.4.2 Synthesis

N,N-di[(2-hydroxyethyl)carbamoylmethyl]aniline (5.3a).[7] A mixture of aniline (**5.1a**) (2.67 g, 28.7 mmol), ethyl bromoacetate (**5.2**) (14.3 g, 83.9 mmol), potassium iodide (2.38 g, 14.3 mmol), and dipotassium hydrogen phosphate (12.5 g, 71.8 mmol) in MeCN (70 mL) was refluxed under nitrogen for 4 h. It was then cooled and poured into water (100 mL). The resulting mixture was extracted with CH_2Cl_2 (100 mL × 3). The extract was dried over anhydrous sodium sulfate and concentrated to give a brown oil. The residue was purified by flash chromatography using hexane/ethyl acetate (5:1, v/v) as elute to give a white solid (6.1 g, 80%). ^{1}H NMR (300 MHz, $CDCl_3$): δ 7.22 (t, J = 7.5 Hz, 2 H, ArH), 6.78 (t, J = 7.2 Hz, 1 H,

ArH), 6.62 (d, J = 8.1 Hz, 1 H, ArH), 4.18-4.25 (m, 4 H, OCH_2), 4.14 (s, 4 H, NCH_2), 1.29 (virtual t, J = 6.6 Hz, 6 H, CH_3).

N,N,N',N'-tetra[(2-hydroxyethyl)carbamoylmethyl]-o-phenylenediamine (5.3b).[6g] A mixture of 1,2-benzenediamine (**5.1b**) (2.2 g, 20.4 mmol), ethyl bromoacetate (**5.2**) (13.4 mL, 121 mmol), sodium iodide (2.6 g, 17 mmol), and diisopropylethylamine (DIPEA) (16.7 ml, 100 mmol) in MeCN (25 mL) was refluxed under nitrogen for 7 h. It was then cooled and poured into water (100 mL). The resulting mixture was extracted with CH_2Cl_2 (100 mL × 3). The extract was dried over anhydrous sodium sulfate and concentrated to give a brown oil. The residue was purified by flash chromatography using hexane/ethyl acetate (4:1, v/v) as elute to give a white solid (5.6 g, 61%). ^{1}H NMR (400 MHz, $CDCl_3$): δ 7.03-7.05 (m, 2 H, ArH), 6.93-6.96 (m, 2 H, ArH), 4.30 (s, 8 H, N-CH_2), 4.08-4.13 (m, 8 H, OCH_2), 1.20 (t, J = 7.2 Hz, 12 H, CH_3).

p-Formyl-N,N-di[(2-hydroxyethyl)carbamoylmethyl]aniline (5.5a).[6g] Compound **5.3a** (0.66g, 2.5 mmol) was dissolved in a mixture of DMF (25 mL) and pyridine (5 mL). The mixture was cooled in an ice bath, then phosphorus oxychloride (**5.4**) (19 mL, 0.2 mmol) was added dropwise in 30 min. The mixture was stirred at 0°C for 1 h and then heated at 75 °C for 2 h. After cooling, the mixture was mixed with CH_2Cl_2 (125 mL) and poured into crushed ice mixed with sodium carbonate (42.4 g, 0.4 mol). The aqueous layer was extracted with CH_2Cl_2 (125 mL × 3). The combined extract was dried over anhydrous sodium sulfate and concentrated in vacuo. The crude product was purified by flash chromatography using CH_2Cl_2/ethyl

acetate (2:1, v/v) as elute to afford a light yellow oil (0.48 g , 65%). ^{1}H NMR (300 MHz, $CDCl_3$): δ 9.79 (s, 1 H, CHO), 7.75 (d, J = 8.7 Hz, 2 H, ArH), 6.67 (d, J = 9.0 Hz, 2 H, ArH), 4.20-4.28 (m, 8 H, OCH_2, NCH_2), 1.29 (d, J = 7.2 Hz, 6 H, CH_3).

4-Formyl-N,N,N',N'-tetra[(2-hydroxyethyl)carbamoylmethyl]-1,2-phenylene-diamine (5.5b).[6g] According to the procedure described for **5.5a**, compound **5.3b** (1.13 g, 2.5 mmol) was converted to **5.5b** as a light yellow solid (0.74 g, 62%). ^{1}H NMR (400 MHz, $CDCl_3$): δ 9.83 (s, 1 H, CHO), 7.60 (virtual s, 1 H, ArH), 7.49 (virtual d, J = 8.4 Hz, 1 H, ArH), 7.10 (d, J = 8.4 Hz, 1 H, ArH), 4.42 (s, 4 H, NCH_2), 4.28 (s, 4 H, NCH_2), 4.09-4.16 (m, 8 H, OCH_2), 1.21 (t, J = 7.2 Hz, 12 H, CH_3).

Monostyryl BODIPY 5.6a. A mixture of triethylene glycol monomethyl substituted BODIPY **2.5** (0.20 g, 0.4 mmol), aldehyde **5.5a** (0.15 g, 0.5 mmol), glacial acetic acid (0.6 mL, 10.5 mmol), piperidine (0.8 mL, 8.1 mmol), and a small amount of $Mg(ClO_4)_2$ in toluene (60 mL) was refluxed for 2 h. The water formed during the reaction was removed azeotropically with a Dean-Stark apparatus. The mixture was concentrated under reduced pressure. The residue was purified by silica gel column chromatography using ethyl acetate/hexane (1:2, v/v) as the eluent. The red fraction was collected and rotary evaporated. It was then further purified by size exclusion chromatography with Bio-beads S-X1 beads using THF as the eluent to afford a purple solid (50 mg, 16%). ^{1}H NMR (300 MHz, $CDCl_3$): δ 7.50 (d, J = 15.9 Hz, 1 H, CH=CH), 7.49 (d, J = 8.4 Hz, 2 H, ArH), 7.18 (d, J = 8.4 Hz, 2 H, ArH), 7.17 (d, J = 15.9 Hz, 1 H, CH=CH), 7.02 (d, J = 8.4 Hz, 2 H, ArH), 6.60 (d, J = 8.4

Hz, 2 H, ArH), 6.57 (s, 1 H, pyrrole-H), 5.97 (s, 1 H, pyrrole-H), 4.17-4.27 (m, 10 H, OCH_2, NCH_2, COOCH2), 3.91 (t, J = 4.8 Hz, 2 H, OCH_2), 3.66-3.80 (m, 6 H, OCH_2), 3.57 (t, J = 4.5 Hz, 2 H, OCH_2), 3.39 (s, 3 H, OCH_3), 2.58 (s, 3 H, CH_3), 1.49 (s, 3 H, CH_3), 1.46 (s, 3 H, CH_3), 1.29 (t, J = 6.9 Hz, 6 H, CH_3); $^{13}C\{^1H\}$ NMR (100.6 MHz, $CDCl_3$): δ 170.6, 159.4, 154.0, 153.8, 148.7, 142.9, 141.7, 139.7, 136.7, 133.5, 131.9, 129.6, 129.3, 127.6, 127.0, 120.8, 117.6, 115.9, 115.2, 112.6, 72.1, 71.0, 70.8, 70.7, 69.9, 67.6, 61.5, 59.2, 53.7, 15.0, 14.8, 14.7, 14.4; MS (ESI): isotopic clusters peaking at *m/z* 742 {20%, $[M-F]^+$}, 762 {15%, $[M+H]^+$}, 784 {100%, $[M+Na]^+$} and 800 {95%, $[M+K]^+$}; HRMS (ESI): *m/z* calcd for $C_{41}H_{50}BF_2N_3NaO_8$ $[M+Na]^+$: 784.3551, found: 784.3543. Anal. calcd for $C_{41}H_{50}BF_2N_3O_8$: C, 64.65; H, 6.62; N, 5.52. Found: C, 64.90; H, 7.06; N, 5.44.

Monostyryl BODIPY 5.6b. According to the procedure described for **5.6a**, a mixture of BODIPY **2.5** (0.20 g, 0.4 mmol), aldehyde **5.5b** (0.24 g, 0.5 mmol), glacial acetic acid (0.6 mL, 10.5 mmol), piperidine (0.8 mL, 8.1 mmol), and a small amount of $Mg(ClO_4)_2$ in toluene (60 mL) was refluxed for 4 h. The crude product was purified by silica gel column chromatography using ethyl acetate/hexane (1:2, v/v) as the eluent. The red fraction was collected and rotary evaporated. It was then further purified by size exclusion chromatography with Bio-beads S-X1 beads using THF as the eluent to afford a purple solid (38 mg, 10%). ^1H NMR (400 MHz, $CDCl_3$): δ 7.51 (d, J = 16.0 Hz, 1 H, CH=CH), 7.30 (virtual d, J = 8.4 Hz, 2 H, ArH), 7.18 (d, J = 8.4 Hz, 2 H, ArH), 7.17 (s, 1 H, ArH), 7.14 (d, J = 19.6 Hz, 1 H, CH=CH), 7.02 (d, J = 8.4 Hz, 2 H, ArH), 7.01 (d, J = 8.4 Hz, 1 H, ArH), 6.56 (s, 1 H,

pyrrole-H), 5.98 (s, 1 H, pyrrole-H), 4.35 (s, 4 H, NCH_2), 4.31 (s, 4 H, NCH_2), 4.19 (t, J = 4.4 Hz, 2 H, OCH_2), 4.10-4.16 (m, 8 H, OCH_2), 3.92 (t, J = 4.8 Hz, 2 H, OCH_2), 3.77-3.79 (m, 2 H, OCH_2), 3.67-3.73 (m, 4 H, OCH_2), 3.56-3.59 (m, 2 H, OCH_2), 3.40 (s, 3 H, OCH_3), 2.58 (s, 3 H, CH_3), 1.47 (s, 3 H, CH_3), 1.43 (s, 3 H, CH_3), 1.22 (t, J = 7.2 Hz, 6 H, CH_3), 1.21 (t, J = 7.2 Hz, 6 H, CH_3); $^{13}C\{^1H\}$ NMR (100.6 MHz, $CDCl_3$): δ 171.0, 170.9, 159.4, 154.6, 153.3, 142.6, 142.5, 142.4, 141.4, 140.1, 136.3, 133.3, 132.2, 131.5, 129.5, 127.5, 122.3, 121.6, 121.5, 121.0, 117.7, 117.6, 115.2, 72.0, 71.0, 70.8, 70.7, 69.8, 67.6, 60.8, 59.2, 52.6, 52.5, 15.0, 14.8, 14.7, 14.3; MS (ESI): isotopic clusters peaking at *m/z* 929 {10%, $[M-F]^+$}, 948 {30%, $[M]^+$} and 949 {20%, $[M+H]^+$}; HRMS (ESI): *m/z* calcd for $C_{49}H_{63}BF_2N_4O_{12}$ $[M]^+$: 948.4498, found: 948.4534.

Monostyryl BODIPY 5.8a. Compound **5.6a** (15 mg, 0.020 mmol) was dissolved in acetonitrile (5 mL) and 2-aminoethanol (**5.7**) (5 mL). The solution was refluxed under nitrogen for 1.5 h. It was then cooled and concentrated in vacuo to remove the acetonitrile before pouring into saturated brine (50 mL). The mixture was neutralized with sodium dihydrogen phosphate, and extracted with CH_2Cl_2 (100 mL × 3). The combined extract was dried over anhydrous sodium sulfate and then concentrated in vacuo. The product was purified by flash chromatography using CH_2Cl_2/methanol (15:1, v/v) as eluent to give a purple solid (11 mg, 70%). ^1H NMR (300 MHz, $CDCl_3$): δ 7.96 (s, 2 H, NH), 7.47-7.50 (m, 3 H, CH=CH, ArH), 7.17 (d, J = 8.1 Hz, 2 H, ArH), 7.15(d, J = 17.7 Hz, 1 H, CH=CH), 7.02 (d, J = 8.4 Hz, 2 H, ArH), 6.57 (s, 1 H, pyrrole-H), 6.53 (d, J = 8.7 Hz, 2 H, ArH), 5.99 (s, 1 H,

pyrrole-H), 4.17 (t, J = 4.8 Hz, 2 H, OCH_2), 3.93 (s, 4 H, NCH_2) 3.90 (t, J = 4.5 Hz, 2 H, OCH_2), 3.67-3.80 (m, 10 H, OCH_2), 3.57 (t, J = 4.5 Hz, 2 H, OCH_2), 3.47-3.46 (m, 4 H, NCH_2), 3.40 (s, 3 H, OCH_3), 2.90 (s, 2 H, OH), 2.58 (s, 3 H, CH_3), 1.46 (s, 3 H, CH_3), 1.43 (s, 3 H, CH_3); $^{13}C\{^1H\}$ NMR (100.6 MHz, $CDCl_3$): δ 171.8, 159.42, 153.8, 153.7, 147.4, 143.1, 141.9, 139.8, 136.7, 133.4, 132.0, 129.6, 129.3, 127.4, 126.8, 120.9, 117.8, 115.7, 115.2, 112.1, 72.1, 71.0, 70.8, 70.7, 69.9, 67.6, 61.5, 59.2, 57.0, 42.5, 31.1, 15.0, 14.8, 14.7; MS (ESI): isotopic clusters peaking at *m/z* 772 {60%, $[M-F]^+$}, 791 {100%, $[M]^+$}, and 792 {60%, $[M+H]^+$}; HRMS (ESI): *m/z* calcd for $C_{41}H_{52}BF_2N_5O_8$ $[M]^+$: 791.3872, found:791.3852. Anal. calcd for $C_{41}H_{52}BF_2N_3O_9$ (**5.8a**·H_2O): C, 60.82; H, 6.72; N, 8.65. Found: C, 60.61; H, 6.93; N, 8.32.

Monostyryl BODIPY 5.8b. According to the procedure described for **5.8a**, a mixture of **5.6b** (19 mg, 0.020 mmol) and 2-aminoethanol (**5.7**) (5 mL) in acetonitrile (5 mL) was refluxed under nitrogen for 1.5 h. The crude product was purified by flash chromatography using CH_2Cl_2/methanol (10:1, v/v) as eluent to afford a purple solid (2.4 mg, 12%). ^1H NMR (400 MHz, $CDCl_3$ with a trace amount of CD_3OD): δ 8.13 (t, J = 5.2 Hz, 2 H, NH), 8.07 (t, J = 5.2 Hz, 2 H, NH), 7.42 (d, J = 16.4 Hz, 1 H, CH=CH), 7.24 (s, 1 H, ArH), 7.18 (d, J = 8.8 Hz, 2 H, ArH), 7.15 (d, J = 7.2 Hz, 1 H, ArH), 7.14 (d, J = 20.8 Hz, 1 H, CH=CH), 7.04 (d, J = 8.8 Hz, 2 H, ArH), 6.93 (d, J = 8.4 Hz, 1 H, ArH), 6.59 (s, 1 H, pyrrole-H), 6.02 (s, 1 H, pyrrole-H), 4.20 (t, J = 4.2 Hz, 2 H, OCH_2), 4.14 (s, 4 H, NCH_2), 4.09 (s, 4 H, NCH_2), 3.92 (t, J = 4.8 Hz, 2 H, OCH_2), 3.77-3.80 (m, 2 H, OCH_2), 3.67-3.73 (m, 4 H, OCH_2), 3.55-3.59 (m, 10 H

OCH_2, NCH_2CH_2), 3.40 (s, 3 H, OCH_3), 2.56 (br, 7 H, CH_3, OH), 1.48 (s, 3 H, CH_3), 1.45 (s, 3 H, CH_3); $^{13}C\{^1H\}$ NMR (100.6 MHz, $CDCl_3$): δ 171.6 159.5, 154.7, 153.0, 143.0, 142.8, 141.7, 140.4, 136.4, 133.4, 132.2, 131.8, 129.5, 127.2, 123.9, 121.4, 120.1, 118.1, 117.5, 115.3, 72.1, 71.0, 70.8, 70.7, 69.9, 67.6, 61.1, 59.2, 56.0, 42.2, 29.8, 14.9, 14.8; MS (ESI): an isotopic cluster peaking at *m/z* 1008 {10%, $[M]^+$}; HRMS (ESI): *m/z* calcd for $C_{49}H_{67}BF_2N_8O_{12}$ $[M]^+$: 1008.4934, found: 1008.4918.

5.5 References

1 (a) Berg, J. M.; Shi, Y. *Science* **1996**, *271*, 1081. (b) Maret, W. *Biometals* **2001**, *14*, 187. (c) Carol, P.; Sreejith, S.; Ajayaghosh, A. *Chem. Asian J.* **2007**, *2*, 338. (d) Domaille, D. W.; Que, E. L.; Chang, C. J. *Nature Chem. Biol.* **2008**, *4*, 168.

2 (a) Bush, A. I. *Curr. Opin. Chem. Biol.* **2000**, *4*, 184. (b) Bush, A. I. *Trends Neurosci.* **2003**, *26*, 207.

3 (a) Satarug, S.; Baker, J. R.; Urbenjapol, S.; Haswell-Elkins, M.; Reilly, P. E. B.; Williams, D. J.; Moore, M. R. *Toxicol. Lett.* **2003**, *137*, 65. (b) Goyer, R. A.; Liu, J.; Waalkes, M. P. *BioMetals* **2004**, *17*, 555.

4 (a) Walkup, G. K.; Burdette, S. C.; Lippard, S. J.; Tsien, R. Y. *J. Am. Chem. Soc.* **2000**, *122*, 5644. (b) Hirano, T.; Kikuchi, K.; Urano, Y; Nagano, T. *J. Am. Chem. Soc.* **2002**, *124*, 6555. (c) Woodroofe, C. C.; Lippard, S. J. *J. Am. Chem. Soc.* **2003**, *125*, 11458. (d) Taki, M.; Wolford, J. L.; O'halloran, T. V. *J. Am. Chem. Soc.* **2004**, *126*, 712. (e) Peng, X.; Du, J.; Fan, J.; Wang, J.; Wu, Y.; Zhao, J.; Sun, S.; Xu, T. *J. Am. Chem. Soc.* **2007**, *129*, 1500. (f) Cheng, T.; Xu,

Y.; Zhang, S.; Zhu, W.; Qian, X.; Duan, L. *J. Am. Chem. Soc.* **2008**, *130*, 16160. (g) Atilgan, S.; Ozdemir, T.; Akkaya, E. U. *Org. Lett.* **2008**, *10*, 4065.

5 (a) Loudet, A.; Burgess, K. *Chem. Rev.* **2007**, *107*, 4891. (b) Ulrich, G.; Ziessel, R.; Harriman, A. *Angew. Chem. Int. Ed.* **2008**, *47*, 1184.

6 (a) Rurack, K.; Kollmannsberger, M.; Resch-Genger, U.; Daub, J. *J. Am. Chem. Soc.* **2000**, *122*, 968. (b) Turfan, B.; Akkaya, E. U. *Org. Lett.* **2002**, *4*, 2857. (c) Goze, C.; Ulrich, G.; Charbonnière, L.; Cesario, M.; Prangé, T.; Ziessel, R. *Chem. Eur. J.* **2003**, *9*, 3748. (d) Bricks, J.; Kovalchuk, A.; Trieflinger, C.; Nofz, M.; Büschel, M.; Tolmachev, A. I.; Daub, J.; Rurack, K. *J. Am. Chem. Soc.* **2005**, *127*, 13522. (e) Zeng, L.; Miller, E. W.; Pralle, A.; Isacoff, E. Y.; Chang, C. J. *J. Am. Chem. Soc.* **2006**, *128*, 10. (f) Miller, E. W.; Zeng, L.; Domaille, D. W.; Chang, C. J. *Nat. Protocols* **2006**, *1*, 824. (g) Wang, J.; Qian, X. *Org. Lett.* **2006**, *8*, 3721. (h)Yuan, M.; Li, Y.; Li, J.; Li, C.; Liu, X.; Lv, J.; Xu, J.; Liu, H.; Wang, S.; Zhu, D. *Org. Lett.* **2007**, *9*, 2313. (i) Du, J.; Fan, J.; Peng, X.; Li, H.; Wang, J.; Sun, S. *J. Fluoresc.* **2008**, *18*, 919. (j) Hudnall, T. W.; Gabbai, F. P. *Chem. Commun.* **2008**, 4596. (k) Ekmekci, Z.; Yilmaz, M. D.; Akkaya, E. U. *Org. Lett.* **2008**, *10*, 461. (l) Fan, J.; Guo, K.; Peng, X.; Du, J.; Wang, J.; Sun, S.; Li, H. *Sensors and Actuators B* **2009**, *142*, 191. (m) Lu, H.; Xiong, L.; Liu, H.; Yu, M.; Shen, Z.; Li, F.; You, X. *Org. Biomol. Chem.* **2009**, *7*, 2554. (n) Jiao, L.; Li, J.; Zhang, S.; Wei, C.; Hao, E.; Vicente, M. G. H. *New J. Chem.* **2009**, *33*, 1888. (o) Lu, H.; Zhang, S.; Liu, H.; Wang, Y.; Shen, Z.; Liu, C.; You, X. *J. Phys. Chem. A* **2009**, *113*, 14081. (p) Dodani, S. C.; He, Q.;

Chang, C. J. *J. Am. Chem. Soc.* **2009**, *131*, 18020. (q) Móczár, I.; Huszthy, P.; Maidics, Z.; Kádár, M.; Tóth, K. *Tetrahedron* **2009**, *65*, 8250. (r) Domaille, D. W.; Zeng, L.; Chang, C. J. *J. Am. Chem. Soc.* **2010**, *132*, 1194. (s) Atilgan, S.; Kutuk, I.; Ozdemir, T. *Tetrahedron Lett.* **2010**, *51*, 892.

7 Gunnlaugsson, T.; Lee, T. C.; Parkesh, R. *Org. Lett.* **2003**, *5*, 4065.

8 Casey, K. G.; Quitevis, E. L. *J. Phys. Chem.* **1988**, *92*, 6590.

9 Bourson, J.; Pouget, J.; Valeur, B. *J. Phys. Chem.* **1993**, *97*, 4552.

10 Nigam, S.; Durocher, G. *J. Phys. Chem.* **1996**, *100*, 7135.

Chapter 6

A Near-Infrared Fluorescent Sensor for Zn^{2+} Ion Based on Silicon(IV) Phthalocyanine

6.1 Introduction

6.1.1 Phthalocyanines

Phthalocyanines were derived from the Greek terms naphtha (rock oil) and cyanine (dark blue). The metal-free unsubstituted derivative was discovered accidentally by Braun and Tcherniac in 1907 as a byproduct in the reaction of phthalamide and acetic anhydride.[1] This class of pigments exhibits unusual stability toward alkaline, acid, and heat. They contain a highly conjugated macrocyclic π system with four imino-isoindoline units (Figure 6.1).[2] Their absorption spectra are characterized by a very strong absorption at ca. 670 nm, which is termed as the Q band, one to two weak absorption band(s) around 600 nm due to the vibrational overtone(s) of the Q band, and a strong Soret absorption peak at ca. 350 nm. These absorptions render a characteristic greenish blue color to these dyes.

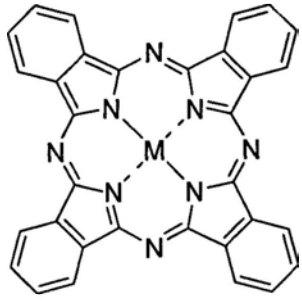

Figure 6.1. General structure of metallophthalocyanines.

Due to their intense color, and high thermal and chemical stability, phthalocyanines were first employed as green and blue colorants in the photographic, printing, plastics, and textile industries.[3] Their intriguing optical and electrical properties also enable them to be used in various technological areas such as photoconductors, optical recording materials, chemical sensors, and catalysts for oxidative degradation of pollutants.[4] Apart from these applications, phthalocyanines are also promising photosensitizing agents for photodynamic therapy.[5]

6.1.2 Silicon(IV) Phthalocyanines

Phthalocyanines with a Group IV metal center can be structurally modified via the attachment of axial substituents. Axially ligated silicon phthalocyanines have advantages over other peripherally substituted phthalocyanines. Firstly these derivatives usually do not exhibit as isomers. Additionally, the axial ligands can not only increase the solubility, but also prevent the aggregation of the phthalocyanines.

The preparation of these silicon phthalocyanines usually involves the silicon phthalocyanine dichloride ($SiPcCl_2$) (**6.2**) as a precursor, which can be prepared by treating 1,3-diiminoisoindoline (**6.1**) with silicon tetrachloride in quinoline (Scheme 6.1).[6] This compound has a poor solubility in common organic solvents and can only be purified by Soxhlet extraction with different solvents. Different axial substituents can then be introduced by replacing the axial chloro ligands by substitution reactions. The resulting axially substituted phthalocyanines usually have improved solubility, which allows their purification by column chromatography.

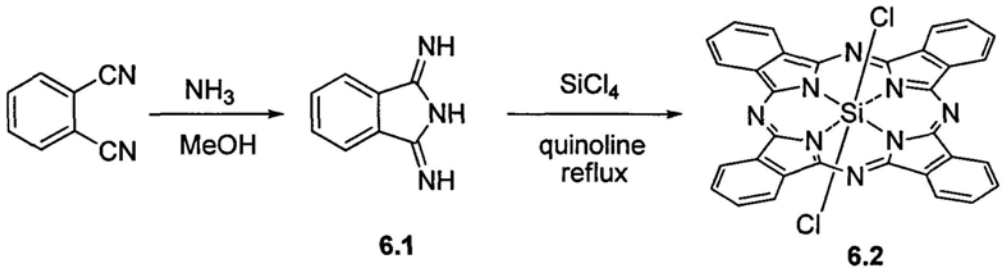

Scheme 6.1. Synthesis of silicon phthalocyanine dichloride (**6.2**).

6.1.3 Design of a Metal Sensor Based on Silicon(IV) Phthalocyanine

As mentioned in Chapter 5, zinc is the second most abundant transition metal element in the human body and it plays an important role in many biological processes.[7] Therefore, the design and development of novel fluorescent probes which can selectively detect and image Zn^{2+} ion in biological systems has received much current interest.[8] Near-infrared (NIR) dyes with emission wavelengths in the region of 650-900 nm are regarded as ideal fluorophores due to their good transmission and low autofluorescence in biological systems.[7b,8c] Silicon(IV) phthalocyanines are desirable candidates for this application because of their strong fluorescence emission at ca. 670 nm and ease of conjugation with various metal chelators. However, phthalocyanine-based fluorescence sensors remain little studied.[9] We describe herein a silicon(IV) phthalocyanine with two axial bis(2-picolyl)amine moieties which can act as a Zn^{2+} ion fluorescence sensor.

6.2 Results and Discussion

6.2.1 Chemical Synthesis and Spectroscopic Characterization

The synthesis of compound **6.6** is depicted in Scheme 6.2. Firstly, N,N-bis(2-picolyl)-2-aminoethanol (**6.5**) was prepared by nucleophilic addition of 2-pyridinecarboxaldehyde (**6.3**) with 2-aminoethanol (**6.4**) followed by reduction with a mixture of sodium cyanoborohydride and acetic acid.[10] It was then reacted with silicon phthalocyanine dichloride (**6.2**) in the presence of NaH in toluene to give the target compound **6.6** in a relatively low yield. This compound was purified by silica gel column chromatography and fully characterized with various spectroscopic methods.

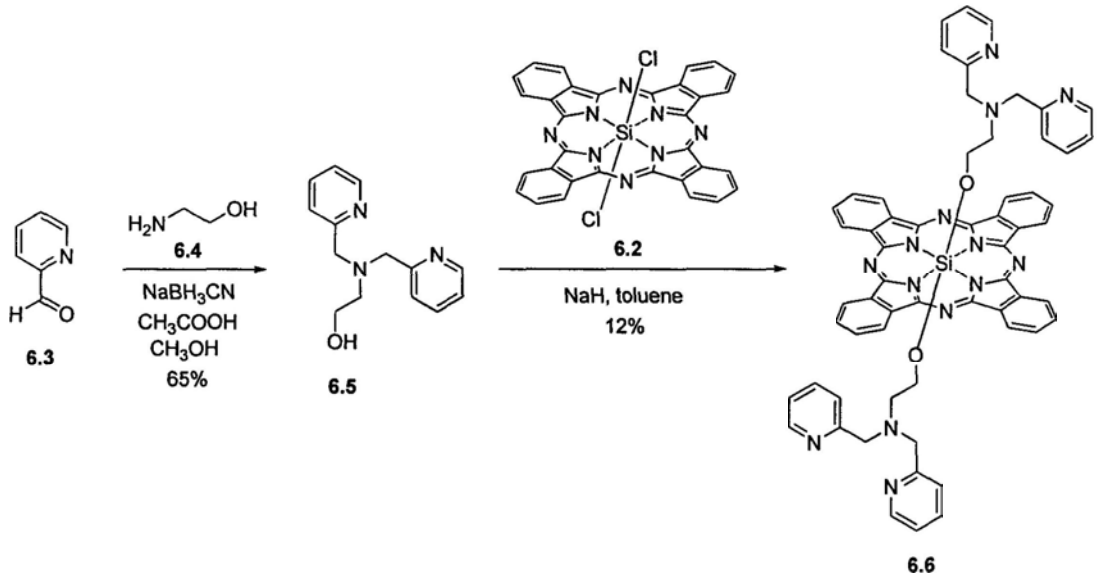

Scheme 6.2. Synthesisof phthalocyanine **6.6**.

Figure 6.2 shows the ^{1}H NMR spectrum of phthalocyanine **6.6** in $CDCl_3$. The two downfield multiplets at 9.54-9.57 and 8.29-8.33 ppm are due to the phthalocyanine α and β ring protons, respectively. The four sets of signals from 5.47

to 7.97 ppm are due to the pyridyl protons. In addition, two well-separated triplets and a singlet are also observed for the methylene protons of the axial moieties. Due to the shielding effect by the ring current, these signals are significantly shifted upfield.

The $^{13}C\{^1H\}$ NMR spectra of this compound showed clearly the expected number of signals. This compound was further characterized with ESI mass spectrometry. The isotopic distribution as well as the exact mass for the $[M + Na]^+$ species was in good agreement with the calculated one.

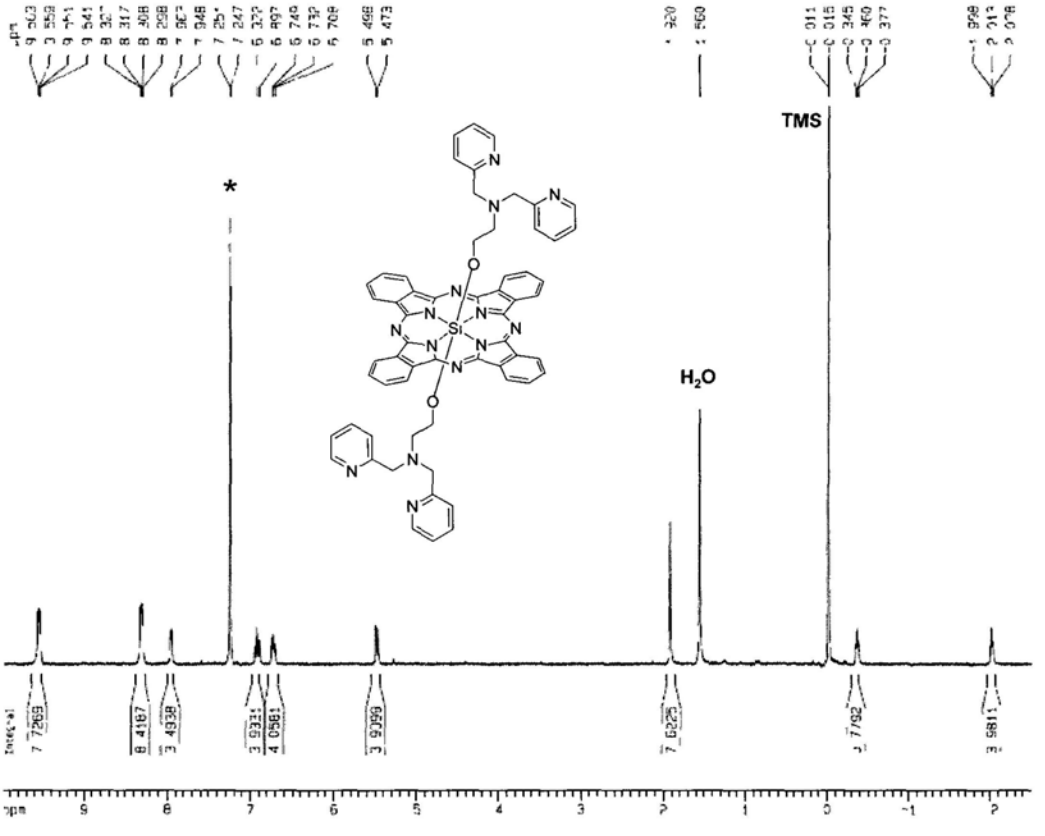

Figure 6.2. ^1H NMR spectrum of phthalocyanine **6.6** in $CDCl_3$; * indicates residual solvent signal.

6.2.2 Spectral Response to Various Metal Ions in MeCN

The electronic absorption spectrum of **6.6** was first recorded in MeCN. It showed a Soret band peaking at 353 nm, an intense and sharp Q band at 672 nm, together with two vibronic bands at 604 and 640 nm. The Q band strictly followed the Lambert Beer's law showing that the compound was non-aggregated in MeCN (Figure 6.3).

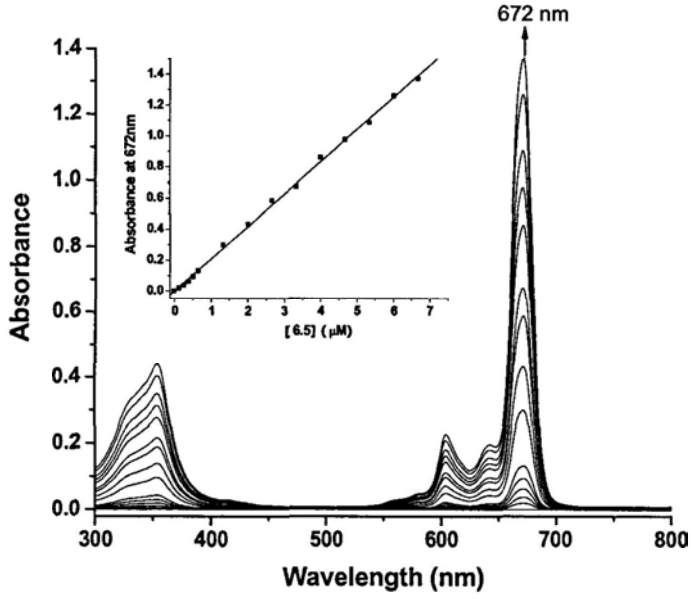

Figure 6.3. Electronic absorption spectra of **6.6** at various concentrations in MeCN. The inset plots the Q-band absorbance versus the concentration of **6.6**.

The spectral response of **6.6** toward various metal ions was then examined and the results are shown in Figure 6.4. Upon addition of Zn^{2+}, Cd^{2+}, Hg^{2+}, Na^{+}, K^{+}, Mg^{2+}, or Ca^{2+} ion, no significant change in the absorption spectrum was observed. However, addition of Cu^{2+} or Pb^{2+} ion induced a bathochromic shift of ca. 10 nm to the Q band.

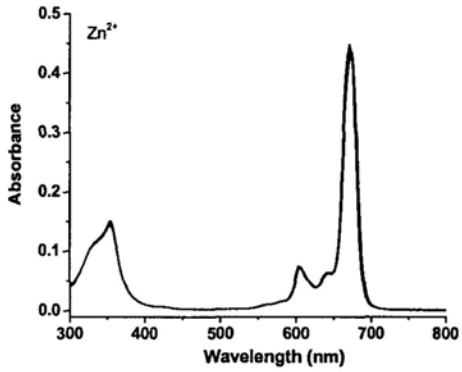
Zn^{2+}
Absorbance
Wavelength (nm)

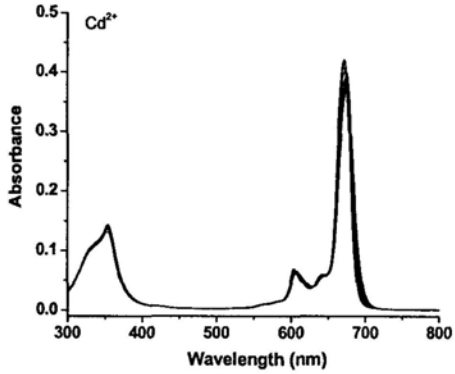
Cd^{2+}
Absorbance
Wavelength (nm)

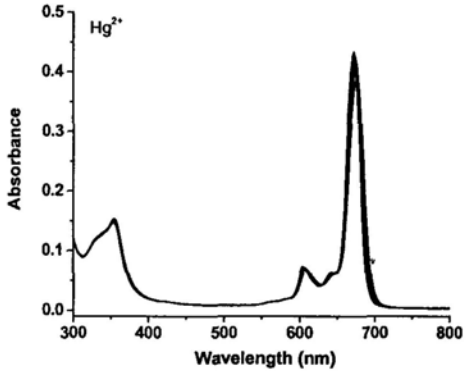
Hg^{2+}
Absorbance
Wavelength (nm)

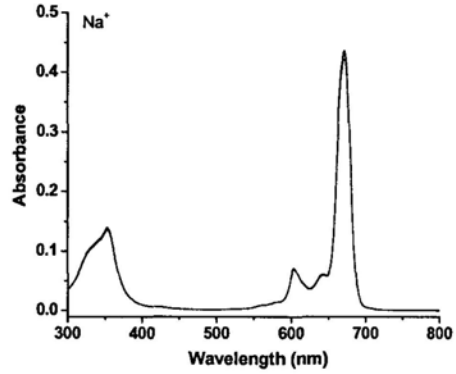
Na^{+}
Absorbance
Wavelength (nm)

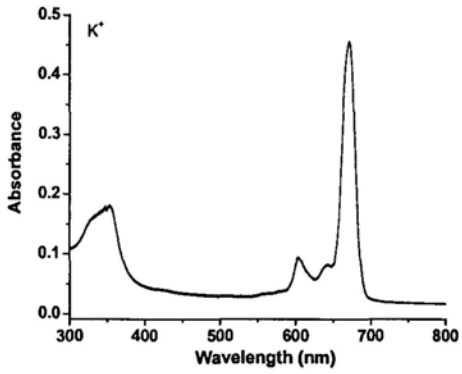
K^{+}
Absorbance
Wavelength (nm)

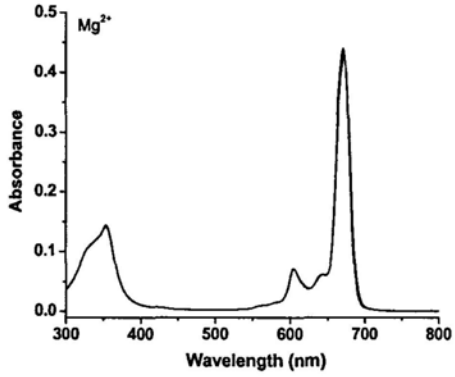
Mg^{2+}
Absorbance
Wavelength (nm)

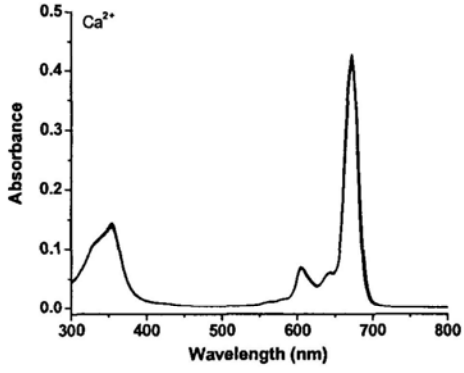
Ca^{2+}
Absorbance
Wavelength (nm)

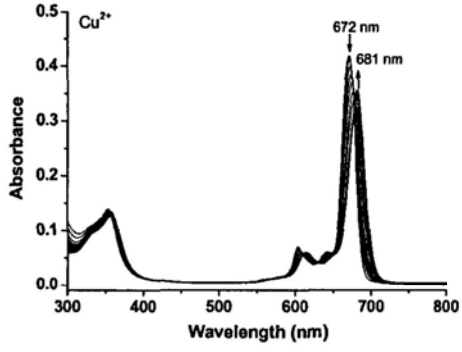
Cu^{2+}
672 nm
681 nm
Absorbance
Wavelength (nm)

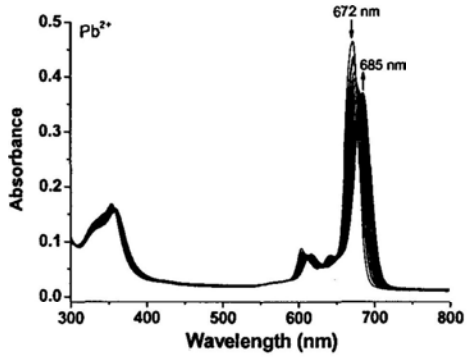

Figure 6.4. Changes in electronic absorption spectrum of **6.6** in MeCN (2 μM) upon addition of various metal ions (0-30 μM).

The fluorescence emission spectrum of **6.6** was also recorded in MeCN. It exhibited a weak fluorescence emission at ca. 680 nm as a result of the efficient photoinduced electron transfer (PET), which quenches the singlet excited state of the silicon phthalocyanine by the lone pair of electrons at the nitrogen atoms in the axial moieties (Figure 6.5). In the presence of Zn^{2+} ion, the lone pair electrons at the nitrogen atoms participated in coordination and the PET process was inhibited. Therefore, upon addition of Zn^{2+} ion, the fluorescence intensity at 676 nm gradually increased and eventually reached a 5-fold enhancement.

The binding stoichiometry of **5.8a** and Zn^{2+} was examined by a Job's plot. The result indicated that **6.6** chelated Zn^{2+} ion with a 1:2 stoichiometry (Figure 6.6). The overall association constant K was determined by a 1:2 nonlinear least-squares analysis[11] of the change in fluorescence intensity with the concentration of Zn^{2+} ion (the inset of Figure 6.5). The value was found to be $(6.2 \pm 0.9) \times 10^{11}$ M^{-2}. The proposed binding mode and the sensing mechanism can be depicted as Figure 6.7.

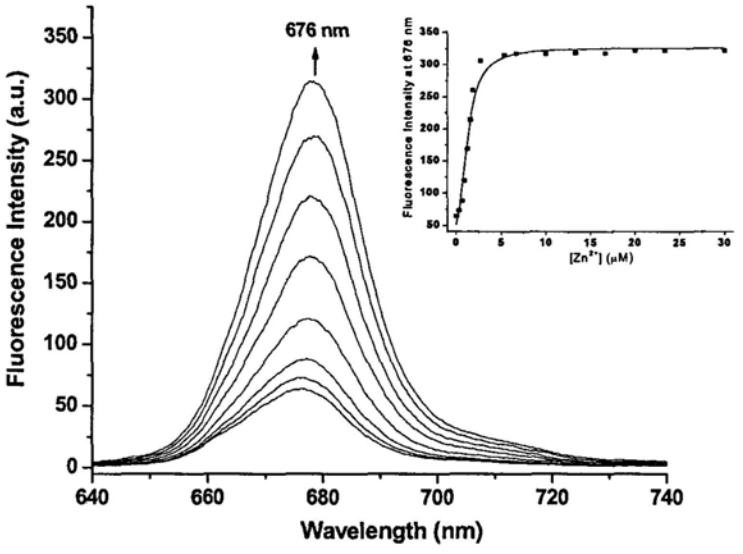

Figure 6.5. Change in fluorescence spectrum (excited at 610 nm) of **6.6** in MeCN (2 μM) upon addition of Zn^{2+} ion (0-30 μM). The inset plots the fluorescence intensity at 676 nm versus the concentration of Zn^{2+} ion.

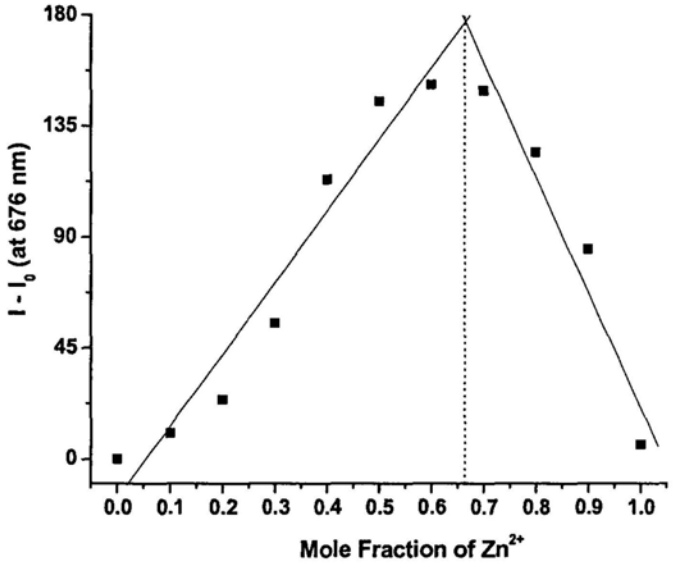

Figure 6.6. Job's plot for the binding of **6.6** with Zn^{2+} ion. The total concentration of **6.6** and Zn^{2+} was fixed at 4 μM.

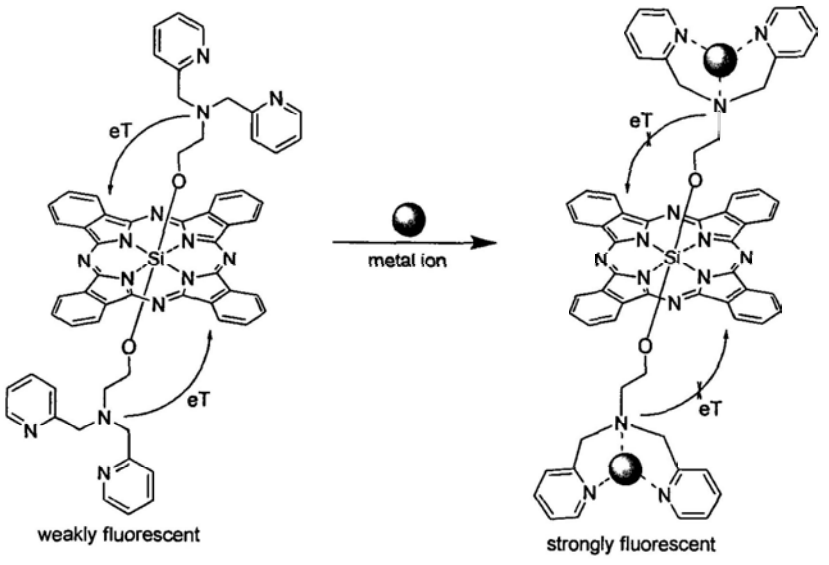

Figure 6.7 Proposed binding mode and the sensing mechanism of **6.6** with metal ions.

The response of the fluorescence emission of **6.6** toward other metal ions was also examined in MeCN (Figure 6.8). The effects for Cd^{2+} and Hg^{2+} ions were similar to that for Zn^{2+}, but somewhat weaker. Mg^{2+}, Ca^{2+}, Na^{+}, and K^{+} ions had little effect on the fluorescence spectrum of **6.6**. Cu^{2+} ion quenched the fluorescence effectively due to electron transfer, while Pb^{2+} ion reduced the emission intensity at 676 nm and at the same time induced a new emission at 688 nm. This band slightly decreased in intensity upon addition of a large excess of Pb^{2+} ion. As shown in Figure 6.9, Zn^{2+} ion induces the greatest fluorescence enhancement. Table 6.1 summarizes all these spectral data including the fluorescence enhancement factor (FEF) and the binding constants of several systems. It can be seen that the FEF increases as the binding constant between **6.6** and the metal ion increases.

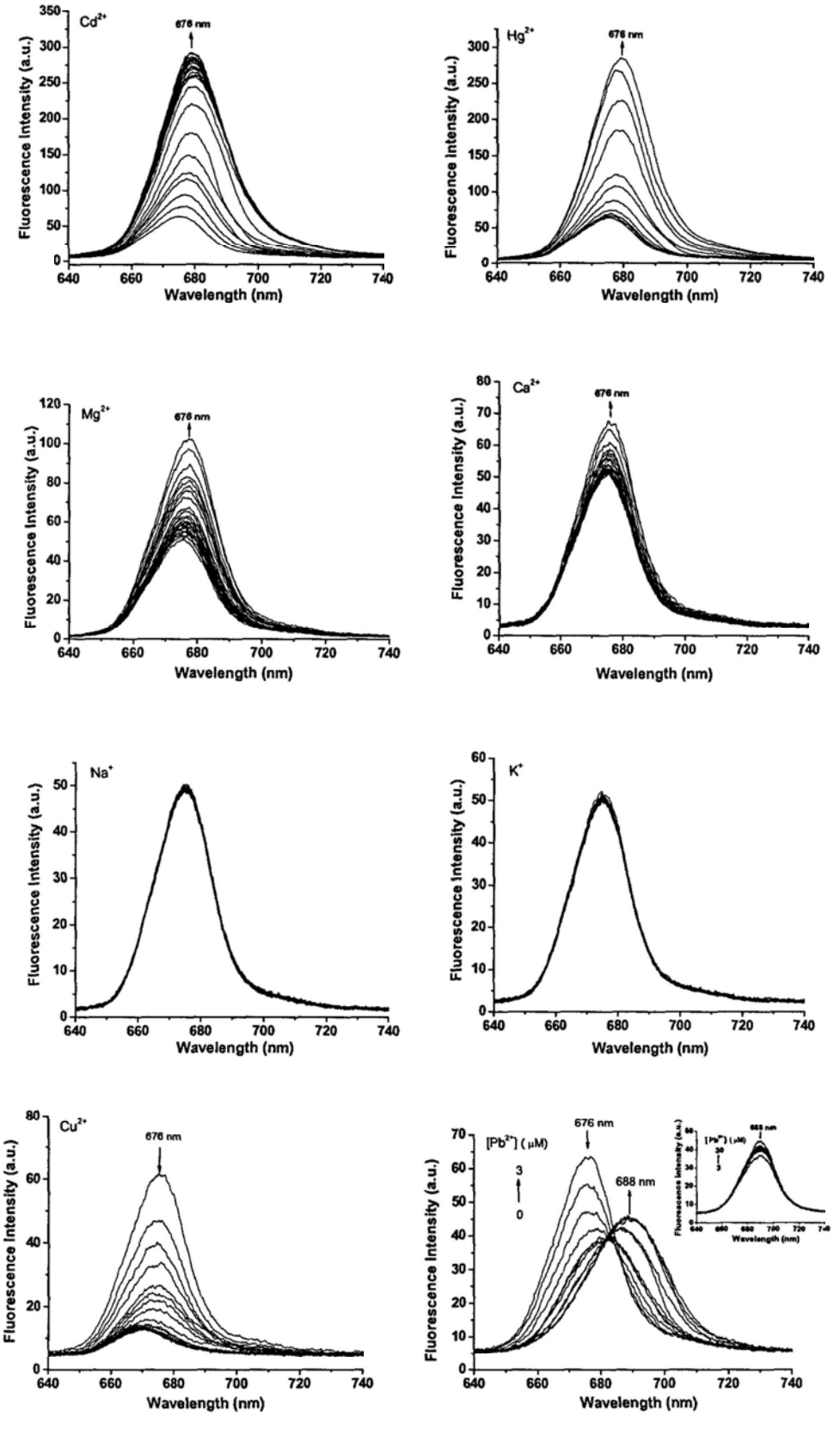

Figure 6.8. Changes in fluorescence emission spectrum of **6.6** in MeCN (2 μM) upon addition of various metal ions (0-30 μM).

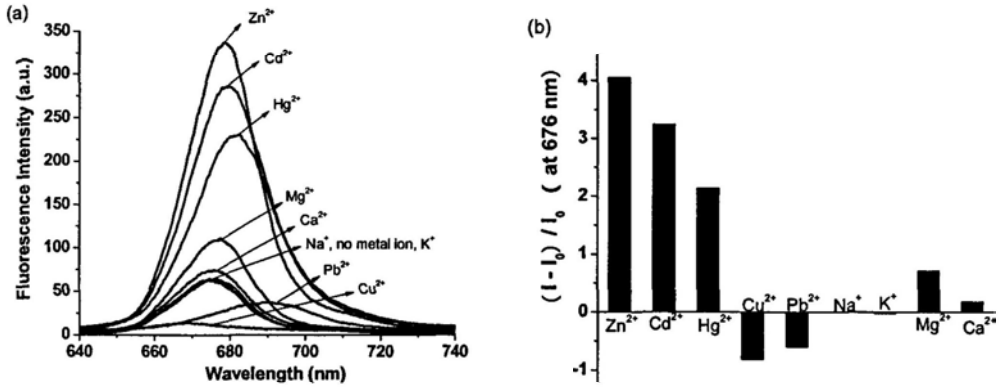

Figure 6.9. Fluorescence emission spectra (a) and change in fluorescence intensity at 676 nm (b) of **6.6** (2 μM) in the presence of 30 μM various metal ions in MeCN.

Table 6.1. Electronic absorption and fluorescence data for **6.6** in the presence of 15 equiv. of various metal ions in MeCN.

Compound	λ_{max} (nm) (log ε)	λ_{em}[a] (nm)	Φ_F[b]	FEF	K (M^{-2})
6.6	674 (5.31)	676	0.04	-	-
6.6-Zn^{2+}	672 (5.32)	678	0.20	5	$(6.2 \pm 0.9) \times 10^{11}$
6.6-Cd^{2+}	675 (5.30)	679	0.17	4.3	$(4.3 \pm 0.6) \times 10^{11}$
6.6-Hg^{2+}	676 (5.29)	680	0.13	3.3	-
6.6-Cu^{2+}	681 (5.25)	668	0.007	0.18	-
6.6-Pb^{2+}	685 (5.27)	689	0.016	0.4	-
6.6-Na^{+}	672 (5.32)	676	0.04	1	-
6.6-K^{+}	672 (5.32)	676	0.04	1	-
6.6-Mg^{2+}	673 (5.31)	678	0.06	1.5	$(4.3 \pm 1.0) \times 10^{9}$
6.6-Ca^{2+}	673 (5.31)	677	0.05	1.3	$(1.4 \pm 0.3) \times 10^{9}$

[a] Excited at 610 nm. [b] Relative to ZnPc (Φ_F = 0.28 in DMF).[12]

6.3 Conclusion

In summary, we have synthesized a novel phthalocyanine which can serve as a fluorescent sensor for Zn^{2+} ion. The complexation leads to fluorescence enhancement due to inhibition of the PET process.

6.4 Experimental Section

6.4.1 General

Experimental details regarding the purification of solvents and instrumentation have been described in Section 2.4.1. The salts used for the complexation studies are the same as those used in Chapter 5.

The association constants were determined by nonlinear least-squares analysis using the 1:2 binding equation: $y = (I_0 + I'Kx^2)/(1 + Kx^2)$,[11] where y is the emission intensity of **6.6** in the presence of metal ion, I_0 is the initial emission intensity of metal-free **6.6**, I' is the ultimate emission intensity of a 1:2 **6.6**-metal ion complex, K is the overall association constant of **6.6** with metal ion, x is the concentration of metal ion.

6.4.2 Synthesis

N,N-bis(2-picolyl)-2-aminoethanol (6.5).[10] To a solution of 2-pyridinecarboxaldehyde (**6.3**) (2.14 g, 20 mmol) in methanol (20 mL) containing sodium cyanoborohydride (0.63 g, 10 mmol) was added dropwise a solution of 2-aminoethanol (**6.4**) (0.61 g, 10 mmol) in anhydrous methanol (20 mL) containing

glacial acetic acid (0.12 g, 2 mmol). After the addition, the solution was stirred at room temperature for 48 h. The solvent was evaporated in vacuo, then water (20 mL) was added. The solution was neutralized by saturated aqueous Na_2CO_3 and extracted with chloroform (50 mL × 2) to give a brown oil. The residue was purified by column chromatography using CH_2Cl_2/MeOH (20:1, v/v) as eluent to afford a light yellow oil (1.58 g, 65%). ^{1}H NMR (300 MHz, $CDCl_3$): δ 8.54 (d, J = 4.8 Hz, 2H, C_5H_4N), 7.61 (t, J = 7.8 Hz, 2H, C_5H_4N), 7.32 (d, J = 7.8 Hz, 2H, C_5H_4N), 7.15 (t, J = 6.6 Hz, 2H, C_5H_4N), 3.93 (s, 4H, NCH_2), 3.69 (t, J = 5.1 Hz, 2H, NCH_2), 2.88 (t, J = 5.1 Hz, 2H, OCH_2).

Phthalocyanine 6.6. A mixture of N,N-bis(2-picolyl)-2-aminoethanol (**6.5**) (0.1 g, 0.41 mmol), silicon phthalocyanine dichloride (**6.2**) (0.125 g, 0.21 mmol), and NaH (20 mg, 0.83 mmol) in toluene (10 mL) was refluxed for 6 h. The solvent was removed in vacuo and the residue was dissolved in dichloromethane and filtered. The filtrate was then dried in vacuo and the residue was subject to column chromatography using $CHCl_3$/MeOH/TEA (100:10:1, v/v) as eluent. The greenish blue solid obtained was further purified by recrystallization from CH_2Cl_2/hexane (1:10, v/v) (26 mg, 12%). ^{1}H NMR (300 MHz, $CDCl_3$): δ 9.55-9.58 (m, 8H, Pc-H_α), 8.31-8.34 (m, 8H, Pc-H_β), 7.80 (d, J = 4.8 Hz, 4H, C_5H_4N), 6.93 (t, J = 7.5 Hz, 4H, C_5H_4N), 6.74 (t, J = 7.5 Hz, 4H, C_5H_4N), 5.50 (d, J = 7.5 Hz, 4H, C_5H_4N), 1.93 (s, 8H, NCH_2), –0.35 (t, J = 4.5 Hz, 4H, NCH_2), –2.00 (t, J = 4.5 Hz, 4H, OCH_2); $^{13}C\{^1H\}$ NMR (75.4 MHz, $CDCl_3$): δ 159.01, 149.20, 147.95, 135.83, 135.51, 130.85, 123.67, 121.25, 120.95, 58.73, 53.41, 53.18; MS (ESI): isotopic clusters

peaking at 782 {70%, $[M - DPA]^+$}, 1047 {5%, $[M + Na]^+$}; HRMS (ESI): *m/z* calcd for $C_{60}H_{48}N_{14}NaO_2Si$ $[M + Na]^+$:1047.3757; found:1047.3747.

6.5 References

1 Braun, A.; Tcherniac, J. *Ber. Deut. Chem. Ges.* **1907**, *40*, 2709.

2 (a) Linstead, R. P. *J. Am. Chem. Soc.* **1934**, *56*, 1016. (b) Linstead, R. P.; Lowe, A. R. *J. Am. Chem. Soc.* **1934**, *56*, 1022. (c) Linstead, R. P.; Lowe, A. R. *J. Am. Chem. Soc.* **1934**, *56*, 1031.

3 (a) *The Phthalocyanines - Properties*; Moser, F. H., Thomas, A. L., Eds.; CRC Press: Florida, **1983**.

4 (a) *Phthalocyanines - Properties and Applications*; Leznoff, C. C., Lever, A. B. P., Eds.; VCH: New York, **1989**, Vol. 1; **1993**, Vols. 2 and 3; **1996**, Vol. 4. (b) *Phthalocyanine Materials: Synthesis, Structure and Function*; McKeown, N. B. Eds.; Cambridge University Press: Cambridge, **1998**.

5 (a) Huang, J.-D.; Wang, S.; Lo, P.-C.; Fong, W.-P.; Ko, W.-H.; Ng, D. K. P. *New J. Chem.* **2004**, *28*, 348. (b) Lo, P.-C.; Huang, J.-D.; Cheng, D. Y. Y.; Chan, E. Y. M.; Fong, W.-P.; Ko, W.-H.; Ng, D. K. P. *Chem. Eur. J.* **2004**, *10*, 4831. (c) Choi, C.-F.; Tsang, P.-T.; Huang, J.-D.; Chan, E. Y. M.; Ko, W.-H.; Fong, W.-P.; Ng, D. K. P. *Chem. Commun.* **2004**, 2236. (d) Lo, P.-C.; Chan, C. M. H.; Liu, J.-Y.; Fong, W.-P.; Ng, D. K. P. *J. Med. Chem.* **2007**, *50*, 2100. (e) Liu, J.-Y.; Jiang, X.-J.; Fong, W.-P.; Ng, D. K. P. *Org. Biomol. Chem.* **2008**, *6*, 4560. (f) Liu, J.-Y.; Lo, P.-C.; Jiang, X.-J.; Fong, W.-P.; Ng, D. K. P. *J. Chem.*

Soc., Dalton Trans. **2009**, 4129. (g) Jiang, X.-J.; Lo, P.-C.; Tsang, Y.-M.; Yeung, S.-L.; Fong, W.-P.; Ng, D. K. P. *Chem. Eur. J.* **2010**, *16*, 4777. (h) Jiang, X.-J.; Lo, P.-C.; Yeung, S.-L.; Fong, W.-P.; Ng, D. K. P. *Chem. Commun.* **2010**, *46*, 3188.

6 Lowery, M. K.; Starshak, A. J.; Esposito, J. N.; Krueger, P. C.; Kenney, M. E. *Inorg. Chem.* **1965**, *4*, 128.

7 (a) Bush, A. I. *Curr. Opin. Chem. Biol.* **2000**, *4*, 184. (b) Carol, P.; Sreejith, S.; Ajayaghosh, A. *Chem. Asian J.* **2007**, *2*, 338.

8 (a) Burdette, S. C.; Frederickson, C. J.; Bu, W.; Lippard, S. J. *J. Am. Chem. Soc.* **2003**, *125*, 1778. (b) Hanaoka, K.; Kikuchi, K.; Kojima, H.; Urano, Y.; Nagano, T. *J. Am. Chem. Soc.* **2004**, *126*, 12470. (c) Leevy, W. M.; Gammon, S. T.; Jiang, H.; Johnson, J. R.; Maxwell, D. J.; Jackson, E. N.; Marquez, M.; Worms, D. P.; Smith, B. D. *J. Am. Chem. Soc.* **2006**, *128*, 16476.

9 Kimura, M.; Hamakawa, T.; Hanabusa, K.; Shirai, H.; Kobayashi, N. *Inorg. Chem.* **2001**, *40*, 4775.

10 Groves, J. T.; Kady, I. O. *Inorg. Chem.* **1993**, *32*, 3868.

11 de la Peña, A. M.; Zung, N. J. B.; Warner, I. M. *J. Phys. Chem.* **1991**, *95*, 3330.

12 Scalise, I.; Durantini, E. N. *Bioorg. Med. Chem.* **2005**, *13*, 3037.

Appendix 1. ^{1}H NMR and $^{13}C\{^{1}H\}$ NMR spectra of compound **2.5** in $CDCl_3$

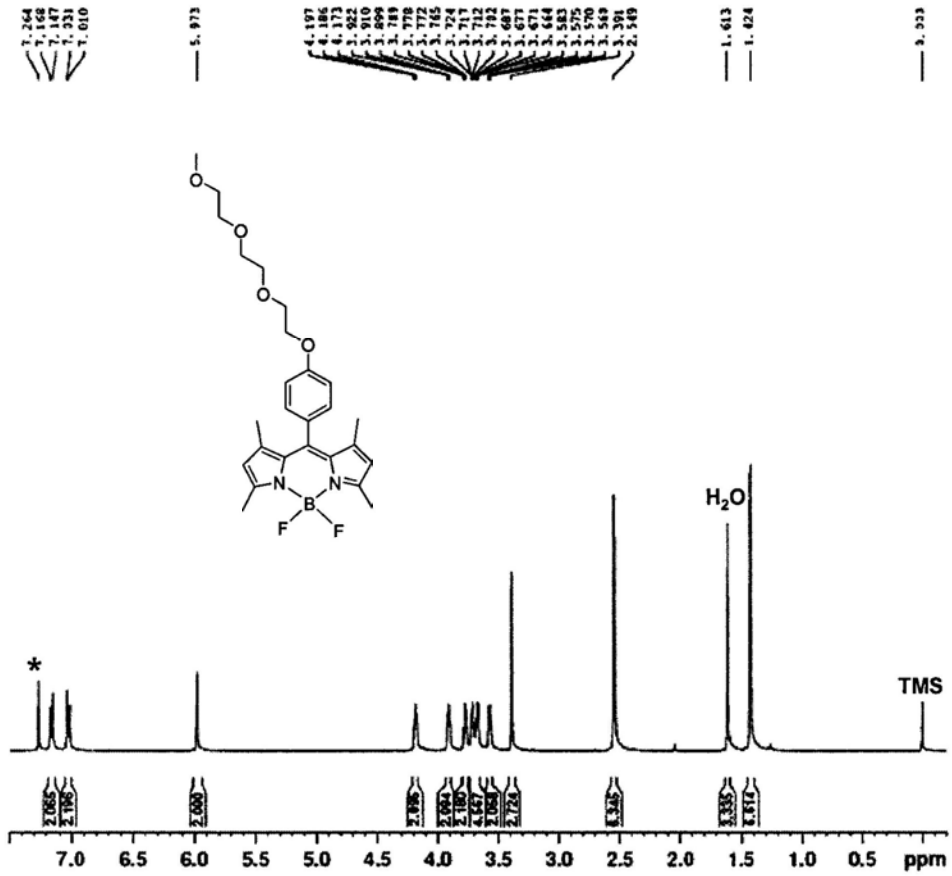

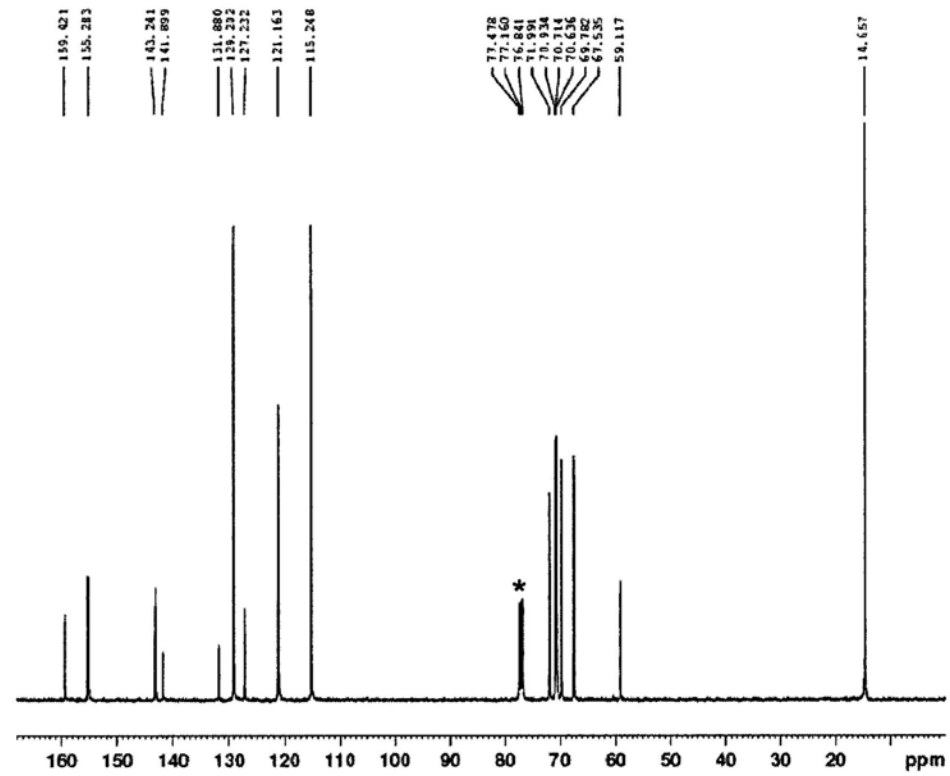

Appendix 2. ^{1}H NMR and $^{13}C\{^{1}H\}$ NMR spectra of compound **2.6** in $CDCl_3$

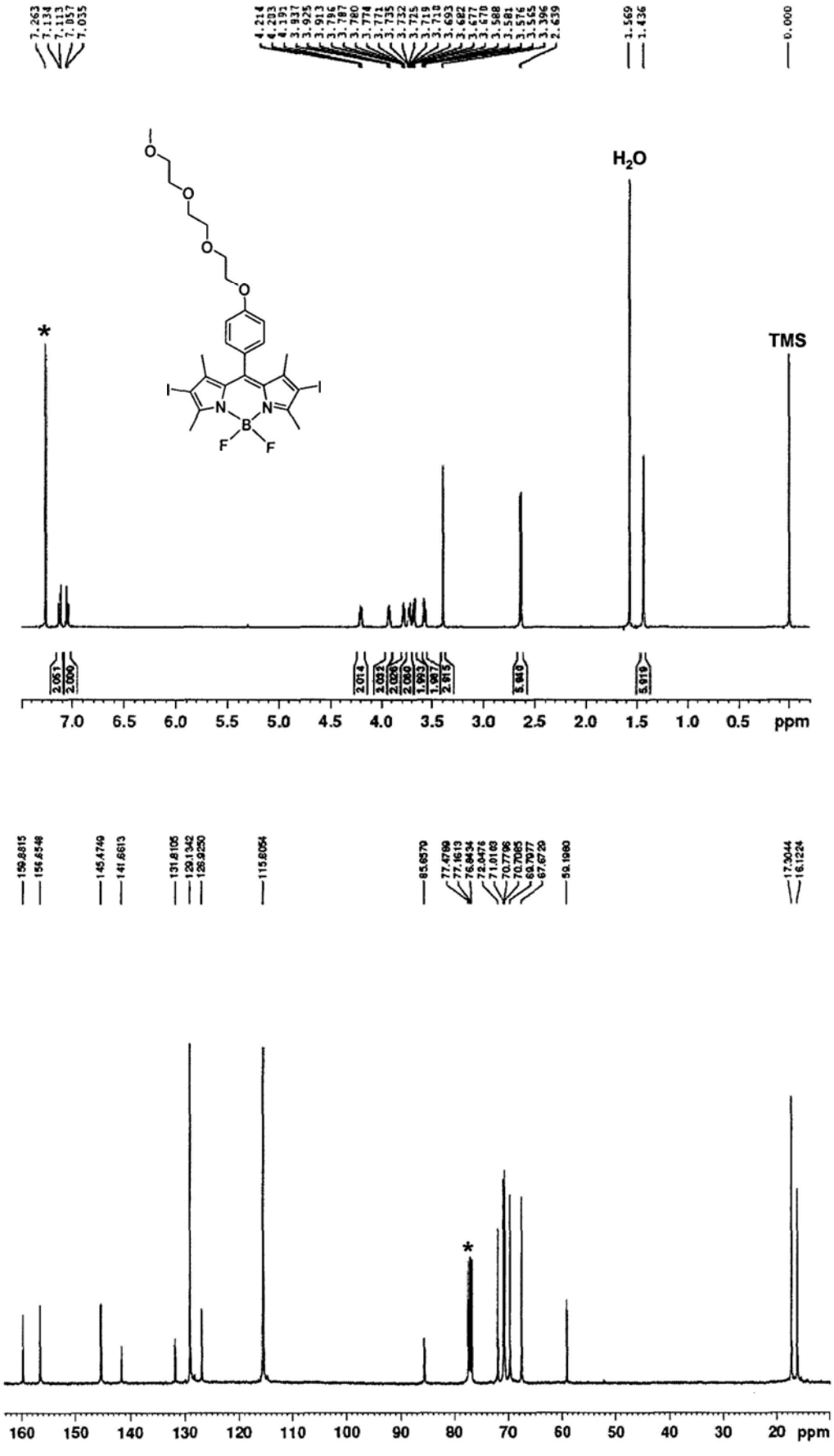

Appendix 3. ^{1}H NMR spectrum of compound **2.9d** in $CDCl_3$

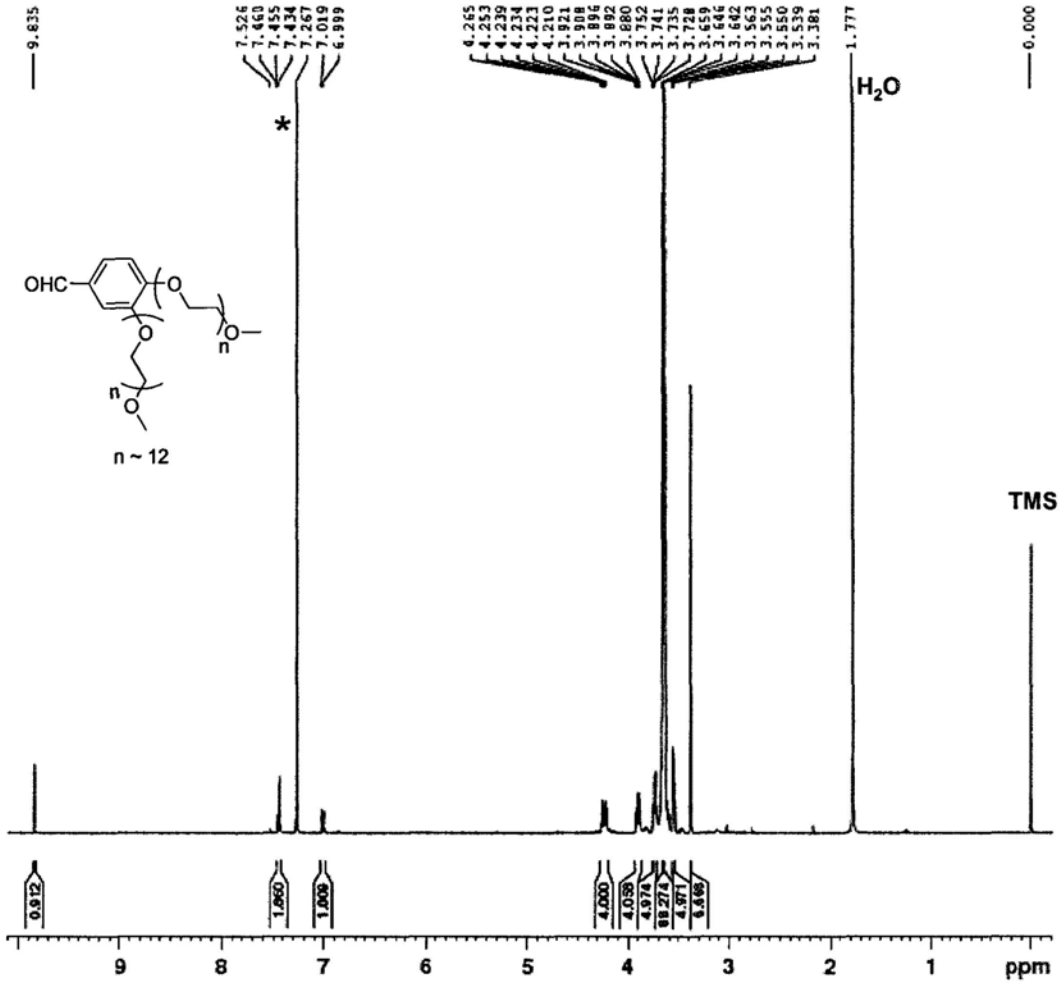

Appendix 4. ^{1}H NMR and $^{13}C\{^{1}H\}$ NMR spectra of compound **2.11a** in $CDCl_3$

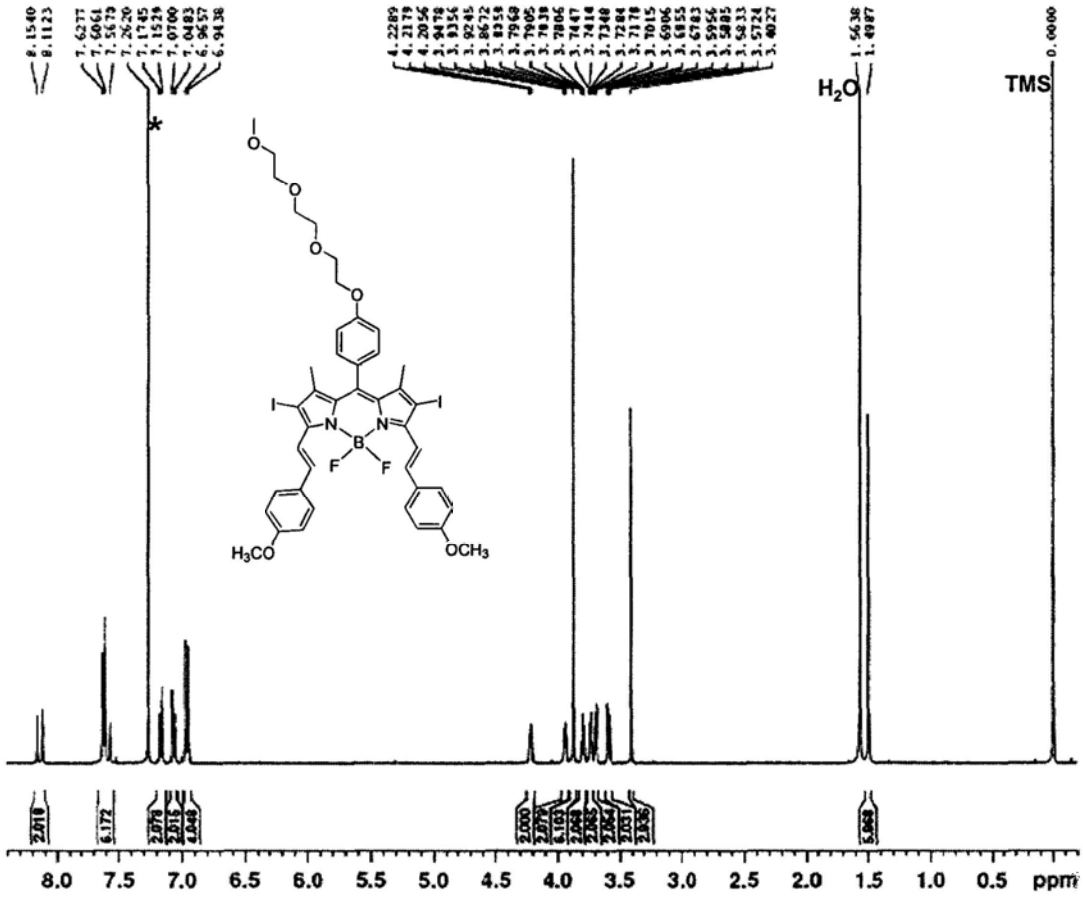

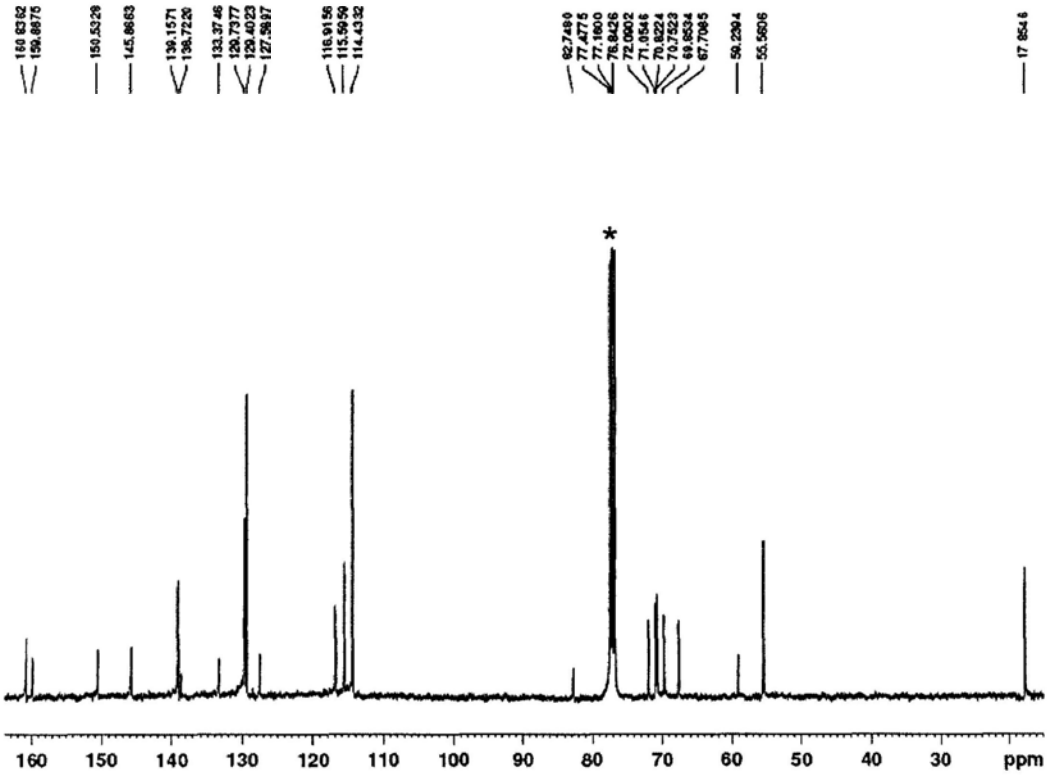

Appendix 5. ^{1}H NMR and $^{13}C\{^{1}H\}$ NMR spectra of compound **2.11b** in $CDCl_3$

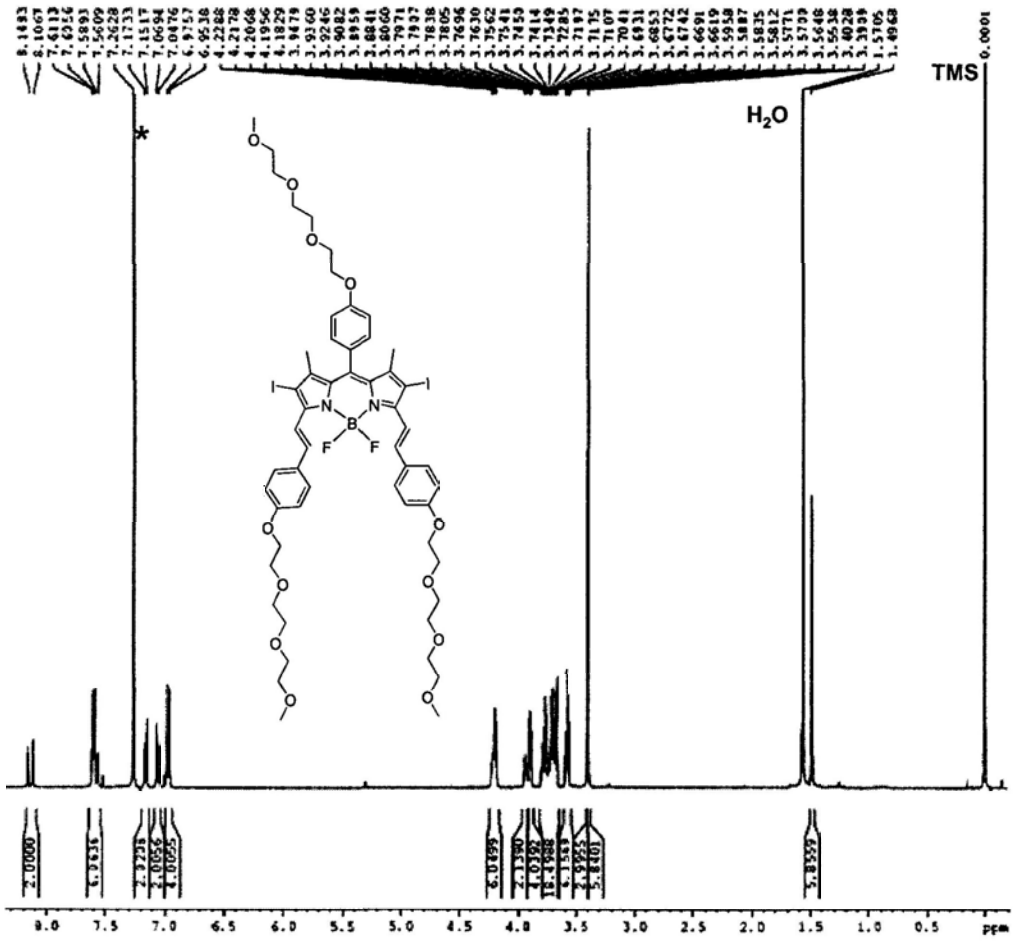

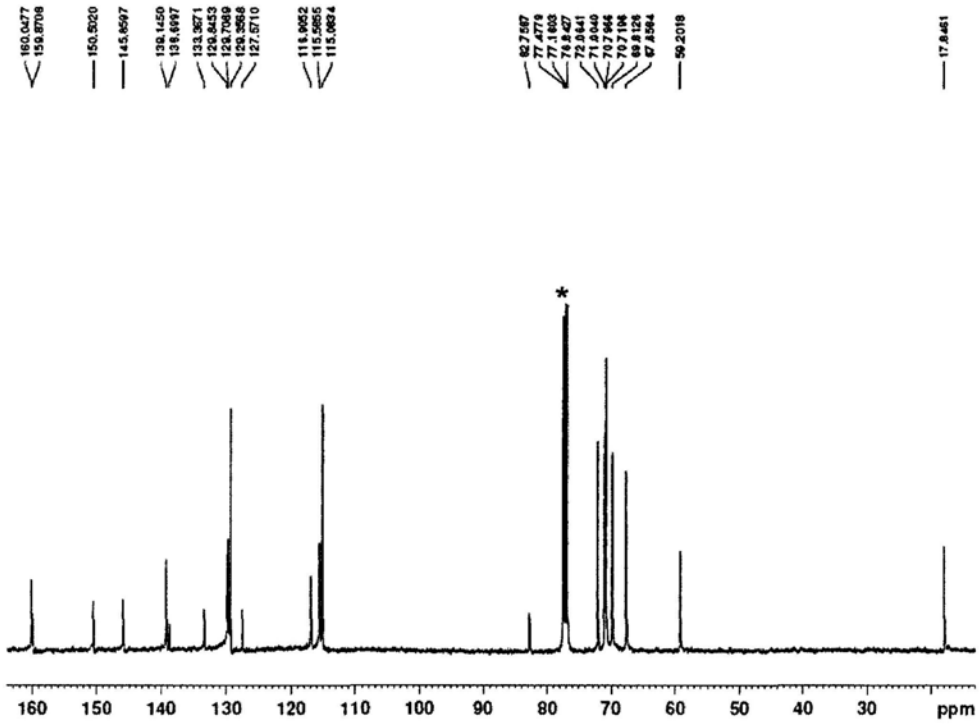

Appendix 6. ^{1}H NMR (in CD_2Cl_2) and $^{13}C\{^{1}H\}$ NMR (in $CDCl_3$) spectra of compound **2.11c**

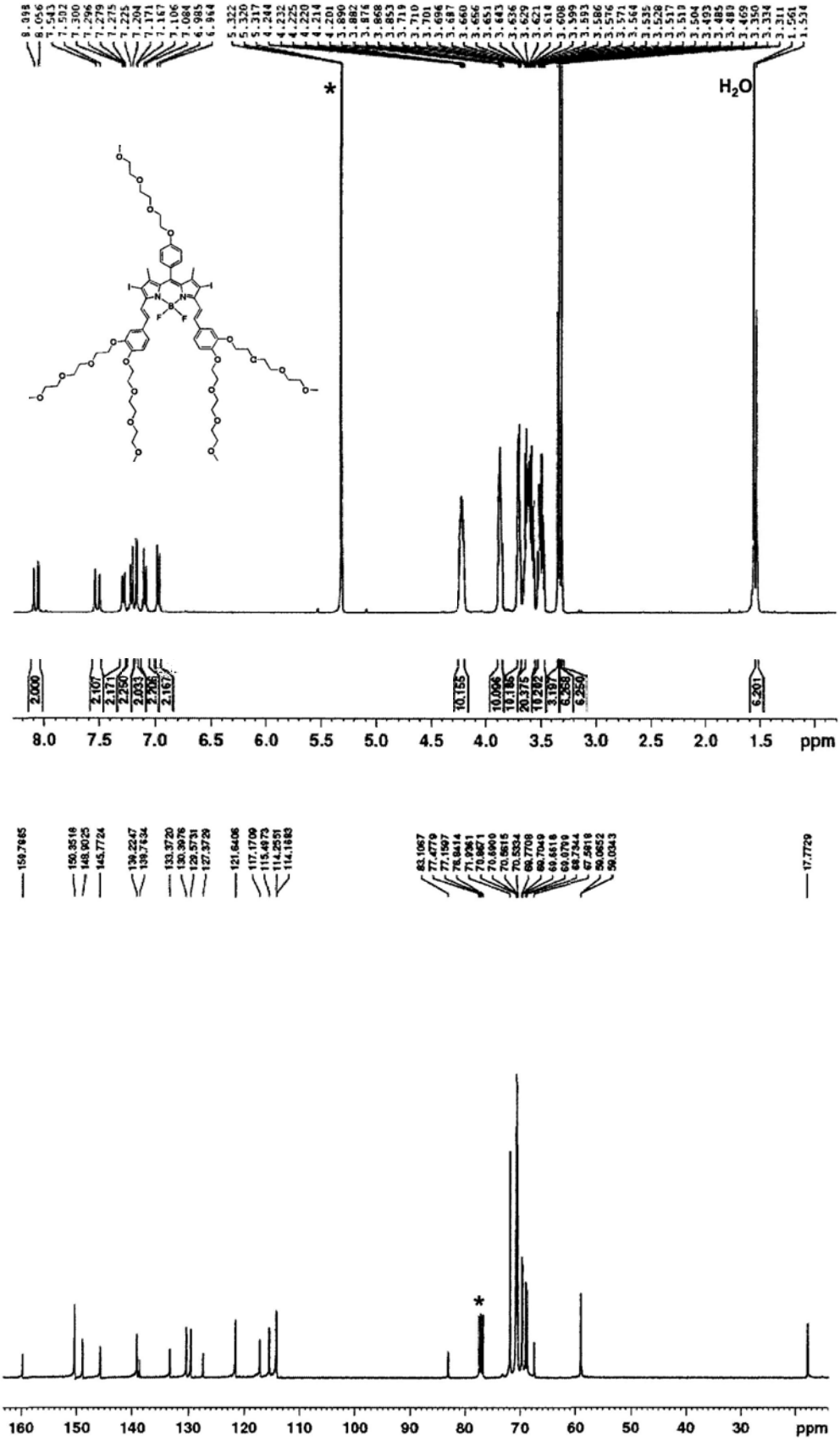

Appendix 7. ^{1}H NMR spectrum of compound **2.11d** in CD_2Cl_2

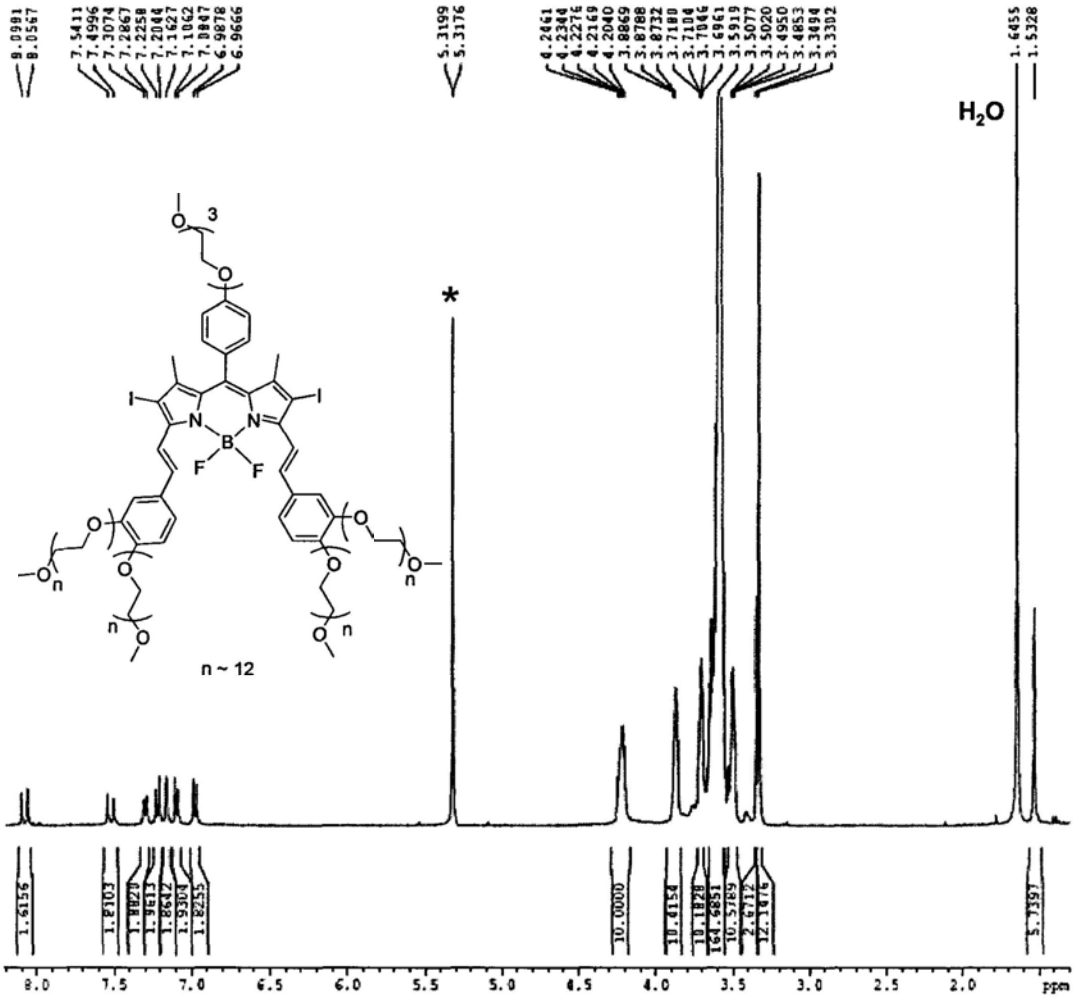

Appendix 8. ^{1}H NMR (in CD_2Cl_2) and $^{13}C\{^{1}H\}$ NMR (in $CDCl_3$) spectra of compound **3.1**

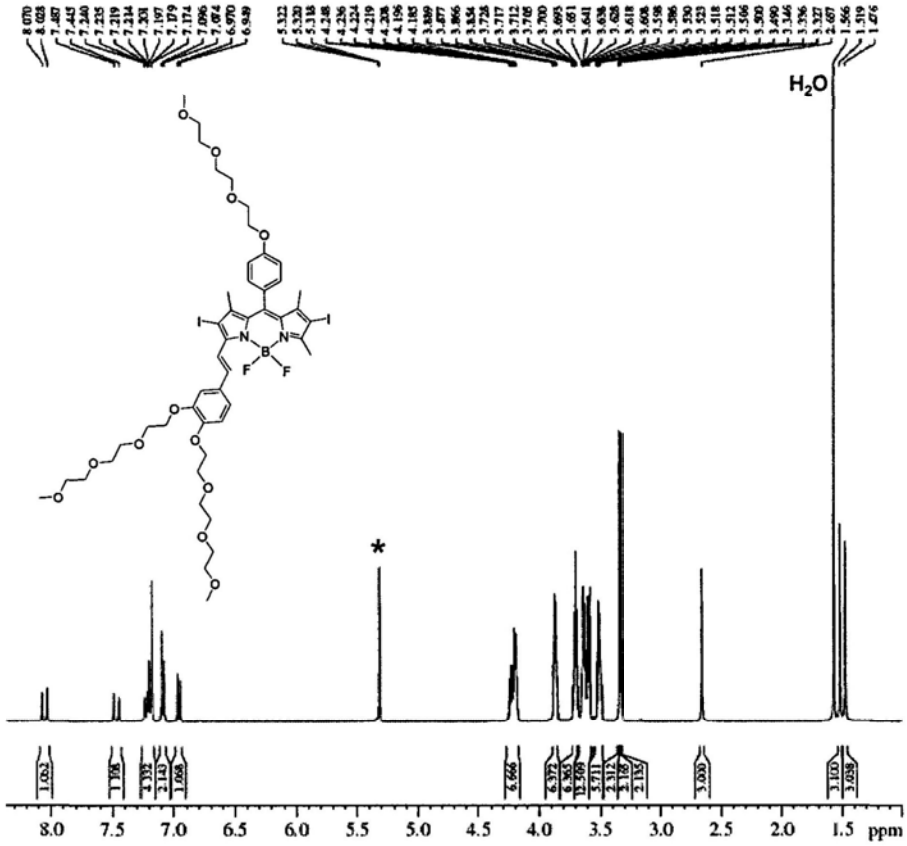

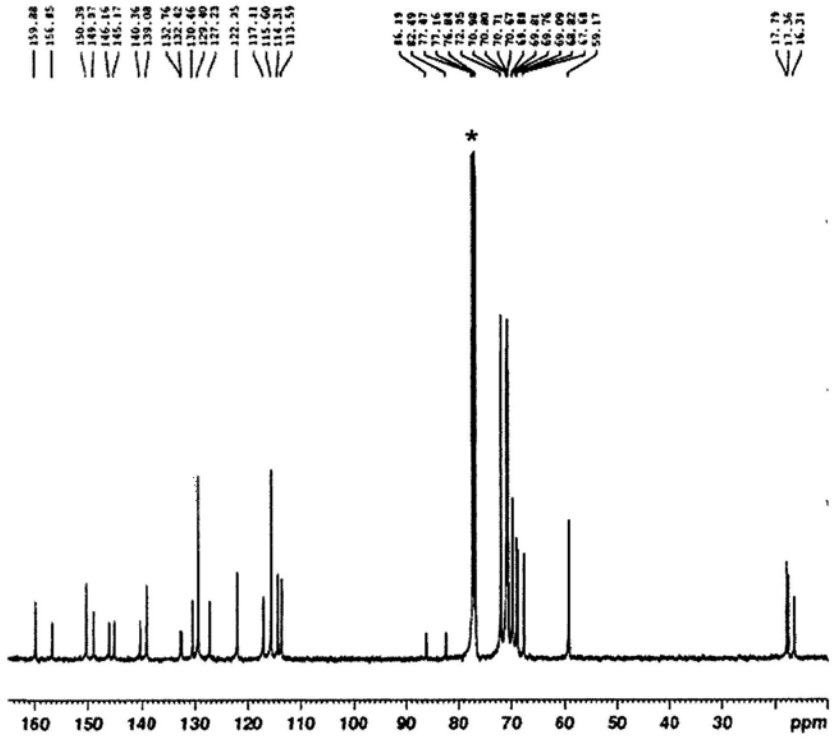

Appendix 9. ^{1}H NMR (in CD_2Cl_2) and $^{13}C\{^{1}H\}$ NMR (in $CDCl_3$) spectra of compound **3.6a**

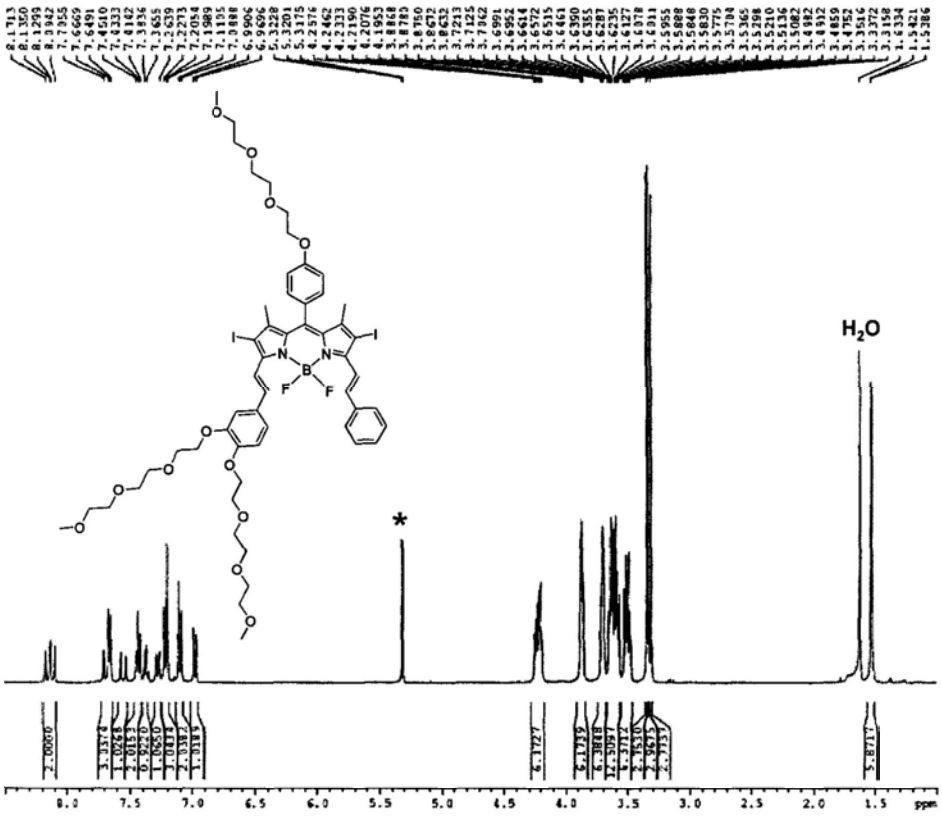

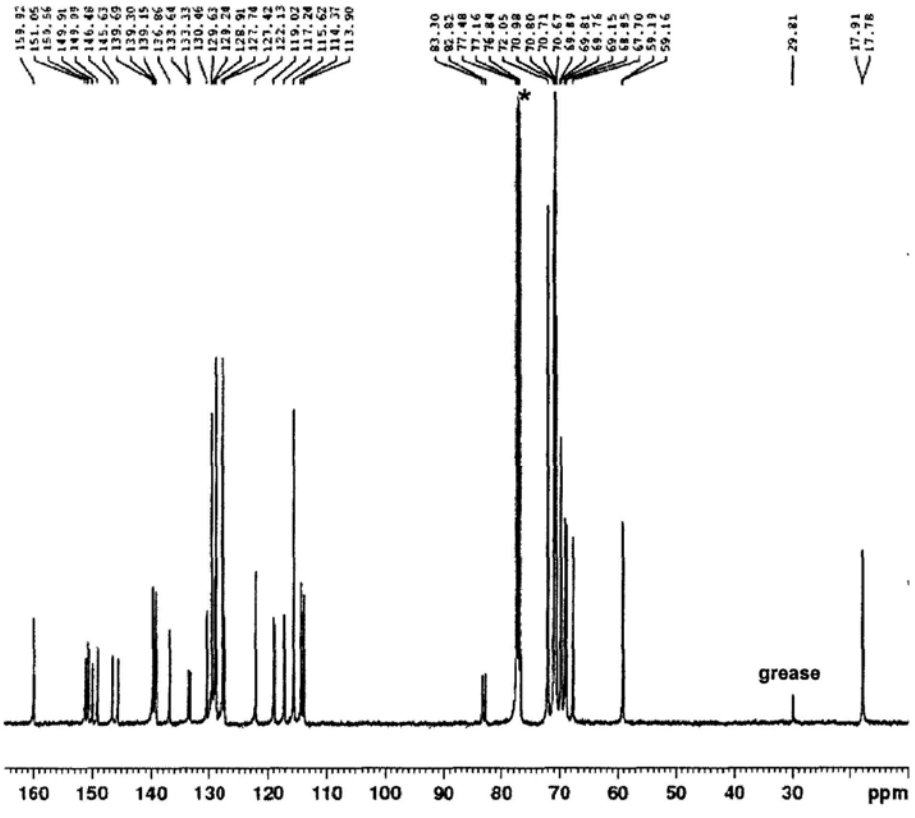

Appendix 10. ^{1}H NMR (in CD_2Cl_2) and $^{13}C\{^{1}H\}$ NMR (in $CDCl_3$) spectra of compound **3.6b**

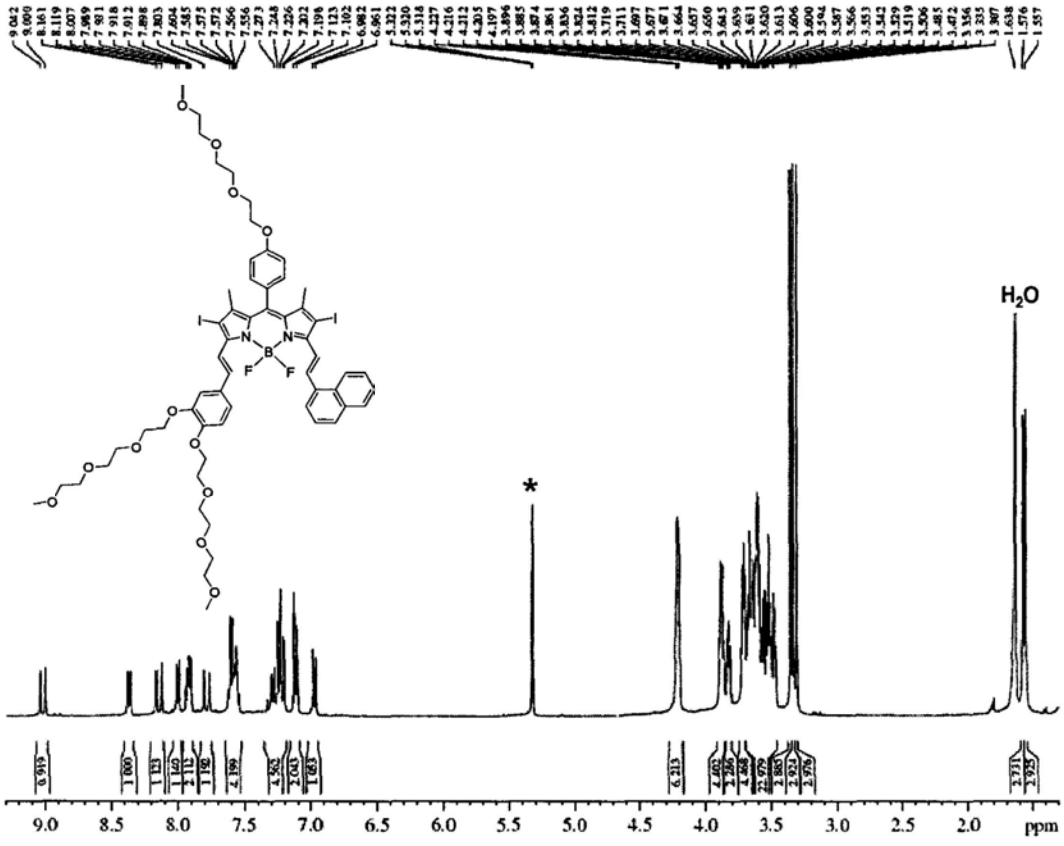

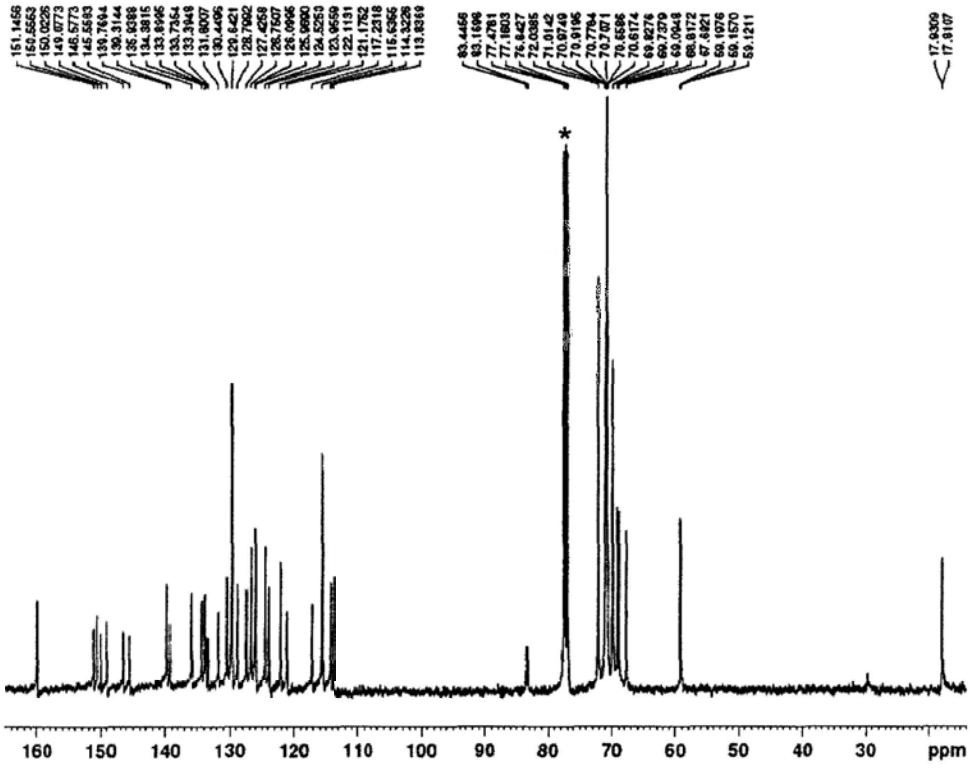

Appendix 11. ^{1}H NMR (in CD_2Cl_2) and $^{13}C\{^{1}H\}$ NMR (in $CDCl_3$) spectra of compound **3.6c**

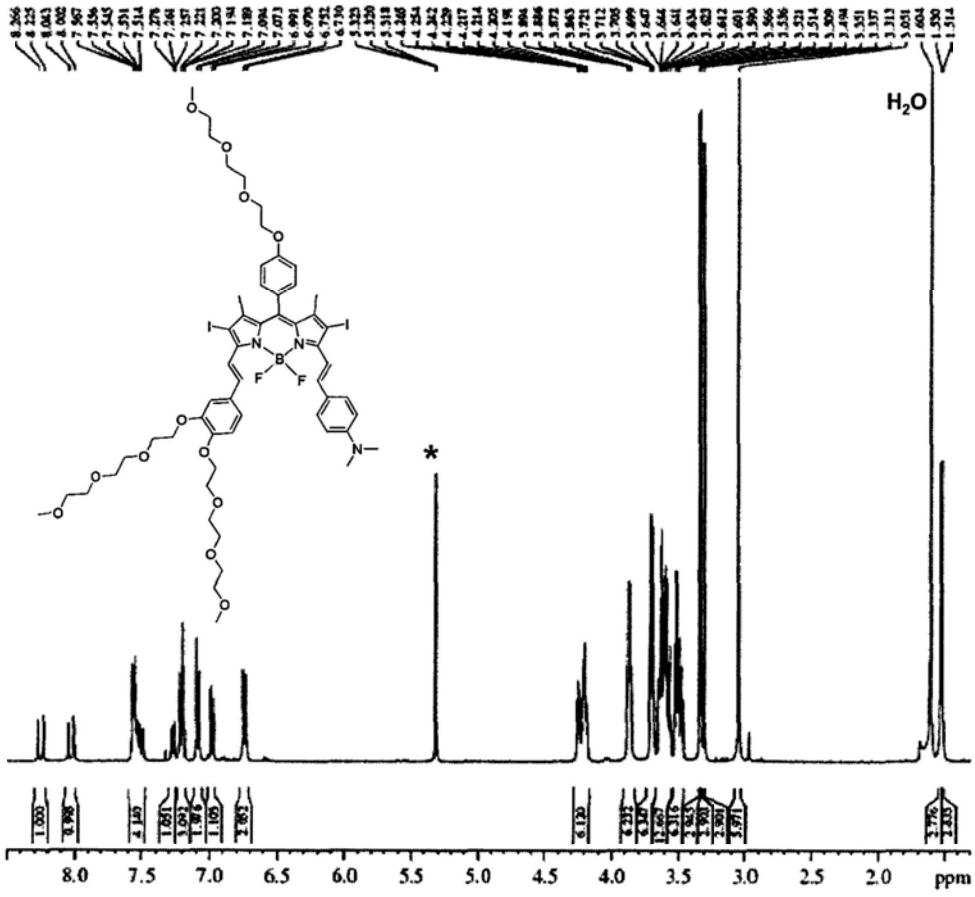

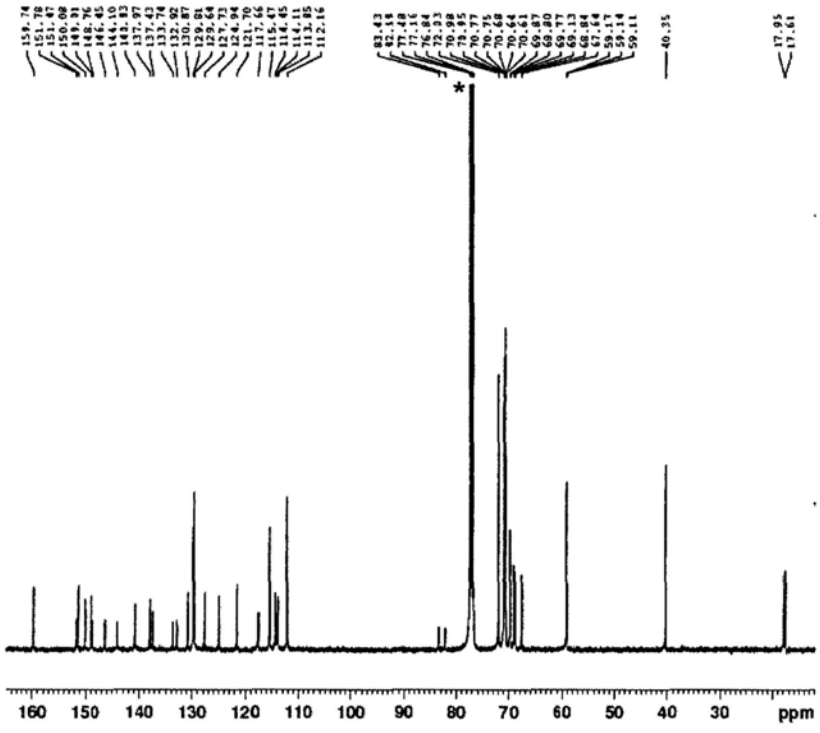

Appendix 12. ^{1}H NMR (in CD_2Cl_2) and $^{13}C\{^{1}H\}$ NMR (in $CDCl_3$) spectra of compound **3.6d**

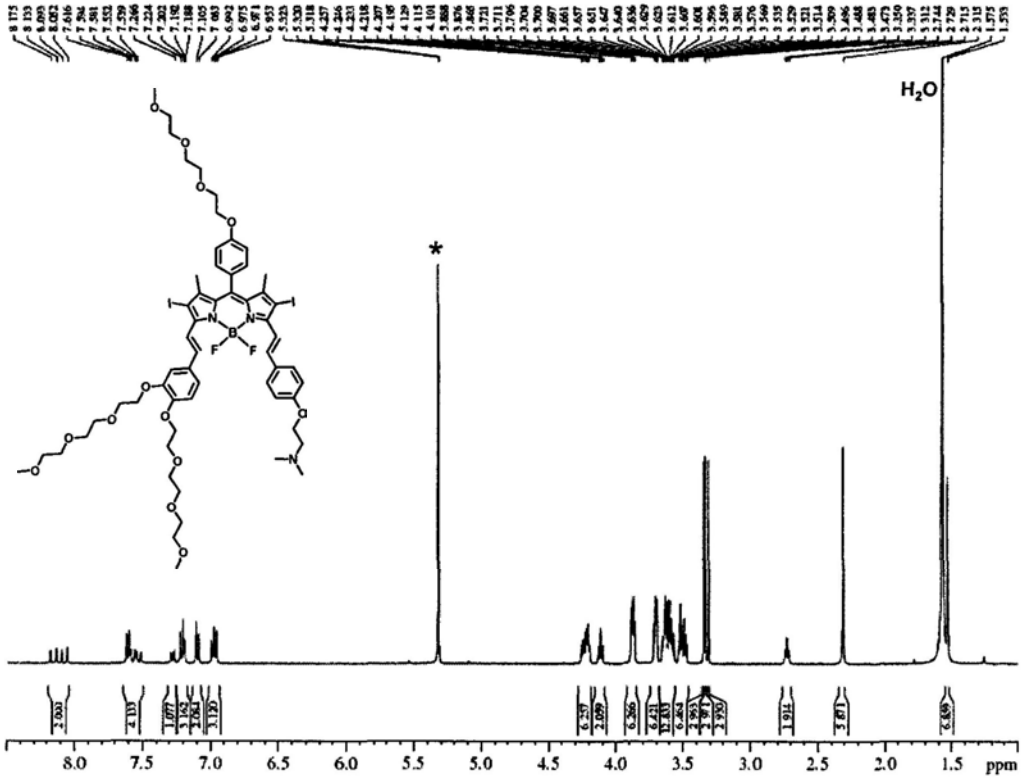

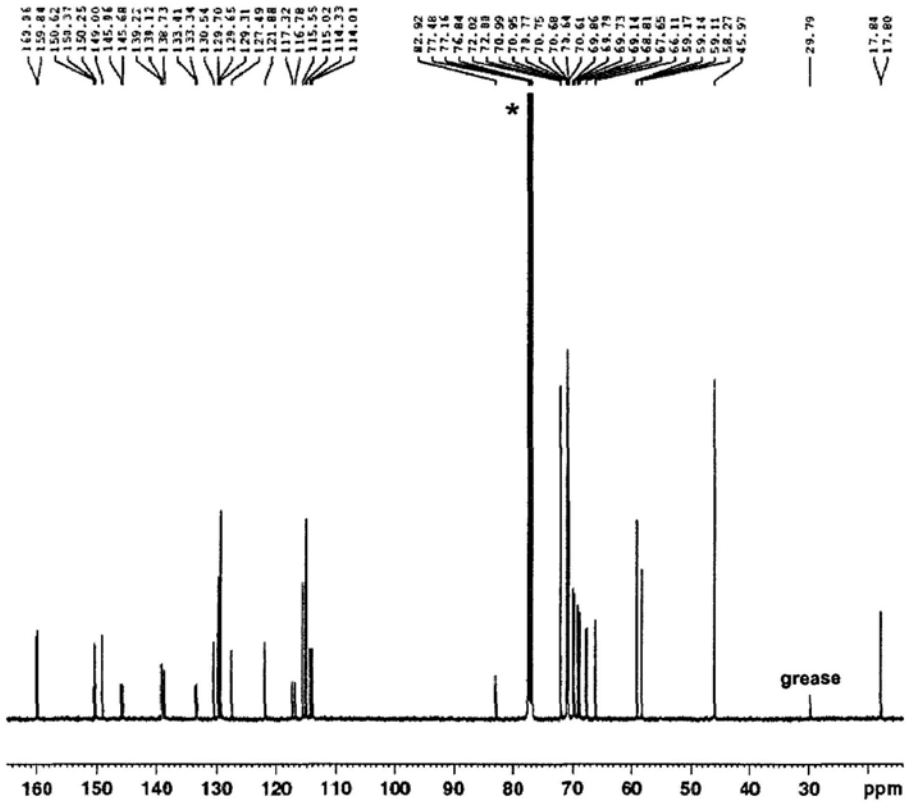

Appendix 13. ^{1}H NMR (in CD_2Cl_2) and $^{13}C\{^{1}H\}$ NMR (in $CDCl_3$) spectra of compound **3.6e**

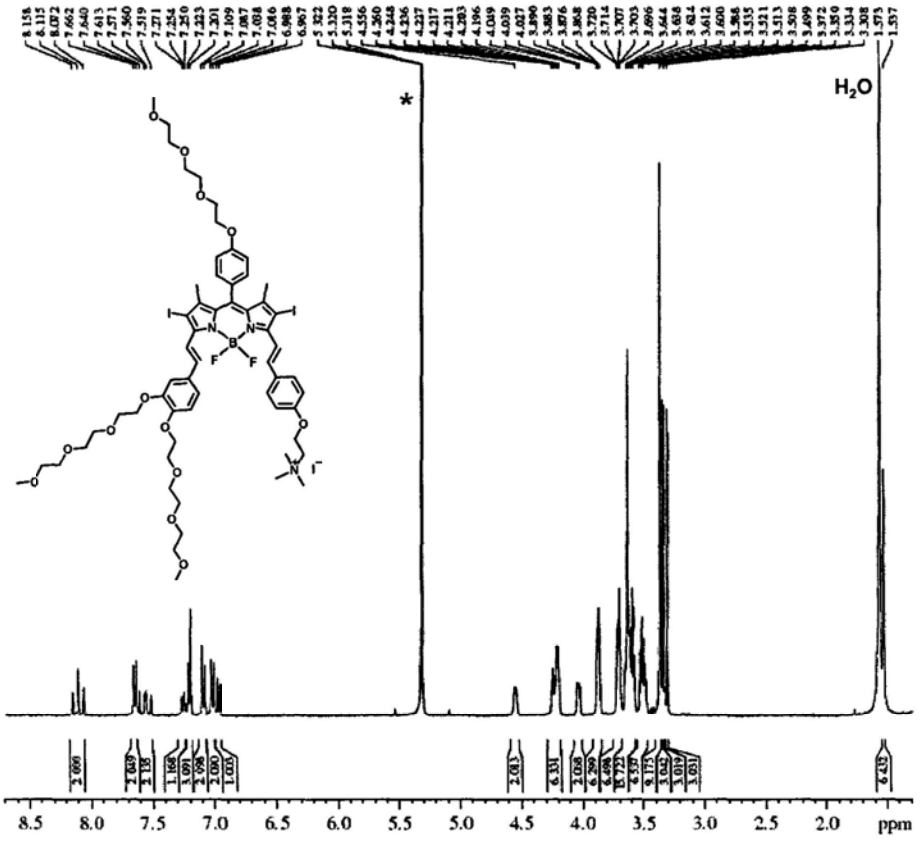

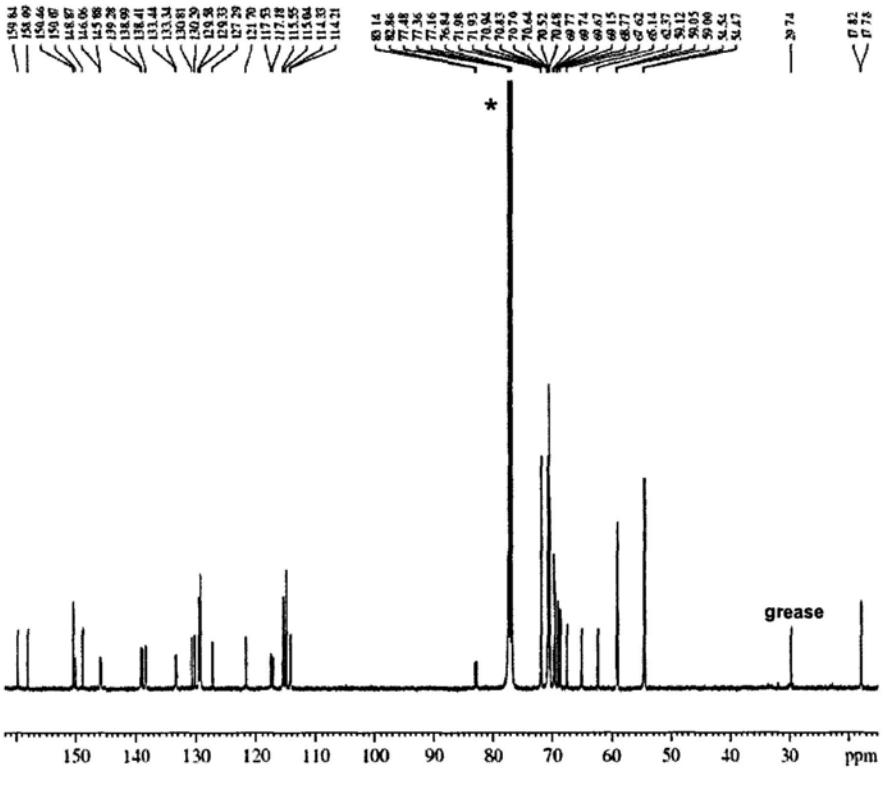

Appendix 14. ^{1}H NMR (in CD_2Cl_2) and $^{13}C\{^{1}H\}$ NMR (in $CDCl_3$) spectra of compound **4.2**

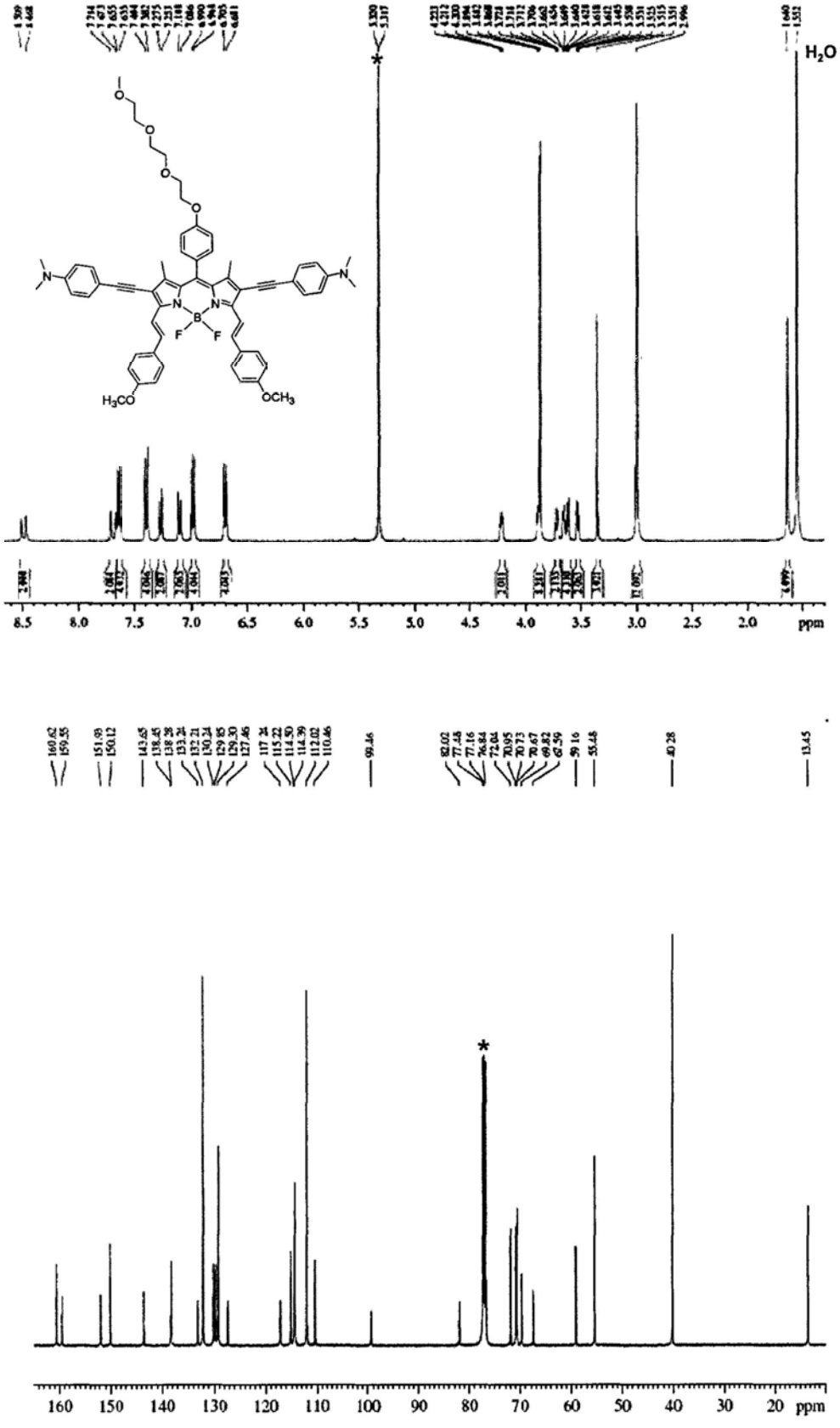

Appendix 15. ^{1}H NMR and $^{13}C\{^{1}H\}$ NMR spectra of compound **5.6a** in $CDCl_3$

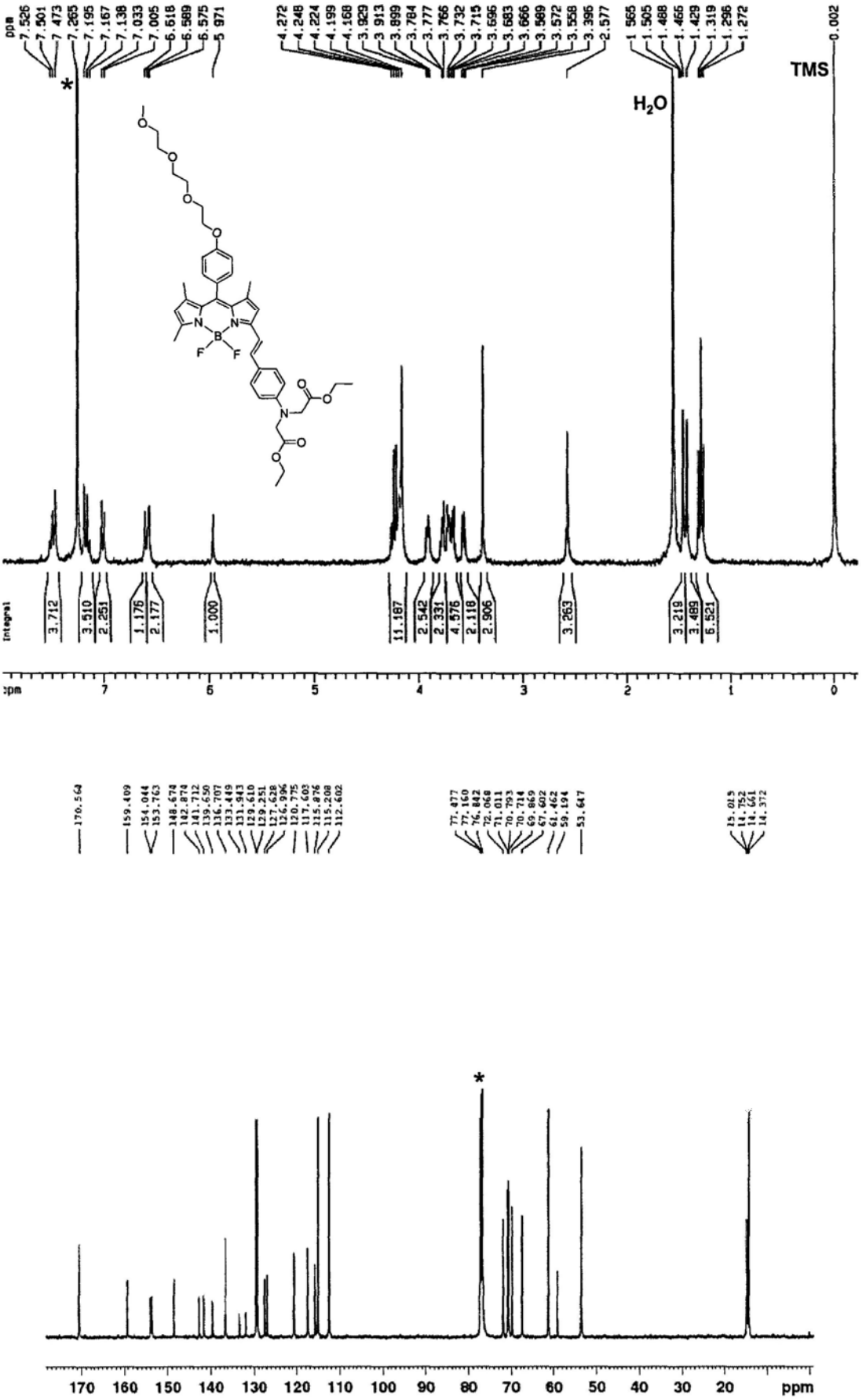

Appendix 16. ^{1}H NMR and $^{13}C\{^{1}H\}$ NMR spectra of compound **5.6b** in $CDCl_3$

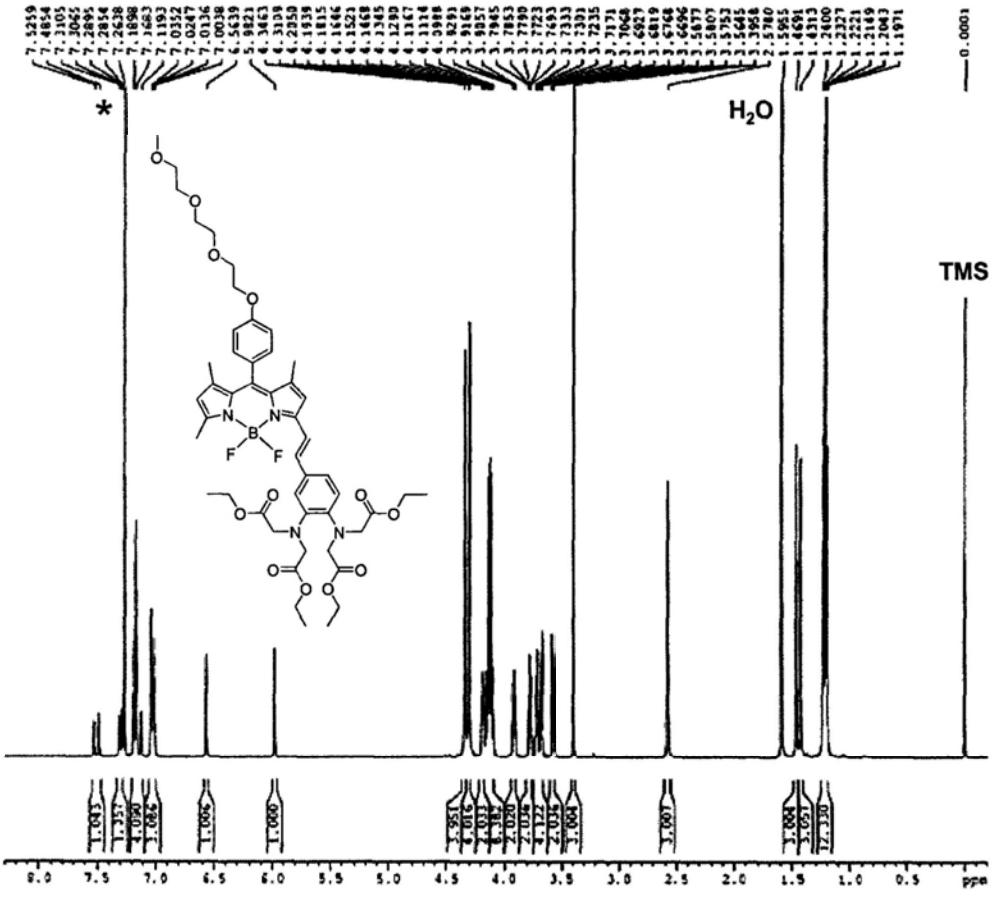

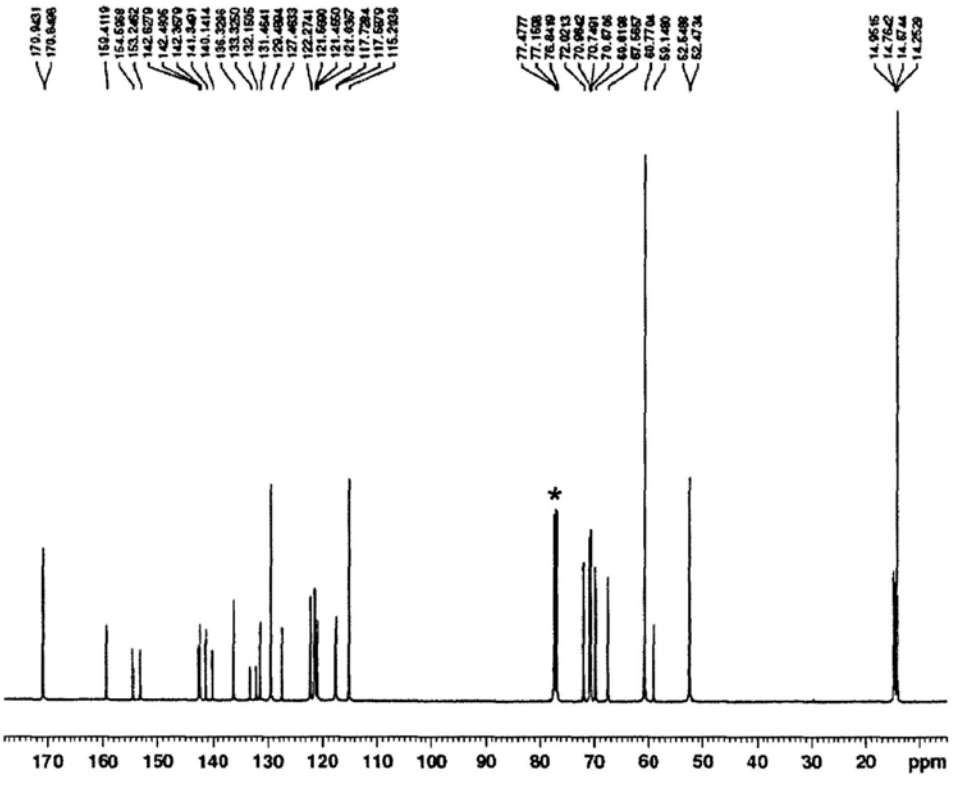

Appendix 17. ^{1}H NMR and $^{13}C\{^{1}H\}$ NMR spectra of compound **5.8a** in $CDCl_3$

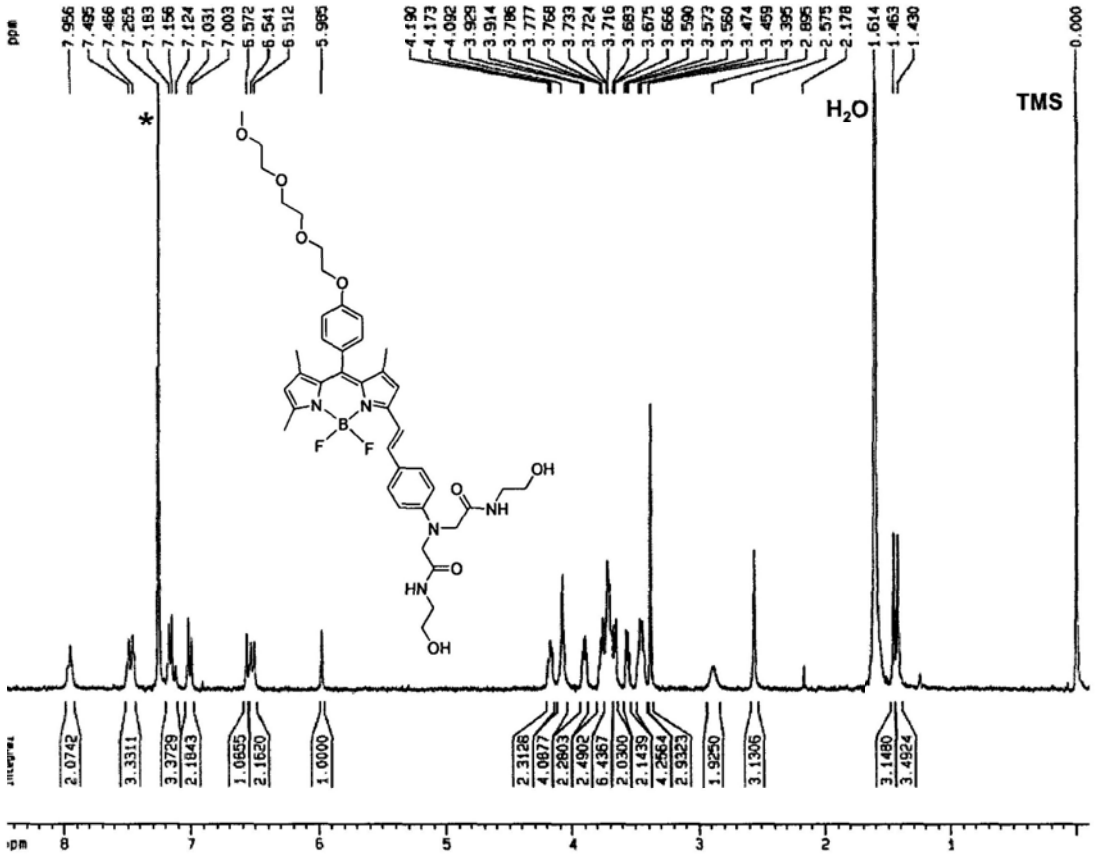

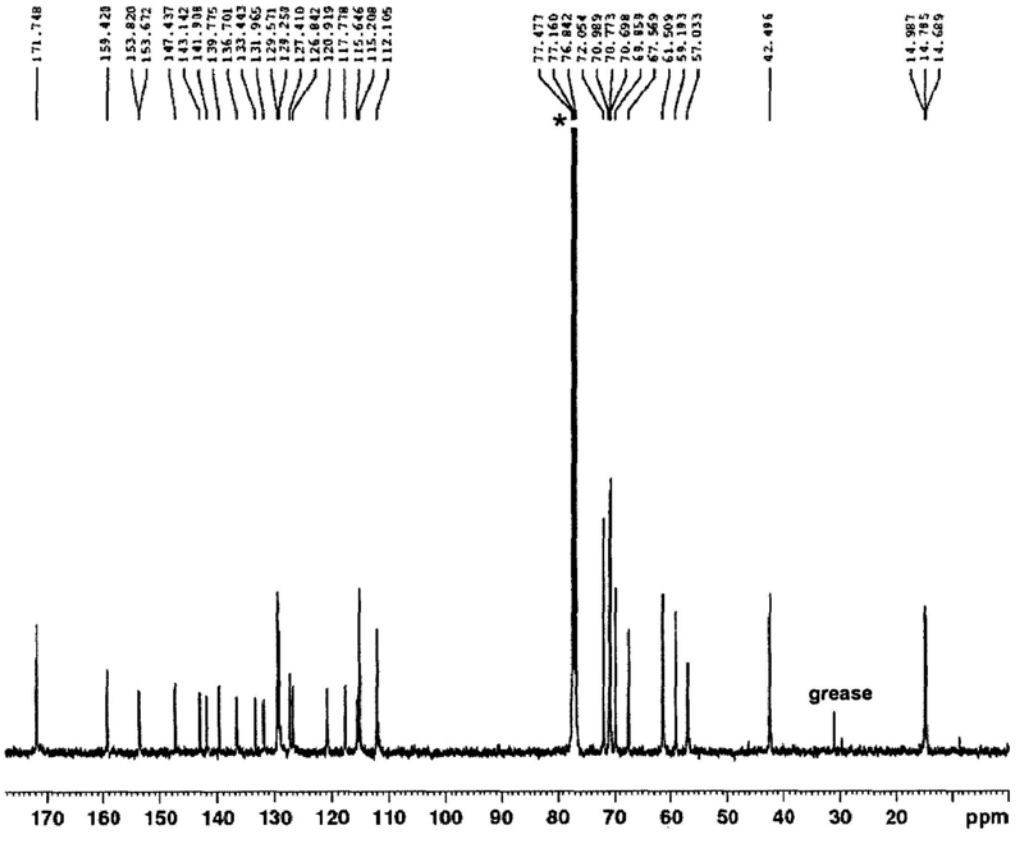

Appendix 18. ^{1}H NMR (in $CDCl_3$ with a trace amount of CD_3OD) and $^{13}C\{^{1}H\}$ NMR (in $CDCl_3$) spectra of compound **5.8b**

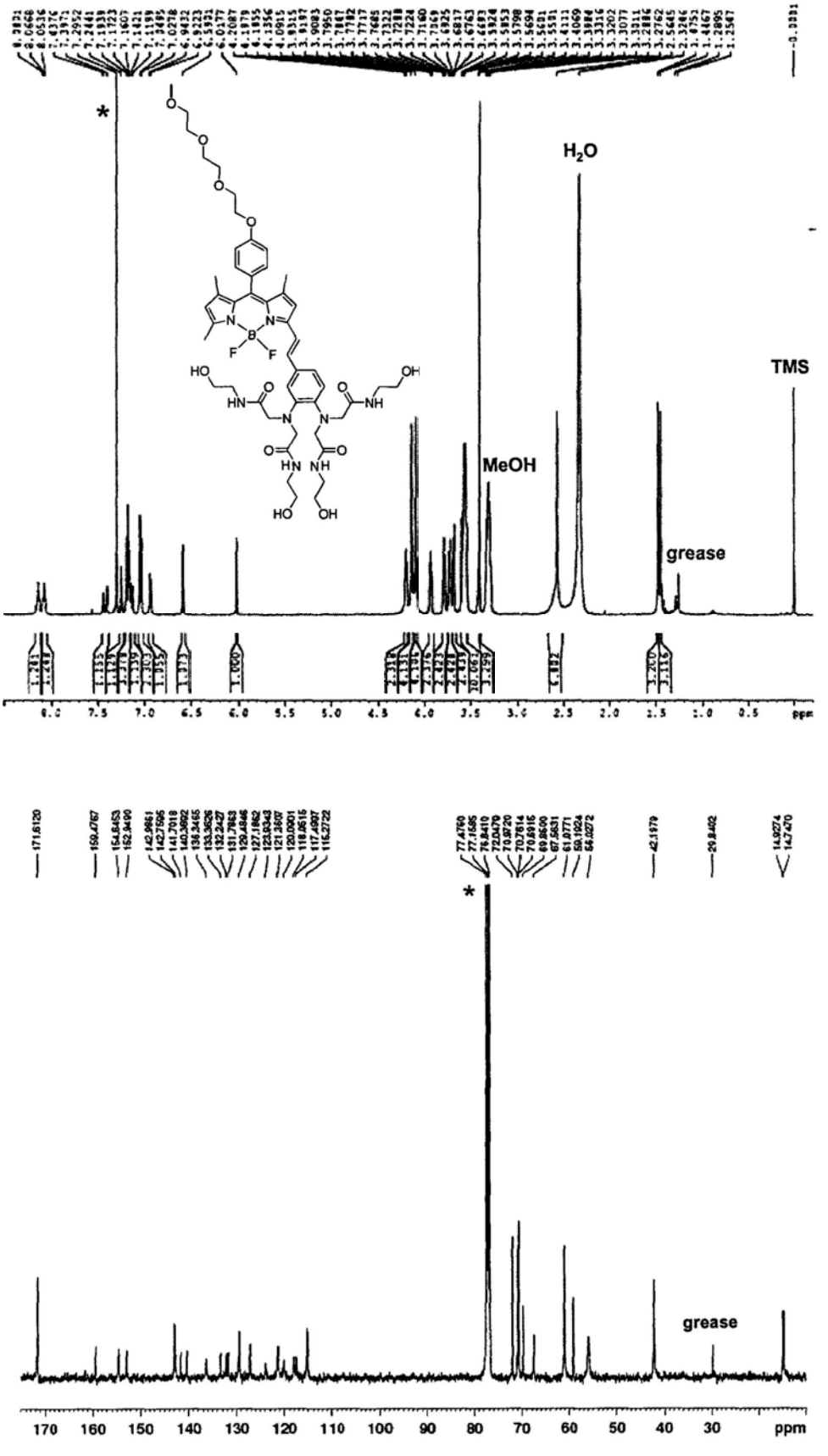

Appendix 19. ^{1}H NMR and $^{13}C\{^{1}H\}$ NMR spectra of compound **6.6** in $CDCl_3$